High-frequency ANN-based Method for Fault Detection, Classification and Location on Multi-terminal HVDC Links

Yang, Qingqing

Award date:
2017

Awarding institution:
University of Bath

High-frequency ANN-based Method for Fault Detection, Classification and Location on Multi-terminal HVDC Links

Qingqing Yang

Thesis submitted for the degree of

Doctor of Philosophy

Department of Electronic and Electrical Engineering

University of Bath

2017

Abstract

This work is the investigation of novel protection schemes for the direct current (DC) link of VSC-based high voltage direct current (HVDC) and multi-terminal high voltage direct current (MTDC) systems, with the purpose of isolating the faulted transmission line rather than tripping the entire network when faults occur on the transmission line. The main essence of the developed method is using the fast Fourier transform (FFT) feeding a multi-layer perceptron (MLP) artificial neural network (ANN) to harness short circuit fault current frequency components for MTDC overhead line relaying. This approach is shown to give more reliable fault detection, classification and location algorithms that are not affected by fault resistance. Detection by analysis of a short circuit fault current only meaning that no voltage signal is required. The protection algorithms are based on the relationship between the magnitudes or phases of fault current frequency component with fault.

A system consisting of two-terminal VSC converters and a three-terminal HVDC system with equivalent grid interconnection and source representation is built using PSCAD/EMTDC software with a detailed switching model for the converter components, which are used for obtaining the fault current data for transmission line terminals. The method is verified by studying different cases with a range of fault resistances in various fault locations, and in addition, external faults. The results show that the proposed method gives fast and reliable fault detection and classification and accurate location for DC line faults.

The method is shown to accurately detect, classify and locate overhead line faults. Unlike existing travelling wave-based methods, which must capture the initial wavefront and require high sampling rates up to 192 kHz, the new approach is more robust since it gives accurate fault detection and fault location over a range of windowed post-fault signals. Furthermore, the proposed method is fault resistance independent meaning even a very high fault impedance has no effect on the accurate fault location.

Acknowledgement

First and foremost, I would like to sincerely express my gratitude to my supervisor Dr. Simon Le Blond for all his support and help. I thank him for his constant patience and all the help during the four years of my research. He is always being there to answer my questions and very thoughtful for my study. He shared with me of his invaluable experience, which is life-long beneficial.

I would like to thank Prof. Furong Li, Prof. Raj Aggarwal, Dr. Francis Robinson, Dr. Miles Redfern, Dr. Chenghong Gu, Dr. Weijia Yuan, Dr. Min Zhang, Dr. Xiaoze Pei, Dr. Martin Balchin, Prof. Manuchehr Soleimani, Mr. Andy Matthews for their willingness to share knowledge and research experience with me. I am grateful to Dr. Ricardo Caneloi dos Santos, for his generous guidance and being supportive.

Thanks to all my other colleagues for their friendship and kindness. I would like to express my gratefulness to all my friends, for the warmest friendship for me in my daily life.

Last but not the least, I thank all my family and especially my parents and my husband Jianwei Li for their love and being always supportive for my PhD study and my life.

Table of Contents

Glossary of Abbreviations

AC	Alternating Current
AI	Artificial Intelligence
ANN	Artificial Neural Network
BP	Back Propagation
CB	Circuit Breaker
CCF	Cross-correlation Function
CDCCB	Capacitor DC Circuit Breaker
CSC	Current Source Converter
DC	Direct Current
DCCB	DC Circuit Breaker
DFT	Discrete Fourier Transform
DSP	Digital Signal Processor
DWT	Discrete Wavelet Transform
EMTDC	Electro-Magnetic Transients including DC
XPS	Expert System Technique
ETO	Emitter Turnoff Device
FACTS	flexible AC transmission system
FFT	Fast Fourier Transform
FL	Fuzzy Logic

GB	Great Britain
GCT	Gate Commutated Turn-off Thyristor
GTO	Gate Turn-off Thyristor
HVDC	High Voltage Direct Current
IEGT	Injection Enhanced Gate Transistor
IGBT	Insulated Gate Bipolar Transistor
IGCT	Integrated Gate Commutated Thyristor
LCC	Line Commutated Converter
MLP	Multi-layer Perceptron
MM	Mathematical Morphology
MMC	Modular Multi-level Converter
MTDC	Multi-terminal High Voltage Direct Current
NG	Negative Pole to Ground
NLM	Nearest Level Modulations
OHL	Overhead Lines
PCC	Point of Common Coupling
PG	Positive Pole to Ground
PI	Proportional Plus Integral
PLL	Phase Lock Loop
PN	Positive Pole to Negative Pole
PSCAD	Power Systems Computer Aided Design

PWM	Pulse Width Modulation
RTDS	Real Time Digital Simulator
RVTW	Reverse Voltage Traveling Wave
SM	Sub-modules
STFT	Short Time Fourier Transform
VSC	Voltage source converter
WT	Wavelet Transform

List of Symbols

C	capacitance
D_{act}	actual fault location
D_{det}	detected fault location
e	relative error
E	a real continuous number system
e_f	amplitude of the superimposed voltage sinusoid
e_i	arbitrary functions refer to the incident travelling wave
e_k	instantenous superimposed voltage
e_r	arbitrary functions refer to the reflected travelling wave
f_s	sampling frequency
$f(t)$	signal sample sequence
$F(\omega)$	spectral component or harmonic
i	current
I_{DInv}	DC current on inverter side
I_{DRec}	DC current on rectifier side
I_{dref}	reference value of current in d axis
I_{qref}	reference value of current in q axis
j	specific neuron
k	index

K_a	reflection co-efficient at terminal a
K_b	reflection co-efficient at terminal b
k_i	integral gain
k_p	proportional gain
K_r	reflection co-efficient
L	line reactance
n	number for the inputs
N	total number of samples
P	active power
P_{ARec}	active power on rectifier side in AC system
P_{DRec}	active power on rectifier side in DC system
P_{rated}	rated active power
P_{ref}	reference value of active power
Q	reactive power
Q_{ARec}	reactive power on rectifier side in AC system
Q_{DRec}	reactive power on rectifier side in DC system
Q_{ref}	reference value of reactive power
R	resistance
s	signal sample sequence
$S(k)$	frequencies between the DC component
t_a	travel time at fault point

t_b	travel time at the end of the line
t_f	fault inception time
T_s	sampling time
t_w	window length
t_0	initial travelling time
U_{DInv}	DC voltage on inverter side
U_{DRec}	DC voltage on rectifier side
v	velocity
V_{dc}	DC voltage
$V_{dcrated}$	rated DC voltage
V_{dcref}	DC voltage reference value
V_n	nominal voltage
w_{ji}	weighting factor
x	fault location
X_{max}	maximum magnitudes for all the training waveforms
X_{min}	minimum magnitudes for all the training waveforms
y	shunt elements
Z	impedance
z	series parameters
Z_c	characteristic impedance
Z_t	impedance of the discontinuity

Z_0	surge impedances of the pole-to-pole
Z_1	surge impedances of the pole-to-ground
ΔP_D	power loss of DC line
ΔU_D	DC line voltage drop
ΔV_n	change in voltage at the corresponding pole
γ	propagation constant
ρ	resistivity of transmission conductor
ω_N	Nth of root of unity
ω_0	fundamental frequency
δ_{dc}	voltage droop
δ_j	factor depending on whether neuron j
$\psi(t)$	mother wavelet
η	learning rate

List of Figures

List of Tables

1 Introduction

1.1 HVDC and MTDC transmission line protection

Within the future energy structure, renewable energy occupies an extremely important role. Solar energy is one of the most basic forms of energy in survival and development of a variety of organisms including humans. The UK makes sufficient use of wind power since the UK is one of the best locations for wind power in the world. Although alternative energy generation has developed rapidly, a large number of problems with such sources still persist. The technology for new energy generation needs to be constantly improved. Intermittency is one criticism of renewable energy. The generation of renewable energy sources, such as wind power and solar power, has a randomness and intermittency when used to generate electricity and may have thus have adverse impacts on the power grid at times. In addition, the best wind resources are often located at a considerable distance from major load centres. Transport of remote wind energy puts additional stress on the transmission network, and enhancement of the transmission infrastructure is required. Recent events have highlighted the need for a balanced energy portfolio. However, the new generation resources are unlikely to be located at the optimum point from the perspective of network loads and power flows. Interconnections between national networks are being recognised as being essential for mutual support and to provide economic access to diverse energy sources. Some of the links now being considered involve considerable transmission distance over land or as submarine links.

Future power grids are expected to be more smart and flexible. A better method of electricity transmission between distributed generations is required. HVDC transmission is the feasible option for the connection of renewable generation. In addition, HVDC technology is one of the technical options that can be considered for the future development of the transmission system in Great Britain (GB). HVDC is the most energy-efficient technology for bulk power transmission losing less electricity than conventional alternating current (AC) transmission over long

distances. Due to its ability to transmit power efficiently over long distances it is an important technology for addressing the unreliability factor of wind energy since many remote sites with different wind conditions may be aggregated.

The development of power system technology has resulted in the formation of interconnected grids around the world. With increasing global requirements to transmit power on an inter-continental scale and the development of new DC breakers, the benefits of a multi-terminal HVDC transmission system are becoming increasingly attractive. MTDC has often been proposed as the most promising technology for an inter-continental super-grid or collecting bulk offshore renewable energy sources [1-3]. Much renewable generation is available at locations remote from load centres, and thus must be transported efficiently over long distances [4]. For example, to interconnect extensive offshore wind sites between the Northern European mainland and the UK, an offshore super-grid is required in the future. Similarly, an MTDC grid could transmit extensive solar power from the deserts of Northern Africa to the load centres of Europe.

With soaring generation capacity in distribution and transmission systems, as well as a steady increase in the voltage level and the distance of transmission lines, stricter requirements are needed for safe operation of power grids. Recent developments in DC circuit breakers (DCCBs) and voltage source converters make MTDC a more technically and economically feasible technology [5]. However, there are many technical challenges in evolving from two-terminal HVDC to MTDC, especially in protection systems.

For HVDC transmission systems, during a fault, the DC line short circuit will not self-extinguish until the current reduces to zero [6]. In typical HVDC two-terminal links, the most common method of isolation is using an AC circuit breaker to trip the entire HVDC system. Hence, the circuit breakers reside on the AC side, and in the event of a fault, the entire link is de-energised [7]. With MTDC, placing breakers on the AC side is not acceptable since they will de-energise the whole system rather than isolating the faulted DC line [8]. Therefore, new methods are required for DC transmission line protection that are able to detect and isolate the faulted DC lines as quickly as possible [9]. In the case of a multi-terminal, it is more desirable to

isolate only the faulted link rather than trip the entire DC grid. DC circuit breakers, presently in the early stages of development, are required to isolate the faulted line. DC breakers require appropriate protective relaying so that the faults can be detected and isolated immediately. In addition, the overall protection system may require online adjustment of zonal relay settings, the faulted line may require maintenance, and the system will need restorative action, all necessitating an accurate and fast fault-location algorithm [3].

This thesis focuses on protection schemes for both HVDC and MTDC systems based on voltage source converters. MTDC is a fairly new technology with only a few systems in operation. After considering all the existing protection methods, this work concludes that a better protection strategy is required to satisfy security, speed, selectivity and robustness. The faulted frequency spectrum is a useful diagnostic to consider in protection schemes because of its dependence on fault location but no other factors. Unlike existing travelling wave-based methods which must capture the initial wavefront and require high sampling rates, the new approach is more robust since it gives accurate fault detection and fault location over a range of windowed post-fault signals. Furthermore, the proposed method is fault resistance independent meaning that even a very high fault impedance has no effect on accurate fault location.

Artificial neural network is a powerful tool to solve non-linear and complex problems. In power systems, it has been used for fault diagnosis and fault location. The ANN technique is selected to interpret the frequency spectrum in this thesis because ANN only requires simulated training data rather than a formal and exhaustive analytical approach. In addition, ANN operation time is extremely fast because it only consists of a number of simple processing units.

To the author's best knowledge, there is no published work on ANNs applied to MTDC transmission protection systems. Hence, this thesis is concerned with the algorithms of the protection scheme for multi-terminal HVDC based on ANN. It proposes a comprehensive novel multi-terminal HVDC protection scheme based on ANN using fault current signals only. Firstly a two-terminal system is simulated in PSCAD/EMTDC software to analyse the steady-state and dynamic responses.

Simulation results validate the proposed method used in the protection scheme. Based on the result, the algorithm is designed. Then, a three-terminal VSC-HVDC system is modelled in PSCAD/EMTDC, which is used for obtaining the fault current data for transmission line terminals. The method is verified by studying different cases with a range of fault resistances in various fault locations, and in addition, external faults. The results show that the proposed method gives fast and reliable fault detection and classification and accurate location for DC line faults.

1.2 Motivation for this study

In power system operation, the network is always under threat due to various conditions, especially from adverse weather. Hence, strict requirements have been put forward to achieve safe operation of power grids. Due the increasing reliance of AC systems on infeed from the DC connection, protection and control of HVDC will be increasingly critical. Transmission lines are fundamental components of power systems because of their wide spread distribution over an array of complex geographic environments. Hence, the probability of faults on the transmission lines is relatively high. Transmission line fault is still one of the main problems causing loss of service. When a line is running under fault caused by adverse environmental conditions or human factors, the safety and reliability of the system will be affected.

A control and protection system is essential to operate and maintain the network in a secure and reliable way. Its perception of the operating status of devices and fast intervention, when required, maintains normal operation of the HVDC system. Rapid action under fault conditions isolates and protects equipment in the first instance. DC control and protection systems mainly consist of the following basic functionalities: fast fault-clearing during a fault, DC power control, DC transmission line control and monitoring every parameter and events in operation.

Recent developments in DC circuit breakers and VSC-based converters make MTDC an increasingly feasible concept. MTDC has the potential to enable electricity to be traded more conveniently between generators and customers thus promoting competition in electricity markets. However, there are many challenges in evolving from two-terminal HVDC to multi-terminal HVDC. Firstly, the main

purpose of the protection system is to maintain the stability of the power system by isolating only the faulted components, whilst leaving as much of the network as possible still in operation. In typical HVDC two-terminal links, the circuit breakers reside on the AC side, and in the event of a fault, the entire link is de-energised. In the multi-terminal case, however, it is more desirable to isolate only the faulted link rather than trip the entire DC grid. Hence, DC breakers are required, and DC protection relays will need to determine when to operate the breakers as well. DC protection relaying requires special consideration over conventional AC methods. Accurate fault location needs to be achieved to support coordination of protection relaying. In conclusion, the objectives of the research work consist of the investigation of possible modelling and protection schemes for the DC link of VSC-based multi-terminal systems, with the purpose of designing a novel protection scheme on the DC side.

1.3 Summary of Key Achievements

- A two-terminal HVDC test system and a three-terminal HVDC test system based on the CIGRE B4 system are simulated in detail, including the converter stations and their control algorithms.
- A sampling rate of 10 kHz is used in signal processing, which is sufficient for the techniques to display a high performance under a whole variety of different system and fault conditions.
- The same feature extraction stage is applied both in fault detection and fault classification improving the overall speed of operation of the proposed scheme and making it easier to implement.
- A novel fault detection, classification and location method based on MLP ANNs using DC current signal only is proposed.
- Fault current is the main criterion for protection relaying. Only the DC side current data from the transmission line is required for the proposed scheme.
- A robust fault detection time of less than 5 ms and a fault location accuracy of less than 1.2 % relative error is demonstrated.

1.4 Outline of the thesis

This thesis has been divided into 9 chapters and is organised as follows:

Chapter 1 – The introduction and outline of the thesis.

Chapter 2 – Overview of basic knowledge of HVDC and MTDC technology and the existing challenges.

Chapter 3 – A literature review of current protection schemes for HVDC and MTDC systems. The principles, advantages and drawbacks of these methods are discussed.

Chapter 4 – The modelling of a two-terminal HVDC system and a three-terminal HVDC system is described. The steady-state condition and transient profile are analysed.

Chapter 5 – Artificial intelligence techniques are introduced with the ANN discussed in detail. The proposed novel protection schemes based on ANNs are presented.

Chapter 6 – The method is applied in the modelled two-terminal HVDC system. The training process and results are shown here.

Chapter 7 – Various faults are simulated from the three-terminal HVDC model established to provide data to examine the performance of the protection scheme. The results are shown and discussed.

Chapter 8 –Conclusions are drawn in this chapter and future work is proposed.

2 High Voltage Direct Current Transmission System

2.1 Introduction

HVDC technology is becoming one of the technical options for the future development of transmission systems around the world. HVDC is more energy efficient over long distances since the losses sustained in conversion are less than the losses due to AC, for example, the skin effect and increased reactive current in cables. It is, therefore, often the best option for onshore/offshore wind farm connection.

This chapter introduces basic knowledge of HVDC and MTDC technology. The advantages of the HVDC system are discussed firstly followed by the current technologies for HVDC and MTDC. The structures and components are introduced. Finally, this section lists the challenges for HVDC and MTDC systems.

2.2 DC versus AC transmission

HVDC transmission technologies associated with an flexible AC transmission system (FACTS) are more applicable nowadays [5]. Even though three-phase AC is commonly used in electrical power transmission systems, there are some limitations in a high-voltage AC transmission system with transmission capacity, the distance constraints and the different frequencies in different networks. Compared with an AC system, HVDC technologies are more desirable and their advantages can be summarised as follows:

- Environmental advantages
- Economical solutions over long distances
- Asynchronous interconnections
- Power flow control

- Improvement of system stability and power quality
- Efficient transmission
- Minimal losses especially for long distance transmission
- Key solution for renewable generation

Specifically, in technical terms, HVDC can connect two systems, which may not be synchronised, and or have different system frequencies. In contrast to limitations caused by inductive and capacitive elements of AC links (especially for cables) on transmission capacity and distance, there is no limitation in a DC network. Economically, HVDC would require less investment for long distance protection. DC is cheaper than AC if the transmission distance is longer than the break-even distance [10]. Power loss is higher in an HVDC converter station compared to that in an AC substation, caused by the conversion between AC and DC. However, the power loss in an HVDC transmission line can be 50% to 70% of that in an equivalent HVAC transmission line [11]. Thus for large distances, an HVDC solution has lower losses. The lower losses beyond the break-even distance and the lower investment cost beyond the break-even distance can be visualised, as seen in Fig. 2-1 and Fig. 2-2 respectively. The investment cost breakdown for VSC HVDC and HVAC is around 50 km for cables and 600 km for overhead transmission line [12, 13]. The DC overhead line may carry about twice as much power as in AC line, and the break-even distance is around 800 km [14]. In conclusion, HVDC has fewer conductors so that less land will be cleared for the transmission corridor. HVDC is also an economical method of long distance transmission and the best way to overcome unreliability factors in renewable generation like wind, solar and hydro by connecting a range of bulk sources of remote renewables to large load centres so that the risk of their unavailability is spread across a portfolio of generators.

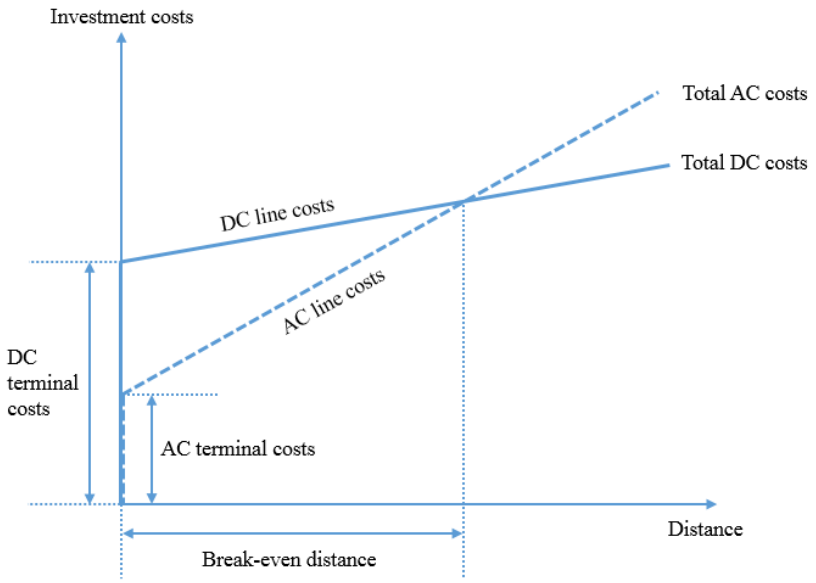

Fig. 2-1 Investment costs for HVAC and HVDC systems [13, 15]

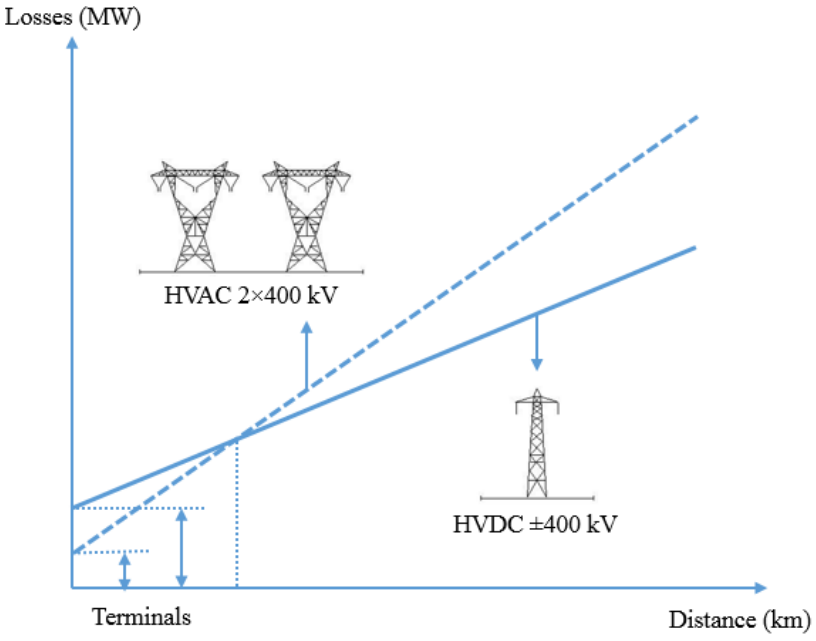

Fig. 2-2 Power losses on HVAC and HVDC systems [15]

2.3 HVDC technology

HVDC has been used for over 50 years, and use can be classified into three categories: back-to-back, two-terminal, and multi-terminal HVDC systems. Following the important milestone in the evolution of HVDC technologies from the paper [16], the development of different types of converter is clearly shown. The

first commercial HVDC links were built in 1954. As time passed, larger power ratings were required due to the increasing demand, hence the new era began with the utilisation of mercury arc valves which perform the conversion from AC to DC, whilst also achieving the power ratings required. In the 1970s, mercury arc valves were replaced by thyristor valves [17, 18]. As technology developed, insulated gate bipolar transistors (IGBTs) and gate turn-off thyristors (GTOs) were embedded to add more control to the switches and higher switching frequencies.

The current source converter (CSC), also called the line commutated converter (LCC), is the most common and the most used technology which is based on commutated thyristor systems (shown in Fig. 2.3 (a)). LCC has a constant DC current, and DC voltage is controlled to alter the power flow of the network [2]. CSCs with thyristor valves are usually used in conventional HVDC systems. However, the application became much more widespread due to the development of fully controllable high-power GTO thyristor and power transistor devices, combined with pulse width modulation (PWM) control which provides low ripple AC current forms smooth switching. The development of HVDC technologies can be ascribed to the continuous improvement of the high-power fully controlled semiconductors (thyristors or transistors) which are described in Table 2-1. The semiconductors can be used under PWM control to balance the frequency difference between the device frequencies and line frequency. The first ever transmission of CSC-HVDC has been in service since 1954; it was designed and installed by ABB from Sweden to the island of Gotland [14].

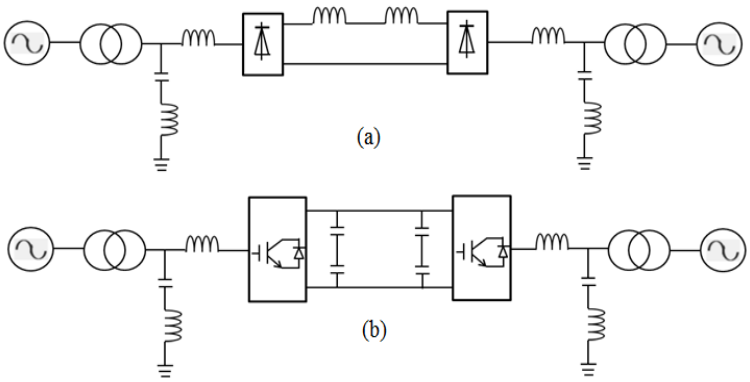

Fig. 2-3 Single-line diagram of (a) CSC-based HVDC and (b) VSC-based HVDC

In order to adopt DC power transmission in the AC power grid, electricity transformation must be achieved at the ends of the DC transmission system, completing rectification and inversion at the sending end and the receiving end. So, power electronic technology support is needed. The development of electronic devices and the application of semiconductors in HVDC has brought in a new era. Voltage source converter (VSC) HVDC has recently evolved with a host of advantages over the conventional CSC HVDC.

The VSC are known as self-commuted converters because the devices are all turn on/off via a gate pulse. Hence, the VSC-based HVDC (shown in Fig 2-3 (b)) was considered as one advanced technology from the mid-1990s [2, 19]. VSC requires semiconductor devices with turn-off capability. The development of IGBT accelerated the utilisation of voltage source converters which had a compact design, four-quadrant operation capability but higher losses [10]. According to the technique introduced in [2], the typical topology of CSC- and VSC-based HVDC are presented in Fig. 2-3 including the most important components. The comparison between CSC and VSC is given in Table 2-2. The first VSC technology was installed and tested and has been working since 1997 in Sweden between Hällsjön and Grängesberg.

Table 2-1 Summary of fully controlled high-power semiconductors

Acronym	**Type**	**Full name**
IGBT	Transistor	Insulated Gate Bipolar Transistor
IEGT	Transistor	Injection Enhanced Gate Transistor
GTO	Thyristor	Gate Turn-off Thyristor
GCT	Thyristor	Gate Commutated Turn-off Thyristor
IGCT	Thyristor	Integrated Gate Commutated Thyristor

Table 2-2 Comparison of different types of converters [10, 20-22]

Converter types	**LCC** (Natural Commutated Converter)	**VSC** (Forced Commutated Converter)
Component	Thyristor	GTO/ IGBT
Semiconductor switch control	Current control	Voltage control
Frequency control	Unavailable	Available
Valves	Thyristor valves	VSC valves
Frequency	50/60 Hz	High frequency
Advantages	System could be controlled rapidly and efficiently	It could control active and reactive power almost instantaneously
From contract date to commissioning	3 years	1 year
Losses per converter	0.7-0.8%	1.7%
DC line constant value	Constant current	Constant voltage

Some of the most significant HVDC projects that have been established in the world, including LCC-HVDC and VSC-HVDC projects, are shown in Appendix A.

2.4 Components of an HVDC system

HVDC systems consist of various equipment using VSC-HVDC as an example (Fig. 2-4). A smoothing reactor, which is used for smoothing ripple current and to oppose over current transients, is placed with the DC converter in series. AC filters, which

are installed between the transformer and phase reactor, are used to reduce the harmonics in the converter. This structure is designed to prevent the undesirable effects of harmonics on the operation of a transformer. A phase reactor is included in the converter which serves the purpose of controlling the flow of reactive and active power and reducing the fault current. The transducer can be divided into a DC current transducer, which is used to measure the DC current for the converter controller, and a DC potential transducer for obtaining the DC line voltage [23-25].

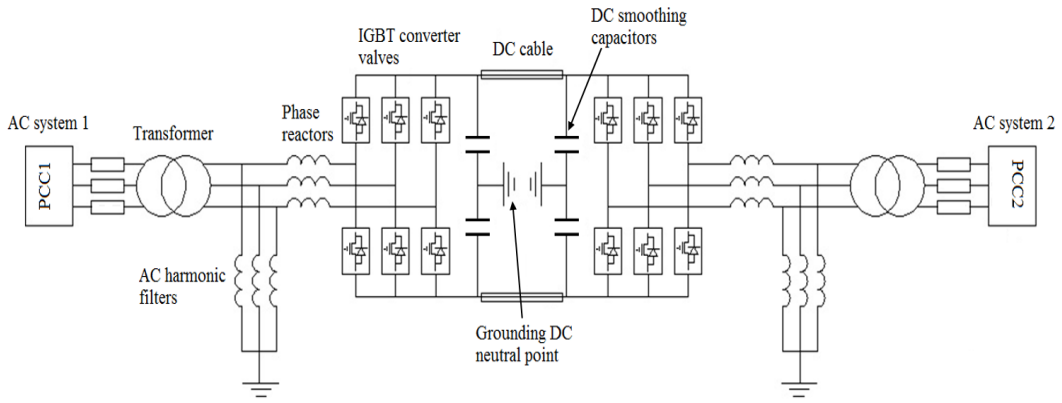

Fig. 2-4 Three-phase representation of a two-terminal VSC-HVDC transmission link showing main components

The converter station is the most important element in the HVDC system. By virtue of the electronic control, the conversion of power from AC to DC and DC to AC can be implemented. From the end of the 1960s, solid-state semiconductor technology was introduced into HVDC converter systems. The first thyristor converters were used in practice in 1972. In recent decades, the use of thyristor valves has been practical and cost effective, with more than 80 GW installed worldwide until 2010. As the technology developed, the capacity of HVDC grew significantly [23, 24, 26]. Valves in HVDC must cause little voltage drop during conduction, be able to withstand high voltages without breaking down, have instant controllable firing and overcurrent capacity during faults. Comparison of different types of valves can be found in Table 2-3.

Table 2-3 Comparison of different types of valves

Types	Thyristor valves	VSC valves
Arrangement	A twelve-pulse group with three quadruple valves	Two level or multilevel converters, phase-reactors and AC filters
Single thyristor valve	Amount of series connected thyristor	A certain number of series connected IGBTs
Material	Fibre optics	Water-cooled and air insulated

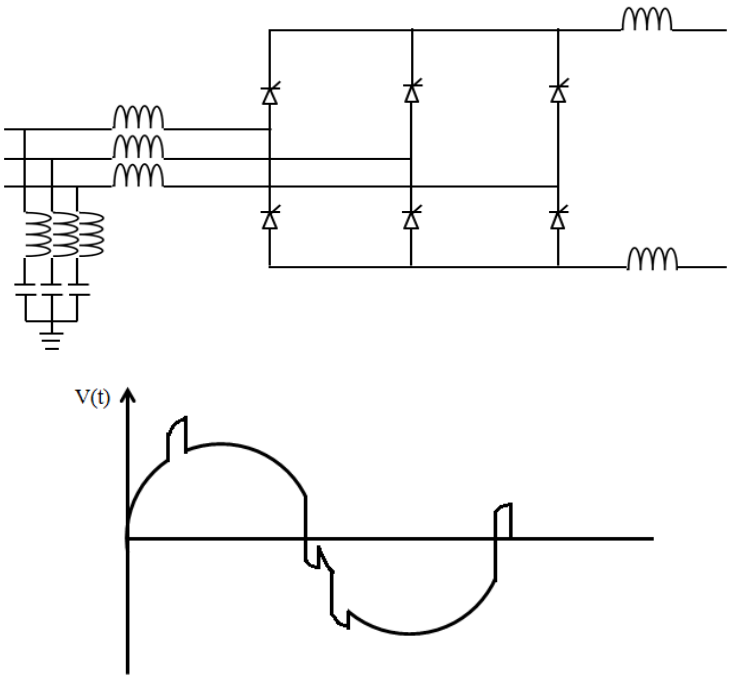

Fig. 2-5 CSC and phase voltage from CSC

CSC: The basic configuration of a conversion unit is the three-phase, full-wave bridge referred to as a 6-pulse or 12-pulse bridge. For a 6-pulse converter, the characteristic harmonics 6K±1 (K is the fundamental frequency), and 6K will be produced on the AC side and DC side respectively. The 12-pulse converter is comprised of two 6-pulse bridges which are connected with 30° difference in series. The even voltage harmonics on the DC side of the converter are of order 12K and the odd current harmonics on the AC side of the converter are of order 12K±1. Two

necessary conditions for current flowing through the valves are indicated: voltage between the anode and cathode must be positive, and there must be firing pulses on the thyristor [10, 19, 24]. CSC and the AC signal from CSC are illustrated in Fig. 2-5.

VSC: For VSC-HVDC, many IGBTs connected in series are used for each semiconductor. The converter is typically controlled through PWM. The harmonics are directly associated with the switching frequency. The active and reactive power could be defined based on the fundamental frequency [27]. VSC can control the undesired harmonics which may be created by CSC. VSC and the signal from VSC are illustrated in Fig. 2-6.

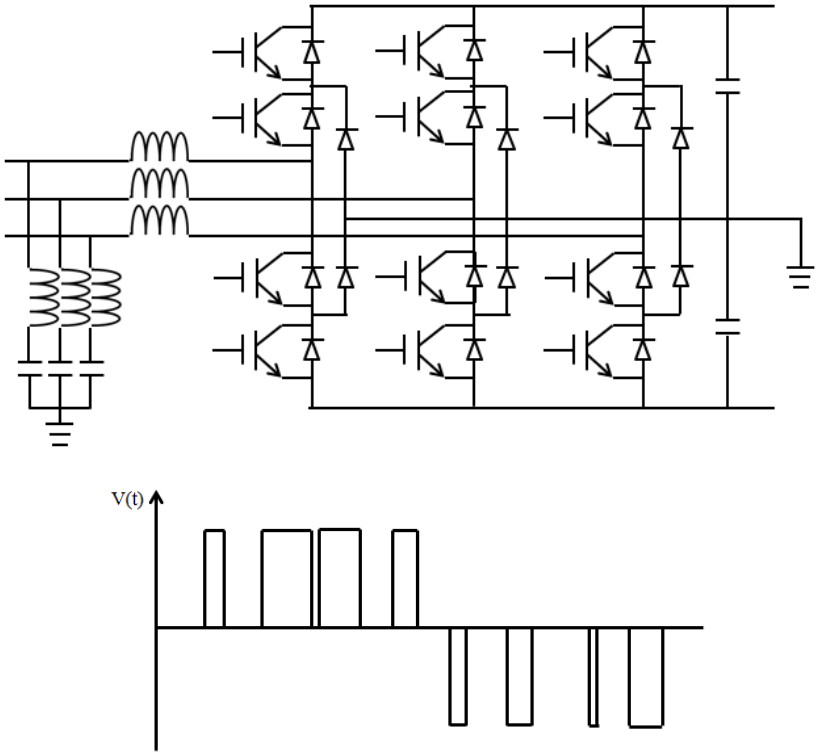

Fig. 2-6 Three-level VSC and phase voltage from three-level VSC

The Modular Multi-level Converter (MMC) is a relatively new VSC technology using sub-modules (SM) to create an arbitrary number of different voltage levels for a better approximation of the AC sinusoidal waveform. The phase potentials can be modulated between several levels instead of two. Multi-level converters have the advantages of extending the low and medium power PWM converter technology

into high power application [5, 28]. In multi-level converters (Fig. 2-7), control can either be achieved by PWM at a high frequency or at lower frequencies based on Nearest Level Modulations (NLM) [29]. Conventional converter topologies are: a neutral point clamped converter, a flying capacitor clamped converter, and a cascaded H-bridge converter which is a state of the art development [30, 31]. The advantages of MMC are obvious, including: being strictly modular concerning industrial implementation; not needing AC-filters; having no DC-link capacitor at the DC-bus; and direct and fast control of the AC- and DC-side. Compared with two-level converters, three-level converters have faster control response and fewer harmonics under a given switching frequency. In order to achieve fast control, PWM is introduced to reduce harmonic content, eliminate low order harmonics, increase the response speed and control the voltage balance on the DC side.

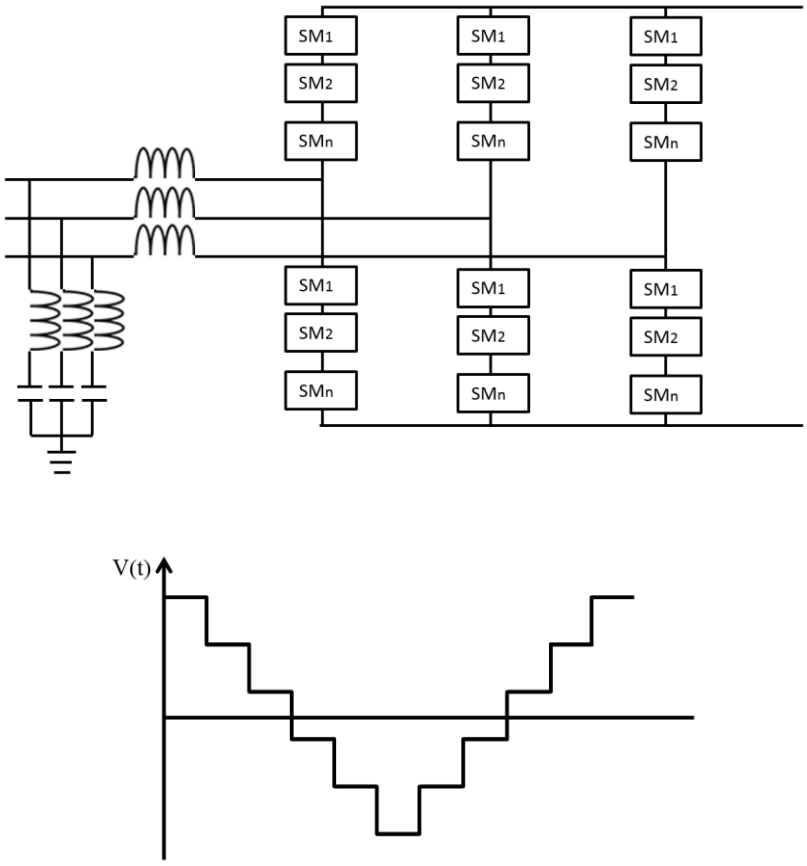

Fig. 2-7 MMC and phase voltage from MMC

For the future converter station design, the main requirements can be found as follows:

- Full controllability in both normal and fault conditions
- Minimisation of filters
- Suitability for common DC-Bus
- Reduced power loss, improved efficiency
- High availability by “inherent redundancy”
- Improved scalability by use of standardised sub components

2.5 Multi-terminal HVDC

As the conventional HVDC systems can only achieve the transmission from two-terminal, the investment cost and operation cost is tremendously increased when using DC interconnection between multiple systems. MTDC has become more attractive due to technical feasibility, which is able to respond more flexibly to different system configurations. Therefore, a multi-terminal HVDC system, which contains more than two converter stations, will play an essential role in the transmission system. What is more, multi-terminal HVDC has often been proposed as a possibility for a super-grid or connecting a large number of onshore/offshore wind farms. The existing multi-terminal HVDC projects are shown in Table A-1 in the appendix A.

Based on different types of HVDC technologies (i.e. converter station), MTDC could be classified into CSC-MTDC, VSC-MTDC and Hybrid-MTDC [32]. A CSC-based multi-terminal HVDC system refers to a system which only consists of CSCs in the network. The existing MTDC systems in the world are using LCC due to the fact that VSC development came about later than the applications. The first two MTDCs are using CSCs in the system. When CSCs are used in multi-terminal systems, the power flow was changed by changing the DC voltage polarity, which is difficult in MTDC. VSC-based MTDC refers to a system that only uses VSCs. VSC-HVDC makes a multi-terminal configuration more straightforward. The capital investment in VSCs is somewhat more than CSCs, but it will operate in a more stable condition when connected to a weak AC grid. Shin-Shinano is the first project which contains VSCs in an MTDC system. Since the VSC converter will provide a constant voltage on the DC transmission line, for MTDC a common

voltage will make a parallel connection easy to build and control. In view of the ability to control both active power and reactive power, VSC can operate in a system with little AC support. Unlike CSC, VSC can change the direction of current so that direction of power flow can be changed more easily [33]. Hybrid MTDC includes both CSCs in some converter stations and some with VSCs. By establishing a middle ground, the hybrid MTDC system is designed to reduce the cost and meet the technical requirement of using VSCs on weak systems. Even though hybrid MTDC would potentially mitigate some problems caused by CSC and VSC systems, there is no existing project in operation so far [20].

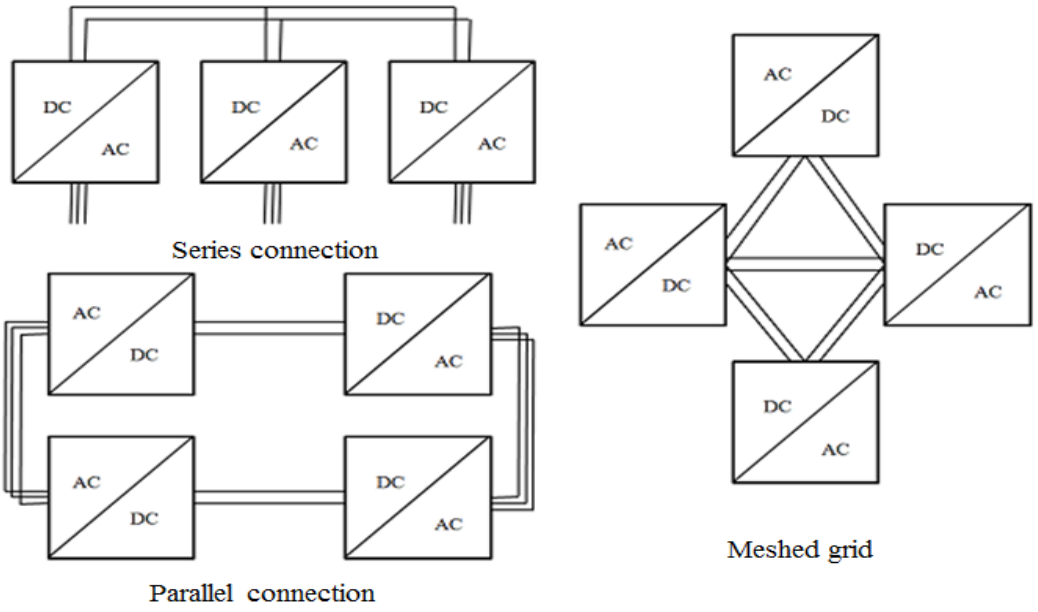

Fig. 2-8 Series connection HVDC system, parallel connection HVDC system and meshed HVDC grid

For multiple HVDC links, converters can be connected in series, in parallel or in a meshed connection as shown in Fig. 2-8. Several small grids under series connections will be connected as in the Shin-Shinano project by using a VSC- and CSC-based Quebec-New England MTDC system. A parallel connection is used for increased power transfer capacity and added redundancy in the system. Paper [34] introduces the multi-terminal UHVDC, which has parallel connected converters. The advantages of connecting converters in parallel are that it will offer more flexibility and lower losses. Highly meshed networks will integrate a large amount of power and are more likely to fulfil N-1 secure operation. However, the

complicated control system may bring some constraints [35].

Using a two rectifier, two inverter systems as an example, the largest converter in charge of DC voltage control and others control their DC current in steady-state conditions. However, both voltage and current control will be used in transient situations. Even though the connection of rectifier and inverter in series is tolerable theoretically, no series-connected (connecting both rectifier and inverter) MTDC transmission system exists, only parallel configurations which could be separated into radial networks and meshed networks [17].

2.6 Basic configurations of HVDC and MTDC systems

Basically, the configuration of HVDC can be divided into four types: back-to-back HVDC systems, monopole HVDC systems, bipolar HVDC systems and multi-terminal HVDCs. Using a CSC-based converter as an example, Fig. 2-9 shows the HVDC systems in different structures. For long distances, especially sea cable transmissions, a return path with the ground or sea electrodes will be the most feasible solution, or a metallic return path, using monopole networks as represented in Fig. 2-9 (a). Monopole with earth returns systems can reduce the cost of a transmission line, but require a higher level of material in overhead lines or land cables. Bipolar transmission (shown in Fig. 2-9 (b)) is used if there are requirements for high capacity or low load rejection. It has significant reliability, fewer losses, and so less adverse environmental impact, but the need for more equipment requires high capital investment. Bipolar systems enable fast power flow reversal and facilitate the control of frequency and power in AC systems. This configuration has many benefits during outage or maintenance on one pole. Back-to-back converters, which can be seen in Fig. 2-9 (c), are usually used for the adjacent systems which cannot be synchronised or connected in a meshed grid [5, 10].

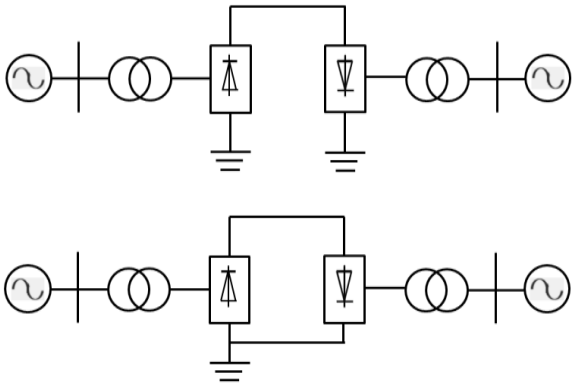

a. Monopole HVDC with earth return and metallic return

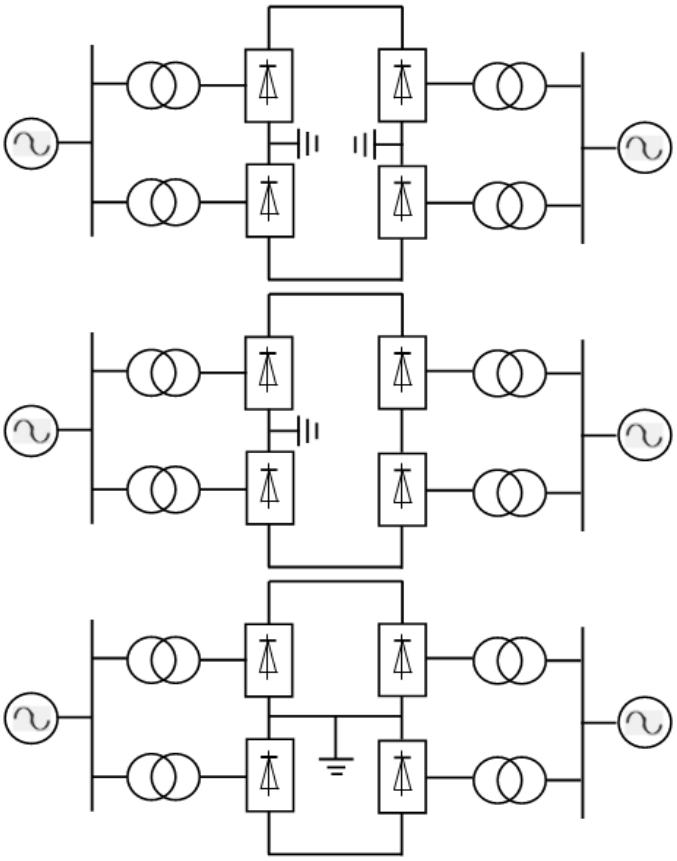

b. Bipolar HVDC with earth return, single wire earth return and metallic earth return

Fig. 2-9 Configurations for HVDC transmission networks

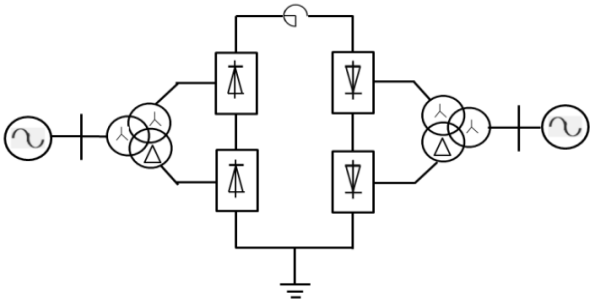

c. Back-to-back HVDC

Fig. 2-9 Configurations for HVDC transmission networks

2.7 Control for VSC-HVDC systems

There are three types of control strategies for VSC-HVDC. Unlike LCC, VSC can control active power and reactive power independently, and mitigate the fluctuations of voltage and frequency caused by wind variations [17, 36, 37]. The active control loop is set to control the active power by one station whilst the DC side voltage is controlled by the other converter station. Likewise, the reactive power control system controls the reactive power and the AC side voltage using two converter stations respectively [37].

Direct control compared with vector control is not an ideal method, because converter current and voltage is used in a three-phase frame. Without an inner-current loop, direct control could not limit the current to protect the valves. The most common method used for VSC-HVDC is vector control since the current and voltage are transformed into the rotating direct-quadrature frame so that the inner-current controllers are designed to improve the response.

Since voltage control is one of the most important parts in a VSC station, the direct-voltage control methods including voltage droop, ratio control, priority control and VMM are introduced in [17]. The load-dependent frequency variations are used as an input signal in a voltage droop method, thus this can be used for both CSC and VSC-based HVDC systems, in that the direct voltage could be regulated by adjusting the converter current. Ratio control is used to overcome the difficulties of voltage droop when steering the power flow in the network. A priority control

strategy is usually used on small MTDC networks as indicated in [17], and VSC has precedence over other kinds of converter in this method. The voltage margin method is proposed to control CSC-MTDC networks.

The voltage margin control method can maintain voltage even after disturbances. Based on [36], local control and master control are introduced in control methods for MTDC. In local control, the transformation of an abc reference frame and dq reference frame is used for active and reactive control. In addition, pulse width modulation, which controls the inverter circuit switching devices on and off, produces a series of voltage pulses which has equal amplitude but varying width. Hence, a sine wave or the required current waveform can be synthesised by these binary voltages with reasonably low harmonic content. According to certain rules of the PWM, the magnitude of output voltage in the inverter circuit and the output frequency could both be changed [28]. A better control method should overcome the non-linear coupling effect and maintain a constant value. Master control, without a requirement for communication, uses the voltage margin method for overall control to coordinate the electric power flows within the MTDC system. One terminal is responsible for DC voltage regulation and the other terminals are responsible for providing active power in case of over-voltage, under-voltage and unstable operation if there is a disturbance or fault.

In [38], cooperative control is selected to be used in a three terminal system. Several strategies are introduced, so these strategies are used to control power sharing among MTDC systems such as autonomous control. This strategy allows the plug and play feature and hence, when any terminal of MTDC system is in outage or curtailed, there is no need to reconfigure the MTDC system or reset new references for their controllers. Moreover, cooperative control has several benefits such as high reliability, and minimising the operation cost. In general, a complex system should be clustered into many subsystems, and it is not necessary for the cooperative control algorithm to communicate with all subsystems as shown in Figure 2-10. Figure 2-10 explains the concept of cooperative control that interacts with subsystems. The two subsystems 1 and 2 are considered to communicate with each other, but subsystem 3 will communicate with the other subsystems through its output. In other words, subsystems 1 and 2 inputs communicate to subsystem 3 in

an indirect way.

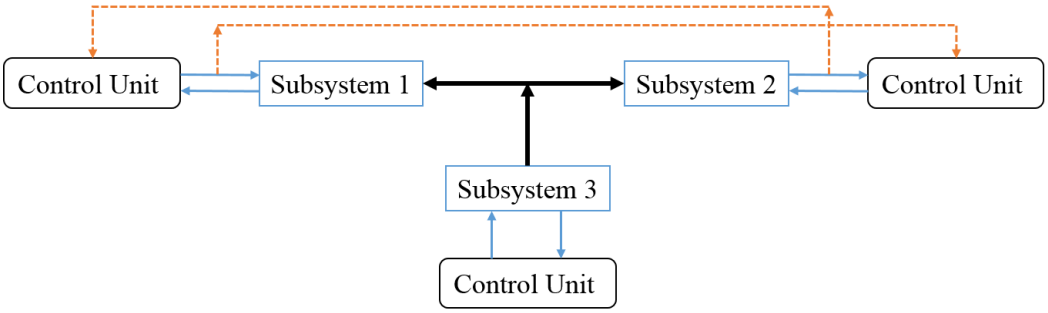

Fig. 2-10 The cooperative control algorithm

2.8 Challenges of HVDC and MTDC transmission systems

HVDC transmission has proved to be a reliable and valuable method of electrical energy transmission. However, there are a number of challenges to overcome. The investment in an HVDC system is high. The power loss in an HVDC converter station is higher compared with an AC substation due to the conversion between AC and DC and the harmonics [11]. In VSC-based HVDC systems, switching losses, which are directly related to high-frequency PWM operation, are one of the most serious and challenging issues that must be overcome. Other significant disadvantages under high frequency operation are electromagnetic interference, transformer insulation stresses, and high frequency oscillations, which require additional filters [5]. Some constraints are also here in the DC side HVDC grid protection such as limited overload capability of power electronics, converter blocks to protect the IGBTs and stability at the DC side. On the AC side, frequency deviations, and in extreme cases, loss of synchronism may occur in any of the connected systems.

2.9 Chapter summary

This chapter reviews the basic introduction of HVDC including HVDC technologies (converter technologies), HVDC components, HVDC configurations and control of HVDC systems. Furthermore, the advantages and challenges of

HVDC and MTDC systems were also reviewed.

CSC-based HVDC is widely used around the world and VSC-based HVDC system is introduced as a promise new solution. With the rapid development of electronic devices, VSC technology stands out from the HVDC technologies and becomes the best option for multi-terminal HVDC systems. Redundancy, resilience and stability are three key objectives for a VSC-based MTDC network [39] which have a number of benefits over other technologies, and so would be successful transmission media. Therefore, the objectives of an MTDC network can be described as follows: to transfer more power; provide redundancy and flexibility for extensions; maintain voltage and frequency, maintain stability; for the healthy sections to continue operating under various fault conditions; and return to a steady-state condition as quickly as possible after disturbance.

3 Overview of the Protection Methods for HVDC and MTDC Systems

3.1 Introduction

The basic principles for protection of HVDC and MTDC systems are introduced in this chapter. The fault profile including the fault types and features are introduced firstly to help to understand the protection principles. The circuit breaker applied in a DC system is presented herein. The basic protection methods used in HVDC and MTDC systems are explained respectively.

3.2 Types of faults

Due to the complexity of current electrical power systems, the occurrence of faults is unavoidable. The target of a protection system is to minimise the damage caused by faults using the appropriate protection scheme. Compared with cables, overhead lines are more easily affected by external situations hence leading to faults. Overhead lines are vulnerable to lightning throughout their length, hence the most common problem is lightning. Other weather conditions such as wind, ice and snow loading, etc. may also cause faults. Birds and animals and trees are also reasons for overhead line faults.

The types of faults on HVDC systems can be classified into two: line-to-ground fault (positive or negative) and line-to-line fault. Depending on the system topology, there are essentially three types of fault including the possibility of pole-to-pole-to-ground fault. However, this type of fault is extremely unlikely and virtually impossible if the two conductors are in separate cables [8].

Overhead lines (OHL) and cables are the two main media for a DC transmission

system. In total, 70-90% of faults are transient in overhead lines, whereas most cable faults are permanent. VSC-based HVDC is usually used in projects involving cables. However, in comparison with cables, an overhead line is more likely to sustain faults. Nonetheless, faults occurring in cables are more likely to be permanent faults. Furthermore, cable fault is mainly caused by insulation deterioration and breakdown [33, 40-42].

Line-to-ground fault (PG and NG in Fig. 3-1) involves insulation failure between a DC conductor and the ground, which is usually caused by lightning strikes and pollution. Line-to-ground faults can be divided into positive line-to-ground faults and negative line-to-ground faults, and they happen when the line is shorted to the ground. When a line-to-ground fault occurs in a bipolar system, the capacitor will be discharged on faulty poles so that it will suffer an overcurrent. On the other hand, a healthy pole capacitor will impose an over voltage. Unlike the permanence of faults in cables, overhead lines can be restored after fault clearance.

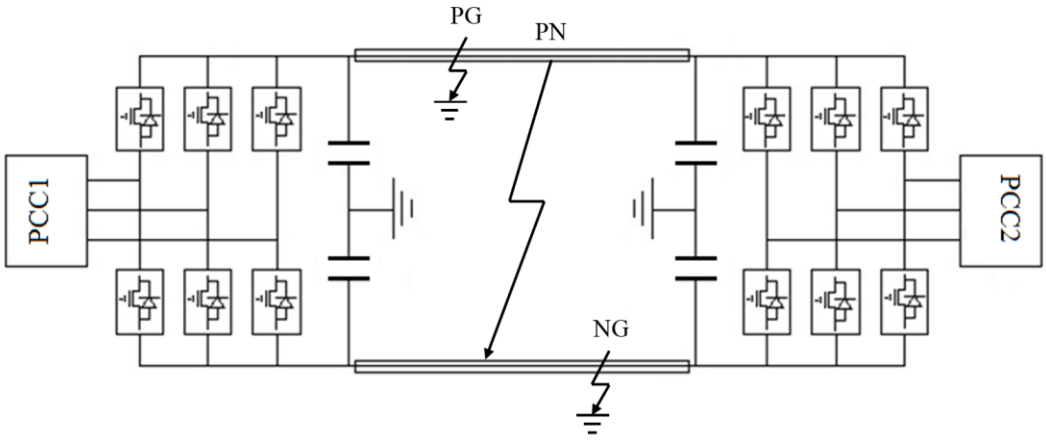

Fig. 3-1 Locations and types of DC line faults

Line-to-line fault (PN in Fig. 3-1) arises from insulation failure between the two DC conductors meaning that the capacitor will be discharged, and the AC system will suffer a three phase short circuit. Except for blocking both converters, a DC line should be isolated from the AC system by using AC breakers or DC breakers. Although rare, line-to-line faults are generally more common on overhead lines than cables since falling objects on exposed conductors may cross the positive line and negative line.

Under line-to-ground faults, overhead line protections are required to detect faults and block and trip the converters, and automate a recovery process is autoreclosing is available. The rebalance of capacitors is the key point before the system restarts. There is a similar process for line-to-line faults to detect faults and block converters. Then DC capacitors can be charged to see whether the DC voltage has been re-established [43].

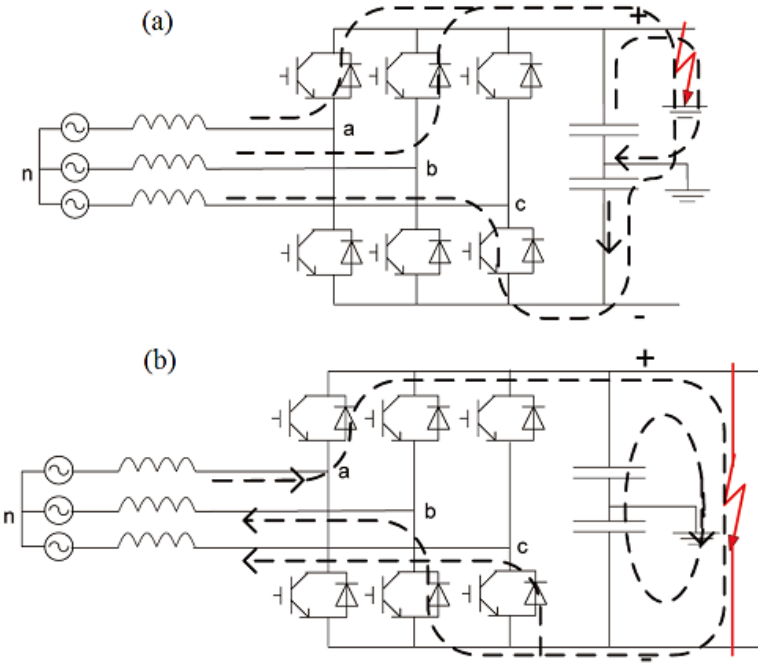

Fig. 3-2 Illustration of VSC-HVDC fault for two paths: (a) line-to-ground (b) line-to-line [43]

A fault on a DC line travels in both directions and the terminals reflect the waveform. The wave front of a transient overvoltage can take two different paths which are illustrated in Fig. 3-2. If the nominal voltage pre-fault is known at any given point along the line, the voltage at the corresponding pole can be characterised by equation 3.1:

$$\Delta V_n = V_n \times \frac{Z_0 - Z_1}{Z_0 + Z_1} \tag{3.1}$$

where: V_n is the nominal voltage, ΔV_n is the change in voltage at the corresponding pole, Z_0 and Z_1 are surge impedances of the pole-to-pole and pole-to-ground paths respectively.

The stability of the power system and the power quality will both be affected by faults on a transmission line. In terms of devices, if the fault cannot be cut immediately, equipment may suffer from severe damage. Some of the equipment can be permanently destroyed in the worst case, and the whole power supply can be lost for a long period. Hence, the protection system is of overriding importance.

In multi-terminal configuration, management of DC side failures have the specific challenges:

• High surge currents after DC-short circuits can lead to mechanical damage and arcing

• Secondary damage of healthy converters at the same DC-Bus can occur

• In normal and transient conditions, resonance currents in the DC-Bus network create further disturbance

3.3 Circuit breakers

The time for the protection system to respond to a fault is particularly critical for MTDC. The present generation of DC circuit breakers needs to operate within a few ms [44] (approximately 5 ms according to one manufacturer) [45, 46] to successfully interrupt the rapidly increasing DC fault current. This is technically challenging but the main fault detection proposed in this paper is always shown to robustly operate at under 5 ms. With ongoing improvements in breaker technology, this will be sufficiently fast either for the current generation of breakers or in the very near future.

Circuit breakers will be positioned on DC transmission lines and work during a fault. The breaker must create an artificial current zero crossing to interrupt the fault current. Different HVDC breakers have been proposed in many studies. Broadly, there are three types of HVDC circuit breakers: electromechanical, solid-state and hybrid circuit breakers [47]. Solid state breakers are fast but expensive, and have high losses. Mechanical breakers making use of auxiliary circuits have a lower cost.

Hybrid breakers combine power electronics and fast disconnector switches. Different grounding schemes should be considered. In addition, passive elements such as inductors are commonly proposed to limit current rise.

Electromechanical types of circuit breakers (shown in Fig. 3-3) can be grouped into three categories: (1) inverse voltage generating method, (2) divergent current oscillating method, and (3) inverse current injecting method. Only the inverse current injecting method can be applied for high ratings of voltage and current. In electromechanical breakers, the current zero can be generated by superimposing the reverse current on the input current by discharging the capacitor via the inductor [47, 48].

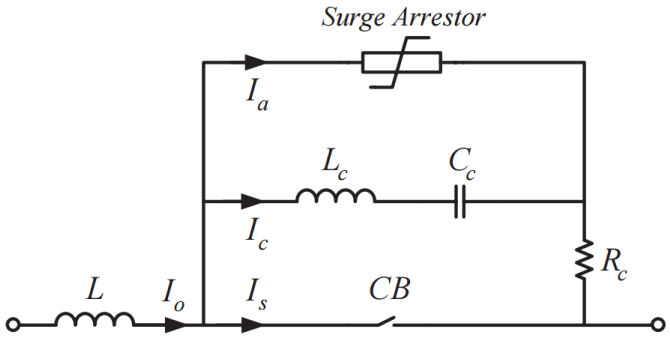

Fig. 3-3 Electromechanical circuit breaker [49]

Solid-state circuit breakers illustrated in Fig. 3-4 are another type of HVDC breaker, which have a much faster interruption time and lower state losses than electromechanical circuit breakers. The interruption time can reach a few milliseconds. This type of CB is based on IGCT instead of IGBT with lower on-state losses. The main disadvantages of these types of circuit breakers are the high capital costs [47, 48].

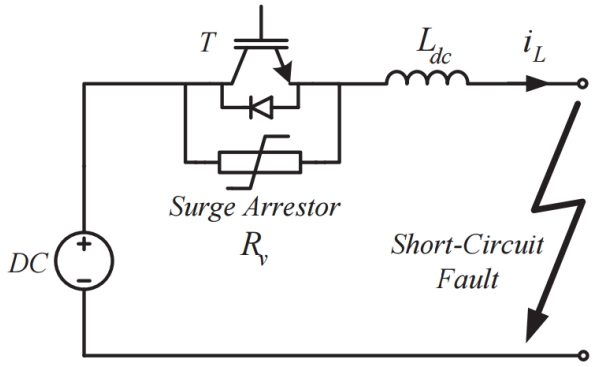

(a) Topology 1

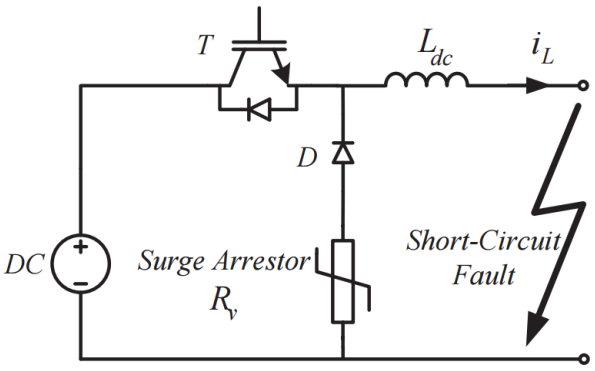

(b) Topology 2

Fig. 3-4 Solid state circuit breaker [49]

The hybrid electromechanical/solid state circuit breaker (Fig. 3-5) is a relatively recent development [50]. It replaces the electromechanical contact with semiconductor switches to achieve the open-circuit disconnection, which has high switching speed and high current carrying capacity [51].

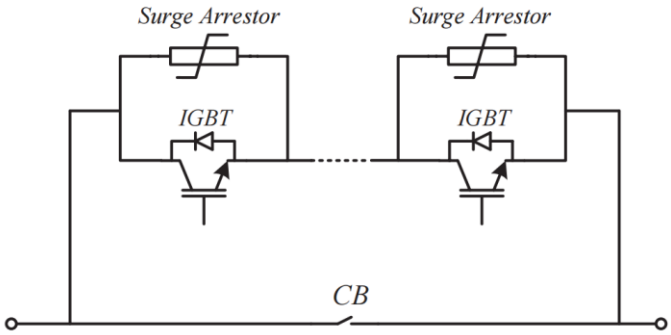

(a) Topology 1

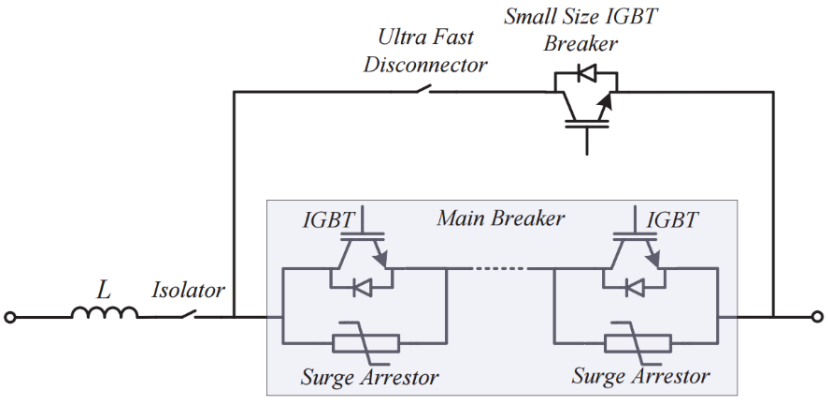

(b) Topology 2

Fig. 3-5 The hybrid circuit breaker [49]

A converter embedded device is another protective device installed in VSC to detect and isolate DC faults. However, the effect is not effective in multi-terminal networks. Capacitor DC circuit breakers (CDCCB) are introduced in [33, 52] by placing a capacitor in series with a circuit breaker. The biggest benefit is that the operational speed is dramatically improved, with the converter back in operation within 10 seconds. The research in paper [53] develops the use of the converter embedded device. Emitter turnoff device (ETO) based CDCCBs, which usually work with snubber circuits are used (Fig. 3-6). With these, the fault can be turned off and interrupted within 10 μs.

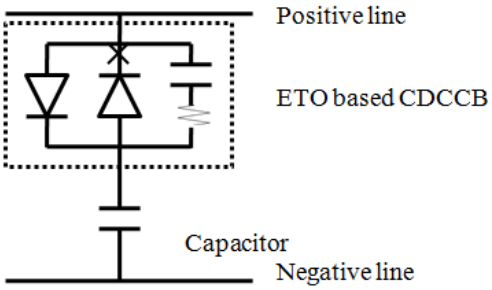

Fig. 3-6 CDCCB protection

The problem of this method using DC protection is that devices may let voltage overshoot when putting converters back into service. Hence, a method introduced in [54] integrated with a chopper circuit may mitigate this problem (as shown in Fig. 3-7).

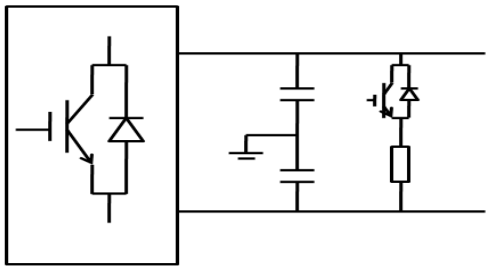

Fig. 3-7 Overvoltage chopper circuit

The chopper in turbines introduced in [55] is to prevent the voltage rise in DC links due to excess energy. When faults occur on the AC side, the dynamic characteristics of a collection grid, which is inertia-less with a slightly larger current, could be determined by converters and corresponding controllers. The result shows that the AC terminal voltage will drop, and DC link voltage will increase to the same value at the connection to the DC chopper. The active power on the wind turbine side will not be impacted because of the use of a DC chopper. The impedance changes from a large to a small value could be seen by relay so that the fault will be detected, resulting also in a change of the angle. The DC voltages will decrease whatever side the fault is on. However, the detection for multi-level converters will be difficult due to many smaller separate capacitors. In conclusion, the maximum disconnection time is 15 ms, and ABB developed the DC breaker in late 2012 to

interrupt the power within 5 ms. Fault detection could be faster using large capacitors which cause a very large discharge current [55].

However, for the moment, operators must work with large numbers of legacy AC devices and, thus, need to compensate for their disadvantages. Accordingly, DC devices are developed to allow the healthy line to keep operating. Most DC breakers are based on semiconductor switches (e.g. IGBT). IGBT circuit breakers are usually regarded as DC protection devices, and they are much cheaper than DC circuit breakers [33, 56]. Like many IGBTs in converters, IGBT circuit breakers using solid state devices consist of an anti-parallel diode. Even though solid state devices have large losses and a high cost, they can clear faults quickly with good performance. The advantage is that the converter will not shut down if a ground fault occurs. However, IGBT-CB is a unidirectional device so that it will not protect the rectifier side. As shown in Fig. 3-8, IGBT-CB will block fault current from a to b if a fault occurs on the DC line.

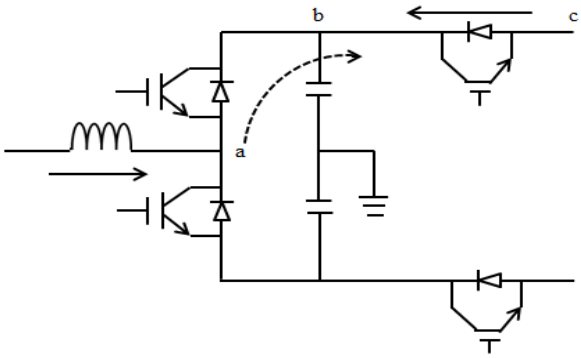

Fig. 3-8 IGBT-CB

In a protection scheme, when a fault occurs, the voltage will start to collapse as the current begins to rise. At the same time, the IGBT is ready to block, and the fast acting DC switch will open once a fault is detected. This technology has also been described in [57]. By considering the constraints caused by the VSC-based multi-terminal system, IGBT-CB has been placed between VSC and DC networks.

3.4 Existing HVDC line protection

A DC line fault will cause the current rise on the converter station, as well as the

collapse of the DC line voltage. The primary objective of line protection is to detect the fault on the DC transmission line, isolate it and recover the line as soon as possible. In the protection of a longer HVDC system with high capacity, the protection of a converter station will not be influenced as much as DC line protection.

For DC protection, a discharge wave will be produced if a fault occurs between shields in DC transmission lines and cables. The surge impedance is typically below 100 ohms. This leads to high short circuit currents. Hence, fault distances could not be devised simply though impedance measurement as for AC systems. Another reason is that there is no complex value of the impedance in DC systems, so distance protection is one dimensional (just resistive) rather than obtaining the X/R locus as would normally be the case in AC systems. Due to the sensitivity of converter stations to overload and high costs, protection should be against overcurrent. Switching DC current is not trivial since DC current will not cross zero. New techniques are therefore required. In a meshed network, the faulted line must be selected within a limited time to keep the remaining system operational after isolating the faulted line. Since DC cable routes usually consist of two independent insulated cables, short circuits between the positive and negative poles are rather unlikely [2].

Four main types of protection principle are currently used in HVDC systems. Travelling wave protection and voltage derivative protection, which are based on the travelling wave concept, are usually used as primary protection. Furthermore, under voltage and differential protection are used as back up protection [58-60]. Some other protection schemes have also been introduced below.

3.4.1 Travelling wave principle

A fault on the transmission line will result in travelling waves on both current and voltage signals, and it will travel in both directions originating from the fault position. The Bewley Lattice diagram can clearly show the propagation of the wave (Fig. 3-9).

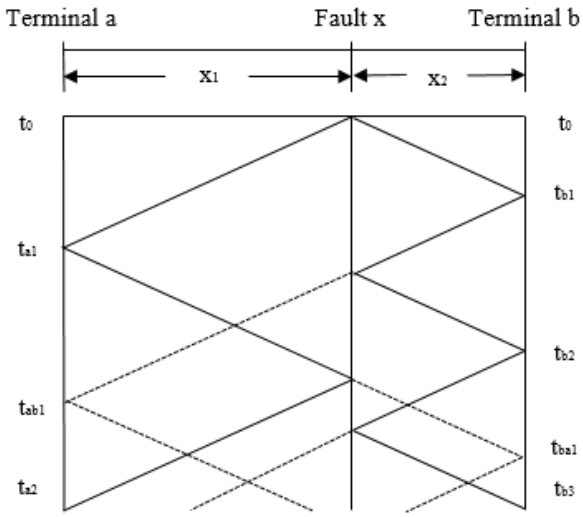

Fig. 3-9 Bewley Lattice diagram [60]

The frequency feature is thus caused by fast travelling wave along the transmission line. For a lossless line these reflections would continue indefinitely but due to losses this energy decays to steady state values after a few transits. The generation of travelling waves results from disturbances on a transmission line, which will bring high frequency oscillations. The travelling wave protection principles are briefly introduced in [6].

Travelling wave-based protection has been successfully applied in both AC and HVDC systems by virtue of development of fast A/D conversion and numeric relay technology [61, 62]. The traditional fault location methods for AC lines are mainly based on the fundamental frequency electrical variables, which cannot be used on DC lines. The current techniques for HVDC transmission lines are mainly based on travelling wave. Travelling wave protection is used for main DC lines. If the threshold is smaller than the difference in current and voltage by detecting the wave front, the protection will operate and determine whether there is sufficient amplitude [63].

However, there are still some problems with this method. First of all, the detection of the wavehead, which is the key point in this method, is not reliable. Secondly, the wave speed, which decides the accuracy of the fault location, depends on the parameters of the line. In addition, a very high sampling frequency has to be used.

Lastly, interference signals may adversely influence the measured fault location.

The most common method of travelling wave-based protection applied to multi-terminal systems, as introduced in [3, 64], is detecting the initial wavefront which has a demonstrably fast and accurate response. Due to its fast computational time and straightforward implementation, the discrete wavelet transform (DWT) is preferred for detecting arrival of wavefronts [65] over using pure frequency or time domain-based methods [66]. However, limitations exist with travelling wave protection [62, 67, 68], such as lack of mathematical tools to model the travelling wave, being easily influenced by noise, inability to detect close-up faults, and requiring knowledge of the surge impedance and a high sampling rate.

The authors in [69] attempt to apply Mathematical Morphology (MM) for analysing the HVDC system faults. Even though the AC line faults are difficult to judge by using travelling wave when the faults occur near the voltage crossing zero, there is no such problem in DC lines. A standard 12-pulse HVDC system in the MATLAB environment is used for analysis in this paper. The voltage magnitude of Reverse Voltage Travelling Wave (RVTW) is calculated based on the data recorded from the rectifier side. . The results show the figure of RVTW during various operating conditions of HVDC systems, including under normal operation and the DC line fault with different distances from the rectifier end. Then the results are analysed using the MM technique. With opening and closing operations on the dilated and eroding objects which are two basic operations in MM, the fault can be measured through the time between two peak values of the closing object and the velocity of the wave. In this paper, the authors claim the accuracy of this method could reach 98.56% [69].

Recently, the main protection strategies for the HVDC system in operation are using travelling wave protection. Even though travelling wave protection has the advantages such as working under higher operating speeds, there are also some specific requirements for the network, such as a high sampling rate. In order to meet the protection requirements under thunder storm conditions, the sensitivity of protection is reduced. Hence, the disadvantages for travelling wave protection are apparent. Travelling wave protection is easily influenced by thunder and

disturbances, as well as being unreliable to the fault with high impedance.

3.4.2 Voltage derivative protection

For so called voltage derivative protection, the initial fault detection is determined by also the derivative of the current. A threshold is set up to compare with the weighted sum of the derivatives. Advantages include speed, and that it could operate for bipolar DC line faults and all other disturbances. The disadvantages are that the derivation depends on fault loop impedance so that it is hard to detect the high impedance faults and faults close to the inverter.

A method which is based on estimating the transmission line impedance including the fault resistance and the total frequency dependant line impedance is introduced in [70]. After inputting the voltage and the current pulses to the system, the obtained impedance can be compared with the measured impedance until there is an acceptable error between them.

3.4.3 Current differential protection

Differential protection based on telecommunication infrastructure is used as backup protection. Communication among different converter stations is via dedicated communication networks, often using optical fibres [37]. The use of telecommunications may bring some risks; therefore, this method is usually used as backup protection.

3.4.4 Under voltage protection

Under voltage protection is used as a backup for voltage derivative or travelling wave protection. Multiple levels of protection will provide adequate backup protection for HVDC lines. The main protection for DC lines should be based on local detection instead of using telecommunication which is dependent on external factors.

3.4.5 Transient-based protection

Boundary protection is a transient-based protection concept which has been proposed in [68]. In a DC system, smoothing reactors and the capacitors installed at both ends of the DC transmission line and the inherent bus bar capacitance represents a natural boundary that does not transmit high frequency signals and thus can be used to rapidly distinguish between internal and external faults [62]. Another transient harmonic current protection method based on the boundary characteristic is introduced in [71]. However, this kind of transient-based protection may mal-operate because of non-fault transients caused by lightning.

3.4.6 Other

The hybrid protection presented in [62] can distinguish both non-fault lightning transients and detect close-up faults, which may be missed by travelling wave methods. However, high sampling frequencies are required, which demand more expensive hardware for sampling and calculation. A method has been proposed in [67] to analyse the relationship between parameters of the DC transmission line and the variation of transient energy obtained from the voltage and current measurements at both terminals, although the technique is not validated with a frequency dependent line model. The authors in [71] present a method utilising transient harmonic current based on the boundary characteristic of DC transmission lines. However, it takes a maximum of 30 ms to identify the faults, which is not quick enough for protection purposes. In addition, the sensitivity of the method will decrease with increasing fault resistance. A differential protection technique for MTDC transmission lines has been proposed in [72], which depends on analysis of the high frequency transients in current signals at each end of the line. As with any differential scheme, this relies on communication between both terminals representing a single point of failure and introducing inherent latency.

The shortcoming of travelling waves, voltage derivative and under voltage protection is that they cannot detect grounding faults with large transition resistance. The detection in differential protection is slow. Hence, some new methods are being developed [59].

Due to the shortcomings, whereby the derivation in voltage and current will be influenced by fault loop impedance in a voltage derivative protection method, a development is introduced in [60]. The fault distance is calculated according to the time difference which relates to the maximum value of cross-correlation function (CCF) and CCF could be determined by the forward and backward travelling wave calculated from the fault injected voltage and current. In addition, the pole mode wave is used for fault location and the ground mode wave is used to identify the faulted pole. In this paper, telecommunication infrastructure was also used to enhance the system by detecting the fault location in a simpler way. In this system both close-up faults and distant faults could be detected in an optimal response time.

3.5 Multi-terminal HVDC protection

The aim of a protection scheme for multi-terminal HVDC systems is to cut the faulted line whilst keeping the remaining converters operational. Not only does this require DC breakers, but also a DC protection relay that will discern when to operate the breakers. DC protection relaying require special consideration over conventional AC methods.

Although HVDC technology has been advanced considerably in recent years, there are still some limitations in multi-terminal systems. More specifically, protection systems still remain problematic in HVDC technology. The existing strategy is to operate the switchgear on the AC side so that the entire DC system will be de-energised. If simply using the original methodology in a MTDC system, the whole network will thus be taken out of service. Moreover, if a fault occurs in the AC transmission system, the DC-Bus voltage will be affected on both ends of the line. Hence, the line may appear faulted as a result of the AC fault. Applications of a protection scheme for MTDC transmission systems have been studied, and the examples can be found in much of the literature.

Conventional CSC-based HVDC systems are currently regulated by connecting a large smoothing reactance in series so that they are robust enough to deal with DC faults. Owing to the DC inductors, CSC HVDC has better ability to withstand short circuit current. Hence, voltage deviation is the key factor in protection strategies

which rely on fault location and travelling wave detection. However, these methods are not applicable in VSC-based HVDC. Due to the ability of VSC-based HVDC to control reactive and active power, it has robustness to withstand AC side disturbances. Nonetheless, it is unable to withstand the DC side fault which is more serious to the network. Therefore, a more appropriate design should be researched for multi-terminal VSC-HVDC [5, 33, 40, 42].

In multi-terminal HVDC systems, different protective strategies are considered based on different factors. The line protection (Fig. 3-10 (a)) with fast breakers at every end of the line gives selective protection to each element. There is no communication between relays and this strategy has the least impact on the grid. A converter station will ride through faults. Line and converter protection (Fig. 3-10 (b)) will have an impact on local converter stations with slower relaying. Open grid protection (Fig. 3-10 (c)) operates all beakers at a bus with fast fault detection and slower fault identification. The protection zones encompass more than one line in grid splitting protection (Fig. 3-10 (d)), which will quickly isolate the faulted zone. Low speed grid protection (Fig. 3-10 (e)) is generally applied in two-terminal HVDC links to block the system.

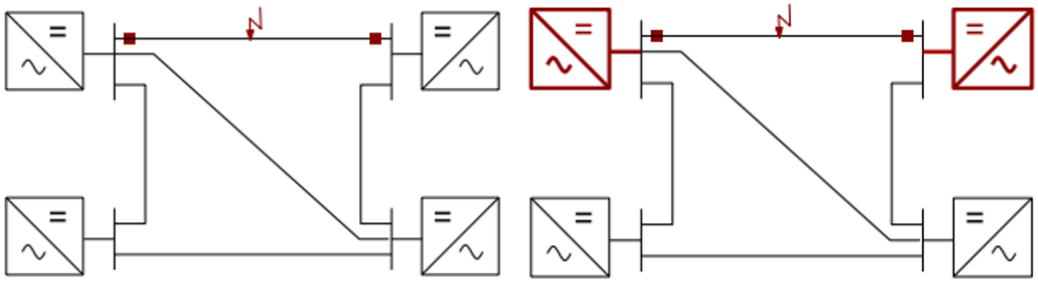

(a) Line protection (b) Line and converter protection

Fig. 3-10 Protection scheme for MTDC systems

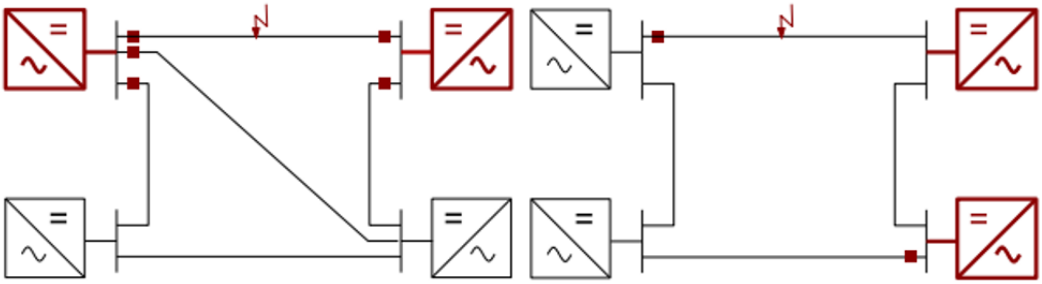

(c) Open grid protection (d) Grid splitting protection

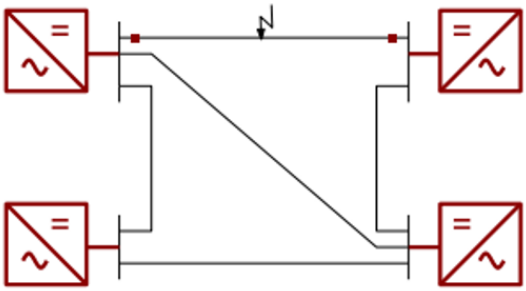

(e) Low speed grid protection

Fig. 3-10 Protection scheme for MTDC systems

For economic reasons, AC counterparts can be used for DC grid protection, which has mature technology and a shorter lead time. AC side breakers can be coordinated to cope with the fault occurring on the DC side in the most economical way. Even so, they cannot satisfy the speed requirement of tripping [33, 40, 42].

The rebalance of the capacitors is the key point of fault recovery, for which [43] gives a detailed solution. Firstly, using high impedance in the grounding system will cause a small discharging current, so that the voltage of the capacitor can be maintained without overcurrent stress. Secondly, the secondary winding of the transformer could change to a Y_n type, so the capacitor could be rebalanced automatically. In addition, using a monopole scheme is better for overhead lines compared with a bipolar system. Lastly, installing equalisation resistors will take a long time to rebalance the voltage. At the end of this paper, the authors give the design philosophy for fast DC breakers.

There are still some other protection methods used in MTDC. [40, 42] have

represented the reverse diode protection method for small scale systems. Here, a reverse diode is installed between the DC overhead line and DC chopper to restrain fault current. This method may be effective for small scale applications, but not practical for large projects.

In addition, the large current charge method compares the current magnitude; the rise time method measures the rise time of the wavehead of the current, and the oscillation pattern method detects the wide pulse without polarity change. These are all the methods used for detecting a faulted line.

A real time closed loop simulation model, which is a ±500 kV, 5000 MW bipolar four-terminal HVDC system, is developed in [73]. Travelling wave protection and derivation protection can be installed in all terminals when used in multi-terminal systems in a similar manner with two-terminal HVDC networks. In order to operate the remaining network when a fault occurs, rectifiers will reduce the current to zero in synchronisation. Meanwhile, the new configuration of a network will be taken into consideration by the master control [73].

A backup protection also should be set up in case of the failure of primary protection. Remote backup protection schemes are the main back up introduced in [53]. The buck converter relay is used as the backup relay for an inverter, the rectifier relay for a buck converter and the fuse relay for a rectifier relay. Also, the overcurrent protection can be used as backup protection. Due to the limited fault current from inverters, traditional overcurrent protection cannot be used for MTDC protections.

In the protection of multi-terminal systems, current and voltage measurement, which are used to detect faults, are more important. In order to provide usable and reliable data for the control and protection system, a measuring system should be installed in the converter station. Then fault location should be identified so that the correct breakers will trigger on both sides of the faulted line. Moreover, the fault current must be detected quickly since VSC is sensitive, and the voltage withstand rating of the converter is about twice the full load rating [33, 53]. The data by a converter station should be collected by redundant systems.

For the purposes of accurate detection, three criteria are used including using voltage wavelet coefficients, current wavelet coefficients, and voltage derivatives. Among these three criteria, if two of them demonstrate the occurrence of the fault, then the breakers will work. In this way, this method overcomes the shortcomings of each of the three criteria facing different situations and the chance of mal operation will be reduced [74]. Furthermore, using “two out of three” can improve the accuracy of judgment when there is the possibility of faults occurring near or far from the bus.

3.6 Chapter summary

An overview of the current protection schemes for HVDC and MTDC networks are discussed in this chapter. Lots of protection schemes such as travelling wave principle, voltage deviation method, and transient-based protection are generally applied as the main protection scheme. Current differential protection and under voltage protection are used as backup protection. Also, some new methods have been studied as well. These technologies are mature methods not only for HVDC systems, but also some of them can be applied in multi-terminal HVDC networks. As all existing protection schemes shown may have some drawbacks, this thesis investigates a novel protection scheme for both two-terminal HVDC systems and multi-terminal HVDC systems.

4 Case Study Model Development and Implementation in PSCAD

4.1 Introduction

This section gives a detailed introduction to the modelling of a two-terminal HVDC system and a three terminal HVDC system which are chosen in the case study. PSCAD software is widely used in power system modelling and is good for transient analysis. Hence, PSCAD is used in this thesis to simulate the two HVDC systems. The PSCAD HVDC system model will serve as the basis for developing the novel protection scheme based on the ANN method which applies the fault current transients. The protection scheme developed herein is based on the analysis of fault current signals.

This section elaborates the software used to model the network and the DC fault behaviour including the steady-state and transient fault phenomena. PSCAD is introduced in the first part, followed by a description of the specific two-terminal HVDC and the multi-terminal HVDC model used for the case study. Different fault types under different conditions (e.g. fault locations, fault resistance, etc.) are conducted. The analysis is based on both an HVDC system and an MTDC system, including the converters without fault blocking capability and surge arresters. The resultant fault current signals are typified and discussed.

4.2 PSCAD/EMTDC introduction

PSCAD/EMTDC is widely used software in electric power systems for electromagnetic transient simulation, which has the function of simulating complicated power systems and providing a powerful element model library as well as an ergonomic user graphical interface. PSCAD (power systems computer aided design) is a pre-processing program for the EMTDC (electro-magnetic transients including DC). The main function of EMTDC/PSCAD is to calculate and simulate

the time domain and frequency domain in power systems. A typical application is to simulate how electric parameters change over time in response to simulated disturbances or changes in network topology. Over the years, with the improvement of the EMTDC element model base and the function, PSCAD can not only study an AC/DC power system, but can be a versatile tool for finishing power electronic simulation and non-linear control. The software can also be used as the Front End for a real time digital simulator (RTDS). Hence, PSCAD/EMTDC simulation analysis software will provide a superior HVDC system model for system fault analysis

4.3 Two-terminal HVDC

4.3.1 Components

A two-terminal VSC-HVDC system is modelled using PSCAD as a platform. The system has been calculated with an equivalent circuit and been tested under steady-state conditions. The model based on the example in PSCAD is selected as the test network. This VSC-HVDC system is a symmetrical monopole system, which consists of a synchronous machine, DC submarine cable, transformers, 6-pulse converters (Rectifier or Inverter), and equivalent 3 phase AC voltage sources represent the AC connections.

Based on the design in the examples, several changes have been made to meet the requirements of this project. The final model is a ground return monopole network with overhead lines. The converter stations use IGBTs instead of GTOs. In addition, the synchronous machine has been replaced by a voltage source behind an equivalent resistance. Detailed modelling for this system is introduced as follows.

Power source

In order to design the connection at the end to be a network with enough short circuit capacity, a voltage source is modelled in sufficient approximation condition in this VSC network. A fixed voltage can be maintained independently no matter how much current is flowing into the network or how much resistance is installed

in this model. In this network, voltage sources are modelled as a synchronous generator and the load.

Converter transformer

Combined with the converter station, the converter transformer plays a key role in an HVDC system. The converter transformer is the power transformer between the converter station valve bridge and the AC system. It realises the connection between the Valve Bridge and the AC busbar and provides a three phase commutation voltage with ungrounded neutrals to the Converter Bridge. Hence, a three phase two winding transformer is built.

Voltage source converter

Compared with a conventional CSC-HVDC system, a VSC-HVDC, using VSC and PWM technology, makes use of IGBT/GTO to complete on-off operations. Using a comparison between a carrier wave and triangular wave, a trigger pulse will be generated respectively for controlling electronic devices. The use of a voltage source converter HVDC for submarine or onshore power transmission is well known to increase the capacity and decrease power losses during transmission. The basic structure of a VSC is made up of 6-pulse converter devices. The designed voltage source converter with a 6-pulse two-level Bridge using IGBT is listed in Fig. 4-1.

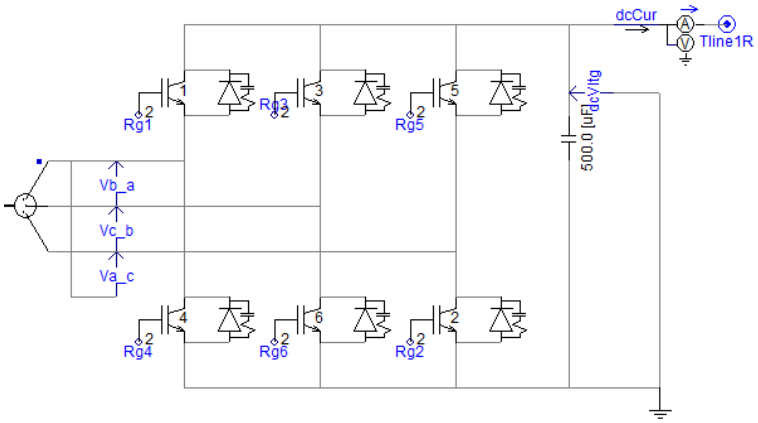

Fig. 4-1 The configuration of a voltage source converter

In this control system, at the rectifier side, the AC voltage is controlled by magnitude control and DC power is controlled by phase shift control with PWM. Meanwhile, on the other side, the AC voltage is controlled by magnitude control independently, and the DC voltage is controlled by phase shift control [75]. Also, there is no need for any existing short circuit capacity in the end AC network at the inverter side.

In contrast to line commutated, so-called current source converter HVDC systems, VSC-HVDC systems function as an ideal DC voltage source so the DC voltage polarity can remain unchanged when the power flow is reversed for a single VSC converter station. These capabilities make the VSC-HVDC suitable for constructing multi-terminal HVDC systems. In the simplest converter architecture, the AC voltage waveform is synthesised using a two-level approach. The converter can be modelled as a controllable voltage source which connects to an AC network through a series reactor at the point of common coupling (PCC) [17, 76]. The basic configuration for a converter station containing the main components as well as the configuration of VSC converters of three-phase, two-level, and six-pulse bridges is presented in Fig. 4-2.

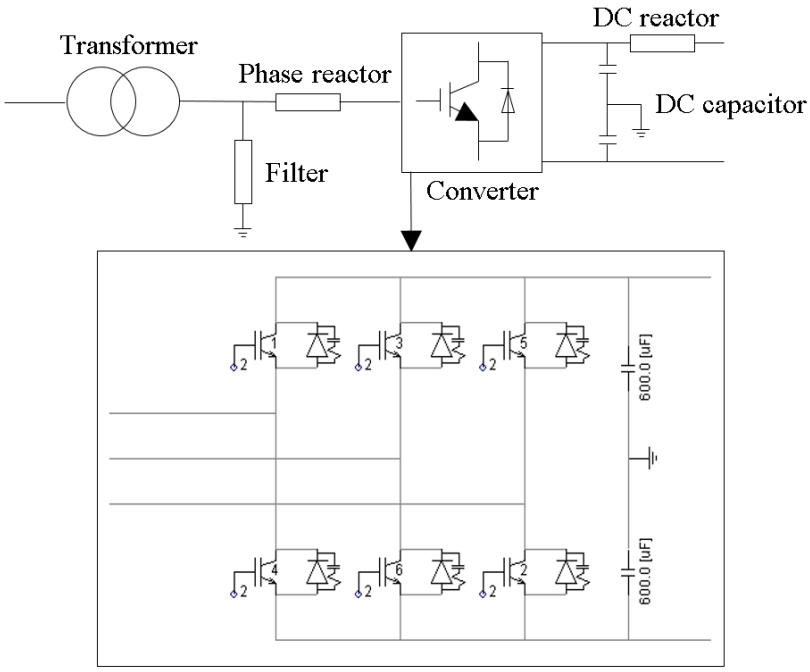

Fig. 4-2 Configuration of a VSC converter station in PSCAD

Although more modern multi-level converter architectures exist, the system here is the well-proven two level converter chosen for its simplicity. On the AC side, phase reactors are applied between transformers and converters to limit both the active and the reactive power flow by regulating currents through them. The phase reactors also function as AC filters to reduce the AC current harmonic content caused by pulse width modulated switching of the converter station. In the well-established two-level converter stations, a low-pass LC-filter is included on the AC side which will suppress high frequency harmonic components. Capacitors on the DC side provide energy storage reducing the DC voltage ripple [77]. In addition, DC reactors are connected after DC capacitors to reduce the rate of rise of DC fault current and reduce harmonic currents.

Transmission line model

Since the transmission line is, in reality, made up of distributed parameters that are frequency dependent, this scheme has been developed with a line model which accurately captures the high frequency transient response. The branches are exclusively overhead lines, where each line is 200 km long with the geometric conductor layout illustrated in Fig. 4-3. Each line is a symmetrically grounded monopole.

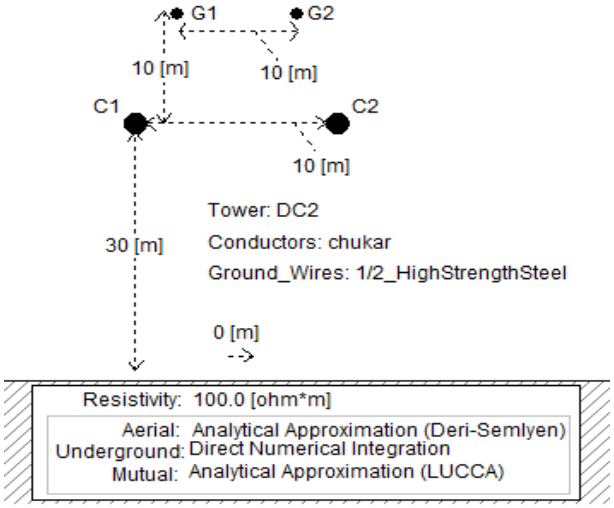

Fig. 4-3 The configuration of the overhead transmission line model

For analysis of steady-state conditions, the transmission line can be modelled using

lumped parameters; however, distributed parameters should be used to accurately reflect transient behaviour [78]. The transmission line or cable can be represented by series impedances and shunt admittances per unit length. The series impedance is inherently frequency dependant due to its imaginary reactance and also due to the skin effect in the conductor and earth wires. Based on these parameters, the characteristic parameters of the line, the surge impedance and propagation constant can be derived, which determine the propagation behaviour of travelling waves on the line [79].

The lumped parameter model is not very accurate compared with distributed parameters, which are more suitable for transient analysis. The line model is, therefore, considered a frequency dependent model which can be seen in Fig. 4-4 [80, 81].

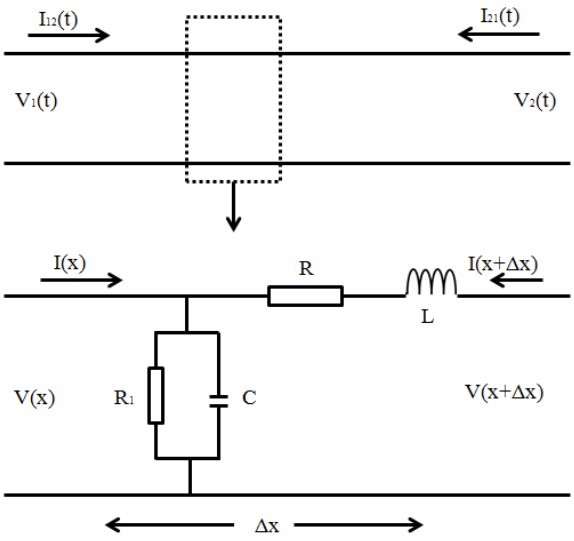

Fig. 4-4 Single-phase distributed parameter line model [81]

It can be noticed that the line is divided into different segments. Each segment can be described by impedance z for series parameters and admittance y for shunt elements as follows (4.1) [81].

$$\begin{cases} z = R + j\omega L \\ y = \frac{1}{R_1} + j\omega C \end{cases} \tag{4.1}$$

The model can be treated as the conventional single-phase distributed parameter line model, and the solutions for voltage and current are shown in:

$$\begin{cases} V_1 = \left(\frac{V_2 - I_{21}Z_c}{2}\right)e^{\gamma l} + \left(\frac{V_2 - I_{21}Z_c}{2}\right)e^{-\gamma l} \\ I_{12} = \frac{V_1}{Z_c} - \frac{V_2}{Z_c}e^{-\gamma l} - I_{21}e^{-\gamma l} \\ I_{21} = \frac{V_2}{Z_c} - \frac{V_1}{Z_c}e^{-\gamma l} - I_{12}e^{-\gamma l} \end{cases} \tag{4.2}$$

where:

$$\begin{cases} \gamma = \sqrt{zy} = \sqrt{(R + j\omega L)\left(\frac{1}{R_1} + j\omega C\right)} \\ Z_c = \sqrt{\frac{z}{y}} = \sqrt{\frac{R + j\omega L}{\frac{1}{R_1} + j\omega C}} \end{cases} \tag{4.3}$$

where: γ is the propagation constant and $Z_c$is the characteristic impedance of the transmission line.

The calculation of line impedance is calculated as:

$$R = \frac{\rho}{l}S \tag{4.4}$$

where: ρ is the resistivity of transmission conductor.

The overhead line was chosen to be a single conductor line. A high voltage tower configuration is represented in Fig. 4-5.

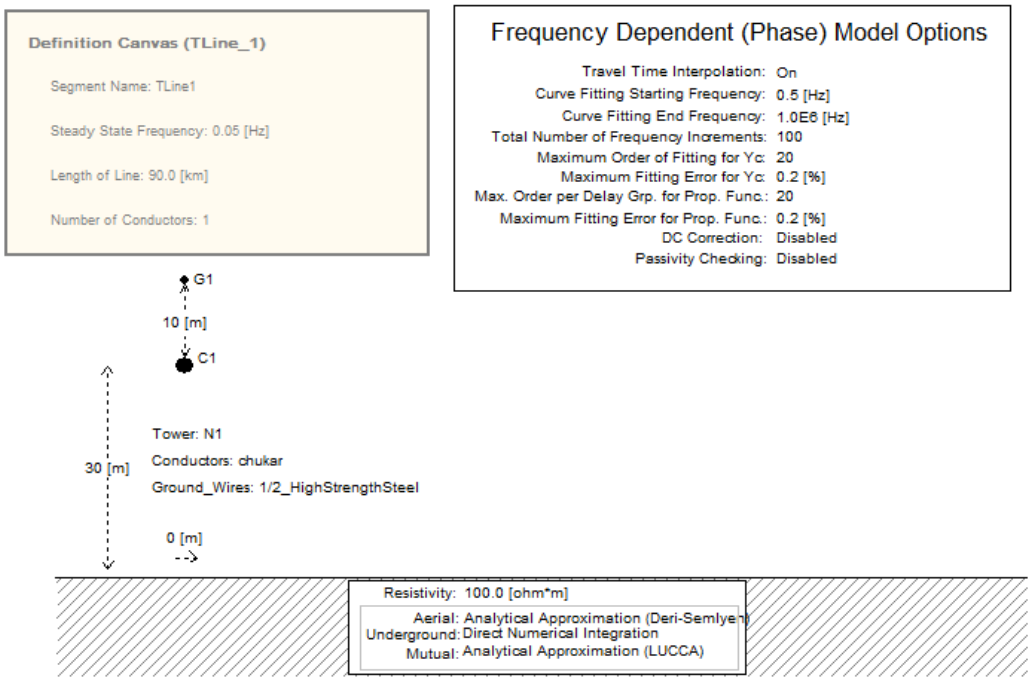

Fig. 4-5 The high voltage tower configuration

4.3.2 Control for two-terminal HVDC links

One or more of the converters connected to the common DC-Bus are generally used to regulate the active power which is to maintain the DC voltage. Hence, the converters at both ends of the line are controlled to work together. Two modes of control are applied independently at each side of the converter.

The AC side voltage is controlled in the sending end converter to achieve power flow. Reactive power generated by the sending end converter is held at a low value by adjusting the magnitude of the voltage on the AC side of the sending end converter. The DC voltage is controlled by adjusting the phase angle of the AC side voltage of the receiving end converter.

4.3.3 Implementation in PSCAD

The implementation is completed based on the above theoretical treatment. The final model can be seen in Fig. 4-6, and the details of the system data are shown in Table 4-1.

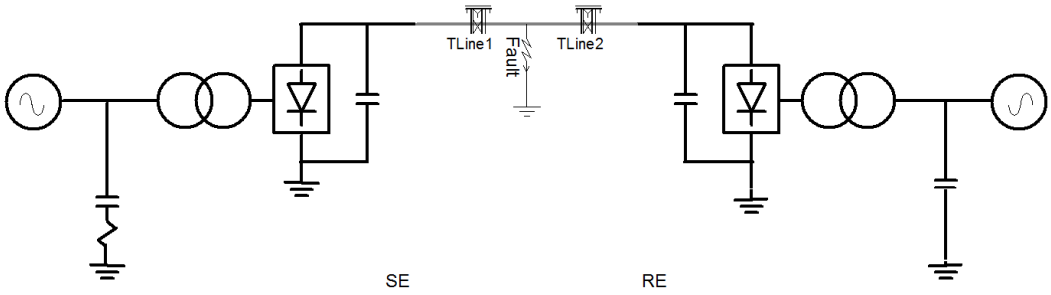

(a) Final VSC-HVDC model

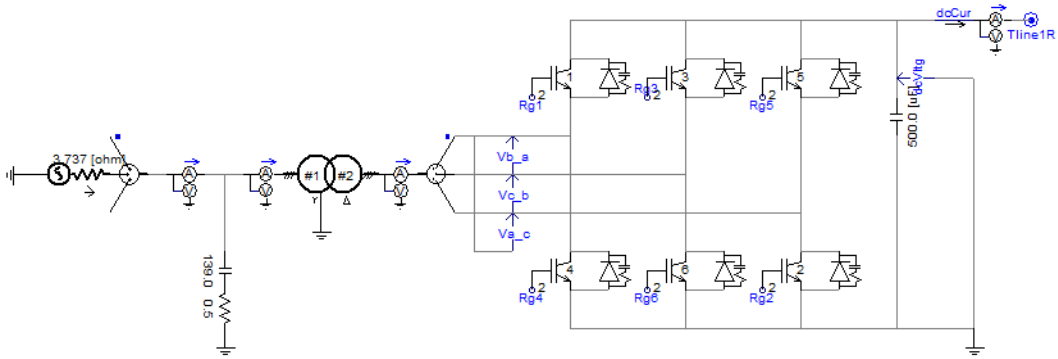

(b) Rectifier side single line diagram

Fig. 4-6 Final model of VSC-HVDC model in PSCAD

Table 4-1 System parameters

System data	Base MVA		100 MVA
	Nominal AC voltage	Rectifier	13.8kV
		Inverter	115 kV
	Nominal DC voltage		110 kV
	System frequency		60 Hz
	Line length		500 km

The basic data from the model are illustrated as follow:

The capacity in voltage source S1 and S2 are both 100 MVA with 60 Hz frequency,

and the resistance of these two voltage sources is $x_d = 3.73\ ohms$. Transformers T1 and T2 also work with 100 MVA. The winding voltage on the rectifier side is 13.8/62.5 kV and the winding voltage on the inverter side is 62.5/130 kV. The DC resistance for the transmission line is 0.03206 ohms/km. The total length of the line is 100 km, and the outer radius of the conductor is 0.0203454 m.

Assuming that the DC voltage utilisation ratio of the PWM technology adopted is 1, the modulation index is between 0 and 1 ($0 \leq M \leq 1$). After testing the modulation index for the two converter station are both 0.85.

4.3.4 Steady-state condition

In steady-state condition, calculation formulas mainly show the relationship of voltage, current, active power, reactive power and angle between the AC side and the DC side of the converter station. Since the system used in this report is a monopole system, the formulas are generally used in a monopole network. The equivalent circuit is created in Fig. 4-7.

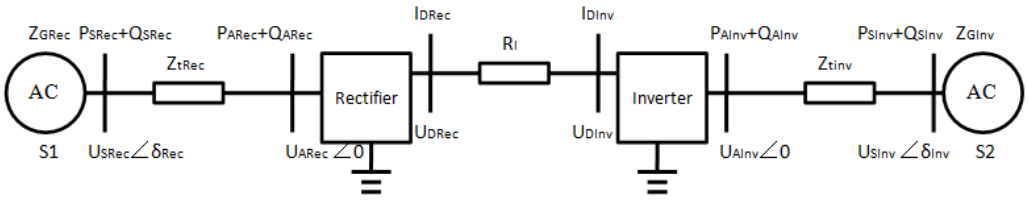

Fig. 4-7 The equivalent circuit of the VSC-HVDC model [82]

In accordance with the equivalent circuit above, the following equation can be obtained where the DC current on the two sides of the converter station have the same value (4.5) [82]:

$$I_{DRec} = I_{DInv} = I_D \tag{4.5}$$

The power injected to the DC side from the rectifier (4.6):

$$P_{ARec} = P_{DRec} = I_{DRec} \times U_{DRec} \tag{4.6}$$

The basic relationship can be obtained from the circuit (4.7):

$$\begin{cases} U_{ARec} = M_{Rec}U_{DRec}/2 \\ U_{SRec}^2 = (U_{ARec} + \Delta U_{Rec})^2 + (\delta U_{DRec})^2 \\ \Delta U_{Rec} = \frac{P_{ARec}R_{Rec}+Q_{ARec}X_{Rec}}{U_{ARec}} \end{cases} \tag{4.7}$$

Hence, the active power and reactive power can be calculated from 4.8 and 4.9:

$$P_{SRec} = P_{ARec} + \frac{(P_{ARec}^2+Q_{ARec}^2)R_{Rec}}{U_{ARec}^2} \tag{4.8}$$

$$Q_{SRec} = Q_{ARec} + \frac{(P_{ARec}^2+Q_{ARec}^2)X_{Rec}}{U_{ARec}^2} \tag{4.9}$$

Also, some factors can be obtained in 4.10 and 4.11 to give the reactive power injected into the converter station on the rectifier side in 4.12:

$$\delta U_{Rec} = \frac{P_{ARec}X_{Rec}-Q_{ARec}R_{Rec}}{U_{ARec}} \tag{4.10}$$

$$\delta_{Rec} = -\tan^{-1}\frac{P_{ARec}R_{Rec}-Q_{ARec}X_{Rec}}{U_{SRec}^2+P_{ARec}R_{Rec}+Q_{ARec}X_{Rec}} \tag{4.11}$$

$$Q_{ARec} = Q_{DRec} - \frac{U_{SRec}^2X_{Rec}}{X_{Rec}^2+R_{Rec}^2} + \frac{\sqrt{U_{ARec}^4X_{Rec}^2-(R_{Rec}^2+X_{Rec}^2)\left[(U_{ARec}^2+P_{ARec}R_{Rec})^2+P_{ARec}^2X_{Rec}^2-U_{Rec}^2U_{Rec}^2\right]}}{X_{Rec}^2+R_{Rec}^2} \tag{4.12}$$

The same procedure may be easily adapted to obtain the active power and reactive power for any other state parameters.

Some other parameters can also be obtained. DC line voltage drop ΔU_D (4.13):

$$\Delta U_D = U_{DRec} - U_{DInv} = RI_D \tag{4.13}$$

Power loss of DC line ΔP_D (4.14):

$$\Delta P_D = P_{DRec} - P_{DInv} = RI_D^2 \tag{4.14}$$

In steady-state power flow calculation, the ideal situation is considered to be when the internal losses of converters are neglected, and the value of converting reactance is around 0.1 to 0.2 p.u. with the rated capacity of the converter as a base. The results of the steady-state condition are shown in Fig. 4-8.

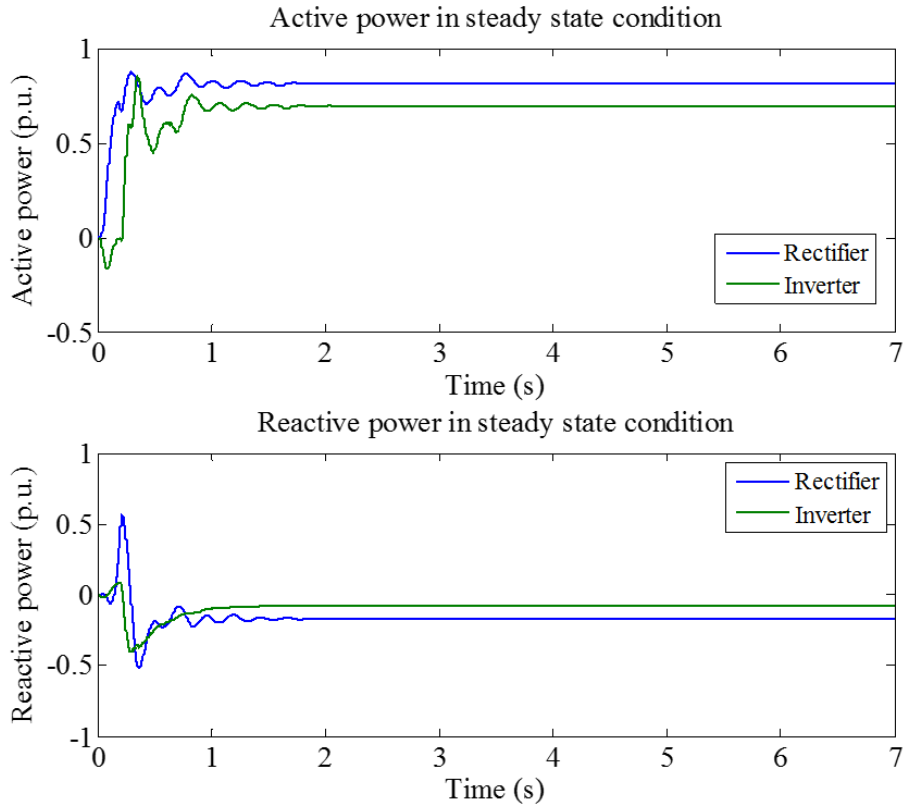

(a) The reactive power and active power generated from the voltage source

Fig. 4-8 Measurement in steady-state condition

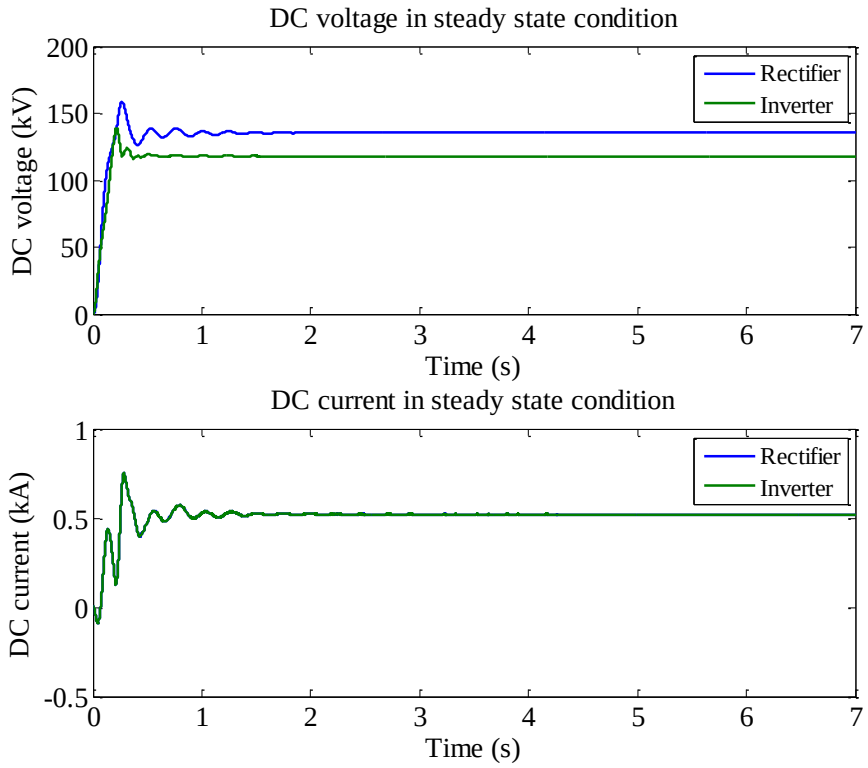

(b) DC voltage and DC current on the transmission line

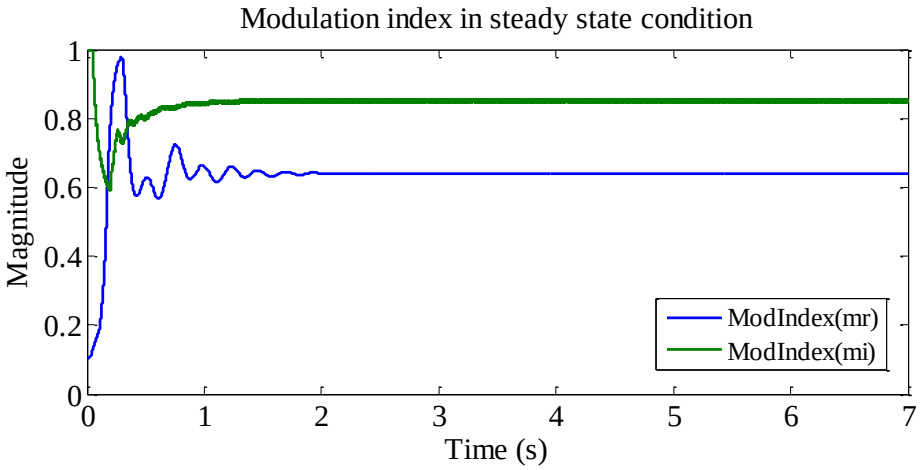

(c) Modulation index

Fig. 4-8 Measurement in steady-state condition

Comparing the calculated values based on (4.5-4.14) with the simulated values in a steady-state condition, the difference between these two values was found to be within 10%. Hence, this model is accurate enough to accomplish the following analysis. The terminal voltage will fluctuate within ±5%. Voltage drop will be no

more than 10%. The result is listed in Table 4-2 in which base MVA is 100 MVA and base voltage is 13.8 kV. The angle in this table is measured in degrees.

Table 4-2 The measurement of the system

Rectifier side			Inverter side		
Value between voltage source and transformer	P	0.727 p.u.	Value between voltage source and transformer	P	0.655 p.u.
	Q	-0.205 p.u.		Q	-0.093 p.u.
	Urms	1 p.u.		U	0.997 p.u.
	A	28.85°		A	7.6°
Value between transformer and converter station	P	0.687 p.u.	Value between transformer and converter station	P	0.69 p.u.
	Q	-0.166 p.u.		Q	-0.138 p.u.
	Urms	4.49 p.u.		U	4.43 p.u.
	A	54.46°		A	-18.57°
Value on DC side	P	0.695p.u.	Value on DC side	P	0.679p.u.
	Urms	8.709p.u.		Urms	8.551p.u.

4.3.5 Fault profile analysis

Based on the model built above, a short circuit fault is implemented in this two-terminal VSC-HVDC network. Fault current generally will be affected by fault types, fault location on the transmission line, ground impedance, short circuit capacity and other factors like converter stations. In addition, some faults are caused by the disconnection of the DC transmission line. The fault analysis mainly focuses on two factors. One is the variation of fault location, and the other is the varying of ground resistance. Through short circuit fault current analysis and high frequency

component analysis, the characteristic of faults occurring on the DC transmission line can be detected.

Fault analysis on transmission lines is mainly based on the measurement of voltage and current with the features generated by the fault, which can generally be divided into time domain analysis and frequency domain analysis.

Considering that a monopole network is applied in this project, only pole-to-ground faults will occur on the DC transmission line which can generally be cleared by the converter station. A single phase short circuit fault is inserted into this model without breakers installed. The fault occurs at t=2 s, lasting 0.5 s. By considering different situations based on different fault locations and different ground resistances, the analysis of the transient component is derived. The granularity of variation is selected to cover all the ranges of faults. For varying locations, with 0.01 Ω ground resistance, the ranges are set to be 10%, 30%, 50%, 70% and 90% on the transmission line to the rectifier. The variation for resistance with the fault on 50% of the line is selected to be 0.01 Ω, 2 Ω, 10 Ω, 50 Ω and 100 Ω.

Time domain response

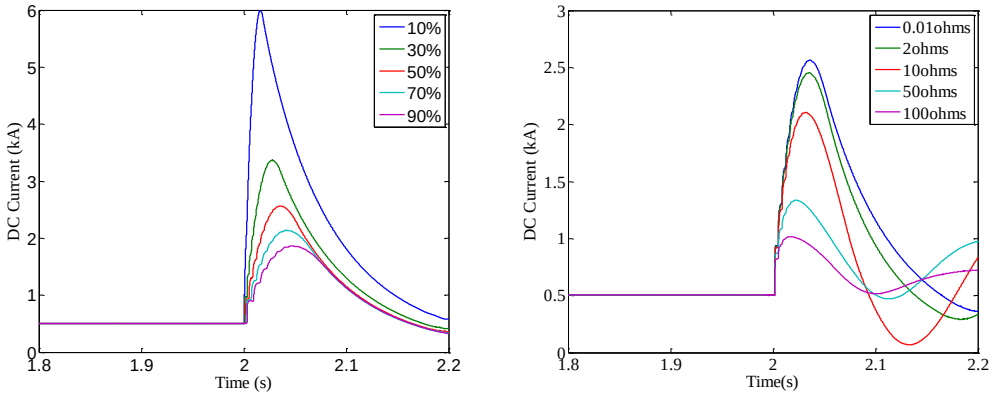

(a) 0.01 Ω fault resistance with varying location *(b) 50% fault location with varying resistance*

Fig. 4-9 Fault current detected from terminal 1

In response to the fault on the transmission line with 0.01 Ω fault resistance at varying locations, the time domain fault current waveform detected on the rectifier side is shown in Fig. 4-9 (a). The fault current waveform detected on faults

occurring at 50% away from the rectifier side with varying ground resistances is shown in Fig. 4-9 (b). The figures shown below are both from 1.8 s to 2.2 s selected from the whole simulation output. Faults are applied at 2 s as indicated.

In response to the fault, the DC current, through the rectifier end of the line, will spike whatever the fault location and fault resistance is. The simulation controls will respond to the higher current, hence, the short circuit fault current will then return to the original current level after reaching the highest value. However, in a real system such high currents because would be interrupted by circuit breakers. Therefore whilst it is unlikely whether the system could sustain these currents without damage before the controls can mitigate them, this is not a realistic scenario to consider. As can be seen in Fig. 4-9 (a), the fault current measured at the rectifier side is reduced while the distance between the fault point and the measuring point increases. The fault current also decreases as the fault resistance increases as shown in Fig. 4-9 (b). The fault current is attenuated due to the response of the converter station control system in the simulation but in practice the fault current would be interrupted by circuit breakers or damage would occur. The measured current $i(t)$ detected from the rectifier side and inverter side is the main source for frequency analysis and is used to find the specified frequency as given by (4.15):

$$i(t) = a\cos\omega_0 t + b\sin\omega_0 t \tag{4.15}$$

where: $i(t)$ is current signal, a and b are constants, ω_0 is the fundamental frequency and $t \in [t_f, t_f + t_w]$ is time, t_f is fault inception time, t_w is the window length.

Frequency domain response

Fault current is generally affected by fault types, fault location on the transmission line, ground impedance, short circuit capacity and other factors like converter stations. In addition, some faults are caused by the disconnection of a DC transmission line. During a fault, the transient signal contains many characteristic frequencies. The reason why a high frequency component is considered to be the most significant factor in this paper is that the frequency components are more

likely to be influenced by fault location rather than other factors like fault resistance. In an HVDC system, the transmission line protection zone is the area between two DC smoothing capacitors at the end of the line, which filter the characteristic harmonics from the AC side. The frequency component is reduced by these DC smoothing capacitors. As a consequence, DC smoothing capacitors can be regarded as the boundary of the transmission of frequency components.

High impedance faults are generally challenging for many protection strategies because of the attenuation of the post-fault characteristics and thus its resemblance to steady-state pre-fault conditions. However, in this paper, the Fast Fourier Transform is used to obtain a frequency spectrum which contains a distinctive feature in the fault current waveform, even in the case of high impedance faults. Analysis of these transient signals using the Fast Fourier Transform is an effective way to analyse the features generated by the fault. The basic form of the FFT is given by (4.16):

$$S(k) = \sum_{j=0}^{N-1} exp\left(-\frac{2\pi k j^2}{N}\right) s(jT_s) \tag{4.16}$$

where: $S(k)$ is defined as the frequencies between the DC component and the sampling frequency, f_s, $s(jT_s) = \mathrm{s}[j]$ is the signal sample sequence, $T_s = 1/f_s$ is the sampling time, k and j are both the index, N is the total number of samples.

The analysis of Fast Fourier Transform is based on the data detected within 6 ms beginning at the fault inception times of 2 s in the simulation. The specified frequencies can be easily obtained as shown in Fig. 4-10 (a)-(e) which indicate the fault location from 10% to 90% varying with fault resistance. Fig. 4-10 (f) shows the line varying with fault location under 0.01 Ω fault resistance.

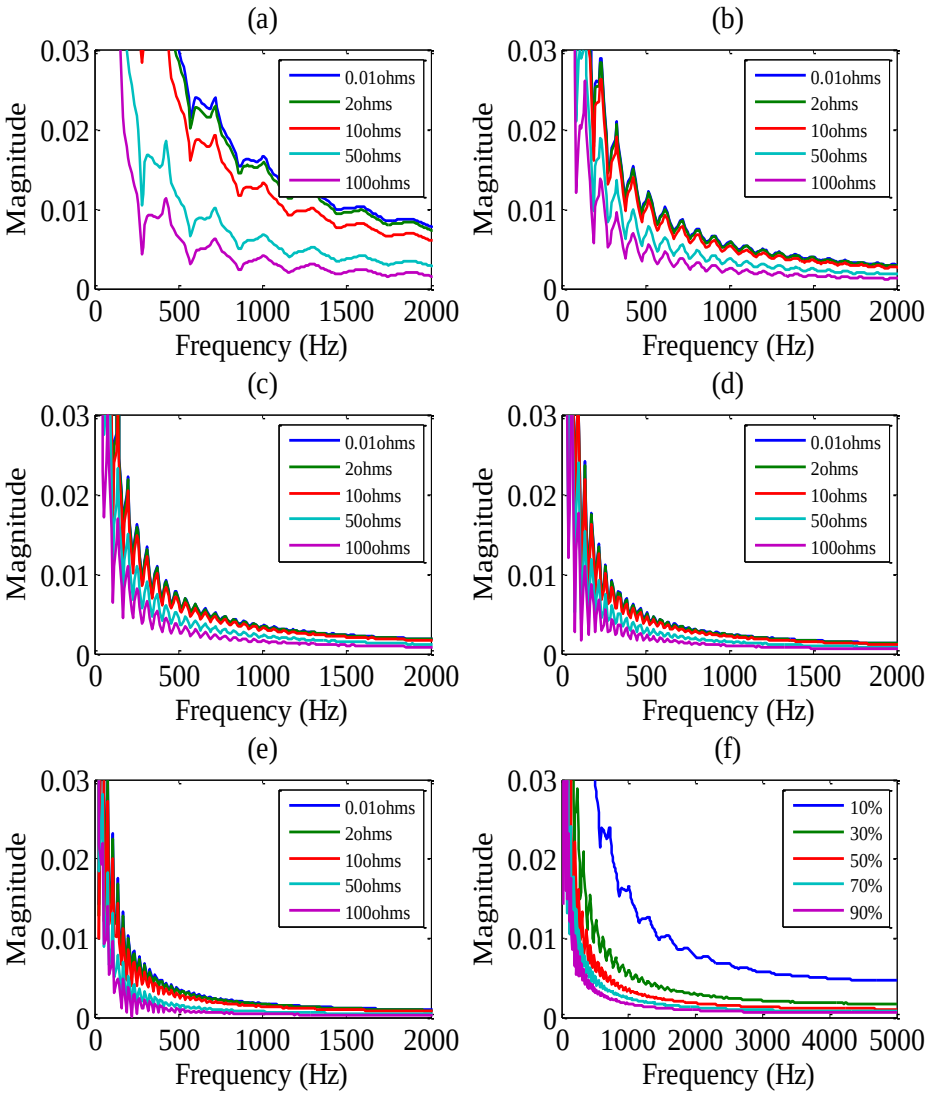

Fig. 4-10 Frequency spectra of the fault current for different fault locations from the rectifier, varying from 10% (a) to 90% (e) and frequency spectra in 0.01 Ω fault resistance (f)

It can be seen that the shapes of the frequency spectrum obtained from the current signal are similar for each specific fault location, regardless of fault resistance. The frequencies with peak values contain higher energy compared with other frequencies; the frequencies with peak values are shown in Table 4-3. This means that the peaks appear in the fixed frequency band for a specific fault location, i.e. two contiguous peak frequencies have a specified gap with a fixed value during the fault occurring at a given location. The closer fault location is to the rectifier side, the larger the gap between two frequencies with peak values. The frequencies spike

at a group of specified frequencies no matter where the fault location is (i.e., 140 Hz, 430 Hz, 720 Hz, 1010 Hz, etc.). Regardless of the magnitude difference caused by fault resistance, the strong dependence on fault location and peak frequency features are apparent.

Table 4-3 Frequency spectrum peak value analysis

Fault Location	Frequency Peak Value (Hz)
10% from T1	140, 430, 720, 1010, 1300, 1590, 1880, etc.
30% from T1	140, 240, 330, 430, 520, 620, 720, 810, 910, 1010, 1100, 1200, 1300, 1400, 1490, 1590, 1690, 1790, 1880, etc.
50% from T1	80, 140, 200, 250, 310, 370, 430, 480, 540, 600, 660, 720, 770, 830, 890, 950, 1010, 1070, 1120, 1180, 1240, 1300, 1360, 1420, 1480, 1530, 1590, 1650, 1710, 1770, 1830, 1880, etc.
70% from T1	60, 100, 140, 180, 220, 260, 300, 340, 390, 430, 470, 510, 550, 590, 630, 690, 720, 760, 800, 840, 880, 920, 970, 1010, 1050, 1090, 1130, 1170, 1220, 1260, 1300, 1340, 1380, 1420, 1470, 1510, 1550, 1590, 1630, 1680, 1760, 1800, 1840, 1880, etc.
90% from T1	50, 80, 100, 140, 170, 200, 240, 270, 300, 330, 360, 390, 430, 460, 490, 520, 560, 590, 620, 650, 680, 720, 750, 780, 810, 850, 880, 910, 940, 980, 1010, 1040, 1070, 1110, 1140, 1170, 1200, 1240, 1270, 1300, 1330, 1370, 1400, 1430, 1460, 1500, 1530, 1590, 1630, 1660, 1690, 1720, 1760, 1790, 1820, 1850, 1880, etc.

The current signal used in analysis is 6 ms long, beginning at 2 s. However, it can also be seen that similar frequency spectra are generated with different sections of post-fault signal with the same range of duration as the 6 ms signal starting from 2.01 s. Hence, for this method any appropriate range of post-fault signal in any section of the signal can be used for detection.

In conclusion, despite the magnitude variations caused by different fault resistance, the overall shape of the frequency spectra generated by current signal is similar for a specific fault location. This feature can be used as the basis of a fault location method.

4.4 Three-terminal HVDC

4.4.1 Control for multi-terminal HVDC links

Since this scheme relies on electromagnetic transients, it is important to model the converter stations in appropriate detail, including their control systems. Using a direct power control strategy does not cancel out the coupling effect among the electrical control variables; therefore, changing one of the electrical control variables will affect the other control variable. Vector control strategy can be implemented using a decoupling feed forward control method which eliminates the effect of the coupling of control variables. Consequently, a vector control strategy is commonly used [83, 84]. The coordinated control of MTDC systems is technically challenging because the power flow and voltage must be carefully controlled at each bus by the switching of the converters. There are various competing methods of achieving this is in the literature [17, 85-88]. In this paper, voltage droop control, based on system droop characteristics as discussed in [88], was chosen for the system control. This was chosen for relative simplicity and robustness since voltage droop control allows multiple converters to regulate the voltage at the same time [86]. Hence, if the control system in one terminal is disconnected, the other terminals can still regulate the voltage levels in the DC system.

The main task of the main control is to calculate the power flow reference and to start or stop sequence. The terminal controller is to achieve the control of active power, reactive power, AC voltage and DC voltage. Initially, the coordinated control is often employed one specific terminal to control DC voltage and the other VSCs controlled active power individually [89]. Gradually, more and more researchers focused on droop-based technology with coordinated control.

The phase voltage, including the amplitude, the angle and the angular frequency can be actuated by the VSC control system. With respect to the AC or DC grid, each VSC station can be controlled in a number of different ways. Due to the decoupled current control, the active and reactive power can be dispatched independently since the two orthogonal dq-current components can be changed independently. In the modelled network shown, terminal 2 is set as a slack bus to balance the system by supplying active power. Such an approach does not require communication between the terminals, because two terminals are responsible for DC voltage regulation and the remaining terminals are responsible for providing active power under both steady-state and transient conditions.

The controller of the VSC consists of two stages which are the inner and the outer controller as shown in Fig. 4-11. The inner controller's inputs are fed from the outer controllers that are responsible for providing current references based on the desired control employed such as the active and reactive power control. The duty of the inner control loops is to prevent overloading during electrical problems and to evaluate the voltage drop value at the AC side.

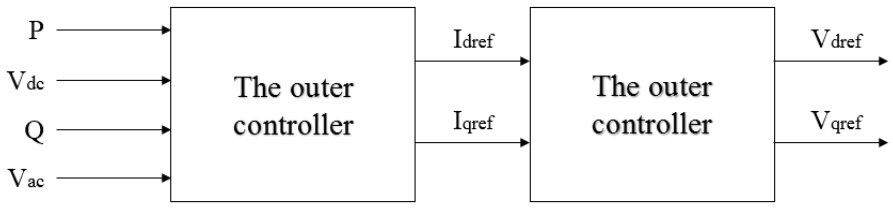

Fig. 4-11 Control structure of VSC

In the basic operation of a VSC-HVDC system, each converter terminal is treated as a controllable-voltage source which connects to an AC network through a series reactor [17]. As is well known, VSC-HVDC can control active power and reactive power independently. The phase voltage including the amplitude, the angle and the angular frequency can be set by the control system of VSC. The voltage droop method is applied here. The droop is defined by the parameter R, which is the percentage of the ratio of normalised voltage deviation to normalised power reference change. The flowchart of the control scheme can be found in Fig. 4-12.

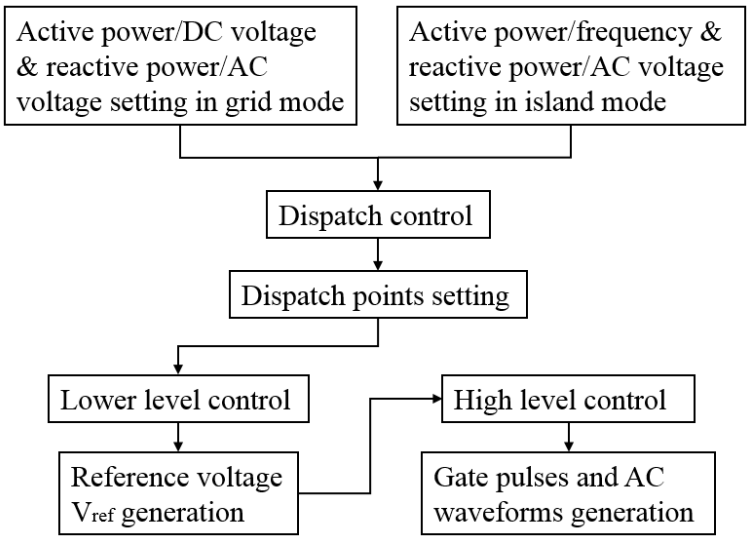

Fig. 4-12 Flowchart of control scheme

From a systems perspective, the DC-Bus voltage and current droop relation is directly linked to the voltage dynamics in the DC system. The current and voltage are transformed into the rotating direct-quadrature frame and the signals are passed to the inner-current PI controllers that must be carefully tuned for stability. Proportional plus integral (PI) control law are applied which is illustrated in equation 4.17 [90].

$$C(s) = k_p + \frac{k_i}{s} \tag{4.17}$$

where k_p is called the proportional gain, k_i is called the integral gain.

Proportional regulation (k_p regulation) responds to the deviation of the system. Once the deviation appears, proportional regulation works to reduce the deviation. The larger the proportion is, the faster the system will respond to regulation so that the error will be reduced. However, if the ratio is too big, the system will become unstable.

Integral regulation (k_i regulation) makes the system eliminate steady-state error. Because of the error, the integral regulation will work until the error returns to zero, and the output of the integral regulation will be a constant output. The strength of the integral action depends on the integral time constant T_i. If T_i is smaller, the

integral action will be strong, and vice versa.

The proportional gain k_p and the integral gain k_i can be determined by:

$$-\frac{1}{k} < k_p < \frac{\tau}{kL}\sqrt{\alpha^2 + \frac{L^2}{\tau^2}} \tag{4.18}$$

$$0 < k_i < \min_{l=1,3\ldots}\{b_l\} \tag{4.19}$$

where:

$$\alpha = \left\{\alpha \middle| \tan(\alpha) = -\frac{\tau}{L}\alpha\,, \alpha \in \left(\frac{\pi}{2}, \pi\right)\right\}$$

$$b_l = b(z_l) = \frac{z_l}{kL}\left(\sin z_l + \frac{\tau}{L} z_l \cos z_l\right)$$

$$z_l = \left\{z \middle| kk_p + \cos z - \frac{\tau}{L} z \sin z = 0\right\}$$

The PI control law can be also expressed in the time domain as:

$$u(t) = k_p e(t) + k_i \int_0^t e(\tau) d\tau \tag{4.20}$$

The PI controller is a linear controller. The control deviation is obtained based on the setting value and the actual output value. The control principle is to linearly combine the deviation of the proportional and integral making a controlled variable to control the objects.

4.4.2 Implementation in PSCAD

A three-terminal VSC-based HVDC system was modelled, based on the CIGRE B4 DC grid test system [91], using the PSCAD software. A portion of the CIGRE B4 DC grid test system, shown in Fig. 4-13, consists of three symmetrical monopole converters, DC link capacitors, passive filters, phase reactors, transformers, DC

transmission lines and AC sources. Detailed modelling can be found in Appendix B.

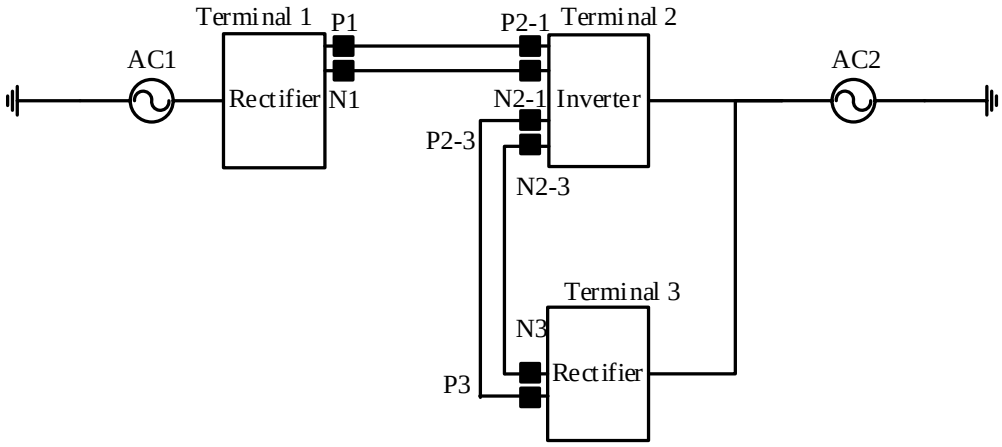

Fig. 4-13 The configuration of the three-terminal HVDC system

The overview of the whole control scheme is shown in Fig. 4-14.

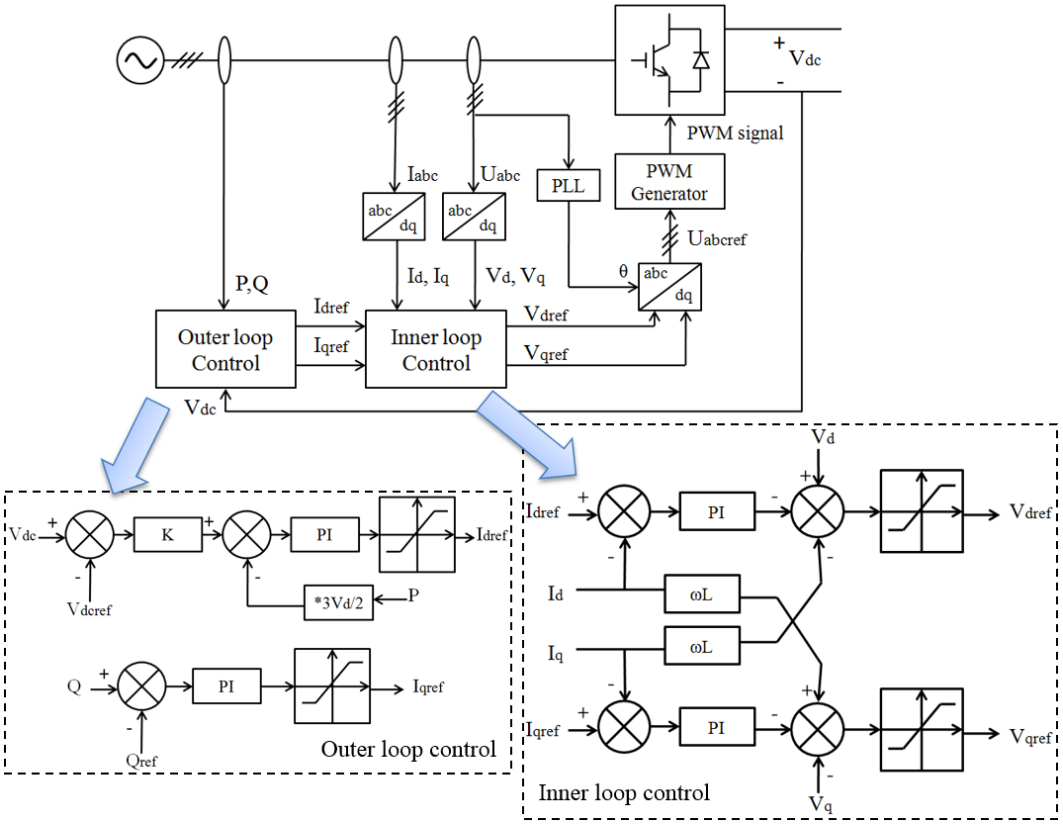

Fig. 4-14 The outer controller and inner controller

The phase voltages calculated by using line voltage will avoid the zero sequence voltages [92]. The phase voltage can be calculated based on Fig. 4-15.

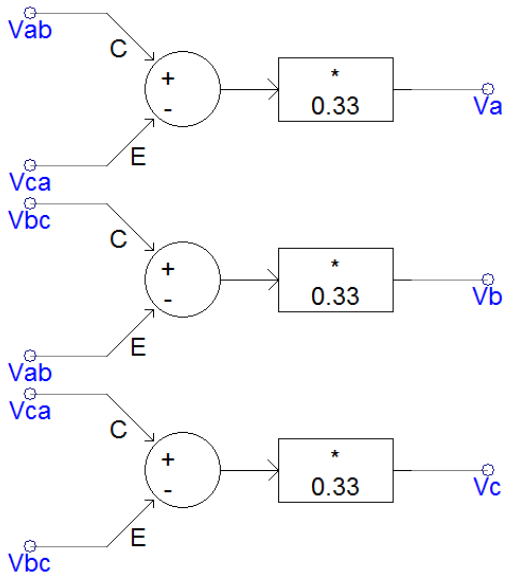

Fig. 4-15 Phase voltage calculation

It is necessary to transform the equation from the abc frame into the dq synchronous frame in order to achieve a decoupled control of active and reactive power. To generate the reference values in the abc frame, dq control is used. The abc to $dq0$ frame conversion is a Park transformation in a rotating reference frame. The $dq0$ to abc frame is an inverse Park transformation.

$$\begin{bmatrix} u_d \\ u_q \\ u_0 \end{bmatrix} = X_{dq} \begin{bmatrix} u_a \\ u_b \\ u_c \end{bmatrix} = \frac{2}{3} \begin{pmatrix} \cos(\theta) & \cos\left(\theta - \frac{2\pi}{3}\right) & \cos\left(\theta + \frac{2\pi}{3}\right) \\ \sin(\theta) & \sin\left(\theta - \frac{2\pi}{3}\right) & \sin\left(\theta + \frac{2\pi}{3}\right) \\ 0.5 & 0.5 & 0.5 \end{pmatrix} \begin{bmatrix} u_a \\ u_b \\ u_c \end{bmatrix} \quad (4.21)$$

The detailed implementation for transforming AC current from the abc to the dq frame is shown in Fig.4-16:

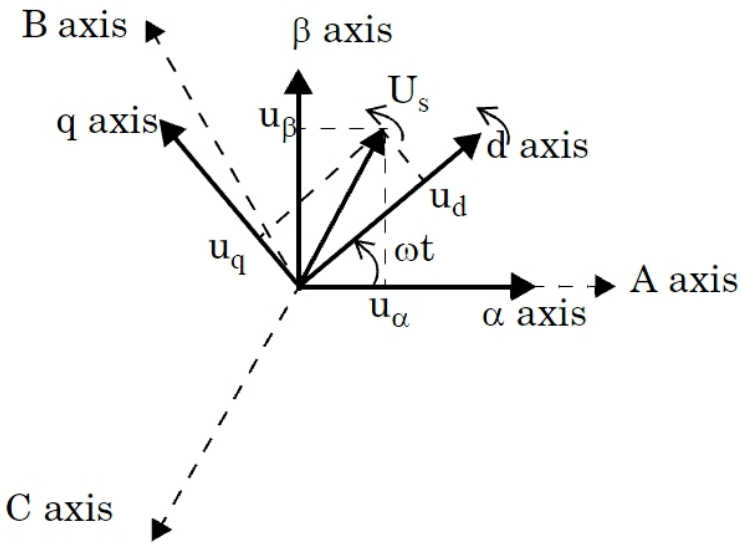

(a) Park transformation [93]

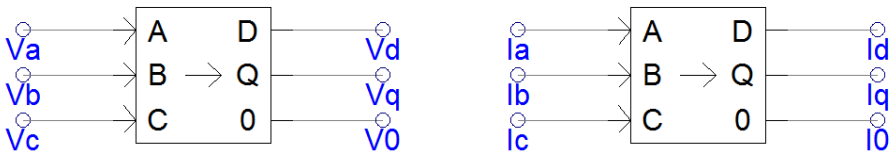

(b) Implementation in PSCAD

Fig. 4-16 Transformation from the abc to the dq frame

The angle th generated from the Phase lock loop (PLL) is the transformation angle generated by the PLL and is used in the abc to dq transformation (Fig. 4-17).

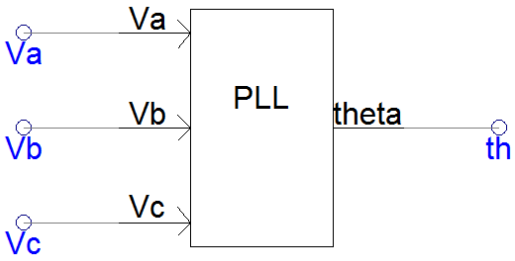

Fig. 4-17 Angle th generation

The outer controller, shown in Fig. 4-18, sets the droop and applies voltage and current limits based on dispatch set points in order to generate V_{ref} in the abc frame using dq0 control. The outer controller can be described by equation 4.22:

$$\begin{cases} I_{dref} = K_P\left(P_{ref} - P\right) + K_P \int \left(P_{ref} - P\right) \\ I_{dref} = K_{dc}\left(V_{dcref} - V_{dc}\right) + K_{dc} \int \left(V_{dcref} - V_{dc}\right) \\ I_{qref} = K_Q\left(Q_{ref} - Q\right) + K_Q \int \left(Q_{ref} - Q\right) \end{cases} \tag{4.22}$$

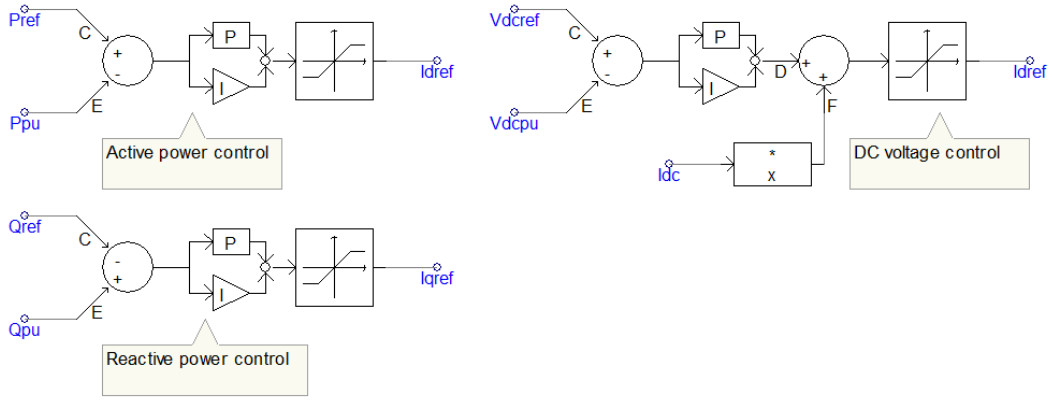

Fig. 4-18 Outer control

The outer controller sets the droop and applies power and DC voltage limits, as shown in Fig. 4-19 and in equation 4.23.

$$\left(V_{dcref} - V_{dc}\right)K - \frac{2}{3V_d}\left(P_{ref} - P\right) = 0 \tag{4.23}$$

where: V_{dcref} is the reference DC voltage, K is the proportional gain, V_d is the reference AC voltage in dq0 reference frame and is desired to have constant value and P_{ref} is the reference active power.

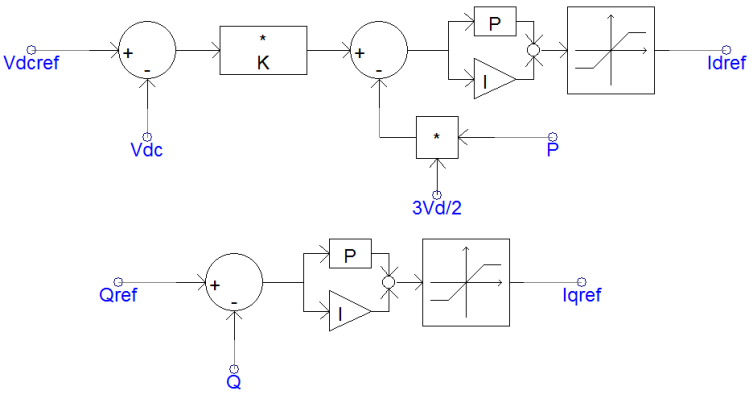

Fig. 4-19 Voltage droop control

Using appropriately tuned PI controllers, the outer controller calculates the reference currents, I_{dref} and I_{qref}, which are the inputs to the inner control. The detailed parameters are listed in Table 4-4. Both active power control, P, and DC voltage control, V_{dc}, are achieved by controlling the reference to the active current controller. The I_{dref} signal is obtained by combining these two types of controllers. The reactive power, Q, controls the reactive current, I_{qref}, via a PI block. The droop is set by equation 4.24 which determines the proportional gain, K.

$$K = \frac{2P_{rated}}{3\delta_{dc}V_d V_{dcrated}} \tag{4.24}$$

where: δ_{dc} is the voltage droop, P_{rated} is the rated active power, $V_{dcrated}$ is the rated DC voltage.

The tuning of the PI controllers is shown in Table 4-4

Table 4-4 PI controllers tuning

DC voltage controller	K_p=3.36, K_i=0.05
Active power controller	K_p=3.36, K_i=0.05
Reactive power controller	K_p=0.43, K_i=0.0266
Inner controller (V_{dc})	K_p=2, K_i= 0.0133
Inner controller (P)	K_p=4, K_i=0.0133

In the inner-current loop, control limits the current to protect the valves. The current and voltage are transformed into the rotating direct-quadrature frame and the signals passed to the inner-current controllers (shown in Fig. 4-20) that must be carefully tuned for stability. The inner control, inputs V_{ref} signals via a capacitor balancing algorithm and circulating current suppression algorithm. In the inner-current loop, direct control limits the current to protect the valves as described by (4.25) and (4.26).

$$\begin{cases} V_d^* = L\frac{dI_d}{dt} = K_p\left(I_{dref} - I_d\right) + K\int\left(I_{dref} - I_d\right) \\ V_q^* = L\frac{dI_q}{dt} = K_p\left(I_{qref} - I_q\right) + K\int\left(I_{qref} - I_q\right) \end{cases} \tag{4.25}$$

$$\begin{cases} V_{cd} = V_{sd} - V_d^* + \omega L I_q \\ V_{cq} = V_{sq} - V_q^* + \omega L I_d \end{cases} \tag{4.26}$$

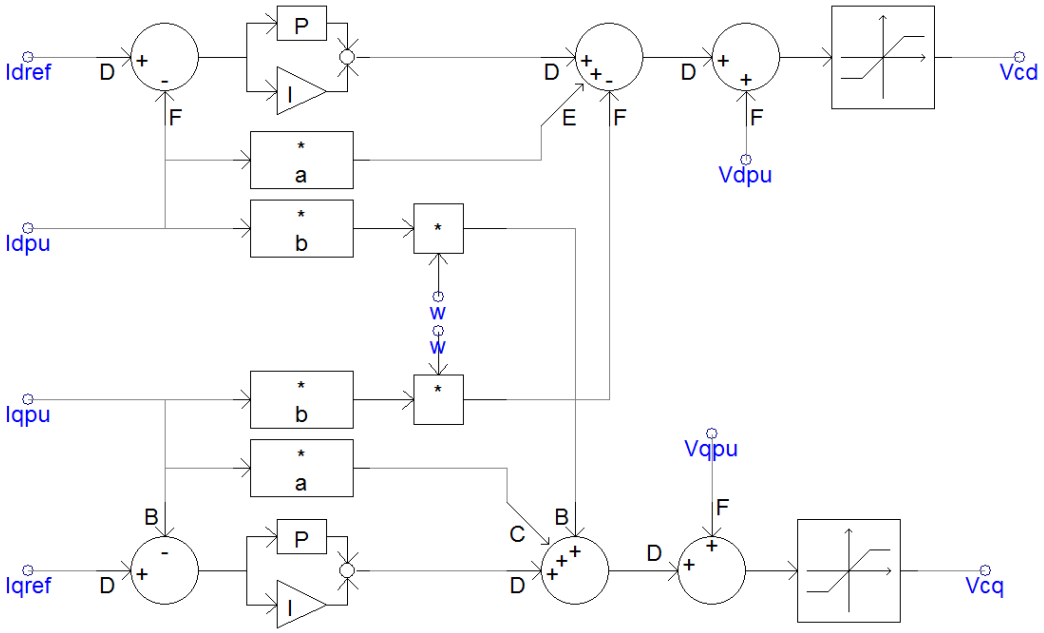

Fig. 4-20 Inner loop control

Transformation from the $dq0$ to the abc frame (Fig. 4-21):

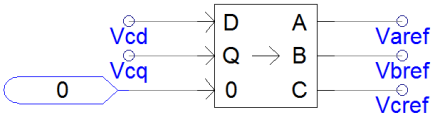

Fig. 4-21 $dq0$ to abc frame transformation

PWM directly controls the inverter circuit switches, producing a series of pulses which have equal amplitude in the output but varying duration. The gate pulses from the PWM give valve specific configurations to synthesise the AC waveform. Controlling the PWM can vary both the magnitude and frequency of the output voltage of the converter circuit [28]. The generation of a PWM triangular carrier

signal and a PWM sinusoidal reference signal are expressed in Fig. 4-22 and Fig. 4-23 respectively. Through a PWM triangular carrier signal and PWM sinusoidal reference signal, the firing pulses are shown in the following control block in Fig. 4-24.

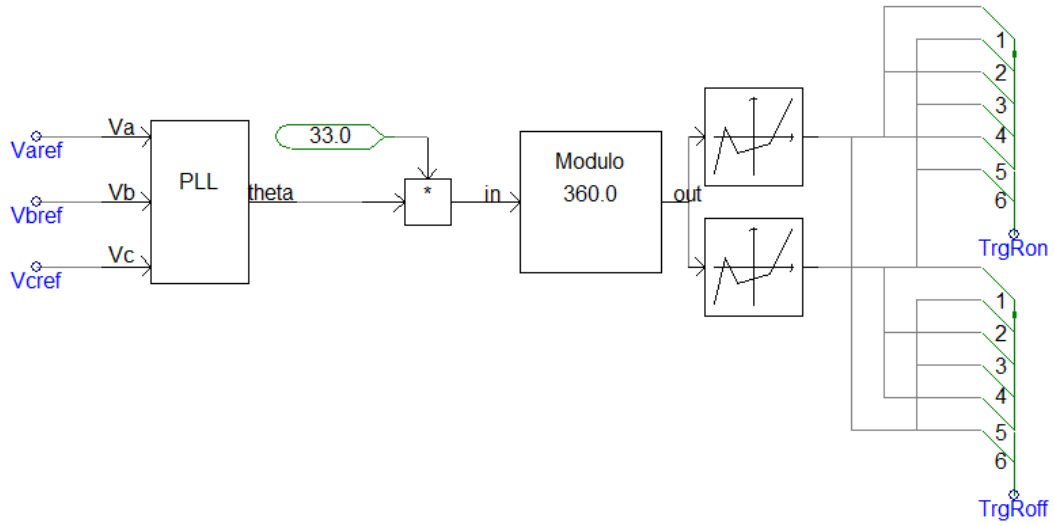

Fig. 4-22 PWM triangular carrier signal

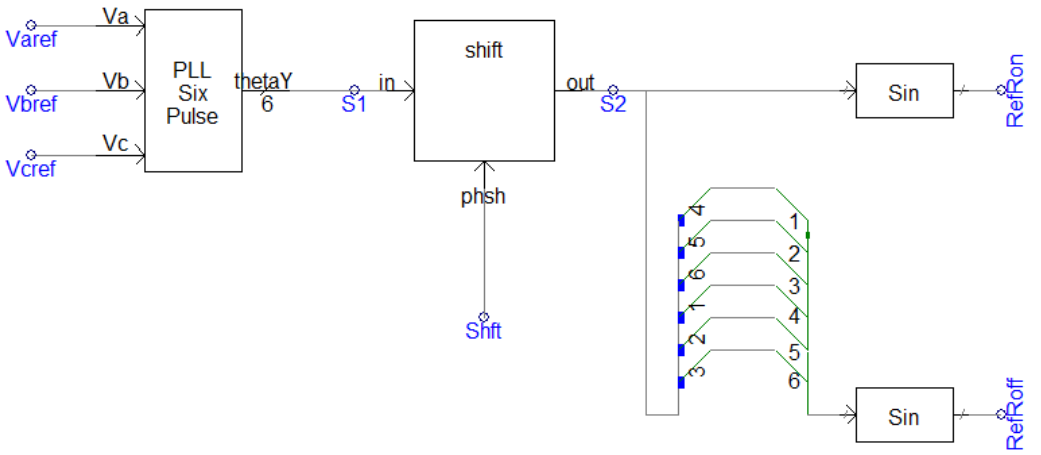

Fig. 4-23 PWM sinusoidal reference signal

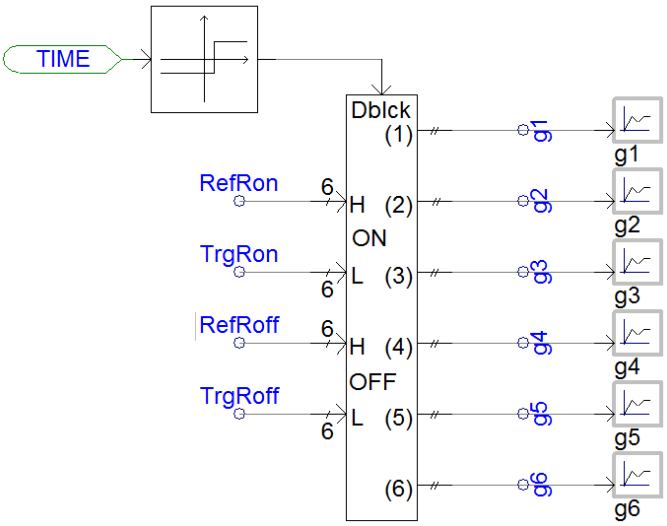

Fig. 4-24 Firing pulses generation

4.4.3 Steady-state condition

Based on the system modelling, the system responses in steady-state conditions are shown in Fig. 4-25.

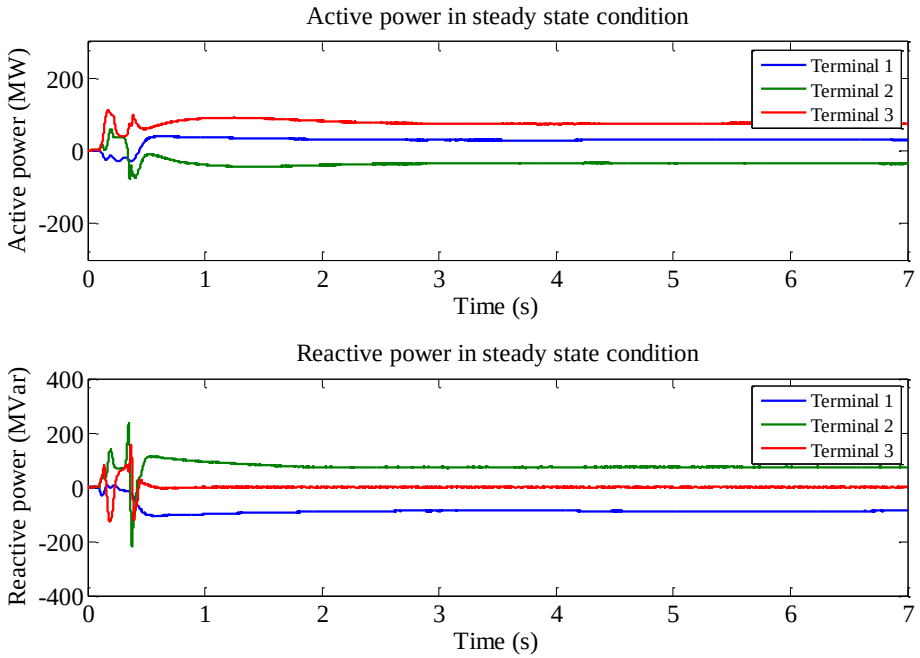

(a) The reactive power and active power generated from the voltage source

Fig. 4-25 Measurement in steady-state conditions

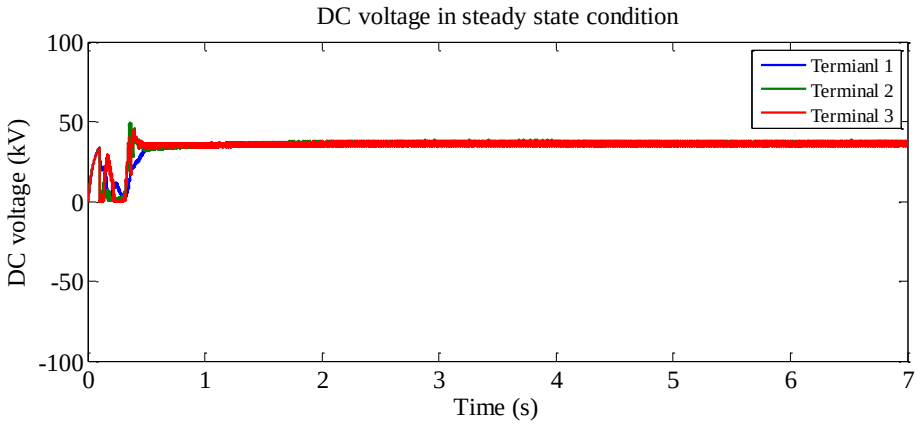

(b) DC voltage on the transmission line

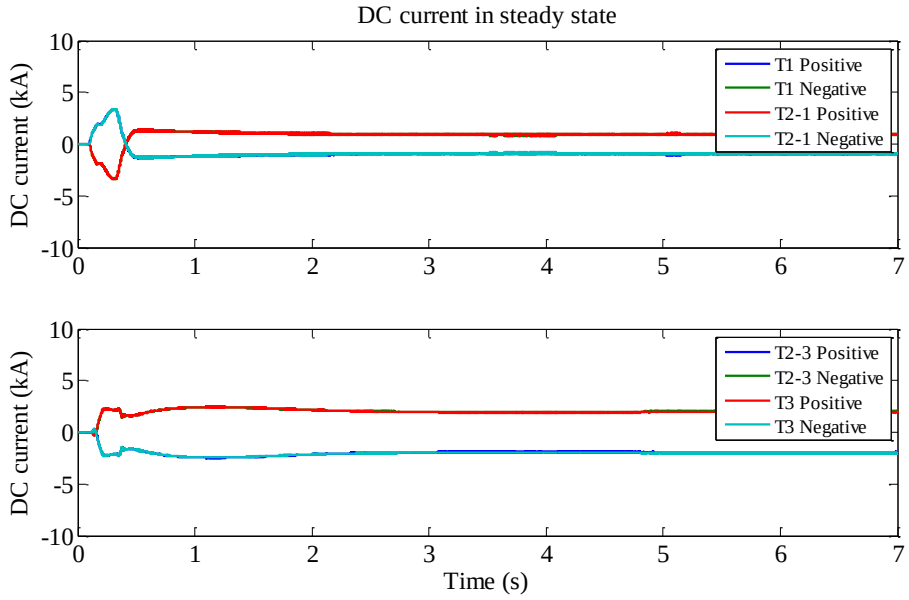

(c) DC current on the transmission line

Fig. 4-25 Measurement in steady-state conditions

4.4.4 Fault profile analysis

Time domain response

On the MTDC system, an example pole-to-pole fault on section 1 between terminal 1 and terminal 2 is applied to show the transient response of the system. The fault is at 30% of the line length from terminal 1 with 0.01 Ω fault resistance. The DC currents and voltages on different terminals clearly have a far more significant

response to the fault on the faulted line compared to the healthy line.

The effect of different types of fault including positive ground fault, negative ground fault and line-line fault can be found in Fig. 4-26, Fig. 4-27 and Fig. 4-28 respectively. Below, negative ground fault, which is 30% away from terminal 1 with 0.01 ohms fault resistance, is used as an example.

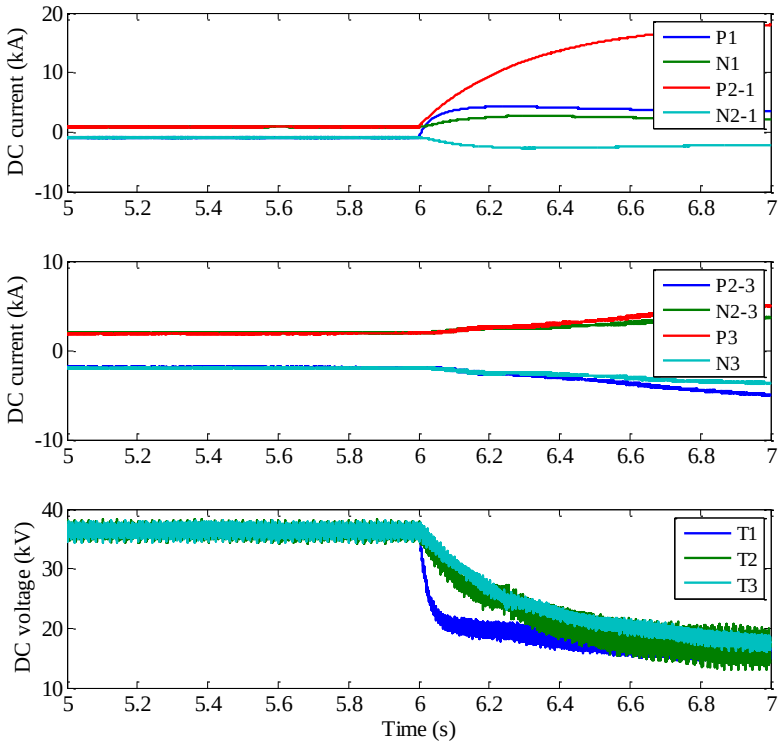

Fig. 4-26 Positive ground fault

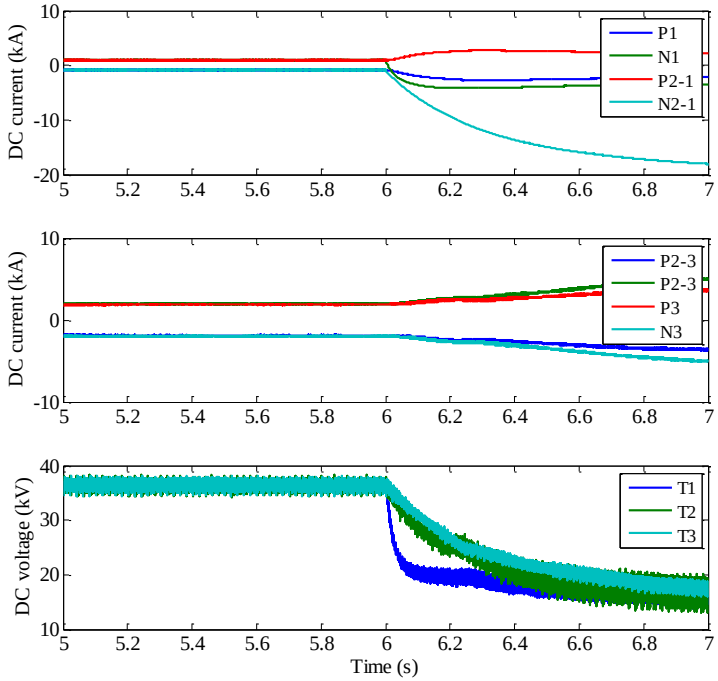

Fig. 4-27 Negative ground fault

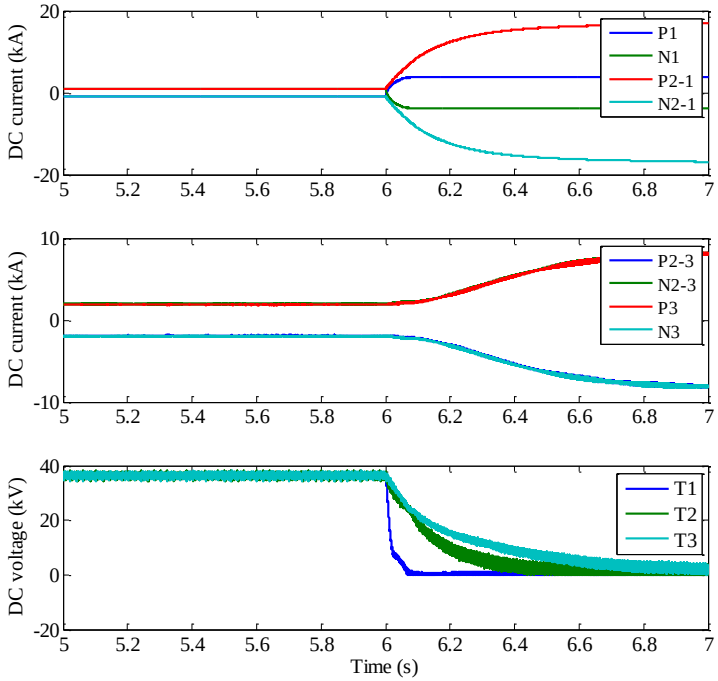

Fig. 4-28 Line-line fault

Different fault location and different fault resistance are two factors that need to be

considered in fault profile analysis. The DC fault current with different fault resistance can be found in Fig. 4-29. As can be seen from the figure, the fault current will decrease with an increase in fault resistance.

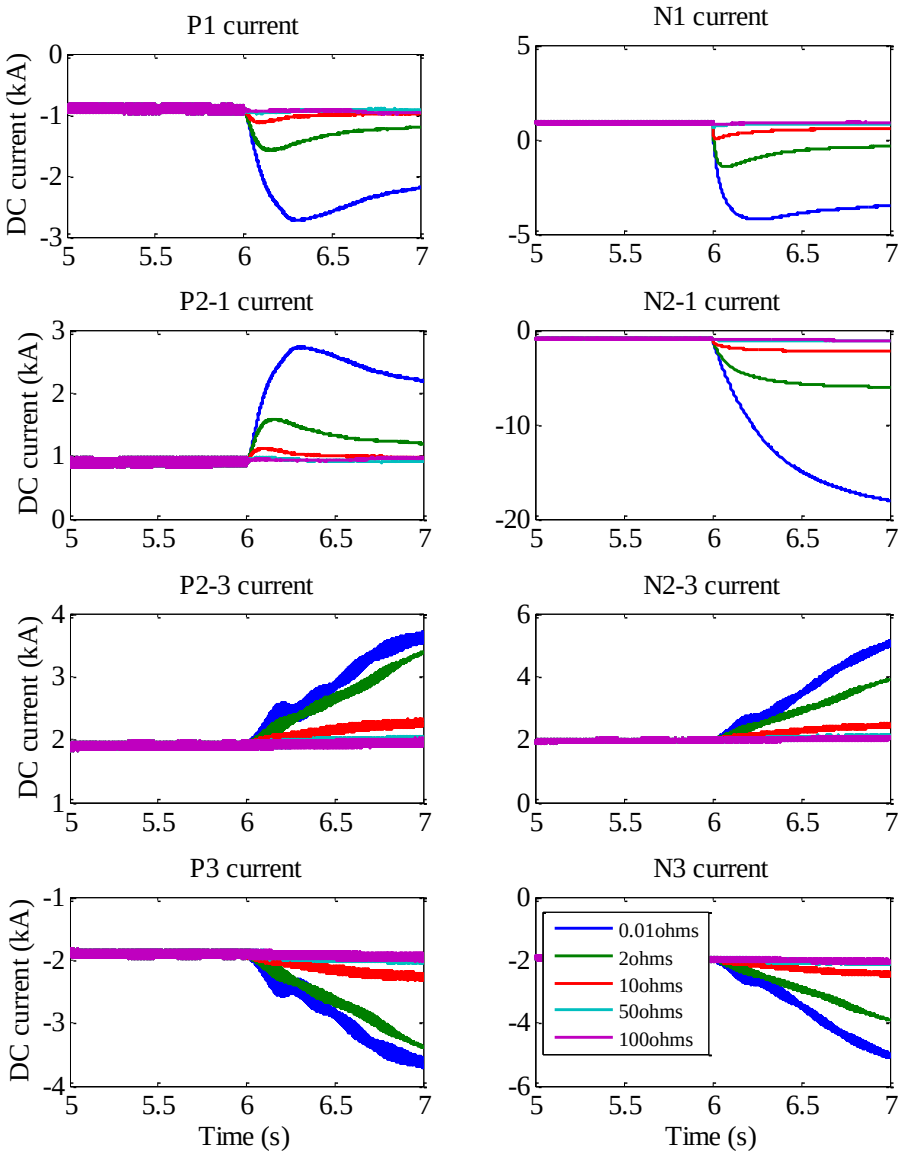

Fig. 4-29 30% negative-pole-to-ground fault with different fault resistance on different terminals

Frequency domain response

Frequency components are important for protection of algorithm design. As

proposed in many previous works, the discrete wavelet transform (DWT) is firstly applied to analyse the signals in the frequency domain. Different from continuous scaling and shifting, the mother wavelet may be scaled and shifted discretely by choosing the set values. The sampling frequency is set to be 10 kHz, and the mother wavelet is selected to be symlets. The level of symlets is 8. The discrete wavelet transform is given by 4.27 [94]:

$$DWT(m,n) = A_0^{-m/2}(\sum x[k]\psi^*[(k - na_0^m b_0)/a_0^m]) \qquad (4.27)$$

where: $\psi(t)$ denotes the mother wavelet, the asterisk presents a complex conjugate, $a, b \in E, , a \neq 0$ are the scaling and shifting parameters respectively, E is a real continuous number system.

The DWT results for DC current and DC voltage are shown in Fig. 4-30, Fig. 4-31, and Fig. 4-32 respectively. As can be seen in the waveforms, the transmission line faults can be clearly presented by the analysis on DC current signals but not DC voltage in a very short time. Hence, the protection method is designed based on the DC current signals.

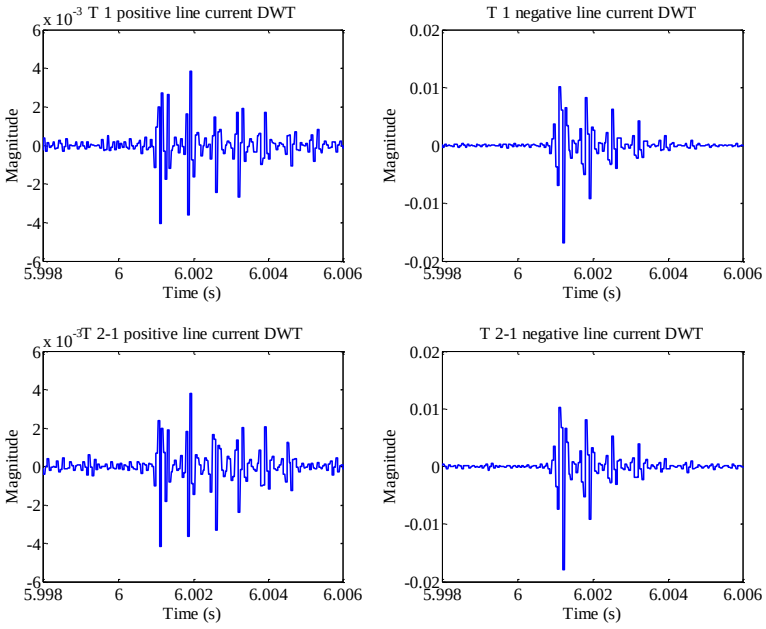

Fig. 4-30 DWT of DC current on line 1

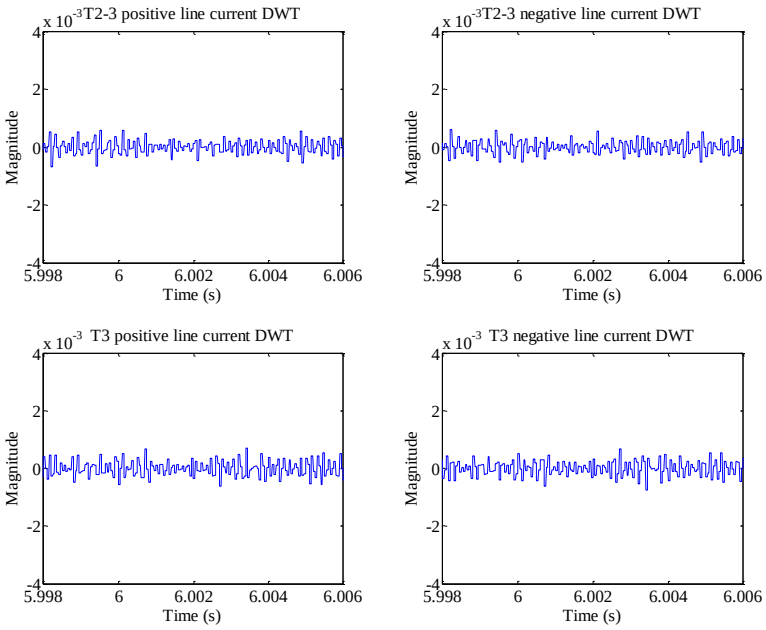

Fig. 4-31 DWT of DC current on line 2

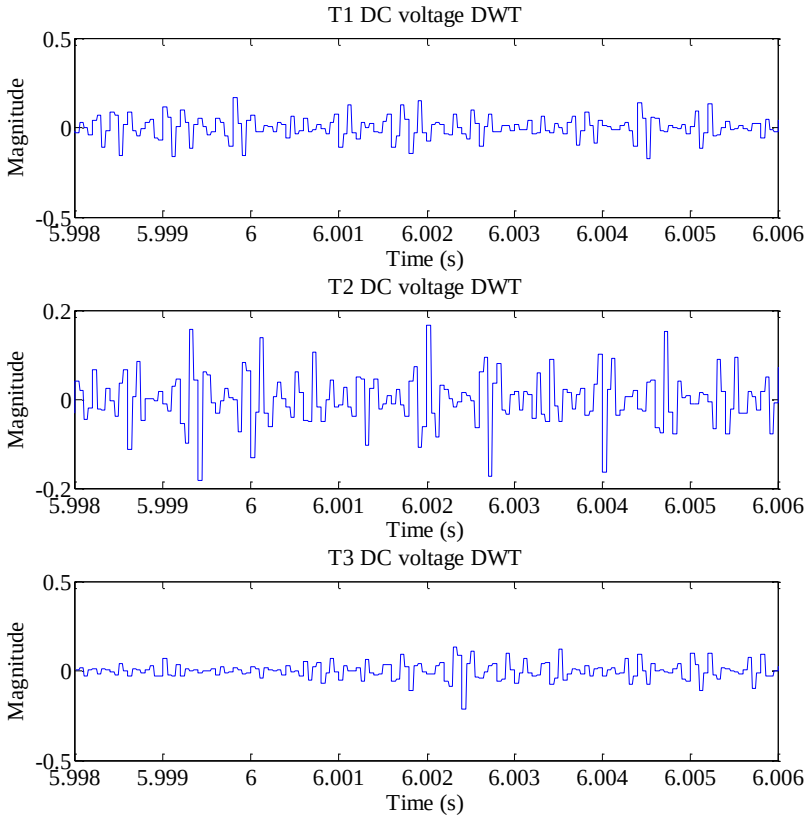

Fig. 4-32 DWT of DC voltage

The Fast Fourier Transform (FFT) is another very powerful signal processing method to convert a time-domain signal into another representation in frequency-domain. Fourier analysis has a high level of technical maturity. An adequate representation in frequency-domain will be presented by FFT with a very short data length (<1s) [95]. In addition, a faster computational time is expediential to meet the time requirement of DC circuit breakers.

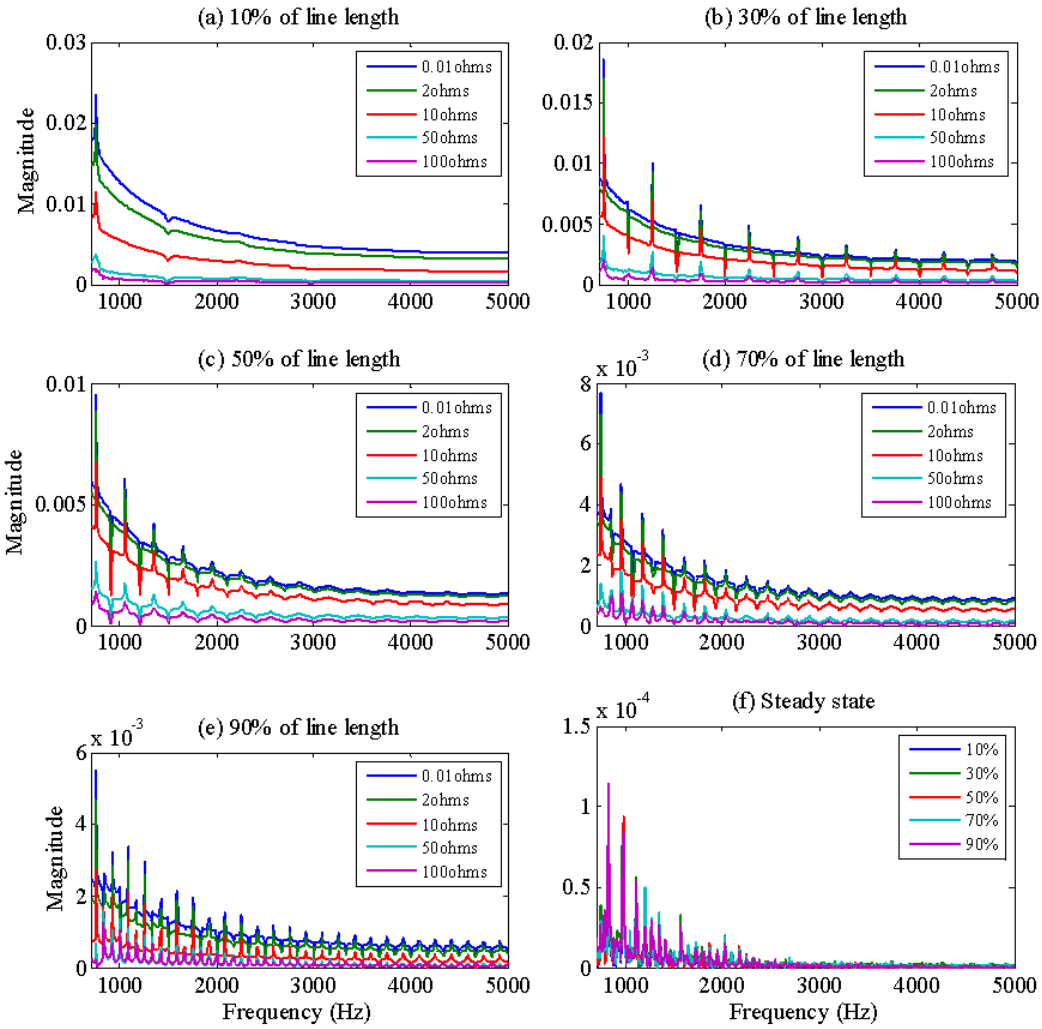

Fig. 4-33 Frequency spectra for different fault locations from the rectifier, varied from 10% (a) to 90% (e) and frequency spectra in 0.01 W fault resistance (f)

In the FFT analysis, the sampling frequency 10 kHz is applied. 10 kHz is found to be sufficient, as 200 samples per 50 Hz AC cycle in this paper for fault location. With 10 kHz sampling frequency, the data processing system will have enough time for calculation. Through signal processing by FFT analysis, the frequency spectrum is generated in Fig. 4-33. From (a) to (e) we can clearly see the frequency change

related to fault location, and the magnitude for fault resistance. The location of the peaks does not change with fault resistance, only the level of the frequency spectrum, whereas location of peaks changes with location of fault.

The frequency spectrum generated from signal processing is shown in Fig. 4-33. Here, the current signal detected at terminal 1 in the system, is shown for the positive pole when a ground-to-pole fault under various conditions is simulated. The signal is windowed from the start of the fault and the window length is 6 ms. Fig. 4-33 (a) to (e) clearly show that only spectral features change with fault location whereas the magnitude of the spectrum changes with fault resistance. In particular, the position of the features, namely valleys and peaks, do not change with varying fault resistance, only the background level of the frequency spectrum. In contrast, the position of the features do vary with the location of the fault. Therefore, these peaks are an important input feature in the fault location ANN.

The high frequency components shown in Fig. 4-33 occur because of the travelling waves that emanate from the fault location due to the sudden step change in circuit conditions. The arrival time of successive travelling waves, both original and reflected, is determined by the fault location and, therefore, the fault location has a direct relationship with the position of features in the frequency spectrum. The post-fault frequency spectrum is largely time-independent. This increases the robustness of this frequency domain approach because, regardless of the window's location on the post-fault time series, it will yield a very similar frequency spectrum for some time after the fault.

Fig. 4-33 (f) shows the frequency spectra generated in steady-state conditions for comparison. The features arise largely due to the switching of the converter stations but the magnitude of these features and the overall spectral energy under steady-state conditions is negligible compared with the fault conditions.

Fault location is based on the detection of the adjacent frequency spectrum. The detection of these high frequency peaks is shown in Fig. 4-34. Peak detection, which is integral in the algorithm, is achieved by a peak finder in MATLAB with subsidiary conditions applied in the algorithm. As can be seen in the figure, the

peaks for all spectra are detected with eye recognition. The pseudo peaks are filtered not to affect the real peak detection.

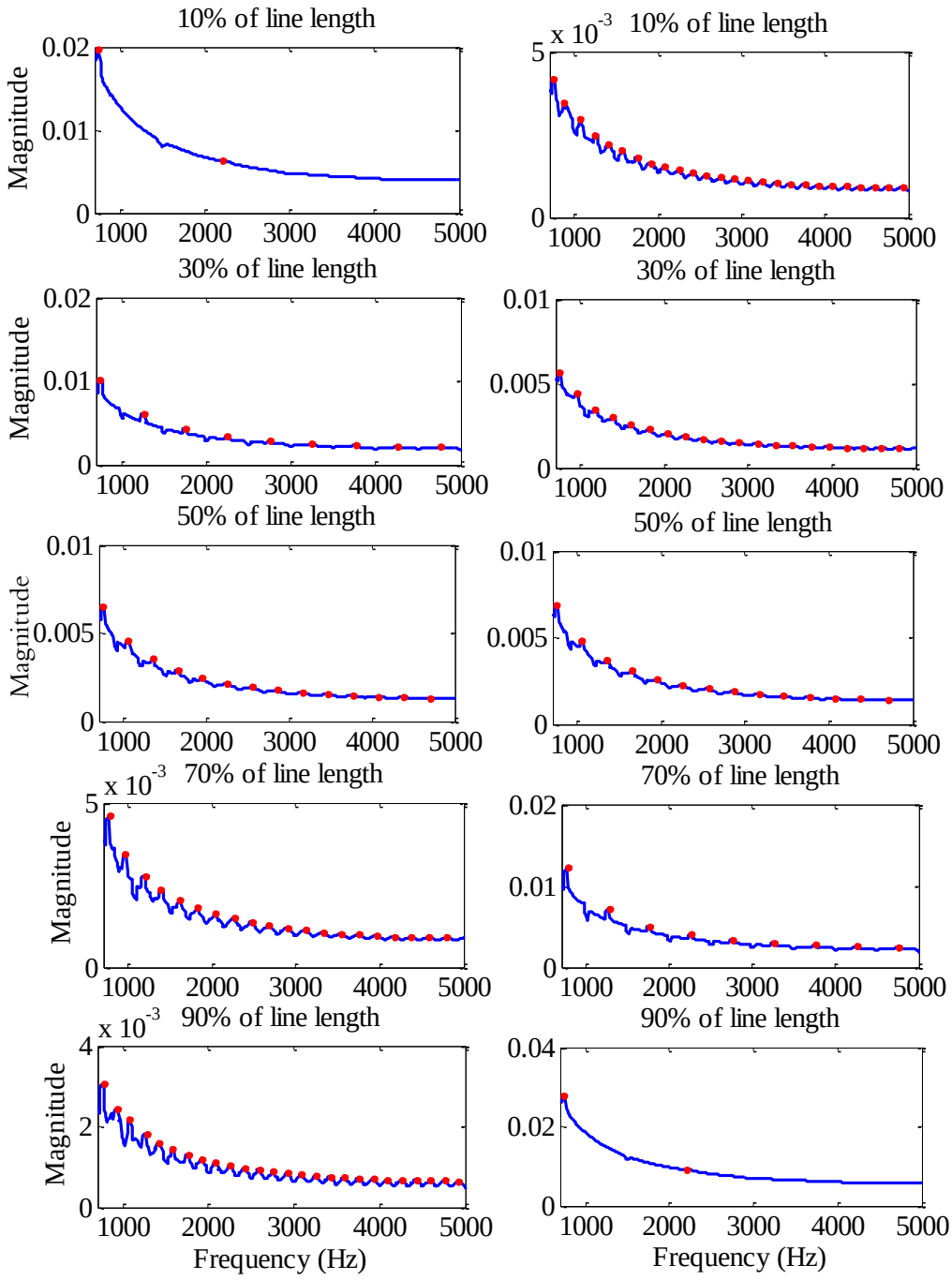

Fig. 4-34 Peak detection in frequency spectrum

Control system response

The control scheme must respond quickly to preserve system stability after the faulted section is de-energised, and this necessitates detailed modelling of the

control to faithfully reproduce the system's transient response. Due to the PWM switching action in VSC-HVDC, the current flowing to the DC side of a converter contains harmonics, which will result in a ripple on the DC side voltage. During disturbances in the AC system (i.e. faults and switching actions), large power oscillations may occur between the AC and the DC side. This in turn will lead to oscillations in the DC voltage and DC overvoltage that may stress the valves. The DC side capacitor can mitigate this problem by providing faster converter response and energy storage to be able to control the power flow. The relatively small time constant allows fast control of active and reactive power.

4.5 Chapter summary

The detailed modelling of a two-terminal HVDC system and multi-terminal HVDC system are introduced. The modelling of each component in the system is discussed firstly, followed by the control scheme implementation. The system modelling is a basis for the fault analysis and protection scheme design, which plays an important role in the project.

Based on these two HVDC models, the system in both steady-state conditions and transient conditions is analysed. The transient conditions are introduced by time domain, frequency domain and control system response – three aspects. Different faults at different fault resistance and locations are simulated. In the frequency response, WT and FFT are both applied to detect the features generated by both current signals and voltage signals. In conclusion, the characteristics of the frequency spectrum can give the best expression to the faults. Significant features can be seen from the fault simulations with FFT analysis. Hence, it can be concluded that the fault currents need to be pre-processed to the frequency domain before being utilised for realising the protection scheme. With the conclusion made in this section, FFT is adopted in the approach for HVDC protection. The detailed feature extraction is discussed in Chapter 6.

5 ANN-based Method in HVDC and MTDC Systems

5.1 Introduction

Based on the network modelling in Chapter 4, the designed protection scheme is applied for fault detection, fault classification, and fault location on these two specified systems. The fault current signals are identified and frequency domain information is extracted using the Fast Fourier Transform (FFT), which, in turn, is interpreted using artificial intelligence techniques. The ANNs are built for both two-terminal HVDC and multi-terminal for testing.

This chapter firstly gives a basic introduction to artificial intelligence (AI), followed by a detailed introduction to artificial neural networks. After an extensive series of studies, the reasons for adopting artificial neural networks (ANNs) in electrical power systems and in the DC transmission line protection scheme developed for HVDC system are given herein. The signal chains as an overview of the proposed methods is introduced. Following the flowchart of the method, the data collection from the system and signal processing are introduced respectively. The detailed description of the ANN including the architecture and the training process is proposed. Lastly, the test results for different fault conditions are illustrated and discussed.

5.2 Artificial intelligence

Artificial intelligence is a powerful collection of computing concepts modelled on the thought and behaviour of human beings and animals. Many AI techniques attempt to automate rational decisions that would usually be made by a human expert, by including missing data, adapting to evolving situations and improving performance over long time horizons based on accumulated experience.

AI technologies have been widely applied in power systems in recent years because of their capability of handling complicated power systems and achieving fast and accurate results. Major AI techniques appropriate for protection are artificial neural networks, Fuzzy Logic systems (FL), and Expert System Techniques (XPSs). ANNs are generally applied in protection, fault diagnosis, power system stabilisers, load forecasting, etc. FLs can be used in power system control, fault diagnosis, state estimation, security assessment, load forecasting, etc. XPS is usually applied in post fault analysis fault diagnosis and settings coordination as a decision making tool.

The advantages of ANN-based methods are that they can discern the non-linear relationship between the inputs and outputs by using appropriate training data. Complex system analysis can be simplified and achieved effectively. They have fast processing speed and are robust. No completed information about the systems and the data are compulsory. In addition, they are fault tolerant [96]. By considering all the benefits illustrated above, the ANN technique is selected in this thesis.

5.3 Artificial neural networks

ANN is a type of Artificial intelligence technique that is inspired by how biological nervous systems, such as the human brain, process information [97, 98]. ANNs have the ability to model both linear and non-linear systems without the need to make assumptions implicitly as in most traditional statistical approaches [99].

As indicated in [100, 101], ANN-based methods are effective for fault detection and fault location on AC grids and HVDC systems due to accuracy, robustness and speed. The ANN is often fed by a feature selection stage, such as the Wavelet Transform (WT). Combined sequentially, these perform fault detection, classification or location [102-104]. As introduced in the literature review section and the results generated in the system modelling chapter, despite using the DWT analysis to extract the most important features, there are still complexities in the processed information that cannot be handled using traditional mathematical techniques [105].

Numerous ANN-based applications have been shown to give improved

performance in power system protection for tasks such as fault location and phase selection. This is because of the ANN's ability to discern classes in complex problem spaces, such as between transients caused by faults and those under healthy conditions [106]. To develop formal relaying schemes, precise mathematical models for each system fault condition must be constructed. However, compared with conventional formal approaches, ANNs can be trained to recognise non-linear relationships between input and output data without requiring knowledge of their internal processes. As such, using its innate ability to recognise patterns, generalise and interpolate within the parameter space, the ANN only requires simulated training data rather than extensive formal and deterministic fault and system models [107]. Importantly, after training, ANN operation time is extremely fast because it only consists of a number of simple, interconnected processing units [107].

ANNs can be classified into feed-forward, for which no loops are formed by the network connections, and feedback such that one or more loops may exist. Feed-forward networks are most commonly used, of which the Multi-layer preceptron (MLP) is the most common type of feed-forward network. An MLP is formed by an input layer, a hidden layer and an output layer which are shown in Fig. 5-1.

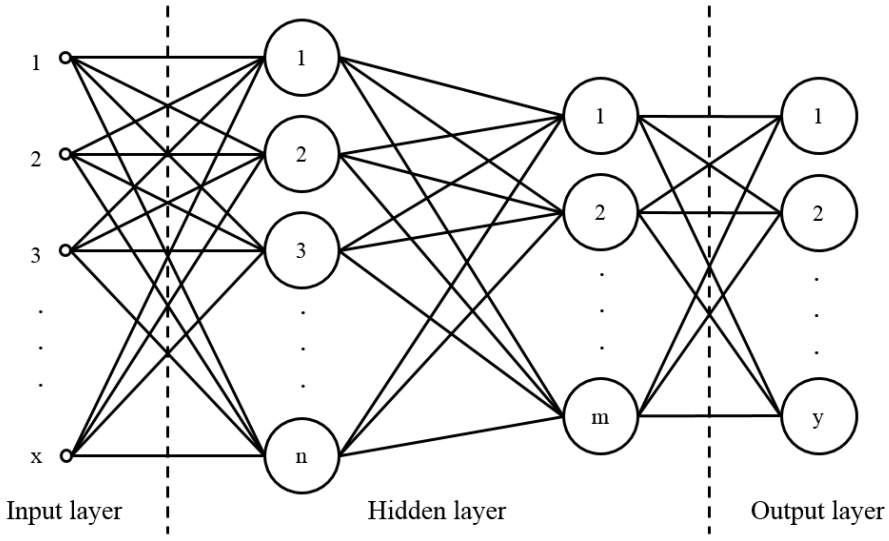

Fig. 5-1 Multi-layer perceptron network

Neurons in the input layer are only used as a buffer to distribute the input signal into the hidden layer (Fig. 5-1) [108]. Each neuron j in the hidden layer sums up its

input signals x_i after weighting them with the strengths of the respective connections w_{ji} from the input layer, and computes its output y_j as a function f(u) , which is shown in Fig. 5-2, of the sum [109].

$$y_j = f\{\sum_{i=1}^{n} w_{ji} x_i\} \tag{5.1}$$

where: w_{ji} is the weighting factor, n is the number for the inputs and j is the specific neuron.

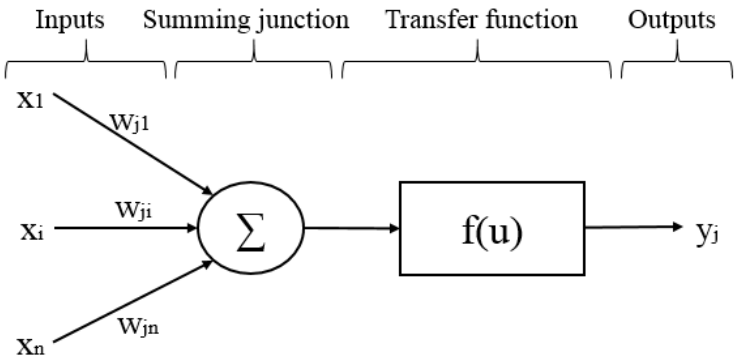

Fig. 5-2 The neuron model

The output of the neurons in the output layer is similarly calculated. As indicated in [110], the backpropagation algorithm, a gradient descent algorithm, is the most commonly adopted MLP training algorithm. It gives the change Δw_{ji} the weight of a connection between neurons i and j as follows:

$$\Delta w_{ji} = \eta \delta_j x_i \tag{5.2}$$

where η is the learning rate and δ_j is the factor depending on whether neuron j is an input neuron or a hidden neuron.

$f(u)$ can be a simple threshold function or a sigmoidal, hyperbolic tangent or radial basis function which is shown in Table 5-1 and Fig. 5-3.

Table 5-1 Activation function

Function type	Expressions
Threshold	$f(u)=\begin{cases}0, u \le 0\\1, u > 0\end{cases}$
Linear	$f(u)=\begin{cases}0, u \le -0.5\\u, -0.5 < u \le 0.5\\1, u > 0.5\end{cases}$
Sigmoid	$f(u)=\frac{1}{1+e^{-u}}$
Hyperbolic tangent	$f(u)=\tanh(u)=\frac{e^{u}-e^{-u}}{e^{u}+e^{-u}}$

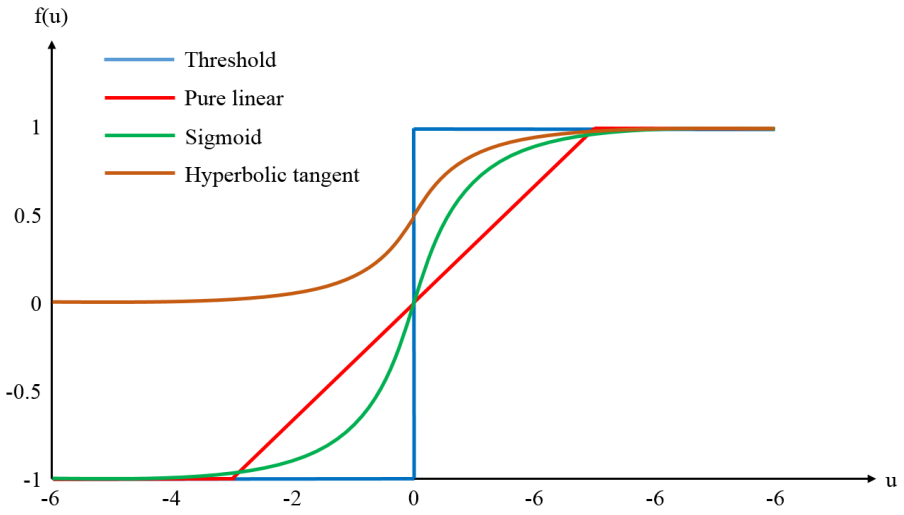

Fig. 5-3 Common transfer function

As shown in Fig. 5-4, the ANNs are usually worked to compare the input data and target data through an iterative process to meet the certain output convergence criteria. The whole process is iteratively repeated by adjusting the weights of ANN

to meet the output target criteria.

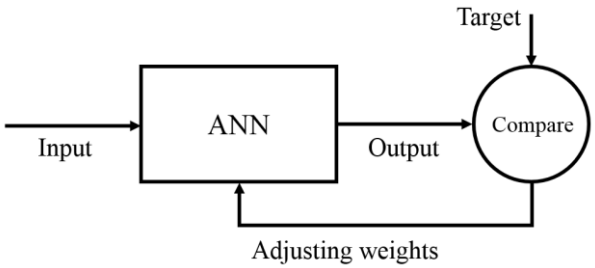

Fig. 5-4 Working principle of ANN

Using the Multi-layer feed-forward neural network as an example, the training process is completed by following the steps below:

- Feature extraction. Selecting the appropriate input data is usually the first step. Extracting the most important features that are applied as the input data in ANN is the basis.
- Data collection. Preparing the data sets is the next step. Sufficient training data is essential for the ANN training. It is imperative for gathering data to train the neural network.
- ANN establishment. Selecting the proper topology of ANN including the determining algorithm and architecture is a key step in the whole process. In addition, the optimal number of hidden layers and neurons should be set by a combination of heuristics and numerous empirical studies.
- Training the ANN. The ANN will be trained using the data sets collected as the input and the selected ANN until the optimal performance is achieved.
- Testing ANN. The data that are not used for training will be used to test the ANN.

Numerous ANN-based applications give excellent performance in power system protection including directional protection, distance protection, differential protection, fault location, phase selection, leading to great improvement in the protection relay's performance [106]. In order to solve the transient problems in power systems, a detailed mathematical model is often required of the relevant parts [107]. The advantages of using ANNs, compared with conventional methods, is that

an ANN can handle complex non-linear phenomena and, as such, only requires training data but not a formal fault model [107]. The ANN can then effectively interpolate for new data it is given, so it is said to be able to generalise. The computation time is very fast after the learning process because ANNs consist of simple processing units [107].

A novel fault detection, fault classification and fault location method based on ANN has been developed for multi-terminal HVDC DC transmission systems in this thesis. The FFT is implemented to detect any surges in the DC current waveform. In the event of a surge, the windowed Fourier transform extracts a feature vector from the current waveform and feeds it to a designed neural network. The neural network determines whether the feature vector belongs to a normal or a fault current surge. Three ANNs are designed for fault detection, fault classification and fault location respectively. These techniques are appropriate when the conventional approaches do not appear as an effective solution.

ANN with a Back Propagation (BP) learning algorithm is widely used to solve various classifications and forecasting problems. The architecture of a multi-Layer Perceptron is selected in this thesis. After detecting the electrical signal through sensors, the signal processing is the second step. The input signal to ANN is modified by the weights w which are associated with each input into the neuron [107].

The Fourier transform extracts a feature vector from the current waveform and feeds it to a purposefully pre-designed neural network. Since the frequency spectrum contains sufficient information about the fault, only current signals from one terminal are required for fault detection and classification. As mentioned earlier, the frequency spectra captured for each fault case express unique features at each fault location. However, due to the complexity of the mapping between spectral features and fault information, a trained ANN is an integral part of the relaying scheme. Firstly one neural network performs fault detection, namely whether the feature vector belongs to a healthy or fault condition. If a fault condition is detected, two further ANNs are trained to perform classification and fault location tasks respectively. In all cases the ANNs are multi-layer perceptron architectures, with

the specific arrangements for each ANN with the hyperbolic tangent sigmoid transfer function used in the hidden layers.

Generally three-layer feed-forward neural networks are used. These are composed of one input layer, one hidden layer and one output layer. More than one hidden layer could be applied in ANNs. By considering the computational time to meet the requirement of a circuit breaker, only one hidden layer is used. In addition, with an extensive series of studies, it is found that one hidden layer is sufficient to cater for the majority of different systems and fault conditions.

The main tasks for the ANNs are to detect the occurrence of fault on the DC transmission line, and to clearly distinguish the fault types (positive pole-to-ground fault, negative pole-to-ground fault, and pole-to-pole ground fault). Another objective is to locate the point of fault.

5.4 Signal chain

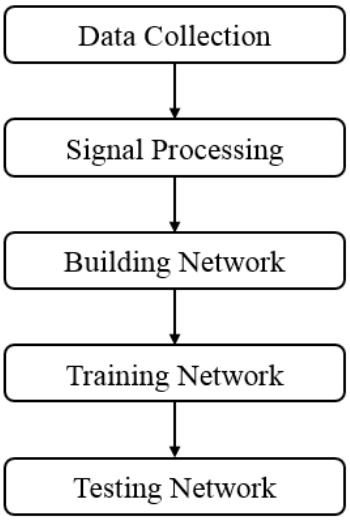

Fig. 5-5 Basic flow chart for ANN design

As proposed in [111], the frequency spectrum of voltage and current contain useful information for protection purposes. The authors in [8] indicate that much of the frequency spectrum combined with an ANN may be used for fault detection and fault location. Hence, the higher frequency components are selected and fed to

suitably-designed ANNs in this work. A comprehensive ANN-based transient protection scheme that accurately and quickly detects, classifies and locates faults on HVDC and MTDC overhead lines is presented. The scheme is shown to have improved performance over previously used protection techniques, such as robustness to high impedance and close-up faults and excellent discrimination of external faults. The process for designing neural networks is expressed in Fig. 5-5.

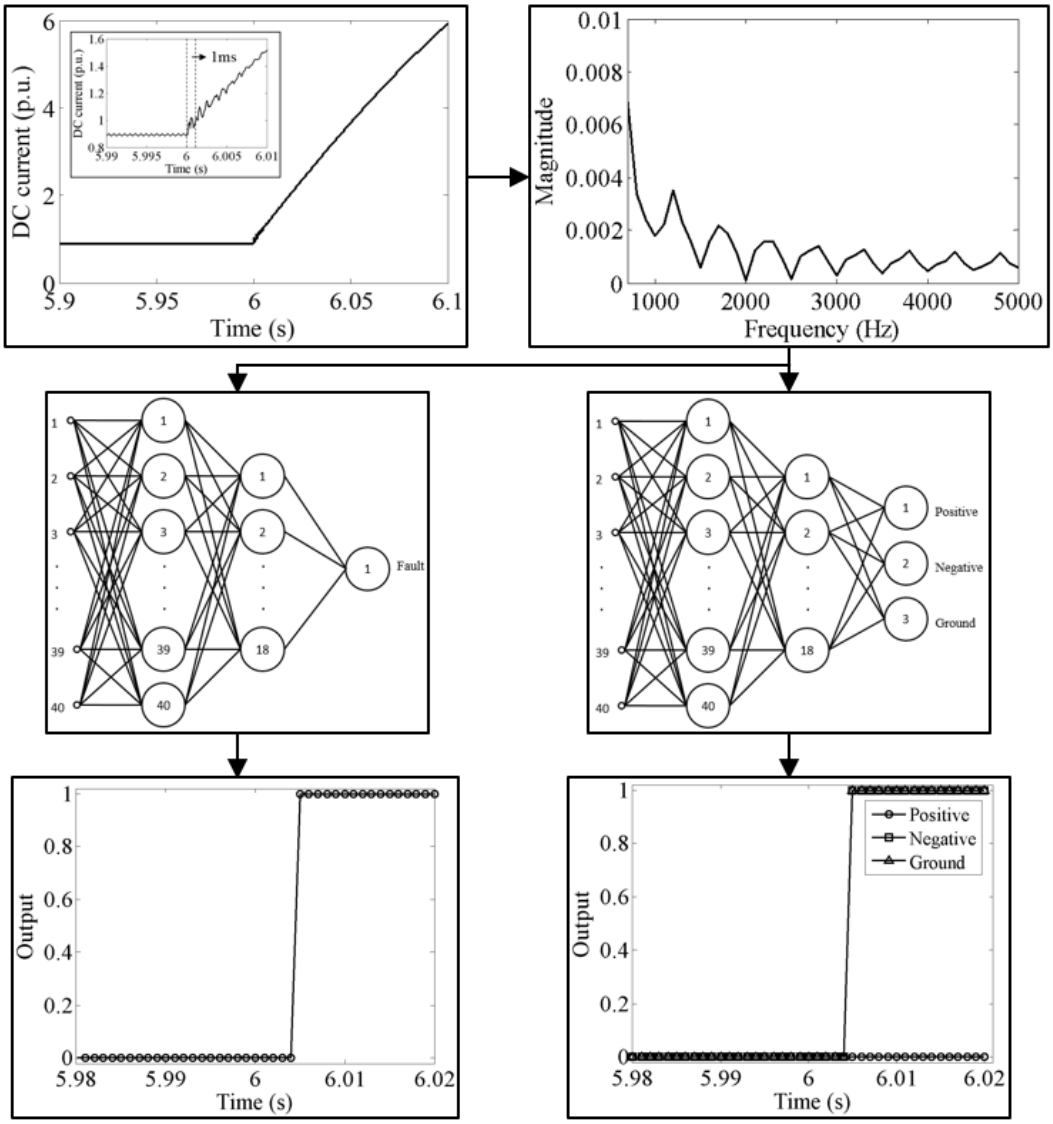

Fig. 5-6 Signal chain for fault detection and classification

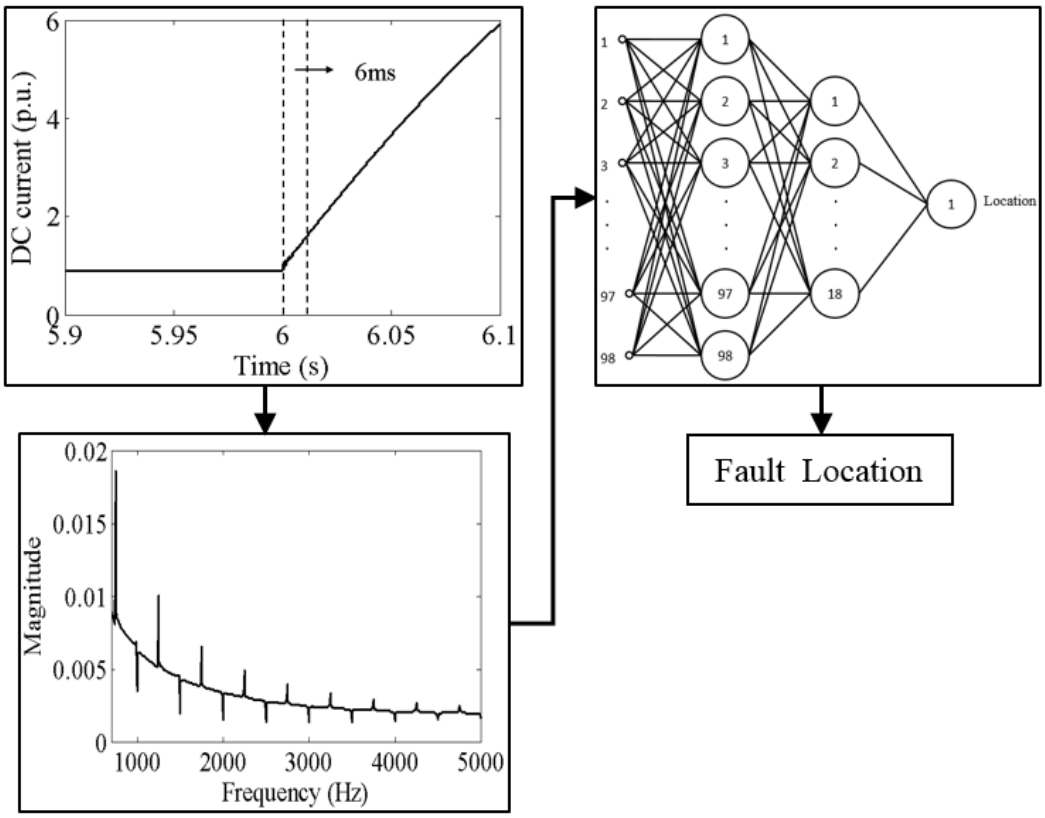

Fig. 5-7 Signal chain for fault location

The fault current signals are generated from the PSCAD model described in Chapter 4. MATLAB was used in signal processing and network training. An overview of the signal chain is presented in Fig. 5-6, for fault detection and fault classification, and Fig. 5-7 for fault location. Firstly, a time series is generated by the digitally sampled current transducer signal. An FFT is applied on the windowed signal to create the input data for the ANN. A counter is then applied to the ANN to generate the diagnostic signal. Each stage is discussed in detail in forthcoming sub-sections.

5.5 Signal processing

The most common approach is using some form of windowed frequency transform on the incoming waveforms for feature selection, and coupling this to an AI method such as ANNs. Any signal can be represented as a time varying amplitude that has a corresponding spectrum. Generally, the frequency spectrum can clearly show harmonics, which are visible as distinct spikes or lines at a particular frequency [112]. Compared with the time-domain signal, the magnitude versus frequency is

more important in this method. The transformation of data between time domain and frequency domain is required. Current versus time representation becomes magnitude versus frequency and phase versus frequency representation that gives enough information for ANN achievement.

The frequency information is generally used for fault diagnosis. In order to obtain this frequency information from the frequency domain, digital signal processing is a mandatory process. For fault detection, classification and location proposes, the transient signals are analysed to extract useful features. The Fourier algorithm is one of the most popular algorithms used for a variety of measurements in control and protection applications [113]. The FFT is a traditional approach for transferring signals from time domain to frequency domain. However, the time domain information is missing through FFT analysis. Hence, an improved technique the Short Time Fourier Transform (STFT) is developed to localise and approximate the signals in both the time and frequency domain to varying extents. There are also some drawbacks in STFT which require a compromise between the resolutions of time domain and frequency domain. The windowed Discrete Fourier Transform (DFT), implemented using the computationally efficient FFT algorithm, is a well-established method for isolating frequency components of a signal, and thus used in a variety of real time control and protection applications [113]. DFT is a suitable option for transient signal analysis. The discrete wavelet transform has the advantage of varying time and pseudo frequency resolutions, and therefore some ANN-based fault detection and fault location algorithms have made use of wavelet transforms but selection of the correct mother wavelet is vital.

The FFT is a more computationally efficient version of the Discrete Fourier Transform DFT [114]. By considering all these approaches, the windowed FFT is selected in the signal processing stage to generate the frequency vs magnitude vs time waveforms. Extensive studies have shown that an adequate representation of frequency domain information can be obtained by an FFT with a very short window length [95]. This leaves more computational time for the rest of the relaying scheme so that the DC circuit breakers can operate within the overall protection time budget.

The data used in signal processing is DC side current data which is detected by the

DC current transformer installed at both ends of the line. The signals are constantly windowed; sliding this window along, a vector of frequency bands that change with time will be obtained. The simulation results of the fault current and fault voltage in both the time domains and frequency domains are discussed extensively in Chapter 4. Because of the characteristics shown by the signals from the frequency domain, the current signals generated from the system will be analysed in the frequency domain for use as the input signal for the ANN-based method. Extraction of the features in the time series is, therefore, performed by the FFT of a moving window.

Analysis of these transient signals using the FFT is an effective way to analyse the features generated by the fault. The complex amplitude is represented by equation:

$$F(\omega) = \frac{1}{N}\sum_{t=0}^{N-1} f(t)\, exp\left(\frac{-j2\pi\omega t}{N}\right) \tag{5.3}$$

where: $F(\omega)$ returns the spectral component or harmonic, $f(t)$is the signal sample sequence, $N$is the number of sample values in each period of the signal. $\omega_N = e^{\frac{-j2\pi\omega t}{\mathrm{N}}}$ is an Nth of root of unity. The variance of the time domain data $f(t)$ can be described by frequency spectrum into spectral components over the frequency domain.

In the feature selection stage, the incoming time series fills a buffer, the buffer undergoes a Hann windowing function (to minimise spectral bias), the FFT of this window is computed, and then the buffer is moved on by one sample and the process is repeated. The Hann window takes the form of (5.4) [114].

$$w(n) = 0.5\left[1.5 - \cos\left(2\prod\frac{n}{N}\right)\right], 0 \le n \le N \tag{5.4}$$

An example Hann window is shown in Fig. 5-8.

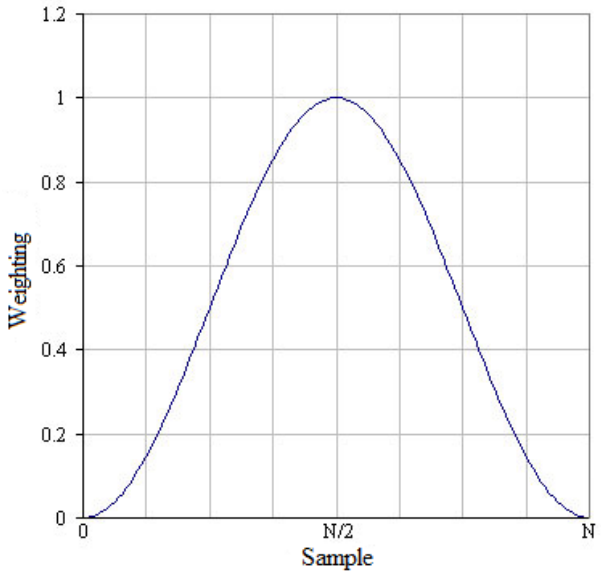

Fig. 5-8 Hann window function

Because the fixed signal is detected in the system, the time dependency would be a constant. Hence, the magnitude of the frequency spectrum lies on the frequency band and the distance. It can be noticed that the magnitude value is closely related to the travelling wave arrival time which leads to the peak magnitude of the frequency.

To be more specific, the current signals have been generated based on the power system studied under different situations such as various fault locations, various fault resistance, etc. For a more robust protection scheme, many situations are considered in the simulations. With the help of the FFT analysis, irrespective of the different types of faults considered herein, there are always some specified peaks corresponding to different fault locations on fault occurrence. These are the very important common features that can be made use of to detect the fault and locate the fault.

The complex and trigonometric forms are related through the magnitude and phase angle. Following the windowed FFT on signal $f(t)$, the complex amplitude is represented by $F(\omega)$ which returns the spectral components. The real parts of $F(\omega)$ are then used to indicate the magnitude at different frequencies in the windowed signal to produce a frequency spectrum. The phase information from the imaginary part of the FFT is discarded.

Take the fault on section 1, 30% away from terminal 1, as an example. The phase of the signal vs frequency results are shown in the following figures under different conditions. The faults are simulated as positive line-to-ground faults (Fig. 5-9), negative line-to-ground (Fig. 5-10), positive line and negative line faults (Fig. 5-11) and steady-state condition (Fig. 5-12).

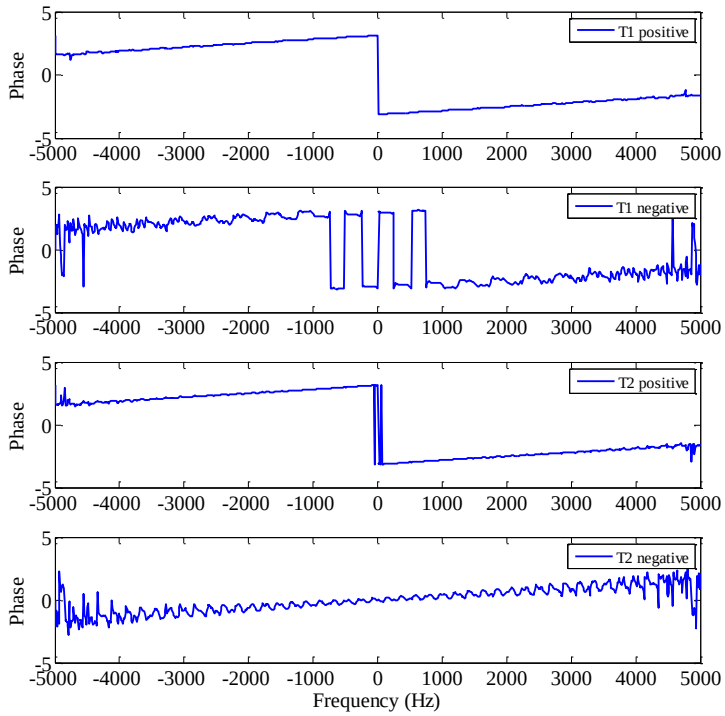

Fig. 5-9 Positive line-to-ground fault

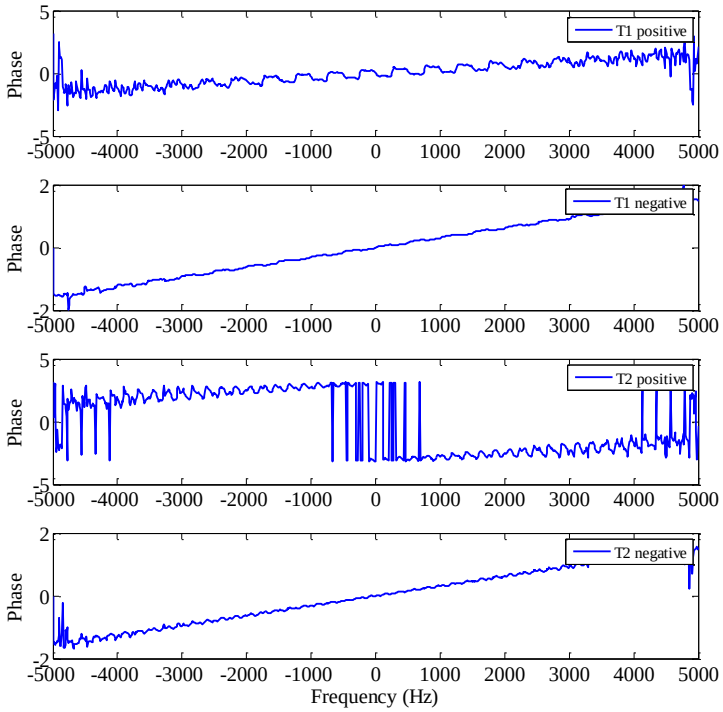

Fig. 5-10 Negative line-to-ground fault

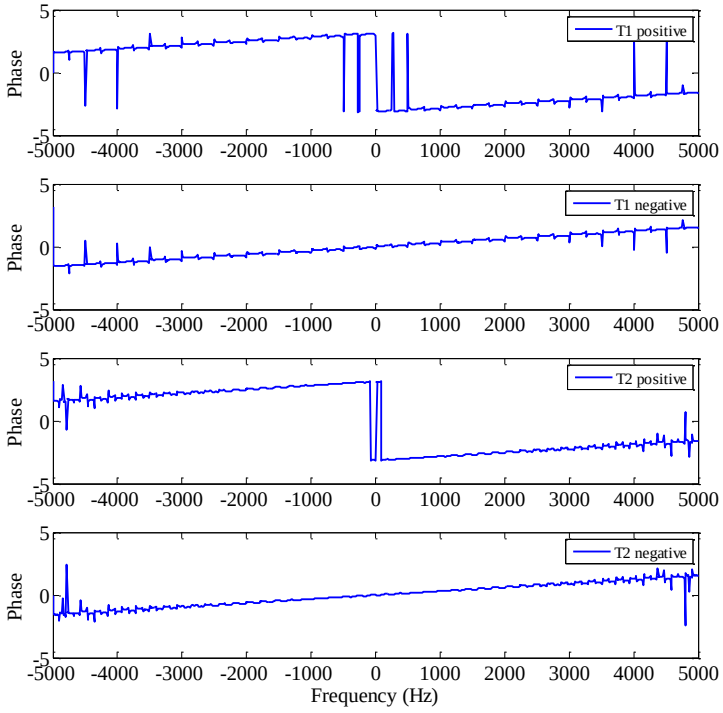

Fig. 5-11 Line-to-line fault

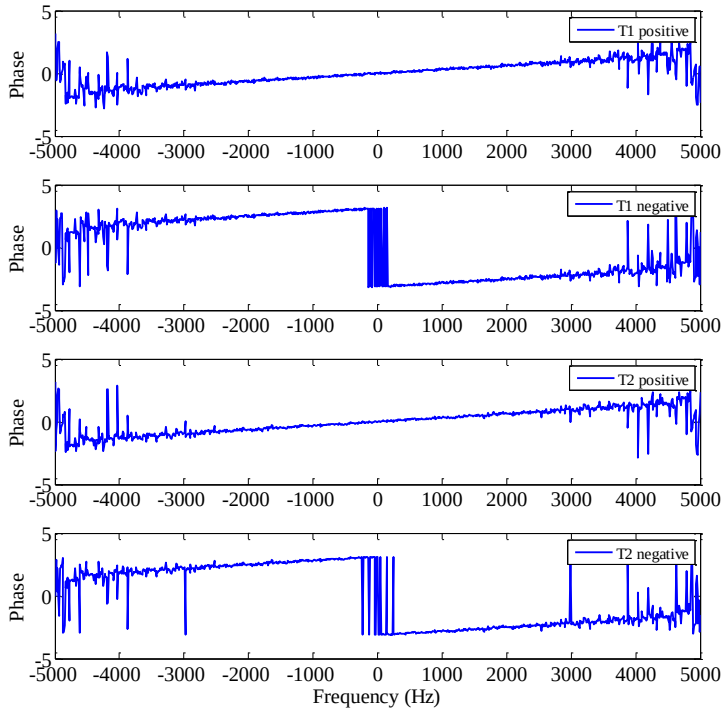

Fig. 5-12 Steady-state condition

According to the phase aspect analysis of the signals, the shape of the figure is fixed under specified conditions, as is concluded in Table 5-2.

Many high frequency components can be detected by analysing the transient signal in the frequency domain because the travelling wave, which is an abrupt signal, is contained in these detected transient signals. Through FFT analysis the feature can be generated by the magnitude aspect to distinguish the faults under different locations and with different resistances.

Table 5-2 Phase analysis under different fault conditions

Fault types	T1 positive	T1 negative	T2 positive	T2 negative
Steady-state				
Positive ground				
Negative ground				
Line-line				

Here use the signal detected from terminal 1 as an example (Ip1). The results show the frequency spectra with varying fault locations under a specified fault resistance. The window length of the signal is 10 ms. The FFT waveform at different fault locations is shown in Fig. 5-13 for 0.01ohms fault resistance and Fig. 5-14 for 2 ohms fault resistance.

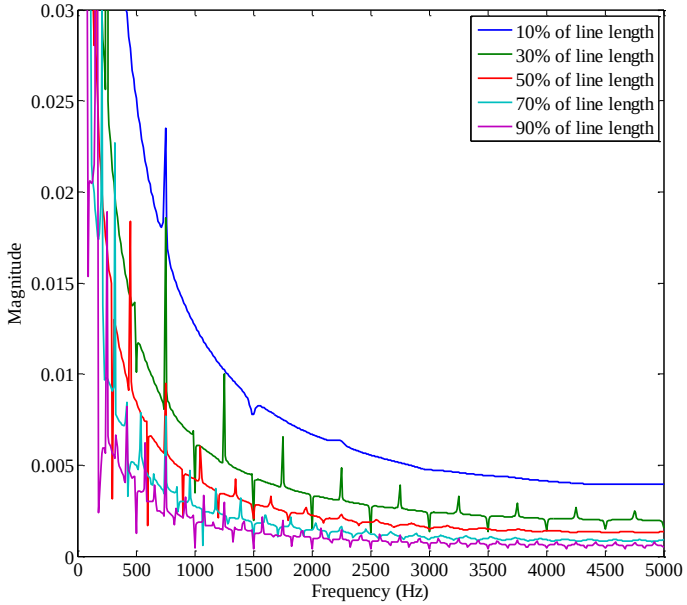

Fig. 5-13 0.01 ohms FFT magnitude at different fault locations

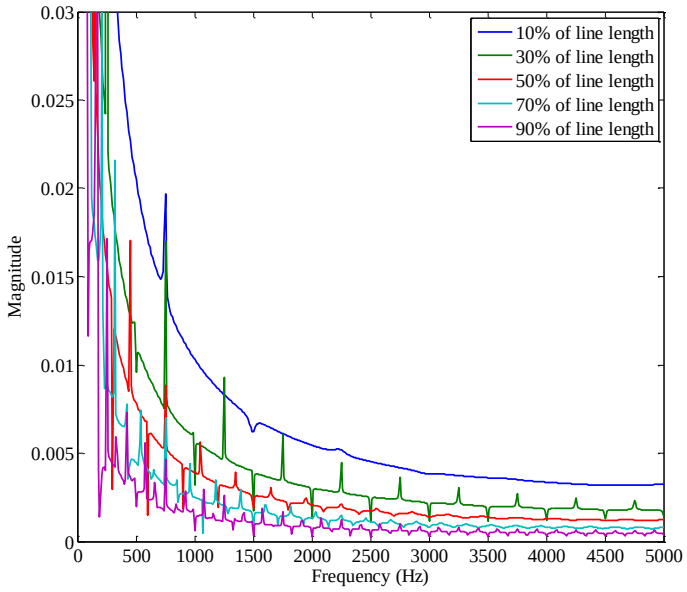

Fig. 5-14 2 ohms FFT magnitude at different fault locations

Take the fault on section 1, 30% away from terminal 1 as an example. The FFT waveform with different fault resistance is shown in Fig. 5-15 with 30% of the line length and Fig. 5-16 with 50% of the line length.

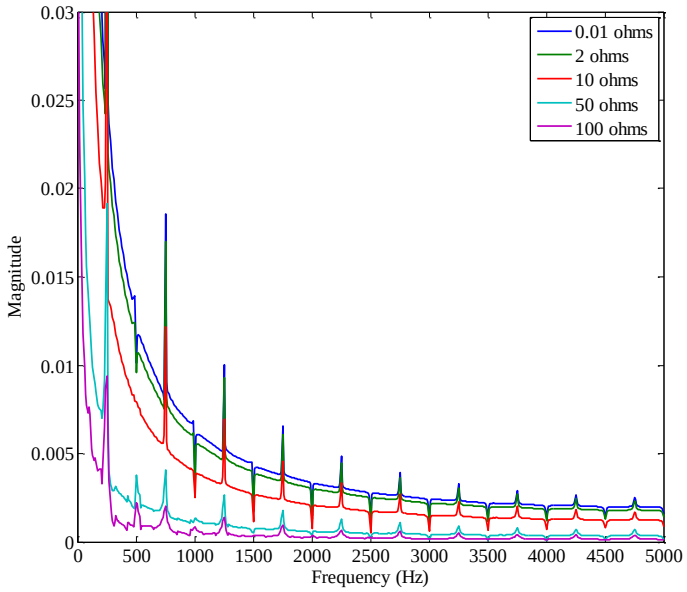

Fig. 5-15 30% fault location FFT magnitude with different fault resistance

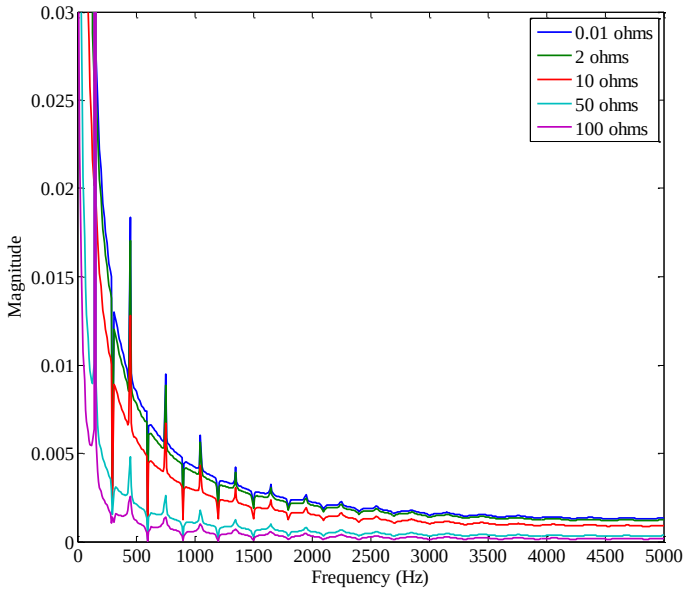

Fig. 5-16 50% fault location FFT magnitude with different fault resistance

Fig. 5-13, Fig. 5-14, Fig. 5-15 and Fig. 5-16 show the analysis of frequency spectra generated by the fault current signal. As can be observed in the frequency spectrum generated from signal processing above, the relationship between the features and fault location or fault resistance are clearly presented. The features specified frequency spectrum varies with fault locations but not fault resistance. Hence, the

features can be used for fault location in the designed protection scheme.

Both the features can be detected from both the two-terminal HVDC system and multi-terminal HVDC system. Even though the DC current and voltage will be influenced during a fault on the other line, the characteristic frequency will only exist on the faulted line.

To be more specific, the current waveforms have been generated based on the power system studied under different situations such as with various fault locations, various fault resistances, etc. Therefore, more situations are considered in the real simulation work. The signal processing results from FFT analysis then become inputs into the ANN for the final decision making in the scheme.

5.6 ANN training cases

There are certain parameters that affect the faulted transient response of the HVDC systems. The fault types, fault location on the transmission line and fault path resistance are the three main factors that should be considered. The investigation concluded that still some other factors had some bearing on the fault signatures, but these were less important than other parameters, and significantly, those that were unknown pre-fault. Hence, the training cases were chosen to reflect the three factors – fault types, fault location and fault resistance.

A multilayer perceptron neural network with the back-propagation learning strategy was applied in fault detection and fault classification. Even though a back-propagation learning strategy is inherently slow in learning, a back-propagation algorithm can provide a very compact distributed representation of complex data for a large training set. The back-propagation algorithm has been chosen as the ideal topology using the Levenberg-Marquardt (trainlm) optimisation technique which brings about significant enhancement of the algorithm performance. In this study, a three-layer feed-forward network with sigmoid hidden neurons and linear output neurons (fitnet), can fit multi-dimensional mapping problems arbitrarily well, given consistent data and enough neurons in its hidden layer.

Normalisation or scaling is usually used in ANNs to learn; it helps significantly when the activation function is Sigmoid. It transposes the input data into the range that the sigmoid activation functions lie in. The input vectors were normalised between 0 and 1 using the maximum and minimum values encountered in the training data for each frequency band, such that 1 was the maximum and 0 was the minimum (i.e. logistic $[0, 1]$). The ANN was trained using backpropagation to produce an output vector of 1 or 0 depending on the type of fault, where '0' represented a heathy signal and '1' represented the fault signal. The transitionary case in which the window captures part healthy and part faulted conditions was not used because of the ambiguity this presents in how the neural network should be trained. The equation for data normalisation in the range 0 to 1 can be found in (5.5). The X_{max} and X_{min} were selected to be the maximum and minimum magnitudes for all the training waveforms.

$$X_i = \frac{X_i - X_{min}}{X_{max} - X_{min}} \tag{5.5}$$

The technical computing environment MATLAB was used for signal processing and neural network design. The sampling frequency of 10 kHz, which translates to 200 samples per 50 Hz AC cycle, was found to be a sufficient compromise between fault location accuracy and providing enough time for the overall relaying speed of the scheme.

5.7 Counter

At the end of the signal chain, a counter, which prevents false trips on account of noise or transitionary conditions, was applied for fault detection and classification to give a stable response. The criteria for distinguishing non-faults (including external faults) and faults were based on the ANN output '0', '1'. However extensive series of studies have shown that, from a practical point of view, the optimal thresholds are applied for clearly distinguishing fault. If the output is less 0.2, then reset output to be 0, indicating non-fault. If the output is greater than 0.72, then reset output to be 1, indicating fault. Specifically a trip signal 1 is generated after 10 consecutive ANN outputs higher than the threshold of 0.8. The counter is

reset if the output falls below the threshold. This process can highly improve the robustness of the system.

5.8 Chapter summary

This chapter has summarised the application of artificial intelligence. By introducing the elementary knowledge of artificial intelligence and artificial neural networks, the ANN-based method is selected to be an appropriate approach for fault detection, classification and location for HVDC systems. The review of applications for ANN in power systems especially for fault diagnosis is given. Finally, the topology of a neural network is introduced to give the best solution in this project. This chapter also presents a new comprehensive approach designed to detect faults on transmission lines, classify fault types and locate the exact fault locations using current data from one end only based on FFT analysis and ANN technique. The frequency components from fault current signals are input to specially trained ANNs. Fault current signals were detected on all terminals in order to create frequency spectra, giving insights into the characteristic frequency components contained within the signal. Through this verification process the proposed method have been tested in a two-terminal HVDC links and a multi-terminal HVDC system, which are introduced in the following two Chapters.

6 ANN-based Fault Detection and Location on HVDC Systems

6.1 Introduction

Based on the methods and techniques presented in the previous chapter, this chapter describes a novel fault detection and fault location scheme using current signal data from only one end of a transmission system to realise the overall power system protection scheme for the HVDC system modelled in Chapter 4. The ANN training cases are presented for ANN detection and fault location. The results and discussion are presented at the end of the chapter.

6.2 ANN training cases for HVDC system

Because a monopole two-terminal HVDC network was modelled, only the pole-to-ground fault may happen on the DC transmission line. Hence, only fault detection and fault location were accomplished in the scheme. Apart from the fault types, the fault location and fault resistance are the two main factors that should be taken into consideration in the ANN training process. The fault resistance depends on how the fault is caused. Technically, there is no upper limit for fault resistance; high impedance faults are much less damaging in terms of fault current so are not considered in this work [114]. Therefore, the fault resistance was varied in the following discrete steps at 0.01, 2, 10, 50 and 100 Ω. One of the objectives of the proposed method was fault location, hence, the location of fault is the most essential parameter. In addition, the features generated were determined by the fault locations. Hence, 10%, 30%, 50%, 70% and 90% of the line length were chosen in the training cases. In conclusion, a total of 35 fault scenarios were considered, (25 DC line fault cases and 10 external fault cases). Of the fault scenarios, the training contained 10 healthy signal windows and 20 post fault input windows. Therefore, 350 fault cases have been taken into consideration. Because the model is a single-pole HVDC system, only the fault detection and fault location were applied. The training data

was split into 70% training samples, 15% validation samples and another 15% testing samples.

6.2.1 Fault detection

Fault detection is the first step in the protection scheme. The main task is to accurately detect the internal fault from the external faults. For HVDC systems, the requirement for HVDC system protection is to distinguish a DC transmission line fault from an external fault including the AC side fault and converter station fault, as well as to distinguish the DC fault from the adjacent lines.

A window of length 1 ms was applied to capture DC current signals for fault detection. In the proposed fault detector, 20 frequency bands from each signal in the range 2800 Hz to 4700 Hz, each approximately 95 Hz in width, showed the best performance used as ANN input. Thus, in total, each ANN had an input layer of 20 neurons of DC current. Fig. 6-1 shows the configuration of ANN 20-12-1 (20 neurons in the input layer, 1 hidden layer with 12 neurons in it and 1 neuron in the output layer) for fault detection.

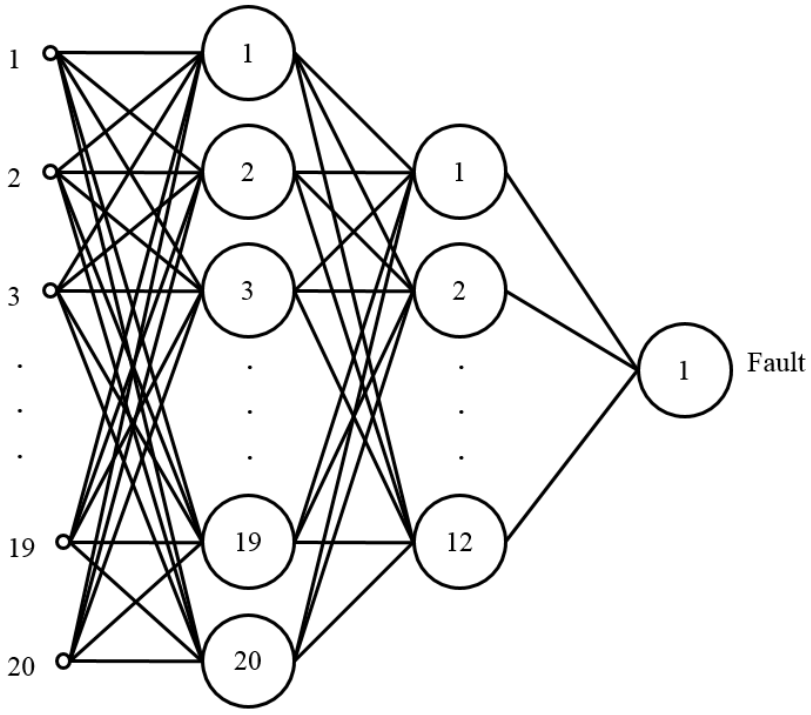

Fig. 6-1 ANN for fault detection

Through a series of tests and modifications, it was found that the ANN presented in Fig. 6-1 gives near optimal performance for this particular application. It is a three-layered network which consists of 20 inputs in the input layer, 12 nodes in the hidden layer and 1 output in the output layer; 20 inputs represented the magnitude of FFT decomposition of the DC fault current; 1 target output demonstrated whether a fault was included in the network. '1' implies a fault in the system and '0' signifies otherwise. In the fault detector, an external fault was treated as no fault on the transmission line, which was implied by '0'. The DC transmission line fault was represented by '1'. Hence, DC transmission line faults can be detected effectively. The examples of input and output are shown in Fig. 6-2 and Fig. 6-3 respectively.

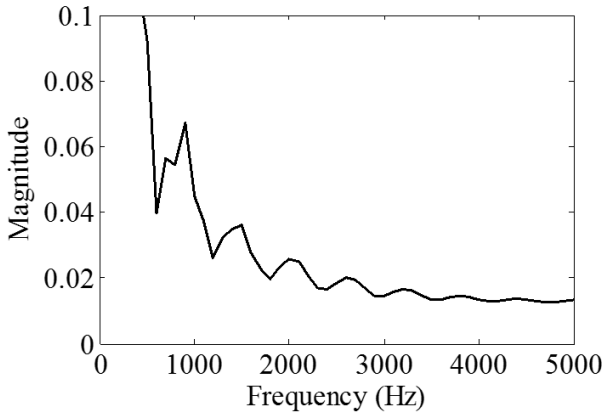

Fig. 6-2 Example of inputs

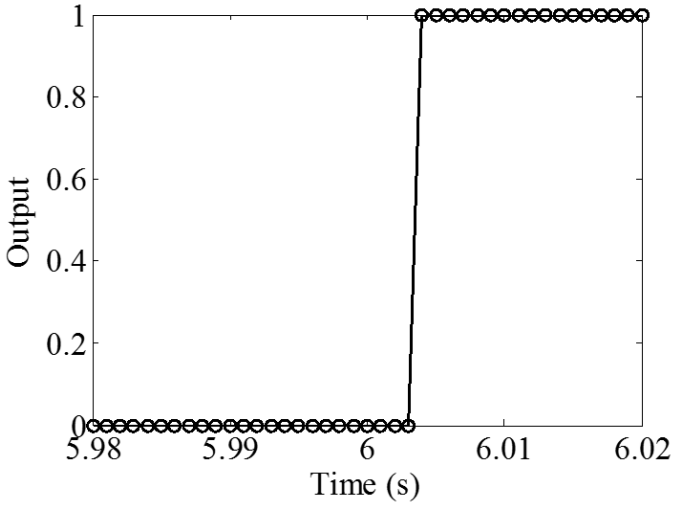

Fig. 6-3 Example of target outputs

The overview of the ANN training is shown in Fig. 6-4 and the regression can be found in Fig. 6-5.

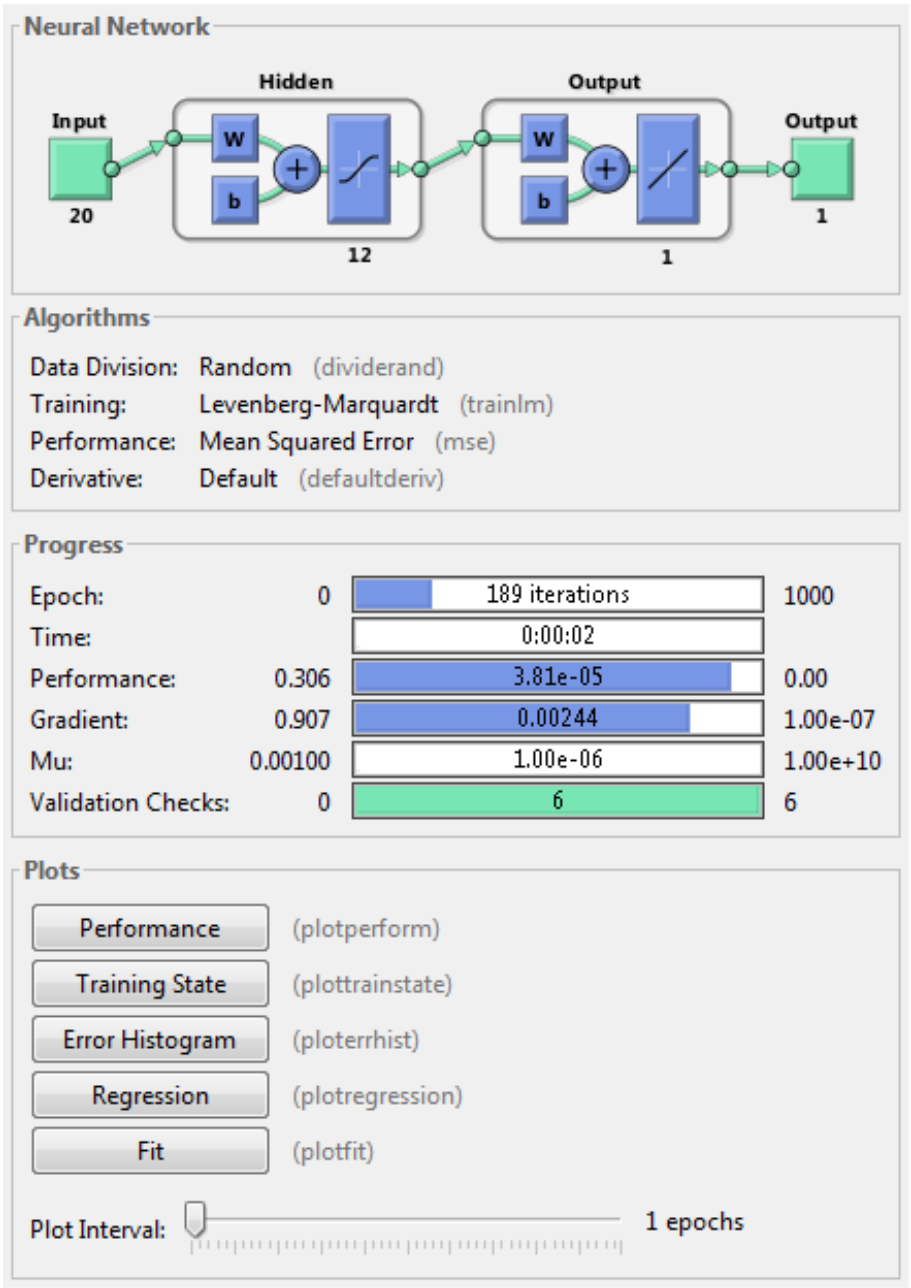

Fig. 6-4 Overview of the ANN training for fault detection

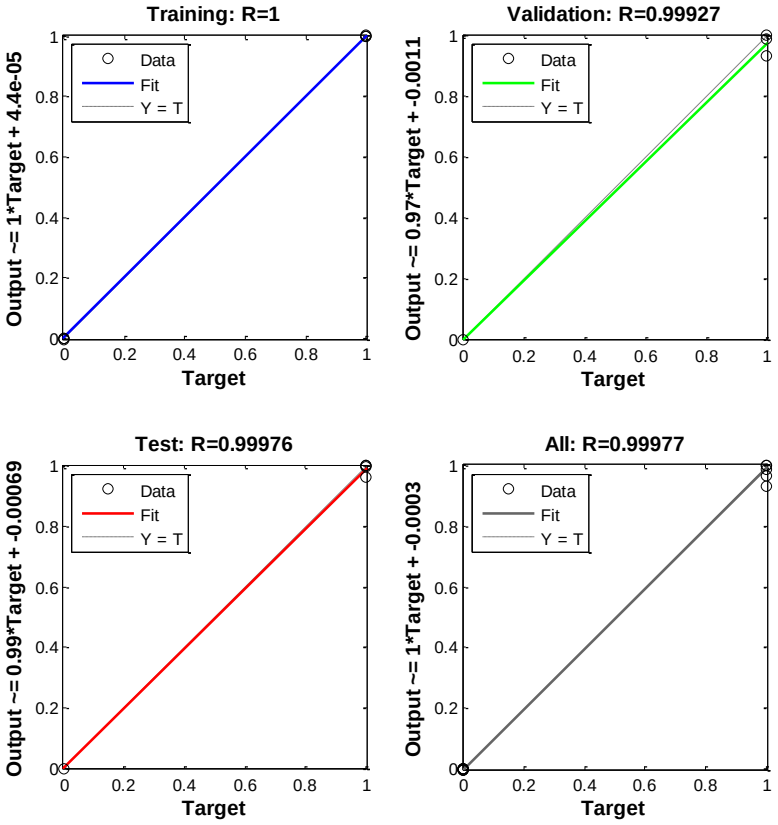

Fig. 6-5 Regression fit for the outputs and targets for the network

For fault detection, the number of epochs is 139. The correlation coefficient is a parameter to measure the target tracking ability in the outputs (0 means no correlation and 1 means complete correlation). The correlation coefficient in this case has been found to be 0.99977 which manifests excellent correlation. The dotted line in the figure indicates the ideal regression fit and the blue (training), green (validation), red (test) and grey (all) solid lines indicate the actual fit of the ANN. It can be seen that both these lines track each other very closely which is an indication of very good performance by the ANN.

Pattern recognition has also been used to test the ANN performance at the fault detection stage by plotting the confusion matrices for the different types of faults. Fig. 6-6 plots the confusion matrix for training, testing and validation. The green cells indicate the cases which have been classified correctly by ANN and the red cells indicate the cases which have been wrongly classified by the ANN. The blue cells indicate the total accuracy of the classification. It can be seen that 100%

accuracy can be achieved in fault detection by the chosen ANN.

Fig. 6-6 Confusion matrices for training, testing and validation phases

6.2.2 Fault location

Fault location is the next step after the fault has been detected in this case. For the fault location ANN, the faulty line current from both ends of the line is required with a 6 ms window length. Thus in total, fault location uses 98 frequency bands between 3.6 kHz and 4.4 kHz, approximately 16 Hz in width, from two terminals (49 input bands). Fig. 6-7 shows the configuration of ANN 49-12-1 (49 neurons in the input layer, 1 hidden layer with 12 neurons in it and 1 neuron in the output layer).

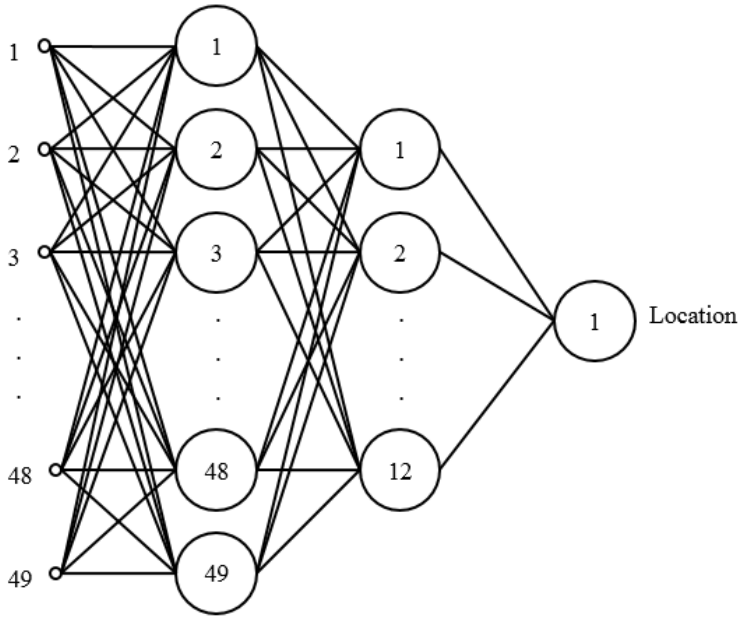

Fig. 6-7 ANN for fault location

A three-layered network, which consisted of 49 inputs in the input layer, 12 nodes in the hidden layer and 1 output in the output layer, was established; 49 inputs which are magnitude of FFT decomposition of the DC fault current; 1 target output was defined as the fault location. The percentage of the line length was limited to between '0' and '1'. The fault location on the tripped transmission line can be measured effectively. The examples of input is shown in Fig. 6-8.

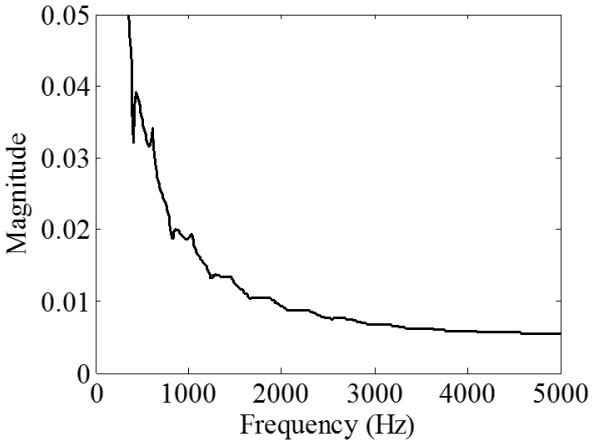

Fig. 6-8 Example of inputs

The overview of the ANN training is shown in Fig. 6-9 and the regression can be found in Fig. 6-10.

The correlation coefficient in this case has been found to be 0.99408 which indicates good correlation. The blue, green, red and grey solid lines meet well with the dotted line indicating the fault locations. The ANN gives a good performance in relation to fault locations.

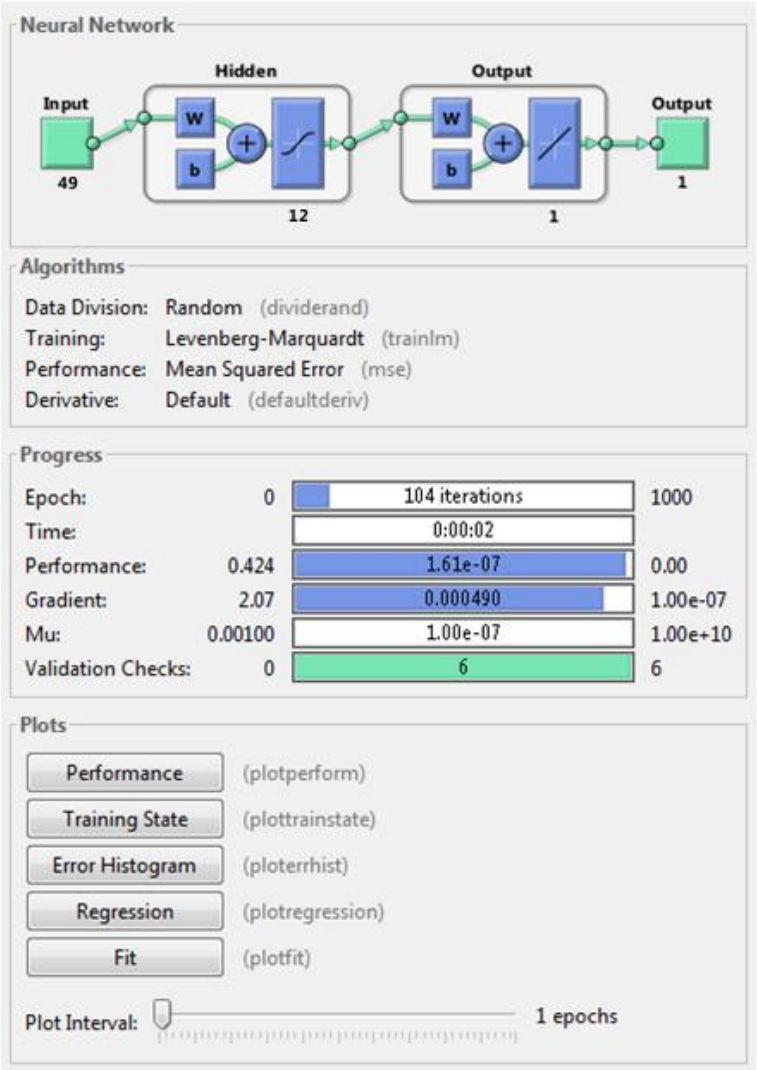

Fig. 6-9 Overview of the ANN training for fault location

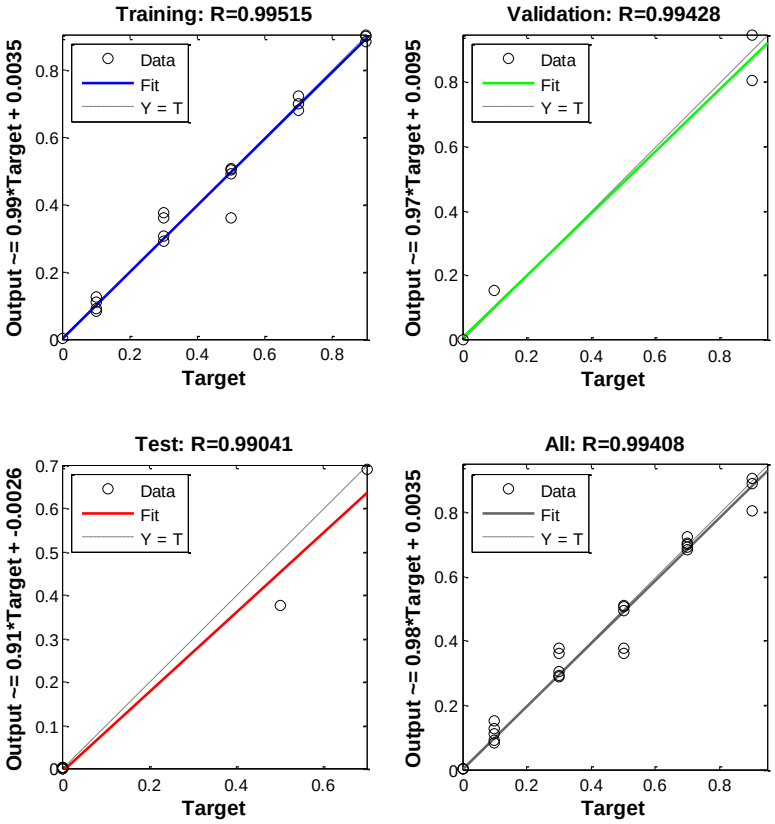

Fig. 6-10 Regression fit for the outputs and targets for the network

6.3 **Results**

Various fault positions were tested respectively. Results in Table 6-1 and Table 6-2 prove the method for fault detection and fault location respectively. It also shows that the scheme accurately predicts the fault occurrence time as well as the fault type.

Table 6-1 Fault detection results

Case	Internal/ external	Fault resistance	Fault location	Fault	ANN output
1	In	0.75	14%	1	0.9649

2	In	4	26%	1	1.0000
3	In	11	38%	1	1.0000
4	In	59	57%	1	0.9981
5	In	32	63%	1	0.9999
6	In	1.8	77%	1	1.0000
7	In	0.3	89%	1	1.0000
13	Ex	0.6	T1	0	0.0000
14	Ex	1.6	T1	0	0.0000
15	Ex	21	T1	0	0.0087
16	Ex	0.9	T2	0	0.0000
17	Ex	2.9	T2	0	0.0000
18	Ex	36	T2	0	0.0000

According to the proposed method, the fault detection and location results are shown in Table 6-1. The accuracy of the fault location method has been evaluated

with (6.1) to calculate the relative error:

$$e = \left|\frac{D_{act} - D_{det}}{L}\right| \tag{6.1}$$

where: D_{act} is actual fault location from the measuring terminal, D_{det} is the detected fault location and L is the total length of the transmission line.

Table 6-2 Fault location results

Case	Internal/ external	Fault resistance	Fault	Fault location	Measured location	Relative Error
1	In	0.75	1	14%	13.70%	0.30%
2	In	4	1	26%	26.82%	0.82%
3	In	11	1	38%	38.65%	0.65%
4	In	59	1	57%	57.74%	0.74%
5	In	32	1	63%	62.73%	0.27%
6	In	1.8	1	77%	77.72%	0.72%
7	In	0.3	1	89%	88.54%	0.46%

Fault detection can be achieved with 100% accuracy using the new ANN-based method. The fault location accuracy can reach 0.83% which is very accurate for

fault location in such a long transmission line.

6.4 Chapter summary

A two-terminal HVDC system was implemented in PSCAD/EMTDC with different types of faults simulated in the DC transmission system. By validating the approach in HVDC system, the generated data are used as ANN training set to build the fault detection ANN and fault location ANN. After the test of these two ANNs, the results show that the proposed method can accurately detect the fault on DC transmission line (reaching to 100%) and the fault location error is as small as 0.83%.

7 ANN-based Fault Detection, Classification and Location on an MTDC System.

7.1 Introduction

This chapter describes how well the proposed ANN-based method works in the multi-terminal HVDC network which is modelled in Chapter 4. The ANN training cases are presented for ANN detection, classification and fault location. The robustness and accuracy of the scheme will be examined under completely different situations in this chapter. The results and discussion are shown in the last part of this chapter.

7.2 ANN training cases for an MTDC system

The training stage used a simulated steady-state condition, external fault condition and fault condition with a thousand scenarios. In order to train all three ANNs, a full range of fault scenarios were considered. Varying fault types, location and fault resistance for many simulation runs produced a comprehensive training set. The study is based on the modelled three-terminal HVDC system; therefore, different sections were considered as well.

Three fault types were considered including pole-to-ground faults (positive pole-to-ground and negative pole-to-ground), pole-to-pole faults and external faults. Therefore, fault resistance was varied in the following discrete steps at 0.01, 2, 10, 50 and 100 Ω. Fault location at 1%, 10%, 20%, 30%, 40%, 50%, 60%, 70%, 80%, 90% and 99% of the line length were chosen in the training cases. The scenarios used included 2 lines, 3 fault types, 11 fault locations and 5 fault resistances so that the variables, shown in Table 7-1, totalled 348 fault scenarios (330 DC line fault cases and 45 external fault cases). Of the fault scenarios, the training contained 5

healthy signal windows and 15 post-fault input windows. In the healthy scenarios, the training contained 30 consecutive windows. Hence, since each window yielded an input vector, training was completed on 6960 input vectors. Because the model was a single-pole HVDC system, only fault detection and fault location were applied. The training data was split into 70% training samples, 15% validation samples and another 15% testing samples. The sampling rate of the PSCAD was 10 kHz, the inverse of the fixed time step of 10 μs.

Table 7-1 Variables

Variable	Details
Fault section	Lines 1 and 2
Fault location	1%, 10%, 20%, 30%, 40%, 50%, 60%, 70%, 80%, 90%, 99%
Fault resistance	0.01 Ω, 2 Ω, 10 Ω, 50 Ω, 100 Ω
External fault	AC side fault at terminals 1, 2 and 3 (single phase, double phase and three phase)

7.2.1 Fault detection

As discussed above, each fault case had its own spectra. The frequency spectra can be expressed as a unique feature for the specified fault location. Because of the complexity of the line, neural network is effective in the protection scheme, giving an effective algorithm to distinguish these different kinds of faults. After comprehensive analysis this was empirically determined to give the best compromise between speed and accuracy for each task. Inputs were taken from standard DC current transducers on only one end and frequencies over 700 Hz of the current waveform were utilised. Inputs were taken from standard current transformers and the band of frequencies between 700 and 5000 Hz of the current

waveform were utilised. The hidden layer consisted of 18 neurons, which gave the best performance.

A window of length 1 ms was applied to capture the DC current signals for fault detection. In the proposed fault detector, 20 frequency bands from each signal in the range 2.8 kHz to 4.7 kHz, each approximately 95 Hz in width, showed the best performance used as ANN input. (Thus, in total, each ANN had an input layer of 40 neurons of DC current, 20 from the positive line and 20 from the negative line).

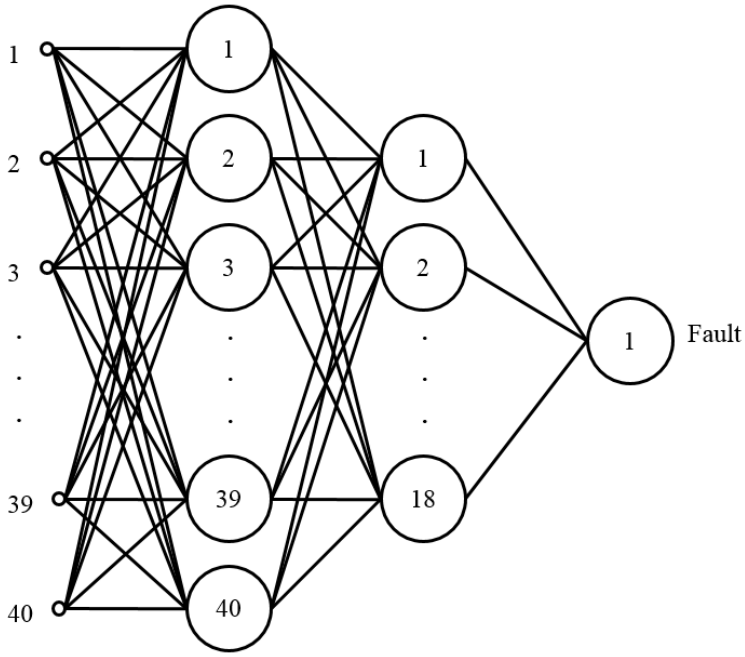

Fig. 7-1 ANN for fault detection

The three-layered network consisted of 40 inputs in the input layer, 18 nodes in the hidden layer and 1 output in the output layer; 40 inputs which are magnitude of FFT decomposition of the DC fault current from both the positive line and negative line; 1 target output demonstrated whether a fault included in the network. The implications of '0' and '1' were the same as for the fault detector in the HVDC system. The DC transmission line faults could be detected effectively. Examples of input and output are shown in Fig. 7-2 and Fig. 7-3 respectively.

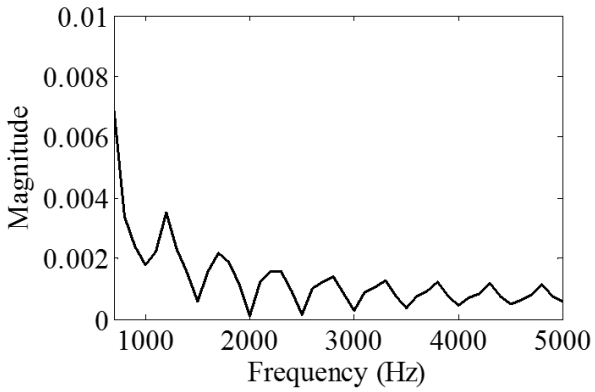

Fig. 7-2 Example of inputs

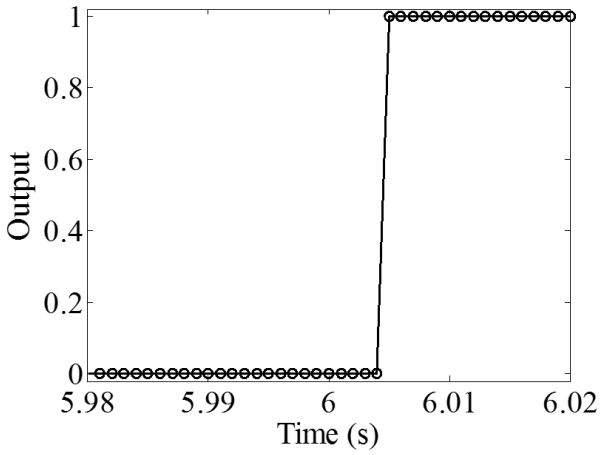

Fig. 7-3 Example of target outputs

The overview of the ANN training is shown in Fig. 7-4 and the regression can be found in Fig. 7-5.

For fault detection, the number of epochs was 260. The correlation coefficient in this case was found to be 0.99995 which indicates excellent correlation, indicating that the fault can be accurately detected.

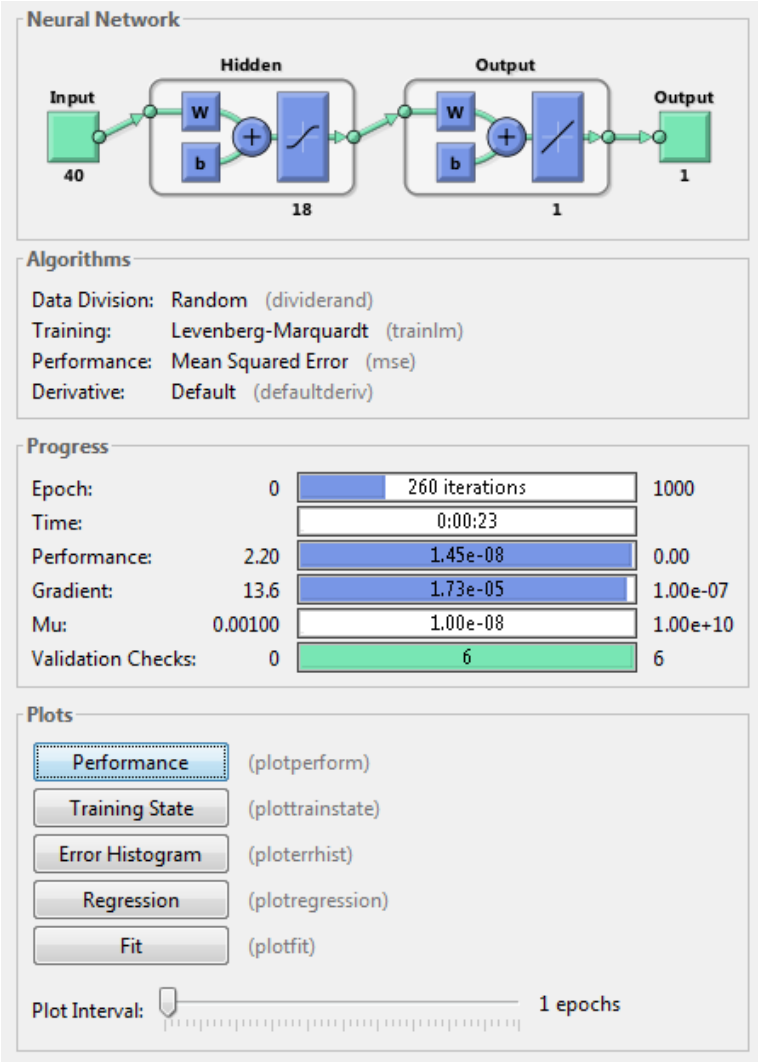

Fig. 7-4 Overview of the ANN training for fault detection

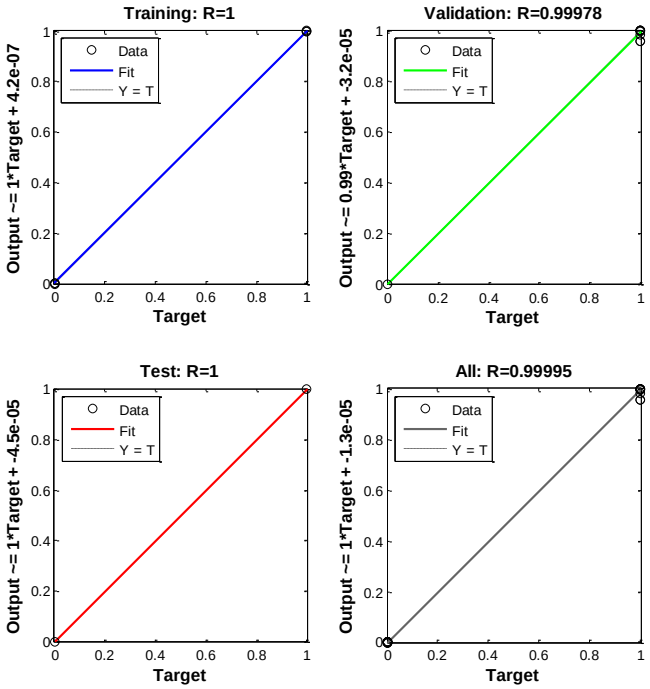

Fig. 7-5 Regression fit of the outputs and targets for the network

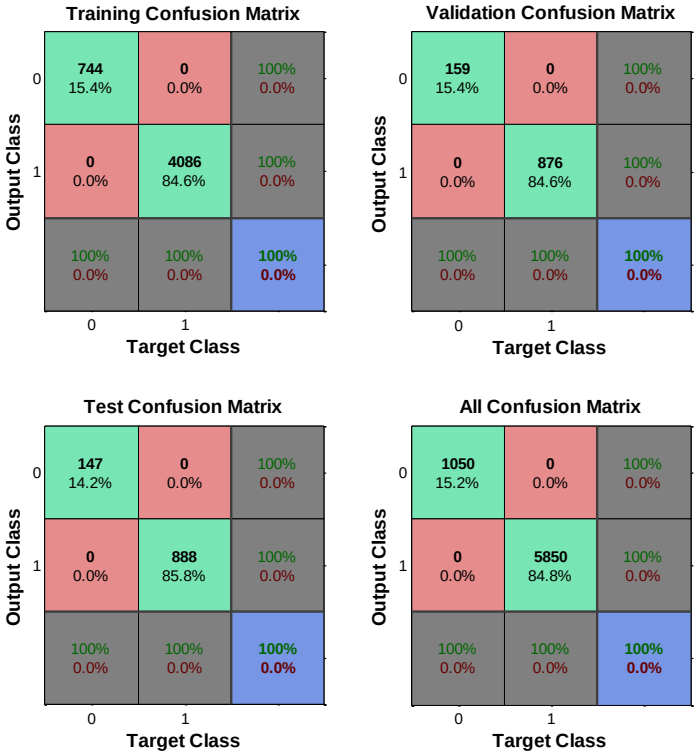

Fig. 7-6 Confusion matrices for training, testing and validation phases

The confusion matrix is also plotted in Fig. 7-6 by pattern recognition. It can be seen that the ANN has 100% accuracy in the validation and test stages for fault detection.

7.2.2 Fault classification

Once a fault was detected on the transmission line, the next step was to identify the fault types. The ANN for fault classification is introduced herein. A window of length 1 ms was applied to capture the DC current signals for fault classification. The fault classification ANN receives an input vector with 40 inputs using the phase information but they worked independently from each other. The neural network for fault classification had 3 outputs, two of them corresponding to the two poles and one output for the ground line. Hence the outputs were either a 0 or 1 denoting the absence or presence of a fault on the corresponding line. P and N denote the two poles of the transmission line and G denotes the ground. Hence the various possible permutations could represent each of the various faults accordingly. Three possible categories of faults could be classified accurately, which are illustrated in Table 7-2.

Table 7-2 Fault classifier ANN outputs for various faults

Fault types	Positive	Negative	Ground
PG	1	0	1
NG	0	1	1
PN	1	1	0

The configuration of the fault classification is shown in Fig. 7-7.

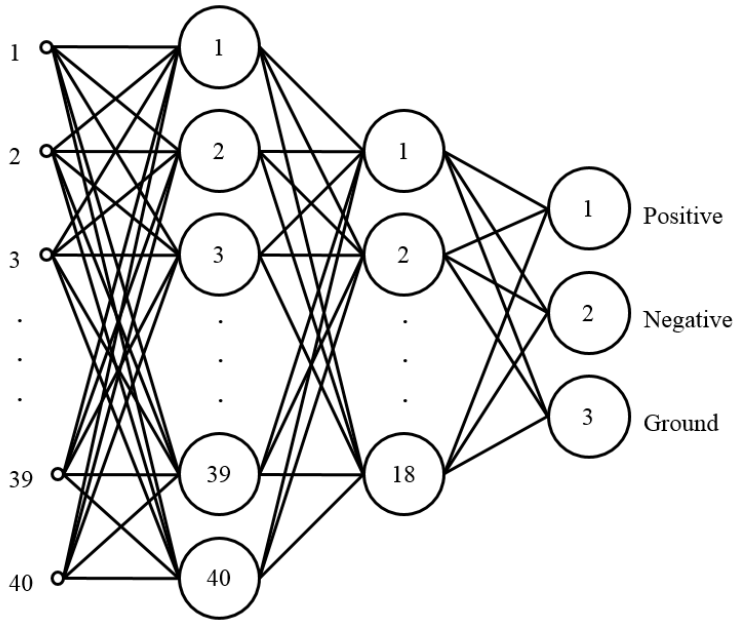

Fig. 7-7 ANN for fault classification

A three-layered network consisted of 40 inputs in the input layer, 18 nodes in the hidden layer and 1 output in the output layer; 40 inputs which are phase of FFT decomposition of the DC fault current from both the positive line and negative line; 3 target outputs are defined to be the fault condition of each of the two poles and one output for the ground line. The examples of input and output are shown in Fig. 7-8 and Fig. 7-9 respectively.

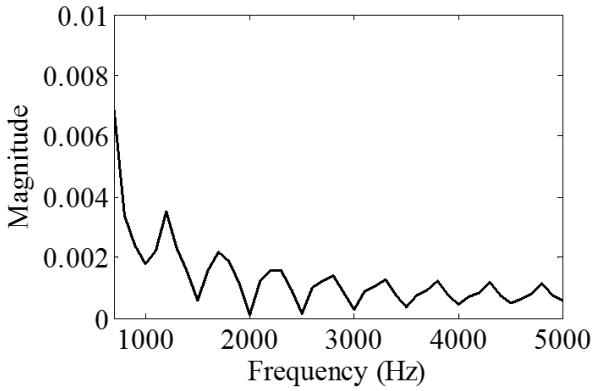

Fig. 7-8 Example of inputs

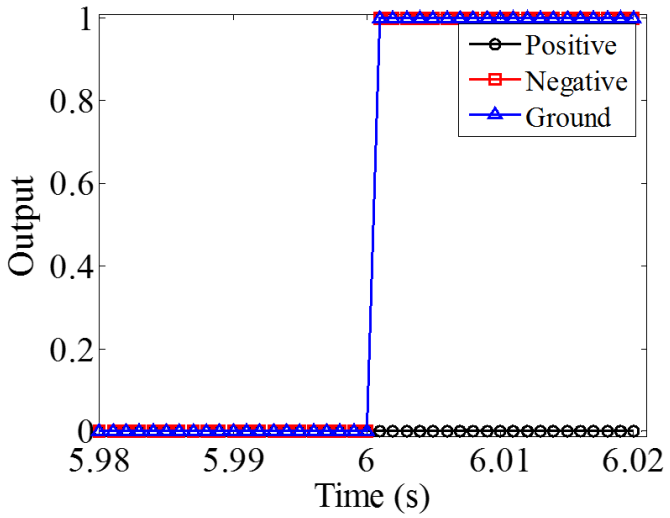

Fig. 7-9 Example of target outputs

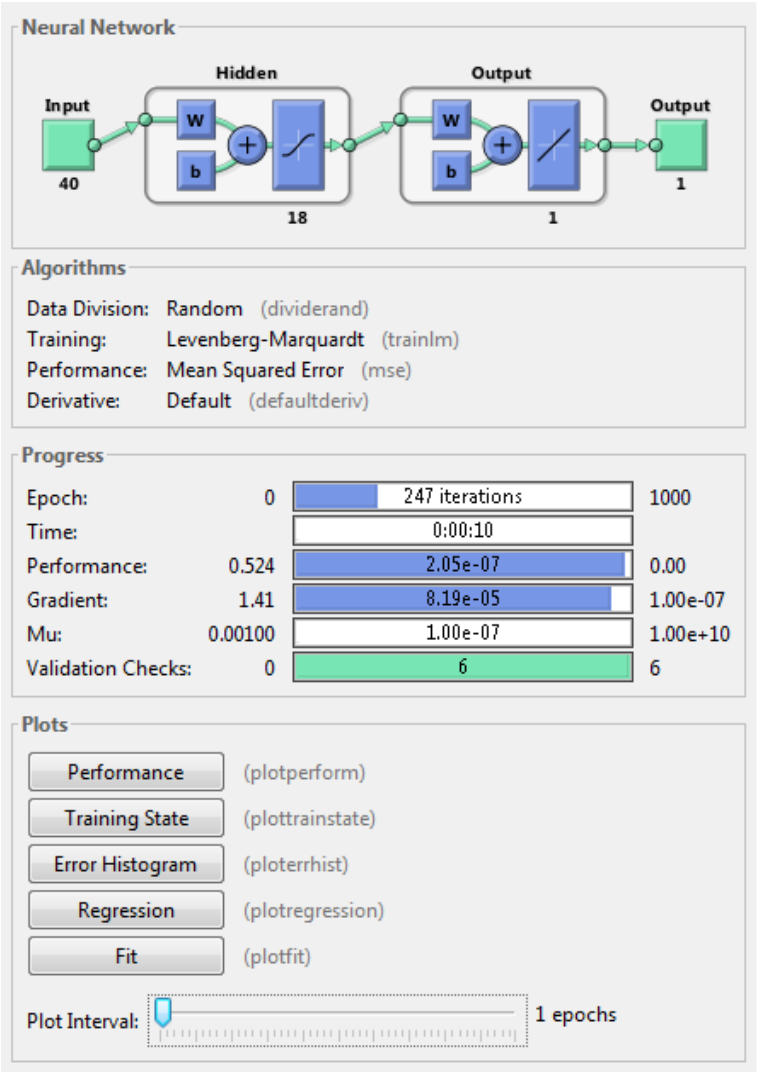

Fig. 7-10 Overview of the ANN training for fault detection

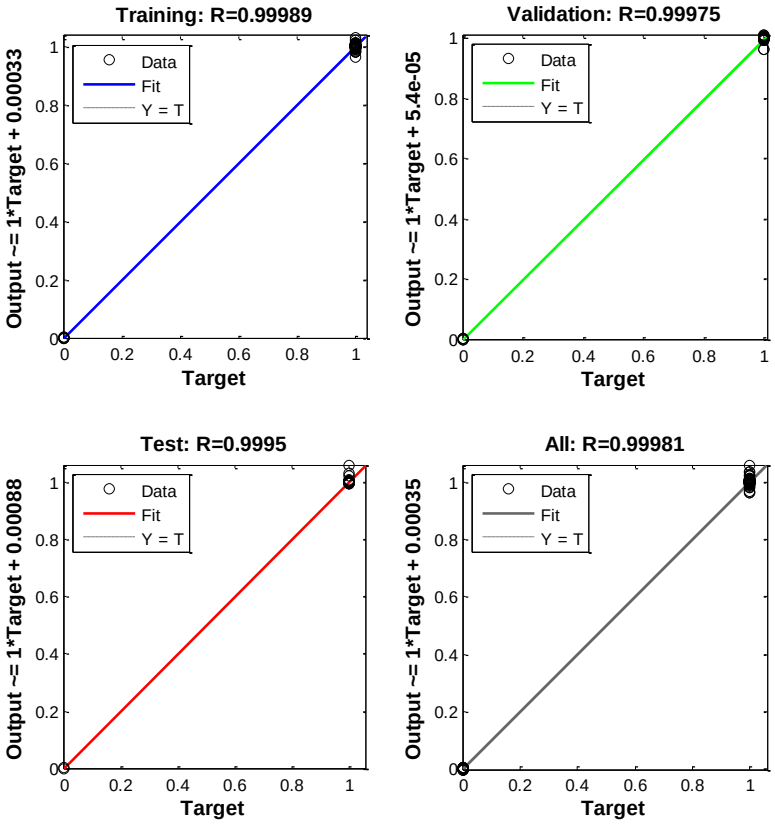

Fig. 7-11 Regression fit for the outputs and targets for the network

Once the ANN was trained, the overview of the ANN training was shown in Fig. 7-10, and the linear regression was plotted in Fig. 7-11 relating the targets to the outputs.

For fault classification, the number of epochs was 247. The correlation coefficient was found to be 0.99981 which indicates satisfactory correlation between the targets and the outputs in this case. The fault location could be found at the point where the solid line meets the dotted line.

7.2.3 Fault location

A 6 ms window was used for fault location. For the fault location ANN (Fig. 7-12), a faulty line current from both ends of the line was required with a 6 ms window length. Thus in total, fault location used 98 frequency bands between 3.6 kHz and 4.4 kHz, approximately 16 Hz in width, from two terminals (49 input bands from

each terminal).

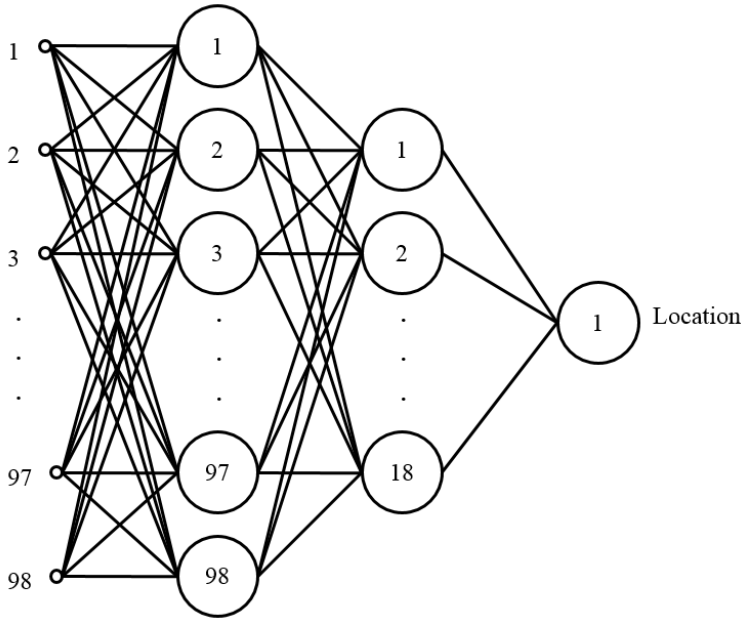

Fig. 7-12 ANN for fault location

A three-layered network consisted of 98 inputs in the input layer, 18 nodes in the hidden layer and 1 output in the output layer; 98 inputs represented the magnitude of FFT decomposition of the DC fault current from both the positive line and negative line; 1 target output represented the fault location. The examples of input and output are shown in Fig. 7-13.

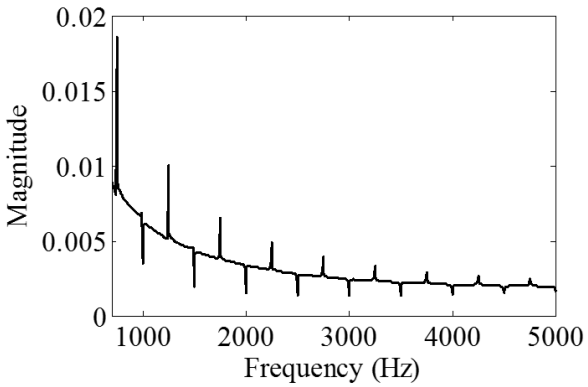

Fig. 7-13 Example of inputs

The overview of the ANN training is shown in Fig. 7-14 and the regression can be found in Fig. 7-15.

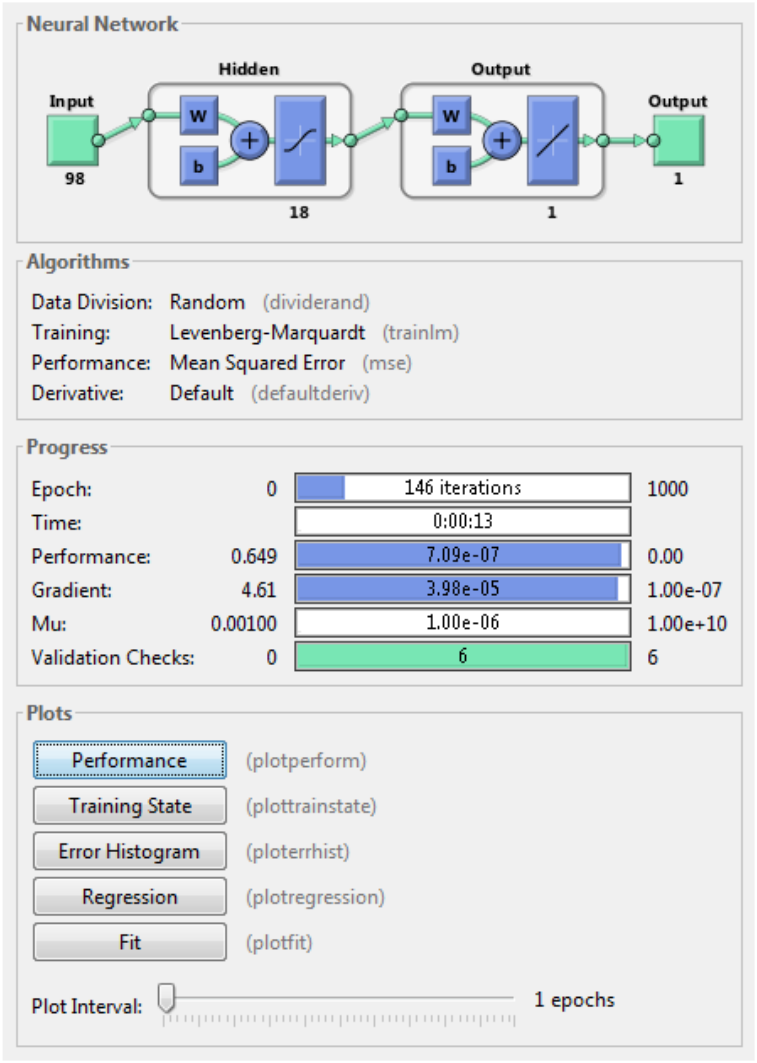

Fig. 7-14 Overview of the ANN training for fault detection

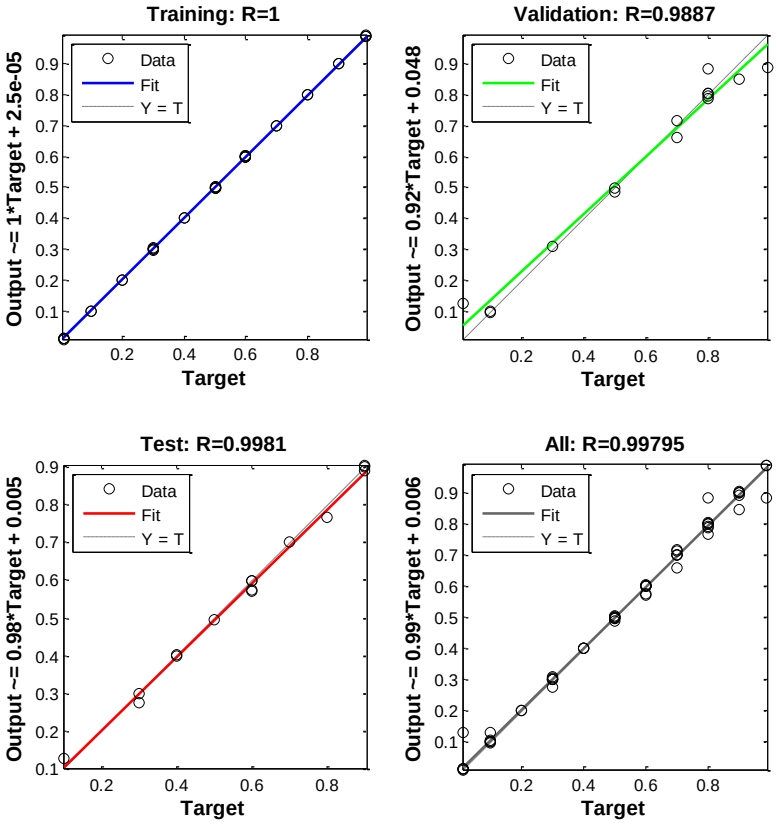

Fig. 7-15 Regression fit for the outputs and targets for the network

The epochs for fault location were 146. The correlation coefficient in this case was found to be 0.99795 which indicates good correlation. ANN gives excellent performance in relation to the fault location.

7.3 **Results**

The protection system was tested with cases not used in the training data, with 15 separate locations and different fault types, such as positive pole-to-ground (PG), negative pole-to-ground (NG) and pole-to-pole (PN). The fault resistance was randomly varied within the limits of the training parameters but values used in training were avoided. The results show that the proposed method can accurately detect, classify and locate these faults with the largest location relative error, calculated by equation (3), being less than 1.16% which is comparable to distance protection. In addition, the results show that the algorithm performs successfully

for a range of fault resistances. According to the proposed method, the fault detection, classification and location results are shown in Table 7-3, Table 7-4, and Table 7-5 respectively.

Table 7-3 Fault detection results

Case	Internal/ external	Section	Type	Fault resistance	Fault location	Fault	ANN output	Detection time (ms)
1	In	S1	PG	0.25	35%	1	1.0000	3.6
2	In	S1	PG	9	67%	1	0.9970	3.7
3	In	S1	NG	69	89%	1	1.0000	3.0
4	In	S1	NG	17	12%	1	1.0000	3.9
5	In	S1	PN	32	34%	1	0.8979	4.5
6	In	S1	PN	1.9	53%	1	0.9992	4.1
7	In	S2	PG	0.33	78%	1	0.9236	3.9
8	In	S2	PG	0.7	58%	1	1.0000	3.6
9	In	S2	NG	8	24%	1	0.9164	4.3

10	In	S2	NG	0.3	46%	1	0.8892	3.9
11	In	S2	PN	1.2	59%	1	0.9886	4.2
12	In	S2	PN	6	72%	1	1.0000	4.1
13	Ex	T1	ABC	0.6	NA	0	0.0000	3.9
14	Ex	T2	AG	1.6	NA	0	0.0000	4.1
15	Ex	T3	BC	1.2	NA	0	0.0000	4.2
16	Ex	T1	AB	0.6	NA	0	0.0972	3.9
17	Ex	T2	BG	1.6	NA	0	0.0126	4.1
18	Ex	T3	AC	1.2	NA	0	0.0000	4.2

Table 7-4 Fault classification result

Case	Internal/ external	Section	Type	Fault resistance	Fault	Fault location	P	N	G	ANN outpour P	ANN outpour N	ANN outpour G	Classification time (ms)
1	In	S1	PG	0.25	1	35%	1	0	1	1.0000	0.0000	0.8930	4.5

2	In	S1	PG	9	1	67%	1	0	1	0.9942	0.0000	0.9968	4.7
3	In	S1	NG	69	1	89%	0	1	1	0.0000	0.9426	1.0000	4.6
4	In	S1	NG	17	1	12%	0	1	1	0.0000	1.0000	0.9527	4.8
5	In	S1	PN	32	1	34%	1	1	0	1.0000	0.8992	0.0000	4.9
6	In	S1	PN	1.9	1	53%	1	1	0	1.0000	0.9751	0.0578	4.9
7	In	S2	PG	0.33	1	78%	1	0	1	0.9427	0.1146	1.0000	4.7
8	In	S2	PG	0.7	1	58%	1	0	1	1.0000	0.0000	0.9538	4.8
9	In	S2	NG	8	1	24%	0	1	1	0.0000	0.9435	0.9727	4.9
10	In	S2	NG	0.3	1	46%	0	1	1	0.0000	1.0000	0.9636	4.9

11	In	S2	PN	1.2	1	59%	1	1	0	1.0000	1.0000	0.0157	4.7
12	In	S2	PN	6	1	72%	1	1	0	1.0000	0,9523	0.0000	4.5

Table 7-5 Fault location result

Case	Internal/ external	Section	Type	Fault resistance	Fault	P	N	G	Fault location	Measured location	Relative error	Location time (ms)
1	In	S1	PG	0.25	1	1	0	1	35%	35.27%	0.27%	15.4
2	In	S1	PG	9	1	1	0	1	67%	65.98%	1.02%	20.5
3	In	S1	NG	69	1	0	1	1	89%	88.65%	0.35%	23.5
4	In	S1	NG	17	1	0	1	1	12%	12.87%	0.87%	23.6
5	In	S1	PN	32	1	1	1	0	34%	34.12%	0.12%	23.8
6	In	S1	PN	1.9	1	1	1	0	53%	52.77%	0.23%	20.4
7	In	S2	PG	0.33	1	1	0	1	78%	77.96%	0.04%	17.5
8	In	S2	PG	0.7	1	1	0	1	58%	58.47%	0.47%	17.8

9	In	S2	NG	8	1	0	1	1	24%	22.84%	1.16%	19.5
10	In	S2	NG	0.3	1	0	1	1	46%	45.68%	0.32%	21.5
11	In	S2	PN	1.2	1	1	1	0	59%	58.79%	0.21%	23.4
12	In	S2	PN	6	1	1	1	0	72%	71.13%	0.87%	25.8

The protection system must be able to discriminate external faults, occurring beyond the protected zone, which, in this case, is the protected DC transmission line. The fault detection algorithm was trained to recognise and ignore a number of external fault conditions: namely, with reference to Table 8-3, DC line faults, AC side faults at terminals 1, 2 and 3, (including single phase to ground (AG), double phase (BC) and three phase faults (ABC)). Using external fault cases not used in the training data showed the fault detection to be 100% successful in avoiding false trips. The fault classification which can be seen in Table 8-4, is 100% accurate. The error of fault location accuracy is small, as low as 1.16%.

7.4 **Discussion**

7.4.1 External fault

External faults occurring beyond the protected link must to be distinguished from the internal. With the presented fault detection method, external faults can be distinguished from internal faults very clearly.

7.4.2 Fault location

In order to design the fault location algorithm and find out the relationship between the fault location and frequency component, the test system was simulated with a

series fault location (the training data sets were from 1% to 99% of the line length). Each fault location had a specified feature versus frequency, and the relationship between fault location and frequency could be distinguished by the designed ANNs. This method can detect a fault location even if the fault points are very near the converter station.

7.4.3 High impedance fault

High impedance faults are generally challenging for many protection strategies because of the attenuation of the post-fault characteristics and thus their resemblance to steady-state pre-fault conditions. For example, it is difficult to detect faults using an overcurrent characteristic alone due to very low fault currents from high impedance faults. Although absolute fault current level is slight, the current signals in the frequency domain contained enough information to indicate fault conditions. The signals in the frequency domain can maximise the characteristics of the faults. Through signal processing by FFT, distinctive features are generated for the protection scheme.

To study the sensitivity of the method proposed in this paper, the training and testing set included a range of simulated fault resistances from 0.01 Ω to 100 Ω. As can be seen in the frequency spectrum for the fault current signal, the frequency features can still be obtained under high fault resistance conditions. Therefore, despite the difficulties that high impedance faults present for many existing protection techniques, the technique presented here is robust for fault impedances of up to 100 Ω. Even though there are some specific difficulties with fault detection and location in conditions with high ground resistance, the simulation work shows very accurate results.

7.4.4 Effect of sampling frequency

Compared with the travelling wave-based fault location method using a 192 kHz sampling frequency [68], the proposed method in this paper uses a relatively low sampling frequency of 10 kHz. It is worth noting that, due to the wideband information that the scheme relies on, the method will work for different sampling

rates, provided the sampling is fast enough to reproduce the frequencies required by the ANN stage.

7.4.5 Effect of noise

Furthermore, by using the windowed FFT, ANN and counter together, the scheme is more robust to noise since several frequency spectra act together to smooth out anomalies. With the windowing of FFT, the ability to withstand noise is increased. To test this, white noise with 50 dB SNR was added to the DC current. Frequency spectra generated before and after the addition of noise had exactly the same performance response to the fault location ANN. The proposed method has the ability to handle extraneous noise that is usually present in the signals

7.4.6 Advantages

Compared with the travelling wave-based fault location method using 192 kHz sampling frequency as indicated in [68], the proposed method in this paper uses a relatively low sampling frequency of about 10 kHz. The fault detection method can distinguish the fault from external faults and terminal faults accurately. This method is sensitive to high fault resistance faults, which have an accurate detection for this boundary of fault. In addition, there is negligible effect for fault location with different sampling frequencies if the sampling frequency is higher than a specified value. Finally, the method applied using ANN is very fast.

7.5 Chapter summary

A three-terminal VSC-based HVDC model based on a CIGRE B4 programme was implemented in PSCAD/EMTDC with different types of faults simulated in the DC transmission system. Three separate neural networks for fault detection, fault classification and fault location were designed for a multi-terminal system. The fault detection feature can detect the internal fault, the faulted section of the MTDC network, and distinguish external faults from internal faults. Both detection and classification only rely on single terminal measurements and so do not require a communication link, whilst the entire scheme relies only on current signals and so

no DC voltage transducers are required. The most important achievement presented is that fault detection and classification can meet the time requirement for DC circuit breakers, and the fault location is accurate and fast enough for online, automation of wider system protection settings if desired. The proposed method is demonstrably robust to high resistance faults and noise. Since the method is purposefully designed for multi-terminal systems, it is robust to faults on other DC lines. In addition, more of the post-fault signal is used, unlike the travelling wave methods that use only the initial wavefront to locate the fault, further improving robustness.

8 Conclusion and Future Work

8.1 Introduction

This closing section presents a summary of the work completed. A summary for each chapter, including the main achievements, is listed. This is followed by the discussion and future avenues of enquiry.

8.2 Thesis summary

In Chapter 1, the basic concepts of power system protection for HVDC and MTDC systems were covered. Beginning with an energy overview, the reason for selecting a HVDC transmission system rather than an AC system was discussed. By choosing the HVDC transmission for renewable energy generation, the challenges facing the current HVDC technology were covered, and particular emphasis was placed on MTDC networks. The biggest challenge for current HVDC technology is the lack of a more appropriate and efficient protection strategy. This is pertinent to this thesis since a novel protection scheme is proposed to give a better solution for HVDC and MTDC protection. The section that followed offered an introduction to the motivation to do this research. The last section gave a brief introduction to each chapter. This chapter gave a basic understanding of the study and put the thesis in context.

Chapter 2 presented a detailed introduction to HVDC technology. The basic knowledge of different HVDC technology including VSC-HVDC and CSC-HVDC was presented. The main components, the configuration and the control scheme of an HVDC system were fully illustrated. The HVDC concept was extended to MTDC networks. Finally, the challenges for HVDC and MTDC systems were listed. This chapter presented the basic principles of an HVDC system, which is the basis for HVDC system modelling and the implementation of the protection scheme.

Chapter 3 presented a literature review on protection methods applied in previous work. Different types of fault which may occur in DC transmission systems were

discussed firstly, followed by the current technologies available for circuit breakers. The main approaches, including the travelling wave principle, voltage derivative protection, current differential protection, under voltage protection, transient-based protection and other methods used in HVDC line protection, were discussed. By discussing the protection method for HVDC as a basis, more protection strategies were introduced for an MTDC system. By considering all the existing protection schemes, a novel protection approach was presented for both multi-terminal HVDC systems and two-terminal HVDC systems based on ANNs.

Chapter 4 detailed the construction and design of a two-terminal VSC-HVDC model and a three-terminal HVDC system model based on the CIGRE B4 model. The initial section summarised the software used to simulate the models. Then the modelling of the two systems was introduced separately from methodology, control scheme, implementation in PSCAD, steady-state validation and fault profile analysis – 5 parts. The methodology discussed the theoretical concepts relevant to the models. This was followed by the detailed control strategy for the models. The detailed implementation was shown here. The models were verified by studying the steady-state conditions, and fault profiles were analysed under a complex interplay of parameters. An array of test cases was conducted on the factors known to affect the short circuit responses. The time domain signals were analysed. Both wavelet transforms and fast Fourier transforms were used to provide frequency analysis in the frequency domain. The main conclusion was that frequency gives a characteristic response through FFT rather than DWT. Significantly, it was found that the frequency features have more bearing on fault locations than fault resistance. Therefore, this was identified as the key point to be addressed by this thesis.

Chapter 5 presented an overview of the application of artificial neural networks. Special emphasis was given to the most relevant techniques for fault detection and fault location. The artificial neural networks were regarded as the central technique in this thesis, and the application was discussed in detail. The chapter concluded with a discussion of how these are best applied to the relevant work in this study.

Chapter 6 dealt with the development of fault detection, classification and location based on ANNs. Following the signal chain displayed in the first section, the signal

processing, ANN training and counters were introduced step by step. The fault DC current waveforms obtained from the system were used for the signal processing. At the signal processing stage, both the magnitude and phase of frequency were used in the input layer of designed ANNs. The frequency domain signals were obtained by FFT analysis. The structure and algorithms used for ANN training were introduced. A counter was designed for more robust detection. An important innovation was the use of three parallel ANNs for fault detection, fault classification and fault location purposes. The algorithm exploits this to give greater robustness.

Chapter 7 discussed the test results demonstrating the proposed method in the modelled two-terminal HVDC system. Since a monopole network was modelled, only fault detection and fault location were achieved by using the two established ANNs. Results were presented that show the algorithm to be 100% successful in fault diagnosis. The fault location accuracy could reach 99.18%.

Chapter 8 demonstrated the proposed method in the modelled multi-terminal HVDC system. This study emphasised generation technology, hence only fault types, fault location and fault resistance were considered. Three ANNs were built in parallel. Results showed the algorithm to be 100% successful in both fault detection and fault classification. The error for fault location accuracy was small, a maximum of just 1.16%.

8.3 Further work

The current work has already taken various faults into consideration. The method is verified by two networks including both the two-terminal HVDC system and the multi-terminal HVDC system. However, more realistic power system conditions can be considered and studied. Moreover, hardware can be applied to test the approach in the future.

From the design method aspect, current ANNs are trained based on the data from the PSCAD simulation model. Various fault cases have been studied in the work. For a more accurate neural network design, more training sets are required. In addition, from a practical point of view, the new fault data will be added into the

database once the fault is detected so the system will constantly learn to improve its performance.

From the protection validation aspect, the proposed protection scheme in this thesis is validated in a two-terminal HVDC system and a three-terminal HVDC system. However, to verify that the protection scheme will work in real time, real time software in the loop and then hardware in the loop tests are suggested. The Real Time Digital Simulator is a dedicated hardware unit capable of solving arbitrary system topologies in real time and it could be used to achieve this in the future.

In addition, more fundamental development is required. More complex multi-terminal HVDC systems are required to be built including those using MMC converters. Also, depending on the requirement of the specific system, new ANNs need to be trained separately and the fault data must to be made available for feature extraction.

Appendix A

Table A Summary of worldwide VSC HVDC projects and their basic parameters [5]

Project name	Year of commission	Power rating	Number of circuits	AC voltage	DC voltage	Lines or cables	Lengths	Comments and reasons for choosing VSC HVDC	Topology	Semiconductors
Hellsjon, Sweden	1997	3 MW ±3 MVar	1	10 KV	±10 KV	Overhead lines	10 km	Test transmission. Synchronous AC grid.	2-level	IGBTs
Gotland HVDC Light, Sweden	1999	50 MW -55 to 50 MVar	1	80 KV	±80 KV	Submarine cables	2×70 km	Wind power (voltage support). Easy to get permission for underground cables	2-level	IGBTs
Eagle Pass, USA	2000	36 MW ±36 MVar	1	138 KV	±15.9 KV	Back-to-back HVDC light station	N/A	Controlled asynchronous connection for trading. Voltage control. Power exchange.	3-level NPC	IGBTs

Tjareborg, Denmark	2000	8 MVA 7.2 MW -3 to 4 MVar	1	10.5 KV	±9 KV	Submarine cables	2×4.3 km	Wind power. Demonstration project. Normally synchronous AC grid with variable frequency control.	2-level	IGBTs
Terrenora Interconnection, Australia	2000	180 MW -165 to 90 Mar	3	110 KV 132 KV	±80 KV	Underground cables	6×59 km	Energy trade. Asynchronous AC grid. Easy to get permission for underground cables.	2-level	IGBTs
MurrayLink, Australia	2002	220 MW -150 to 140 MVar	1	132 KV 220 KV	±150 KV	Underground cables	2×180 km	Controlled asynchronous connection for trading. Easy to get permission for underground cables.	3-level ANPC	IGBTs
CrossSound, USA	2002	330 MW ±150MVar	1	345 KV 138 KV	±150 KV	Submarine cables	2×40 km	Controlled asynchronous connection for power exchange. Submarine cables.	3-level ANPC	IGBTs
Troll A offshore, Norway	2005	84 MW -20 to24	2	132 KV 56 KV	±60 KV	Submarine cables	4×70 km	Environment, CO2 tax. Long submarine cables	2-level	IGBTs

		MVar						distance. Compactness of converter on platform electrification.		
Estlink, Finland	2006	350 MW ±125 MVar	1	330 KV 400 KV	±150 KV	Submarine and underground cables	2×31 km 2×74 km	Length of land cable, sea crossing and non-synchronous AC system.	2-level	IGBTs
Nord E.ON 1, Germany	2009	400 MW	1	380 KV 170 KV	±150 KV	Submarine and underground cables	2×75 km 2×128 km	Offshore wind farm to shore. Length of land and sea cables. Asynchronous system.	N/A	IGBTs
Caprivi Link, Namibia	2009	300 MW	1	330 KV 400 KV	350 KV	Overhead lines	970 km	Synchronous AC grids. Long distance, weak networks.	N/A	IGBTs
Valhall offshore, Norway	2009	78 MW	1	300 KV 11 KV	150 KV	Submarine cables	292 km	Reduce cost and improve operation efficiency of the field. Minimize emission of greenhouse gases.	2-level	IGBTs

Appendix B

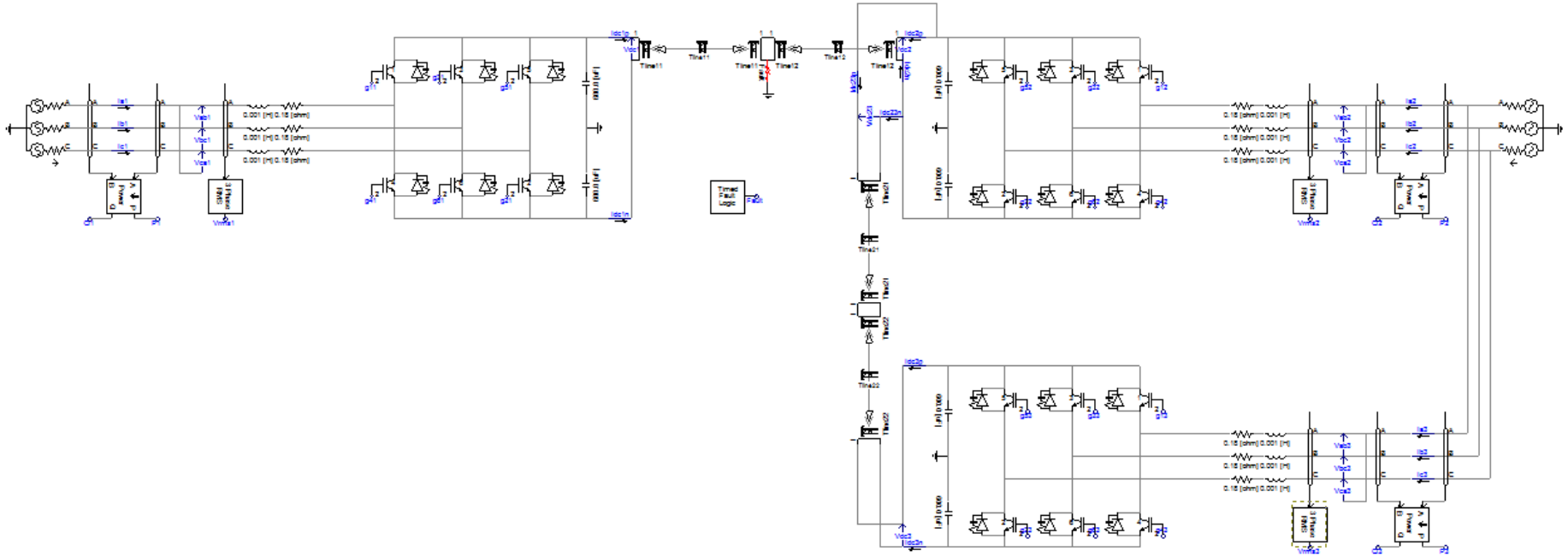

Fig. B Configuration of three-terminal HVDC system

References

[1] S. Gordon, "Supergrid to the rescue," *Power Engineer,* vol. 20, pp. 30-33, 2006.

[2] D. Van Hertem and M. Ghandhari, "Multi-terminal VSC HVDC for the European supergrid: Obstacles," *Renewable and sustainable energy reviews,* vol. 14, pp. 3156-3163, 2010.

[3] S. Azizi, M. Sanaye-Pasand, M. Abedini, and A. Hassani, "A Traveling-Wave-Based Methodology for Wide-Area Fault Location in Multiterminal DC Systems," *Power Delivery, IEEE Transactions on,* vol. 29, pp. 2552-2560, 2014.

[4] O. Gomis-Bellmunt, J. Liang, J. Ekanayake, R. King, and N. Jenkins, "Topologies of multiterminal HVDC-VSC transmission for large offshore wind farms," *Electric Power Systems Research,* vol. 81, pp. 271-281, 2011.

[5] N. Flourentzou, V. G. Agelidis, and G. D. Demetriades, "VSC-Based HVDC Power Transmission Systems: An Overview," *Power Electronics, IEEE Transactions on,* vol. 24, pp. 592-602, 2009.

[6] D. Naidoo and N. Ijumba, "HVDC line protection for the proposed future HVDC systems," in *Power System Technology, 2004. PowerCon 2004. 2004 International Conference on*, 2004, pp. 1327-1332.

[7] K. Sano and M. Takasaki, "A surgeless solid-state DC circuit breaker for voltage-source-converter-based HVDC systems," *Industry Applications, IEEE Transactions on,* vol. 50, pp. 2690-2699, 2014.

[8] S. P. Le Blond, Q. Deng, and M. Burgin, "High frequency protection scheme for multi-terminal HVDC overhead lines," in *Developments in Power System Protection (DPSP 2014), 12th IET International Conference on*, 2014, pp. 1-5.

[9] Z. Ying, T. Nengling, and X. Bin, "Fault Analysis and Traveling-Wave Protection Scheme for Bipolar HVDC Lines," *Power Delivery, IEEE Transactions on,* vol. 27, pp. 1583-1591, 2012.

[10] H. V. D. C. Transmission–Proven, "Technology For Power Exchange, SIEMENS," ed, 2006.

[11] B. Andersen, "HVDC transmission-opportunities and challenges," in *AC*

and DC Power Transmission, 2006. ACDC 2006. The 8th IEE International Conference on, 2006, pp. 24-29.

[12] B. Van Eeckhout, D. Van Hertem, M. Reza, K. Srivastava, and R. Belmans, "Economic comparison of VSC HVDC and HVAC as transmission system for a 300 MW offshore wind farm," *European Transactions on Electrical Power,* vol. 20, pp. 661-671, 2010.

[13] R. Rudervall, J. Charpentier, and R. Sharma, "High voltage direct current (HVDC) transmission systems technology review paper," *Energy week,* vol. 2000, 2000.

[14] N. G. Hingorani, "High-voltage DC transmission: a power electronics workhorse," *IEEE spectrum,* vol. 33, pp. 63-72, 1996.

[15] ABB, "Economic and environmental advantages," *ABB,* vol. http://new.abb.com/systems/hvdc/why-hvdc/economic-and-environmental-advantages.

[16] R. Rudervall, J. Charpentier, and R. Sharma, "High voltage direct current (HVDC) transmission systems technology review paper," *Energy Week,* 2000.

[17] R. T. Pinto, P. Bauer, S. F. Rodrigues, E. J. Wiggelinkhuizen, J. Pierik, and B. Ferreira, "A novel distributed direct-voltage control strategy for grid integration of offshore wind energy systems through MTDC network," *Industrial Electronics, IEEE Transactions on,* vol. 60, pp. 2429-2441, 2013.

[18] J. Arrillaga, Y. H. Liu, and N. R. Watson, *Flexible power transmission: the HVDC options*: John Wiley & Sons, 2007.

[19] M. P. Bahrman and B. K. Johnson, "The ABCs of HVDC transmission technologies," *Power and Energy Magazine, IEEE,* vol. 5, pp. 32-44, 2007.

[20] T. K. Vrana, R. E. Torres-Olguin, B. Liu, and T. M. Haileselassie, "The North Sea Super Grid - a technical perspective," in *AC and DC Power Transmission, 2010. ACDC. 9th IET International Conference on*, 2010, pp. 1-5.

[21] A. M. Abbas and P. W. Lehn, "PWM based VSC-HVDC systems: A review," in *Power & Energy Society General Meeting, 2009. PES '09. IEEE*, 2009, pp. 1-9.

[22] E. Csanyi, "Principles and Characteristics of Distance Protection," 2012.

[23] L. Livermore, L. Jun, and J. Ekanayake, "MTDC VSC Technology and its applications for wind power," in *Universities Power Engineering Conference (UPEC), 2010 45th International*, 2010, pp. 1-6.

[24] F. Nozari and H. S. Patel, "Power electronics in electric utilities: HVDC power transmission systems," *Proceedings of the IEEE,* vol. 76, pp. 495-506, 1988.

[25] W. Zhao, "HVDC Engineering Technology," *China Electricty Come Out,* 2010.

[26] H. Stomberg, B. Abrahamsson, and O. Saksvik, "Modern HVDC thyristor valves," *ABB Power Systems, Ludvika, Sweden,* 1996.

[27] Z. Xu and H. Chen, "Review and Applications of VSC HVDC," *High Voltage Engineering,* vol. 30, pp. 1-10, 2007.

[28] A. Lindberg and T. Larsson, "Pwm And Control Of Three Level Voltage Source Converters In An Hvdc Back-to-back Station," in *AC and DC Power Transmission, Sixth International Conference on (Conf. Publ. No. 423)*, 1996, pp. 297-302.

[29] M. Guan, Z. Xu, and H. Chen, "Control and modulation strategies for modular multilevel converter based HVDC system," in *IECON 2011-37th Annual Conference on IEEE Industrial Electronics Society*, 2011, pp. 849-854.

[30] D. Soto-Sanchez and T. Green, "Control of a modular multilevel converter-based HVDC transmission system," in *Power Electronics and Applications (EPE 2011), Proceedings of the 2011-14th European Conference on*, 2011, pp. 1-10.

[31] C. Chen, G. P. Adam, S. Finney, J. Fletcher, and B. Williams, "H-bridge modular multi-level converter: control strategy for improved DC fault ride-through capability without converter blocking," *IET Power Electronics,* vol. 8, pp. 1996-2008, 2015.

[32] N. Nosaka, Y. Tsubota, K. Matsukawa, K. Sakamoto, H. Nakamura, M. Takasaki*, et al.*, "Simulation studies on a control and protection scheme for hybrid multi-terminal HVDC systems," in *Power Engineering Society 1999 Winter Meeting, IEEE*, 1999, pp. 1079-1084.

[33] J. Candelaria and J.-D. Park, "VSC-HVDC system protection: A review of current methods," in *Power Systems Conference and Exposition (PSCE), 2011 IEEE/PES*, 2011, pp. 1-7.

[34] V. F. Lescale, A. Kumar, L. E. Juhlin, H. Bjorklund, and K. Nyberg,

"Challenges with Multi-Terminal UHVDC Transmissions," in *Power System Technology and IEEE Power India Conference, 2008. POWERCON 2008. Joint International Conference on*, 2008, pp. 1-7.

[35] T. K. Vrana and O. B. Fosso, "Technical aspects of the North Sea super grid," *CIGRE Electra, November,* 2011.

[36] Z. Jiebei and C. Booth, "Future multi-terminal HVDC transmission systems using Voltage source converters," in *Universities Power Engineering Conference (UPEC), 2010 45th International*, 2010, pp. 1-6.

[37] M. P. Bahrman, J. G. Johansson, and B. A. Nilsson, "Voltage source converter transmission technologies: the right fit for the application," in *IEEE Power Engineering Society General Meeting*, 2003, pp. 1840-1847.

[38] H. Alsiraji, "Cooperative Power Sharing control in Multi-terminal VSC-HVDC," UWSpace, 2014.

[39] N. Mossadegh, "A System Representative Model to Study Frequency Excursions in the National Electricity Transmission System and the potential for MT-HVDC Support," University of Bath, 2014.

[40] J. Yang, J. E. Fletcher, and J. O'Reilly, "Multi-terminal DC wind farm collection and transmission system internal fault analysis," in *Industrial Electronics (ISIE), 2010 IEEE International Symposium on*, 2010, pp. 2437-2442.

[41] Y. Xu, D. Shi, and S. Qiu, "Protection coordination of meshed MMC-MTDC transmission systems under DC faults," in *TENCON 2013-2013 IEEE Region 10 Conference (31194)*, 2013, pp. 1-5.

[42] J. Yang, J. E. Fletcher, and J. O'Reilly, "Multiterminal DC wind farm collection grid internal fault analysis and protection design," *Power Delivery, IEEE Transactions on,* vol. 25, pp. 2308-2318, 2010.

[43] Y. Jie, Z. Jianchao, T. Guangfu, and H. Zhiyuan, "Characteristics and Recovery Performance of VSC-HVDC DC Transmission Line Fault," in *Power and Energy Engineering Conference (APPEEC), 2010 Asia-Pacific*, 2010, pp. 1-4.

[44] O. G.-B. Dirk Van Hertem, Jun Liang, *HVDC Grids: For Offshore and Supergrid of the Future*. IEEE Press series on power engineering, April 2016.

[45] M. Callavik, A. Blomberg, J. Häfner, and B. Jacobsen, "The hybrid HVDC breaker. An innovation breakthrough enabling reliable HVDC grids. ABB Grid Systems," ed, 2013.

[46] ABB, "ABB's Hybrid HVDC Circuit Breaker," *http://new.abb.com/about/events/cigre2014/hvdc-breaker,* 2014.

[47] C. M. Franck, "HVDC circuit breakers: A review identifying future research needs," *Power Delivery, IEEE Transactions on,* vol. 26, pp. 998-1007, 2011.

[48] N. Kostoulas, V. Sitokonstantinou, M. Idris, P. Sterling, S. Sayed, and P. Karaiskos, "DC circuit breakers and their use in HVDC grids," *Report, Imperial College, London, UK*.

[49] A. Mokhberdoran, A. Carvalho, H. Leite, and N. Silva, "A review on HVDC circuit breakers," in *Renewable Power Generation Conference (RPG 2014), 3rd*, 2014, pp. 1-6.

[50] C. Meyer, S. Schroder, and R. W. De Doncker, "Solid-state circuit breakers and current limiters for medium-voltage systems having distributed power systems," *IEEE transactions on power electronics,* vol. 19, pp. 1333-1340, 2004.

[51] M. M. R. Ahmed, G. Putrus, L. Ran, and R. Penlington, "Development of a prototype solid-state fault-current limiting and interrupting device for low-voltage distribution networks," *IEEE Transactions on Power Delivery,* vol. 21, pp. 1997-2005, 2006.

[52] N. Mahajan, "Systems Protection for Power Electronic Building Block Based DC Distributed System," *NCSU,* 2004.

[53] M. E. Baran and N. R. Mahajan, "Overcurrent Protection on Voltage-Source-Converter-Based Multiterminal DC Distribution Systems," *Power Delivery, IEEE Transactions on,* vol. 22, pp. 406-412, 2007.

[54] J. Wu, S. Zhang, and D. Xu, "Modeling and control of multi-terminal HVDC with offshore wind farm integration and DC chopper based protection strategies," in *Industrial Electronics Society, IECON 2013-39th Annual Conference of the IEEE*, 2013, pp. 1013-1018.

[55] J. I. Marvik and H. G. Svendsen, "Analysis of Grid Faults in Offshore Wind Farm with HVDC Connection," *Energy Procedia,* vol. 35, pp. 81-90, // 2013.

[56] L. Tang and B.-T. Ooi, "Locating and isolating DC faults in multi-terminal DC systems," *Power Delivery, IEEE Transactions on,* vol. 22, pp. 1877-1884, 2007.

[57] L. Tang and B.-T. Ooi, "Protection of VSC-multi-terminal HVDC against DC faults," in *Power Electronics Specialists Conference, 2002. pesc 02.*

2002 IEEE 33rd Annual, 2002, pp. 719-724.

[58] D. Naidoo and N. M. Ijumba, "HVDC line protection for the proposed future HVDC systems," in *Power System Technology, 2004. PowerCon 2004. 2004 International Conference on*, 2004, pp. 1327-1332 Vol.2.

[59] Z. Jiankang, S. Jiale, J. Zaibin, S. Guobing, and S. Xiaohua, "A Fast Full-Line Tripping Distance Protection Method for HVDC Transmission Line," in *Power and Energy Engineering Conference (APPEEC), 2012 Asia-Pacific*, 2012, pp. 1-5.

[60] D. Naidoo and N. M. Ijumba, "A protection system for long HVDC transmission lines," in *Power Engineering Society Inaugural Conference and Exposition in Africa, 2005 IEEE*, 2005, pp. 150-155.

[61] V. Pathirana and P. McLaren, "A hybrid algorithm for high speed transmission line protection," *Power Delivery, IEEE Transactions on,* vol. 20, pp. 2422-2428, 2005.

[62] X. Liu, A. H. Osman, and O. P. Malik, "Real-time implementation of a hybrid protection scheme for bipolar HVDC line using FPGA," *Power Delivery, IEEE Transactions on,* vol. 26, pp. 101-108, 2011.

[63] J. L. Blackburn and T. J. Domin, *Protective relaying: principles and applications*: CRC press, 2006.

[64] O. Nanayakkara, A. D. Rajapakse, and R. Wachal, "Traveling-wave-based line fault location in star-connected multiterminal HVDC systems," *Power Delivery, IEEE Transactions on,* vol. 27, pp. 2286-2294, 2012.

[65] O. M. K. K. Nanayakkara, A. D. Rajapakse, and R. Wachal, "Location of DC Line Faults in Conventional HVDC Systems With Segments of Cables and Overhead Lines Using Terminal Measurements," *Power Delivery, IEEE Transactions on,* vol. 27, pp. 279-288, 2012.

[66] M. M. Saha, J. J. Izykowski, and E. Rosolowski, *Fault location on power networks*: Springer Science & Business Media, 2009.

[67] X. Zheng, T. Nengling, Y. Guangliang, and D. Haoyin, "A transient protection scheme for HVDC transmission line," *Power Delivery, IEEE Transactions on,* vol. 27, pp. 718-724, 2012.

[68] X. Liu, A. Osman, and O. Malik, "Hybrid traveling wave/boundary protection for monopolar HVDC line," *Power Delivery, IEEE Transactions on,* vol. 24, pp. 569-578, 2009.

[69] A. Swetha, P. K. Murthy, N. Sujatha, and Y. Kiran, "A NOVEL

TECHNIQUE FOR THE LOCATION OF FAULT ON A HVDC TRANSMISSION LINE," *Journal of Engineering & Applied Sciences,* vol. 6, 2011.

[70] M. Shukr, D. W. P. Thomas, and P. Zanchetta, "VSC-HVDC transmission line faults location using active line impedance estimation," in *Energy Conference and Exhibition (ENERGYCON), 2012 IEEE International*, 2012, pp. 244-248.

[71] Z. Xiao-Dong, T. Neng-Ling, J. S. Thorp, and Y. Guang-Liang, "A transient harmonic current protection scheme for HVDC transmission line," *Power Delivery, IEEE Transactions on,* vol. 27, pp. 2278-2285, 2012.

[72] A. E. Abu-Elanien, A. A. Elserougi, A. S. Abdel-Khalik, A. M. Massoud, and S. Ahmed, "A differential protection technique for multi-terminal HVDC," *Electric Power Systems Research,* vol. 130, pp. 78-88, 2016.

[73] M. Hu, C. Fu, J. S. Wang, H. Rao, and H. B. Liu, "Real time digital simulation of the parallel multi-terminal HVDC transmission system," in *Power System Technology (POWERCON), 2012 IEEE International Conference on*, 2012, pp. 1-5.

[74] K. De Kerf, K. Srivastava, M. Reza, D. Bekaert, S. Cole, D. Van Hertem, *et al.*, "Wavelet-based protection strategy for DC faults in multi-terminal VSC HVDC systems," *Generation, Transmission & Distribution, IET,* vol. 5, pp. 496-503, 2011.

[75] M. H. R. C. Inc., "Applications of PSCAD® / EMTDC™," 2007.

[76] J. Beerten, S. Cole, and R. Belmans, "Modeling of multi-terminal VSC HVDC systems with distributed DC voltage control," *Power Systems, IEEE Transactions on,* vol. 29, pp. 34-42, 2014.

[77] D. Jovcic and K. Ahmed, *High Voltage Direct Current Transmission: Converters, Systems and DC Grids*: John Wiley & Sons, 2015.

[78] C. Wadhwa, *High voltage engineering*: New Age International, 2007.

[79] A. Wasserrab and G. Balzer, "The significance of frequency-dependent overhead lines for the calculation of HVDC line short-circuit currents," *Electrical Engineering,* pp. 1-11, 2015.

[80] R. Dhua and C. Koley, "Simulation of Frequency Dependent Transmission Line for Identification of Faults and Switching over Voltages," in *Proceedings of the International Conference on Frontiers of Intelligent Computing: Theory and Applications (FICTA)*, 2013, pp. 311-320.

[81] O. electrical, "Frequency Dependent Line Model," *http://www.openelectrical.org/wiki/index.php?title=Frequency_Dependent_Line_Model*.

[82] L. Gengyin, Z. Ming, H. Jie, L. Guangkai, and L. Haifeng, "Power flow calculation of power systems incorporating VSC-HVDC," in *Power System Technology, 2004. PowerCon 2004. 2004 International Conference on*, 2004, pp. 1562-1566.

[83] V. Sood and H. Patel, "Comparison between direct and vector control strategy for VSC-HVDC system in EMTP-RV," in *Power Electronics, Drives and Energy Systems (PEDES) & 2010 Power India, 2010 Joint International Conference on*, 2010, pp. 1-6.

[84] H. Alsiraji, "Cooperative Power Sharing control in Multi-terminal VSC-HVDC," 2014.

[85] J. Khazaei, Z. Miao, L. Piyasinghe, and L. Fan, "Minimizing DC system loss in multi-terminal HVDC systems through adaptive droop control," *Electric Power Systems Research,* vol. 126, pp. 78-86, 2015.

[86] C. Dierckxsens, K. Srivastava, M. Reza, S. Cole, J. Beerten, and R. Belmans, "A distributed DC voltage control method for VSC MTDC systems," *Electric Power Systems Research,* vol. 82, pp. 54-58, 2012.

[87] X. Zhao and K. Li, "Droop setting design for multi-terminal HVDC grids considering voltage deviation impacts," *Electric Power Systems Research,* vol. 123, pp. 67-75, 2015.

[88] T. M. Haileselassie, "Control of multi-terminal VSC-HVDC systems," 2008.

[89] T. M. Haileselassie, M. Molinas, and T. Undeland, "Multi-terminal VSC-HVDC system for integration of offshore wind farms and green electrification of platforms in the North Sea," in *Nordic Workshop on Power and Industrial Electronics (NORPIE/2008), June 9-11, 2008, Espoo, Finland*, 2008.

[90] D. L. Yali Xue, Feng Xu, Chongde Lv, "Parameter Tuning and Evaluation for Optimal PI Controllers," *J Tsinghua Univ (Sci & Tech),* vol. 44, pp. 1067-1070, 2004.

[91] T. K. Vrana, Y. Yang, D. Jovcic, S. Dennetire, J. Jardini, and H. Saad, "The CIGRE B4 DC grid test system," *System,* vol. 500, p. D1, 2013.

[92] T. Kalitjuka, "Control of Voltage Source Converters for Power System Applications," 2011.

[93] Mathworks, "Global Optimization Toolbox: User's Guide (r2016b)," *The MathWorks, Inc.,* 2016.

[94] A. Ukil and R. Živanović, "Abrupt change detection in power system fault analysis using adaptive whitening filter and wavelet transform," *Electric Power Systems Research,* vol. 76, pp. 815-823, 2006.

[95] E. C. Ifeachor and B. W. Jervis, *Digital signal processing: a practical approach*: Pearson Education, 2002.

[96] R. P. Nath and V. N. Balaji, "Artificial intelligence in power systems," *IOSR Journal of Computer Engineering (IOSR-JCE), e-ISSN,* pp. 2278-0661, 2014.

[97] S. S. Haykin, S. S. Haykin, S. S. Haykin, and S. S. Haykin, *Neural networks and learning machines* vol. 3: Pearson Upper Saddle River, NJ, USA:, 2009.

[98] S. Sivanandam and S. Deepa, *Introduction to neural networks using Matlab 6.0*: Tata McGraw-Hill Education, 2006.

[99] D. R. Nayak, A. Mahapatra, and P. Mishra, "A survey on rainfall prediction using artificial neural network," *International Journal of Computer Applications,* vol. 72, 2013.

[100] M. Mirzaei, M. Ab Kadir, E. Moazami, and H. Hizam, "Review of fault location methods for distribution power system," *Australian Journal of Basic and Applied Sciences,* vol. 3, pp. 2670-2676, 2009.

[101] N. Zhang and M. Kezunovic, "Transmission line boundary protection using wavelet transform and neural network," *Power Delivery, IEEE Transactions on,* vol. 22, pp. 859-869, 2007.

[102] K. Silva, B. Souza, and N. Brito, "Fault detection and classification in transmission lines based on wavelet transform and ANN," *Power Delivery, IEEE Transactions on,* vol. 21, pp. 2058-2063, 2006.

[103] A. L. O. Fernandez and N. K. I. Ghonaim, "A novel approach using a FIRANN for fault detection and direction estimation for high-voltage transmission lines," *Power Delivery, IEEE Transactions on,* vol. 17, pp. 894-900, 2002.

[104] F. Martín and J. A. Aguado, "Wavelet-based ANN approach for transmission line protection," *Power Delivery, IEEE Transactions on,* vol. 18, pp. 1572-1574, 2003.

[105] R. Aggarwal and Y. Song, "Artificial neural networks in power systems. I.

General introduction to neural computing," *Power Engineering Journal,* vol. 11, pp. 129-134, 1997.

[106] Q.-H. Wu, Z. Lu, and T. Ji, *Protective relaying of power systems using mathematical morphology*: Springer Science & Business Media, 2009.

[107] T. S. Dillon and D. Niebur, *Neural networks applications in power systems*: CRL Publishing London, 1996.

[108] I. Abu-Mahfouz, "Drilling wear detection and classification using vibration signals and artificial neural network," *International Journal of Machine Tools and Manufacture,* vol. 43, pp. 707-720, 2003.

[109] K. Guney, C. Yildiz, S. Kaya, and M. Turkmen, "Artificial neural networks for calculating the characteristic impedance of air-suspended trapezoidal and rectangular-shaped microshield lines," *Journal of Electromagnetic Waves and Applications,* vol. 20, pp. 1161-1174, 2006.

[110] D. Pham and X. Liu, "Neural Networks for Identification, Prediction and Control," *Springer-Verlag, London,* 1995.

[111] S. Le Blond, R. Bertho, D. Coury, and J. Vieira, "Design of protection schemes for multi-terminal HVDC systems," *Renewable and Sustainable Energy Reviews,* vol. 56, pp. 965-974, 2016.

[112] G. Maral, *VSAT networks*: John Wiley & Sons, 2004.

[113] Y. Guo, M. Kezunovic, and D. Chen, "Simplified algorithms for removal of the effect of exponentially decaying DC-offset on the Fourier algorithm," *Power Delivery, IEEE Transactions on,* vol. 18, pp. 711-717, 2003.

[114] S. Le Blond, "Intelligent autoreclosing for systems of high penetration of wind generation with real time modelling, development and deployment," University of Bath, 2011.

Publications

1) Yang, Q., Le Blond, S., Aggarwal, R., Wang, Y., & Li, J. 2017. New ANN method for multi-terminal HVDC protection relaying. Electric Power Systems Research, 148, 192-201.

2) Yang, Q., Le Blond, S., Liang, F., Yuan, W., Zhang, M., & Li, J. 2017. Design and Application of Superconducting Fault Current Limiter in a Multi-terminal HVDC System. IEEE Transactions on Applied Superconductivity, 27(4), 1-5.

3) Yang, Q., Li, J., Le Blond, S., & Wang, C., 2016. Artificial Neural Network Based Fault Detection and Fault Location in the DC Microgrid. Energy Procedia, 103, 129-134.

Electric Power Systems Research 148 (2017) 192–201

Contents lists available at ScienceDirect

Electric Power Systems Research

journal homepage: www.elsevier.com/locate/epsr

New ANN method for multi-terminal HVDC protection relaying

Qingqing Yang, Simon Le Blond, Raj Aggarwal, Yawei Wang, Jianwei Li*

Department of Electronic and Electrical Engineering, University of Bath, United Kingdom

ARTICLE INFO

Article history:
Received 18 November 2016
Received in revised form 22 March 2017
Accepted 24 March 2017

Keywords:
Artificial neural network
Fault current signal
Fault detection
Fault location
Transmission line
VSC-HVDC system

ABSTRACT

This paper proposes a comprehensive novel multi-terminal HVDC protection scheme based on artificial neural network (ANN) and high frequency components detected from fault current signals only. The method is shown to accurately detect, classify and locate overhead line faults. Unlike existing travelling wave based methods which must capture the initial wavefront and require high sampling rates, the new approach is more robust since it gives accurate fault detection and fault location over a range of windowed post-fault signals. Furthermore, the proposed method is fault resistance independent meaning even a very high fault impedance has no effect on accurate fault location. A three-terminal VSC-HVDC system is modelled in PSCAD/EMTDC, which is used for obtaining the fault current data for transmission line terminals. The method is verified by studying different cases with a range of fault resistances in various fault locations, and in addition, external faults. The results show that the proposed method gives fast (<5 ms) and reliable (100%) fault detection and classification and accurate location (<1.16%) for DC line faults.

1. Introduction

Multi-terminal High Voltage Direct Current (MTDC) has often been proposed as the most promising technology for an inter-continental super-grid or collecting bulk offshore renewable energy sources [1,2]. Much renewable generation is available at locations remote from load centres, and thus must to be transported efficiently over long distances [3]. For example, to interconnect extensive offshore wind sites between Northern Europe and the UK, an offshore super-grid may be required in the future. Similarly an MTDC grid could transmit extensive solar power from the deserts of Northern Africa to the load centres of Europe.

Recent developments in DC circuit breakers and voltage source converters (VSC) make MTDC a more technically and economically feasible technology [4]. However, there are many technical challenges in evolving from point-to-point HVDC to MTDC, especially in protection systems. In typical HVDC point-to-point links, the most common method of isolation is using an AC circuit breaker to trip the entire HVDC system. Hence, the circuit breakers reside on the AC side, and in the event of a fault, the entire link is de-energised [5]. In the multi-terminal case, however, it is more desirable to isolate only the faulted link rather than trip the entire DC grid. DC circuit breakers, presently in the early stages of development, are required to isolate the faulted line. DC breakers require appropriate protective relaying, so the faults may be detected and isolated immediately. In addition, the overall protection system may require online adjustment of zonal relay settings, the faulted line may require maintenance, and the system will need restorative action, all necessitating an accurate and fast fault-location algorithm [2].

Travelling wave based protection has been successfully applied in both AC and HVDC systems by virtue of development of fast A/D conversion and numeric relay technology [6,7]. The most common method of travelling wave based protection in multi-terminal systems, as introduced in [2,8], is detecting the initial wavefront which has a demonstrably fast and accurate response. Due to its fast computational time and straightforward implementation, the discrete wavelet transform (DWT) is preferred for detecting arrival of wavefronts [9] over using pure frequency or time domain based methods [10]. However, limitations exist with travelling wave protection [7,11,12], such as lack of mathematical tools to model the travelling wave, difficulty in the detection of the wave-head, being easily influenced by noise, inability to detect close-up faults, unequal travelling wave velocities in line and underground cables, and requiring knowledge of the surge impedance and a high sampling rate.

De Kerf et al. proposed a DC fault detection algorithm for multi-terminal VSC-HVDC systems using three independent fault criteria, including voltage wavelet analysis, current wavelet analysis and voltage derivative and magnitude [13]. Even though the detection time reaches 1 ms, the method is only proved for a fault resistance of 0.01 Ω. In practice the fault impedance will vary, and the method

* Corresponding author.
E-mail addresses: jl977@bath.ac.uk, keorwei@gmail.com (J. Li).

http://dx.doi.org/10.1016/j.epsr.2017.03.024
0378-7796/

presented in this new work is shown to be robust to this variation. A non-unit protection is proposed by same authors [14] based on the reflection of the travelling wave at an inductive termination, which uses both voltage and current signals compared with a pre-selected threshold. However this method requires accurate and fast current and voltage sensors, leading to higher overall system costs than a method that relies on current signals only, such as that presented in this paper. Boundary protection is a transient-based protection concept which has been proposed in [12]. In a DC system, smoothing reactors and the capacitors installed at both ends of the DC transmission line and the inherent bus bar capacitance represent a natural boundary that does not transmit high frequency signals, and thus can be used to rapidly distinguish between internal and external faults [7]. Another transient harmonic current protection method, based on the boundary characteristic is introduced in Ref. [15]. However, this kind of transient based protection may maloperate because of non-fault transients caused by lightning. A low speed protection for mechanical DC breakers is proposed in Ref. [16], where the total fault clearing time is in total 60 ms, a prohibitively long relaying time for most DC breakers. The backup protection proposed in the paper requires fault current limiting equipment resulting in additional costs. In Ref. [17] a data based primary fault detection method using current signals is proposed. However the fault detection relies on information from several buses in the system, and thus necessitates a fast communication link, unlike the method presented here, which uses single ended measurements for fault detection and classification. The hybrid protection presented in Ref. [7] can distinguish both non-fault lightning transients and detect close-up faults, which may be missed by travelling wave methods. However, high sampling frequencies are required, which demand more expensive hardware for sampling and calculation. Another method [11] is based on the relation between parameters of the DC transmission line and the variation of transient energy obtained from the voltage and current measurements at both terminals, although the technique is not validated with a frequency dependent line model. The authors in Ref. [15] present a method utilising transient harmonic current based on the boundary characteristic of DC transmission lines. However, it takes a maximum of 30 ms to identify faults, which is not quick enough for protection purposes. In addition, the sensitivity of the method will decrease with increasing fault resistance. A differential protection technique for MTDC transmission lines has been proposed in Ref. [18], which depends on analysis of the high frequency transients in current signals at each line terminal. As with any differential scheme, this relies on communication between both terminals representing a single point of failure and introducing inherent latency.

The time for the protection system to respond to a fault is particularly critical for MTDC. The present generation of DC circuit breakers need to operate within a few ms [19] (approximately 5 ms according to a manufacturer) [20] to successfully interrupt the rapidly increasing DC fault current. This is technically challenging but the main fault detection proposed in this paper is always shown to robustly operate under 5 ms. With ongoing improvements in breaker technology the authors believe this will be sufficiently fast either for the current generation of breakers or in the very near future.

Artificial Intelligence (AI) is a powerful collection of computing concepts modelled on the thought and behaviour of human beings and animals. Many AI techniques attempt to automate rational decisions that would usually be made by a human expert, by including missing data, adapting to evolving situations and improving performance over long time horizons based on accumulated experience. Researchers have shown that ANNs can successfully be applied to a wide array of applications, for example reservoir inflow forecasting in hydrology [21,22]. As indicated in Ref. [23], ANN based methods are effective for fault detection and fault location on AC grids and HVDC systems due to accuracy, robustness and speed. The ANN is often fed by a feature selection stage, such as the Wavelet Transform (WT). Combined sequentially, these perform fault detection, classification or location [24,25]. However, to the authors' best knowledge, there is no published work for ANNs applied to MTDC transmission protection systems.

As proposed in Ref. [26], the frequency spectrum of voltage and current contains useful information for protection purposes. The authors in Ref. [27] indicate that much of the frequency spectrum combined with an artificial neural network may be used for fault detection and fault location. Hence, the higher frequency components are selected and fed to suitably designed ANNs in this work. This paper presents a comprehensive ANN-based transient protection scheme that accurately and quickly detects, classifies and locates faults on MTDC overhead lines. The scheme is shown to have improved performance over previously used protection techniques, such as robustness to high impedance and close-up faults and excellent discrimination of external faults.

This comprehensive protection scheme based on ANNs overcomes the drawbacks of previous work, and for the first time, successfully uses wide-band information from the frequency domain for HVDC protection, opening new research avenues. The proposed method uses a larger section of the signal for detection and thus reduces the uncertainty inherent in existing travelling wave methods that rely on detection of the intial wavefront. With ANNs, the computational time is far improved, not only for fault detection, but also for fault location. The accuracy of fault detection is shown to be 100% within 4.5 ms, and location accurate to 1.16% within 25 ms compared with 1.5 s in Ref. [28] and up to 36 s in Ref. [29].

2. Multi-terminal HVDC system modelling

A three-terminal VSC based HVDC system was modelled using the PSCAD software, based on the CIGRE B4 DC grid test system [30,31]. A portion of the CIGRE B4 DC grid test system, shown in Fig. 1, consists of three symmetrical monopole converters, DC link capacitors, passive filters, phase reactors, transformers, DC transmission lines and AC sources.

2.1. Converter station modelling

In contrast to line-commutated, so-called current source converter (CSC) HVDC systems, VSC HVDC systems function as an ideal DC voltage source so the DC voltage polarity can remain constant when the power flow is reversed for a single VSC converter station. These capabilities make the VSC-HVDC suitable for constructing multi-terminal HVDC systems. In the simplest converter architecture, the AC voltage waveform is synthesized using a two-level approach. The converter can be modelled as a controllable voltage source which connects to an AC network through a series reactor at the point of common coupling (PCC) [32–34]. The basic configuration of the converter station, as well as the configuration of VSC converters of three-phase, two-level, and six-pulse bridges are presented in Fig. 2.

Although more modern multi-level converter architectures exist, the system chosen here is the well-proven two level converter for its simplicity. On the AC side, phase reactors are applied between transformers and converters for limiting both the active and the reactive power flow by regulating currents through them. The phase reactors also function as AC filters to reduce the AC current harmonic content caused by pulse width modulated (PWM) switching of the converter station. In the well-established two-level converter stations, a low-pass LC-filter is included on the AC side which will suppress high frequency harmonic components.

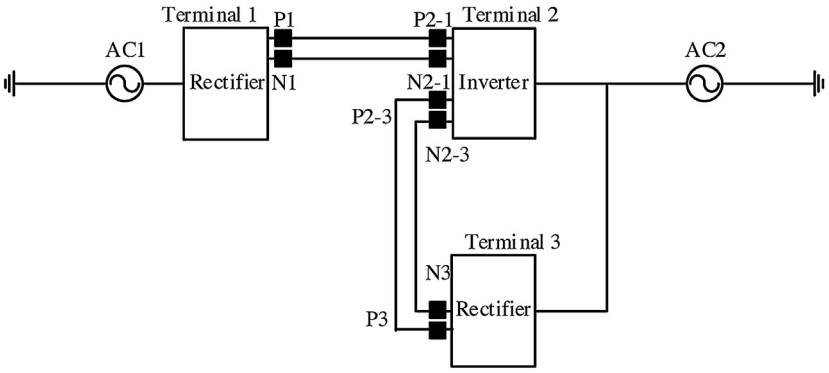

Fig. 1. The configuration of three-terminal HVDC system.

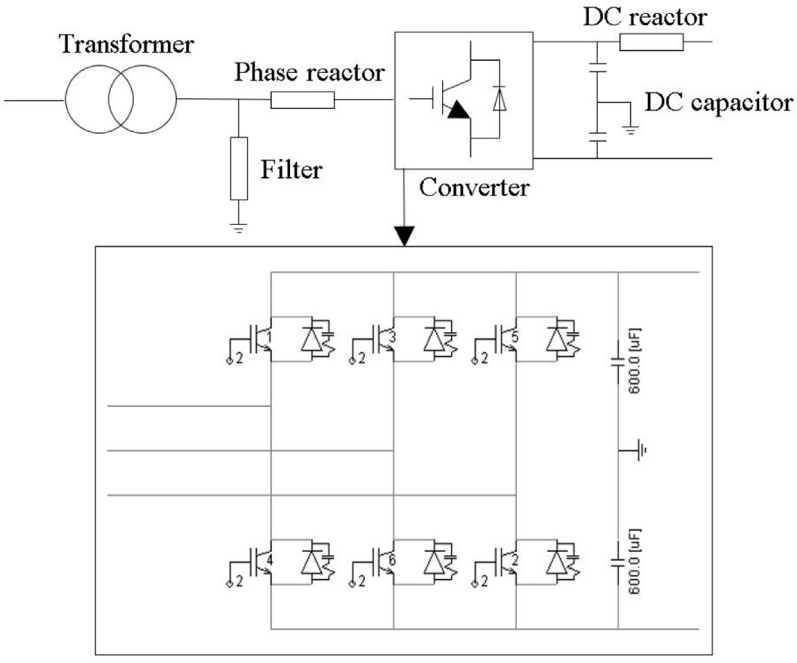

Fig. 2. Configuration of VSC converter station.

Capacitors on the DC side provide energy storage reducing the DC voltage ripple [35,36]. In addition, DC reactors are connected after DC capacitors to reduce the rate of rise of DC fault current and mitigate harmonic currents.

2.2. Transmission line model

Since the transmission line is in reality made up of distributed parameters that are frequency dependent, this scheme has been developed with such a line model to accurately capture the high frequency transient response. The branches are exclusively overhead lines, where each line is 200 km long with the geometric conductor layout illustrated in Fig. 3. Each line is a symmetrically grounded monopole.

For analysis of steady state conditions, the transmission line can be modelled using lumped parameters, however, distributed parameters should be used to accurately reflect transient behaviour [37]. The transmission line or cable can be represented by series impedances and shunt admittances per unit length. The series impedance is inherently frequency dependant due to its imaginary reactance and also due to the skin effect in the conductor and earth wires. Based on these parameters, the characteristic parameters

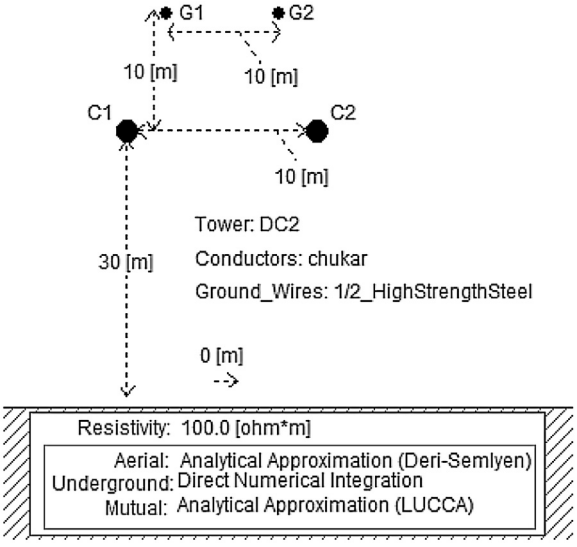

Fig. 3. The configuration of overhead transmission line model.

of the line, the surge impedance and propagation constant can be derived, which determine the propagation behaviour of travelling waves on the line [38].

2.3. Controller model

Since this scheme relies on electromagnetic transients, it is important to model the converter stations in appropriate detail, including their control systems. The coordinated control of MTDC systems is technically challenging because the power flow and voltage must be carefully controlled at each bus by the switching of the converters. There are various competing methods of achieving this in the literature [39–43]. In this paper, voltage droop control, based on system droop characteristics as discussed in Refs. [42,44], was chosen for the system control. This was chosen for relative simplicity and robustness since voltage droop control allows multiple converters to regulate the voltage at the same time [43]. Hence, if the control system in one terminal is disconnected, the other terminals can still regulate the voltage levels in the DC system.

The phase voltage, including the amplitude, the angle and the angular frequency can be actuated by the VSC control system [45]. With respect to the AC or DC grid, each VSC station can be controlled in a number of different ways. Due to the decoupled current control, the active and reactive power can be dispatched independently since the two orthogonal dq-current components can be changed independently. In the modelled network shown in Fig. 1, terminal 2 is set as a slack bus to balance the system by supplying active power. Such an approach does not require communication between the terminals, because two terminals are responsible for DC voltage regulation and the remaining terminals are responsible for providing active power under both steady state and transient conditions.

To generate the reference values in the abc frame, dq control is used. The outer controller sets the droop and applies power and DC voltage limits, as shown in Fig. 4 and in Eq. (1).

$$\left(V_{dcref} - V_{dc}\right) K - \frac{2}{3V_d}\left(P_{ref} - P\right) = 0 \tag{1}$$

where: V_{dcref} is the reference DC voltage, K is the proportional gain, V_d is the reference AC voltage in the dq0 reference frame and is desired to have constant value and P_{ref} is the reference active power.

Using appropriately tuned PI controllers, the outer controller calculates the reference currents, I_{dref} and I_{qref}, which are the inputs to the inner control. Both active power control, P, and dc voltage control, V_{dc}, are achieved by controlling the reference to the active current controller. The I_{dref} signal is obtained by combining these two types of controllers. The reactive power, Q, controls the reactive current, I_{qref}, via a PI block as shown in Fig. 4. The droop is set by Eq. (2) which determines the proportional gain, K.

$$K = \frac{2P_{rated}}{3\delta_{dc} V_d V_{dcrated}} \tag{2}$$

where: δ_{dc} is the voltage droop, P_{rated} is the rated active power, $V_{dcrated}$ is the rated DC voltage.

From a *systems* perspective, the DC bus voltage and current droop relation is directly linked to the voltage dynamics in the DC system. The current and voltage are transformed into the rotating direct-quadrature frame and the signals are passed to the inner-current PI controllers (shown in Fig. 4) that must be carefully tuned for stability. In the inner-current loop, control limits the current to protect the valves. PWM directly controls the inverter circuit switches, producing a series of pulses which have equal amplitude in the output but varying duration. The gate pulses from the PWM give the valve specific configurations to synthesise the AC waveform. Controlling the PWM can vary both the magnitude and frequency of the output voltage of the converter circuit [46].

2.4. System transient response

Because of their widespread distribution over an array of complex terrains and their exposure to the environment, transmission lines experience the highest occurrence of faults of any part of the power system, and therefore correct operation of their protection systems is crucial.

The most common overhead line short circuit faults, namely pole-to-pole faults and pole-to-ground faults are analysed in the simulated network. After the occurrence of a fault, low frequency steady state components and high frequency transient components due to travelling waves will be generated on the transmission line.

On the system depicted in Fig. 1, an example pole-to-pole fault on Section 1 between terminal 1 and terminal 2 is applied to show the transient response of the system. The fault is at 30% of the line length from terminal 1 with 0.01 Ω fault resistance. Fig. 5 depicts the DC currents and voltages on different terminals clearly have a far more significant response to the fault on the faulted line compared to the healthy line.

The control scheme must respond quickly to preserve system stability after the faulted section is de-energised, and this necessitates detailed modelling of the control to faithfully reproduce the system's transient response. Due to PWM switching action in VSC-HVDC, the current flowing to the DC side of a converter contains harmonics, which will result in a ripple on the DC side voltage. During disturbances in the AC system (i.e. faults and switching actions) large power oscillations may occur between the AC and the DC side. This in turn will lead to oscillations in the DC voltage and DC overvoltage that may stress the valves. The DC side capacitor (shown in Fig. 2) can mitigate this problem by providing faster converter response and energy storage to be able to control the power flow. The relatively small time constant allows fast control of active and reactive power.

3. Signal chain

3.1. Overview of signal chain

An overview of the signal chain is presented in Fig. 6, for fault detection and fault classification, and Fig. 7 for fault location. Firstly, a time series is generated by the digitally sampled current transducer signal. A fast Fourier transform (FFT) is applied on the windowed signal to create the input data for the ANN. A counter is then applied to the ANN to generate the diagnostic signal. Each stage is discussed in detail in forthcoming sub-sections.

3.2. Signal processing

With the high frequency component method, the detected characteristic frequency will not propagate onto the adjacent line due to the DC shunt capacitors in the current path. Therefore even though the DC current and voltage will be influenced during a fault on the other line, the characteristic frequency will only exist on the faulted line.

The windowed discrete Fourier transform (DFT), implemented using the computationally efficient FFT algorithm, is a well-established method for isolating frequency components of a signal, and thus used in a variety of real time control and protection applications [47]. Extensive studies have shown that an adequate representation of frequency domain information can be obtained by an FFT with a very short window length [48]. This leaves more computational time for the rest of the relaying scheme so that the

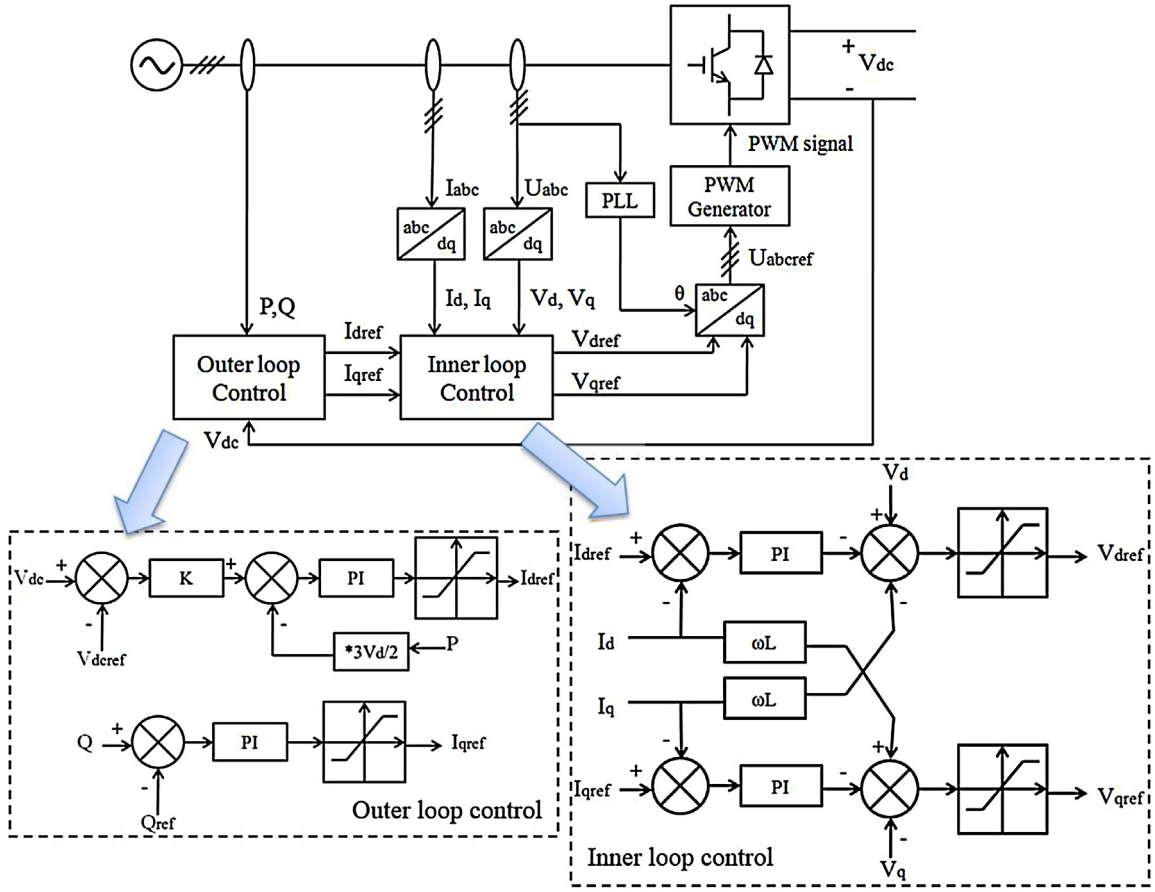

Fig. 4. The outer controller and inner controller.

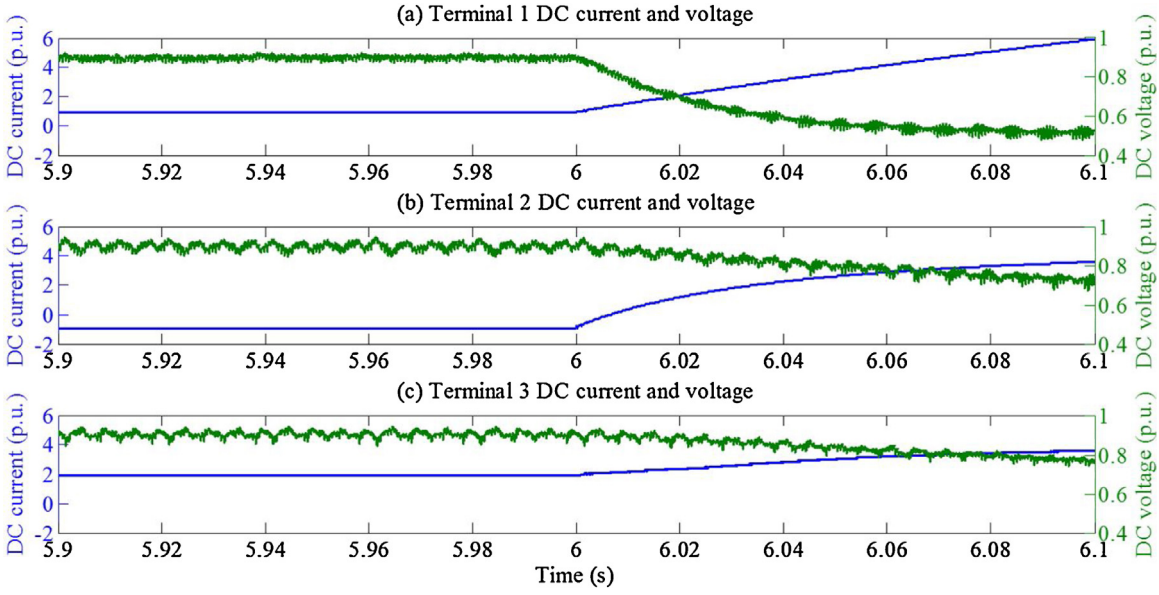

Fig. 5. The configuration of overhead transmission line.

DC circuit breakers can operate within the overall protection time budget.

Following the windowed FFT on signal $f(t)$, the complex amplitude is represented by $F(\omega)$ which gives the signal's spectral components. The real parts of $F(\omega)$ are then used to indicate the magnitude at different frequencies in the windowed signal to produce a frequency spectrum. The phase information from the imaginary part of the FFT is discarded.

The technical computing environment MATLAB was used for signal processing and neural network design. The sampling frequency of 10 kHz, which translates to 200 samples per 50 Hz AC cycle, was found to be a sufficient compromise between fault loca-

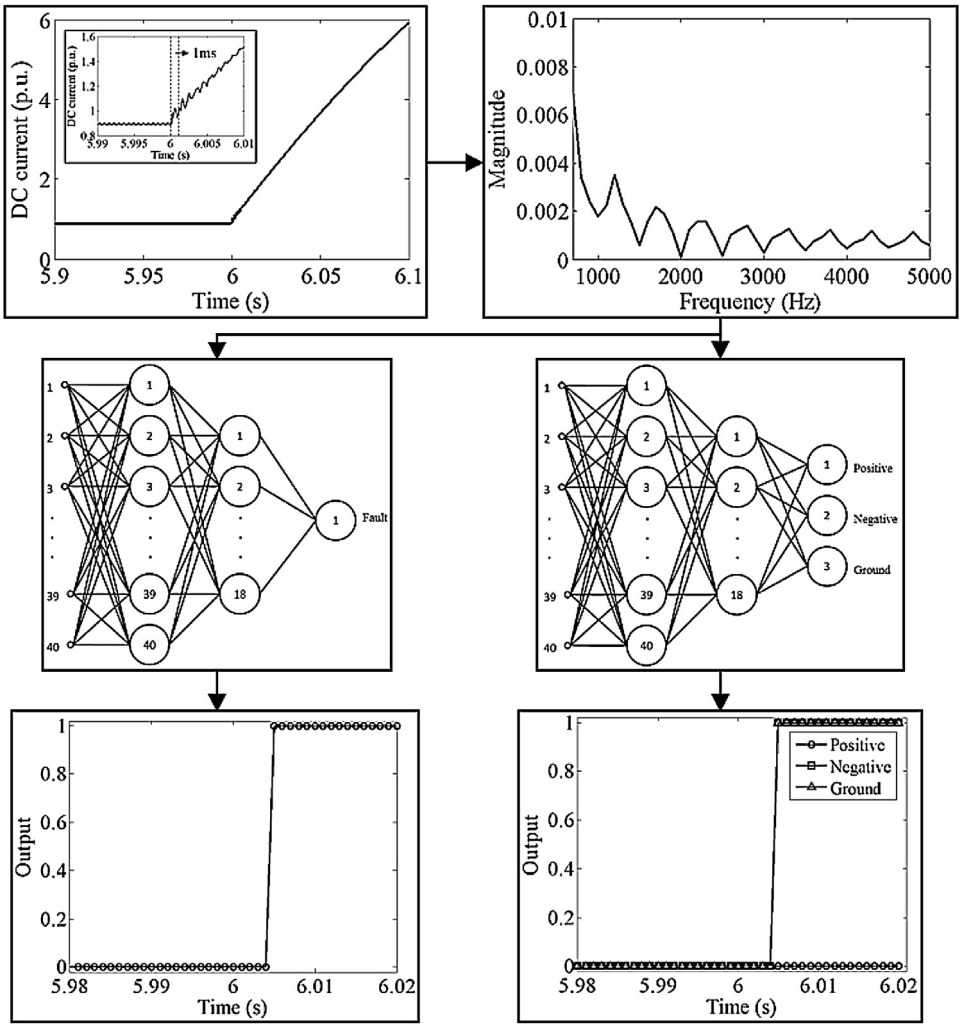

Fig. 6. Signal chain for fault detection and classification.

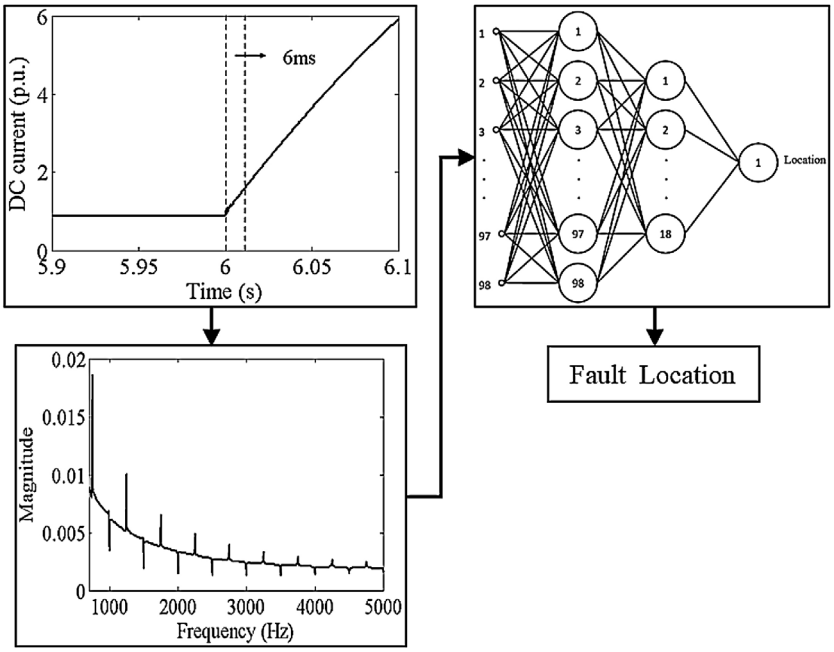

Fig. 7. Signal chain for fault location.

tion accuracy and to provide enough time for the overall relaying speed of the scheme.

The frequency spectrum generated from signal processing is shown in Fig. 8. Here, the current signal detected at terminal 1 in the system depicted in Fig. 1, is shown for the positive pole when a ground to pole fault under various conditions is simulated. The signal is windowed from the start of the fault and the window length is 6 ms. Fig. 8(a)–(e) clearly shows that only spectral features change with fault location whereas the magnitude of the spectrum changes with fault resistance. In particular, the position of the features, namely valleys and peaks, do not change with varying fault resistance, only the background level of the frequency spectrum. In contrast, the position of the features *do* vary with the location of the fault. Therefore these peaks are an important input feature to the fault location ANN.

The high frequency components shown in Fig. 8 occur because of the travelling waves that emanate from the fault location due to the sudden step change in circuit conditions. The arrival time of successive travelling waves, both original and reflected, is determined by the fault location and therefore the fault location has a direct relationship with the position of features in the frequency spectrum. The post fault frequency spectrum is largely time-independent. This increases the robustness of this frequency domain approach because regardless of the window's location on the post fault time series, it will yield a very similar frequency spectrum for some time after the fault.

Fig. 8(f) shows the frequency spectra generated in steady state conditions for comparison. The features arise largely due to the switching of the converter stations but the magnitude of these features and the overall spectral energy under steady state conditions is negligible compared with the fault conditions.

3.3. Artificial neural network

Numerous ANN-based applications have been shown to give improved performance in power system protection for tasks like fault location and phase selection. This is because of the ANN's ability to discern classes in complex problem spaces, such as between transients caused by faults and those under healthy conditions [49]. To develop formal relaying schemes, precise mathematical models of each system fault condition must be constructed. However, compared with conventional formal approaches, ANNs can be trained to recognise non-linear relationships between input and output data without requiring knowledge of their internal processes. As such, using its innate ability to recognise patterns, generalise and interpolate within the parameter space, the ANN only requires simulated training data rather than extensive formal and deterministic fault and system models [50]. Importantly, after training, ANN operation time is extremely fast because it only consists of a number of simple, interconnected processing units [50].

The Fourier transform extracts a feature vector from the current waveform and feeds it to a purposefully pre-designed neural network. Since the frequency spectrum contains sufficient information about the fault, only current signals from one terminal are required for fault detection and classification. As mentioned earlier, the frequency spectra captured for each fault case express unique features at each fault location. However due to the complexity of the mapping between spectral features and fault information, a trained ANN is an integral part of the relaying scheme. Firstly one neural network performs fault detection, namely whether the feature vector belongs to a healthy or fault condition. If a fault condition is detected, two further ANNs are trained to perform classification and fault location tasks respectively. In all cases the ANNs are multi-layer perceptron (MLP) architectures, with the specific arrangements for each ANN shown in Figs. 6 and 7 with the hyperbolic tangent sigmoid transfer function used in the hidden layers.

Table 1
Variables.

Variable	Details
Fault location	1%, 10%, 20%, 30%, 40%, 50%, 60%, 70%, 80%, 90%, 99%
Fault resistance	0.01 Ω, 2 Ω, 10 Ω, 50 Ω, 100 Ω
External fault	AC side fault at terminals 1–3 (single phase, double phase and three phase)

A window of length 1 ms is applied to capture DC current signals for fault detection and classification, whilst a 6 ms window is used for fault location. After comprehensive analysis these window lengths were empirically determined to give the best compromise between speed and accuracy for each task. Inputs are taken from standard DC current transducers and frequencies over 700 Hz of the current waveform are utilized. In the proposed fault detector and classifier, 20 frequency bands from each signal in the range 2800 Hz–4700 Hz, each approximately 95 Hz in width, show the best performance used as ANN input. (Thus, in total, each ANN has an input layer of 40 neurons of DC current, 20 from the positive line and 20 from the negative line.) The fault detection and fault classification ANN receives the same input vector with 40 inputs but they work independently from each other. For the fault location ANN, the faulty line current from both ends of the line are required with 6 ms window length. Thus in total, fault location uses 98 frequency bands between 3600 Hz and 4400 Hz, approximately 16 Hz in width, from two terminals (49 input bands from each terminal). The hidden layer consists of 18 neurons. The training data was split into 70% training samples, 15% validation samples and another 15% testing samples. For fault detection, the number of epochs was 247, for fault classification, 279, and for fault location, 189.

In order to train all three ANNs, a full range of fault scenarios were considered. Varying fault types, location, and fault resistance, for many simulation runs produced a comprehensive training set. In addition, the full range of possible healthy operational conditions of the MTDC system, including steady state conditions, external faults, such as external DC line fault condition were simulated. Using the simulation of the system in Fig. 1 and with the variables shown in Table 1, a total of 73 fault scenarios were considered, (55 DC line fault cases and 18 external fault cases). Of the fault scenarios, the training contained 10 healthy signal windows and 20 post fault input windows. In the healthy scenarios the training contained 30 consecutive windows. Hence, since each window yielded an input vector, training was completed on 2190 input vectors.

The input vectors were normalised between 0 and 1 using the maximum and minimum values encountered in the training data for each frequency band, such that 1 is the maximum and 0 is the minimum. The ANN was trained using backpropagation to produce an output vector of 1 or 0 depending on the type of fault, where '0' represents a healthy signal and '1' represents the fault signal. The transitionary case where the window captures part healthy and part faulted conditions was not used because of the ambiguity this presents in how the neural network should be trained.

At the end of the signal chain, a counter, which prevents false trips on account of noise or transitionary conditions, is applied for fault detection and classification to give a stable response. Specifically a trip signal 1 is generated after 10 consecutive ANN outputs higher than the threshold of 0.72. The counter is reset if the output falls below the threshold.

4. Test results

Using the proposed method illustrated in the flowchart shown in Figs. 6 and 7, the fault detection, classification and location results

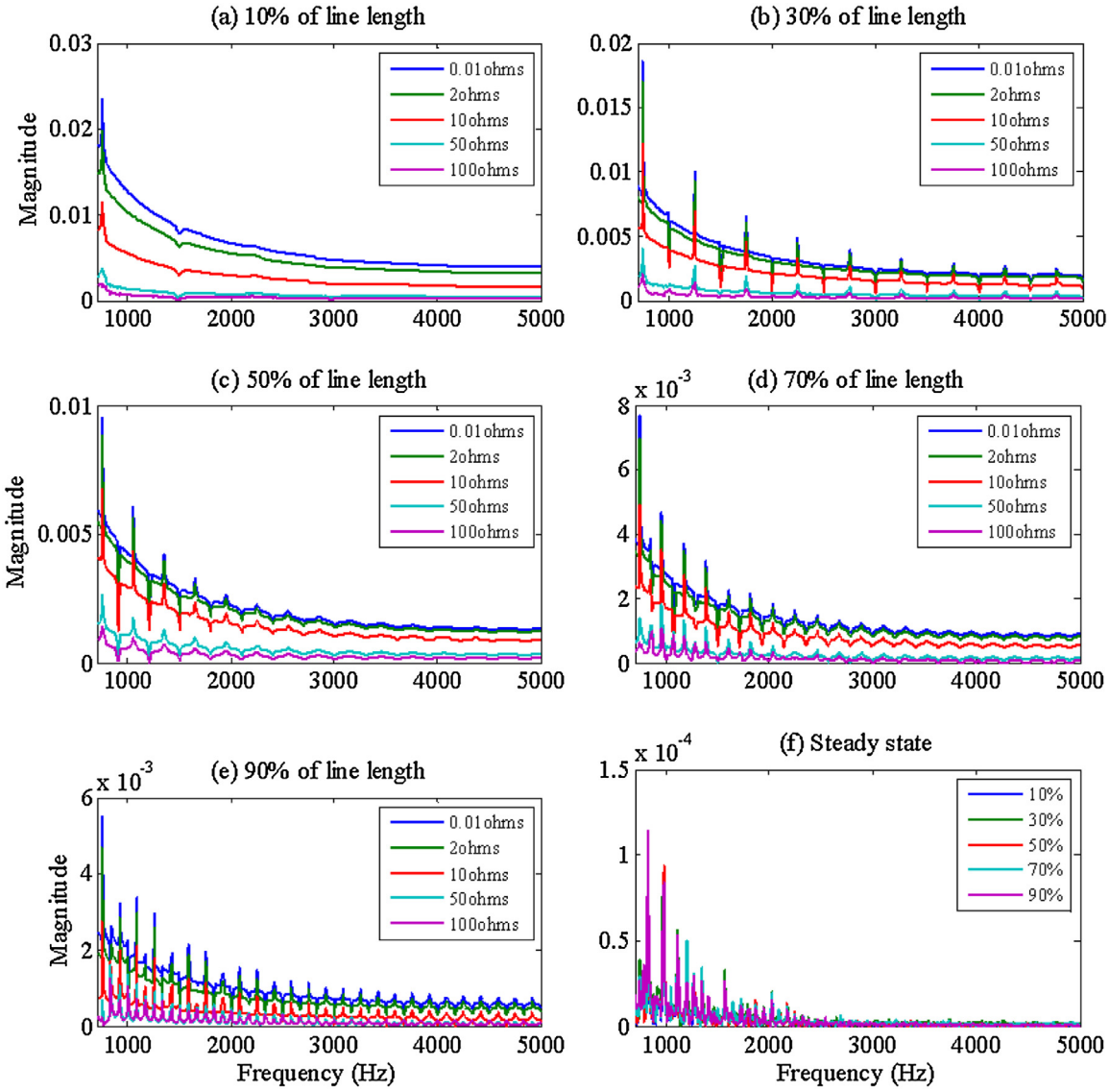

Fig. 8. Frequency spectra for different fault locations from the terminal 1, varied from 10% (a) to 90% (e) and steady state condition (f).

are shown in Table 2. The accuracy of the fault location method has been evaluated with Eq. (3) to calculate the relative error:

$$e = |\frac{D_{act} - D_{det}}{L}| \quad (3)$$

where: D_{act} is actual fault location from the measuring terminal, D_{det} is the detected fault location and L is the total length of the transmission line.

The protection system was tested with cases not used in the training data, with 15 separate locations and different fault types, such as positive pole to ground (PG), negative pole to ground (NG) and pole to pole (PN). The fault resistance was randomly varied within the limits of the training parameters but values used in training were avoided. The results show that the proposed method can accurately detect, classify and locate these faults with the largest location relative error, calculated by Eq. (3), being less than 1.16% which is comparable to distance protection. In addition the results show that the algorithm performs successfully for a range of fault resistances. As can be seen in Table 2, with the increase in fault resistance, the percentage of error does not increase, hence, the method is not adversely affected by changing fault resistance. The maximum time for fault detection is within 4.5 ms, acceptable for DC breaker operation. The fault can be located within 26 ms which is acceptable for the automated post-fault reconfiguration of wider system settings. To achieve a fast fault location in this scheme, the error is 1%, but if a longer fault location time is permitted, the accuracy can be improved.

The protection system must be able to discriminate external faults, occurring beyond the protected zone, which in this case is the protected DC transmission line. The fault detection algorithm was trained to recognise and ignore a number of external fault conditions: namely, with reference to Table 2, DC line faults, AC side faults at terminals 1–3, (including single phase to ground (AG), double phase (BC) and three phase faults (ABC)). Using external fault cases not used in the training data showed the fault detection to be 100% successful in avoiding false trips (see Table 2).

High impedance faults are generally challenging for many protection strategies because of the attenuation of the post fault characteristics and thus their resemblance to steady state pre-fault conditions. For example, it is difficult to detect faults using an overcurrent characteristic alone due to very low fault current from high impedance faults. Although absolute fault current level is slight, the current signals in the frequency domain contain enough information to indicate fault conditions. To study the sensitivity of the

Table 2
Fault location result.

Case	Internal/ external	Section	Fault type	Fault resistance Ω	Fault detection	Positive	Negative	Ground	Fault location	Measured location	Relative error	Detection time (ms)	Classification time (ms)	Location time (ms)
1	In	S1	PG	0.25	1	1	0	1	35%	35.27%	0.27%	3.6	4.5	15.4
2	In	S1	PG	9	1	1	0	1	67%	65.98%	1.02%	3.7	4.7	20.5
3	In	S1	NG	69	1	0	1	1	89%	88.65%	0.35%	3.0	4.6	23.5
4	In	S1	NG	17	1	0	1	1	12%	12.87%	0.87%	3.9	4.8	23.6
5	In	S1	PN	32	1	1	1	0	34%	34.12%	1.12%	4.5	4.9	23.8
6	In	S1	PN	1.9	1	1	1	0	53%	52.77%	0.23%	4.1	4.9	20.4
7	In	S2	PG	0.33	1	1	0	1	78%	77.96%	0.04%	3.9	4.7	17.5
8	In	S2	PG	0.7	1	1	0	1	58%	58.47%	0.47%	3.6	4.8	17.8
9	In	S2	NG	8	1	0	1	1	24%	22.84%	1.16%	4.3	4.9	19.5
10	In	S2	NG	0.3	1	0	1	1	46%	45.68%	0.32%	3.9	4.9	21.5
11	In	S2	PN	1.2	1	1	1	0	59%	58.79%	0.21%	4.2	4.7	23.4
12	In	S2	PN	6	1	1	1	0	72%	71.13%	0.87%	4.1	4.5	25.8
13	Ex	T1	ABC	0.6	0	NA	NA	NA	NA	NA	NA	3.9	NA	NA
14	Ex	T2	AG	1.6	0	NA	NA	NA	NA	NA	NA	4.1	NA	NA
15	Ex	T3	BC	1.2	0	NA	NA	NA	NA	NA	NA	4.2	NA	NA

method proposed in this paper, the training and testing set includes a range of simulated fault resistances from 0.01 Ω to 100 Ω. As can be seen in the frequency spectrum of the fault current signal in Fig. 8, the frequency features can still be obtained under high fault resistance conditions. Therefore despite the difficulties that high impedance faults present to many existing protection techniques, the technique presented here is robust to fault impedances up to 100 Ω. Compared with the travelling wave based fault location method using a 192 kHz sampling frequency [12], the proposed method in this paper uses a relatively low sampling frequency of 10 kHz. It is worth noting that due to the wideband information that the scheme relies on, the method will work for different sampling rates, provided the sampling is fast enough to reproduce the frequencies required by the ANN stage. Furthermore by using the windowed FFT, ANN and counter together, the scheme is more robust to noise since several frequency spectra act together to smooth out anomalies. To test this, white noise with 50 dB SNR was added to the DC current. Frequency spectra generated before and after addition of noise had exactly the same performance response to the fault location ANN.

5. Conclusion

This paper described a comprehensive novel MTDC protection scheme based on artificial neural networks. The high frequency components from fault current signals are input to specially trained ANNs. A three-terminal VSC-based HVDC model based on CIGRE B4 programme was implemented in PSCAD/EMTDC with different types of faults simulated in the DC transmission system. The general approach is valid for any MTDC system, or indeed, HVDC link, provided the system can be first simulated to generate custom ANN training data for calibration. Fault current signals were detected on all terminals in order to create frequency spectra, giving insights into the characteristic frequency components contained within the signal. Three separate neural networks for fault detection, fault classification and fault location were designed. The fault detection can detect the internal fault for both line-to-ground faults and line-to-line faults, the faulted section of the MTDC network, and distinguish external faults from internal faults. Both detection and classification only rely on single terminal measurements and so do not require a communication link, whilst the entire scheme relies only on current signals and thus DC voltage transducers are not required. The most important achievement presented is that the fault detection and classification can meet the time requirement of DC circuit breakers, and the fault location is accurate and fast enough for online, automation of wider system protection settings if desired. The proposed method is demonstrably robust to high resistance faults and noise. Since the method is purposefully designed for multi-terminal systems, it is robust to faults on other DC lines. Although it is sufficiently fast, the fault detection is not as fast as some existing methods, but importantly unlike the travelling-wave methods that only rely on the initial wavefront, more of the post-fault signal is used, offering the 100% reliability demonstrated in the results.

With the rapid development of HVDC technology, MMC converters are now the state of the art. However there are a wide range of competing MMC topologies available, from different manufacturers, with no one option prevailing across the few installed systems across the world. Thus for the sake of simplicity, and to demonstrate the approach on the most developed technology, the well-established 2-level converter was used to validate the presented method. In future work, this new method will be demonstrated on a wide range of MMC converter systems. However, regardless of the nature of the converter station, the authors are

confident the method will be valid as long as training data is available for the ANNs via simulation.

The training process is important for the robustness of the method. Since the simulation work must prove the concept first on one system, the training data is limited to one system in this paper. In order to reduce the uncertainties, more training data will be used to produce a more generic system in later work. In order to achieve the best compromise between fault location time and the accuracy, a comparison between different window lengths will be conducted to investigate the best performance between speed and accuracy. More extensive training data from different systems will be used to generalise the ANN responses.

Acknowledgements

The authors gratefully acknowledge the support and use of facilities in the department of Electronic and Electrical Engineering, University of Bath, UK. Q. Yang would like to thank the support provided by Chinese Scholarship Council.

References

[1] D. Van Hertem, M. Ghandhari, Multi-terminal VSC HVDC for the European supergrid: obstacles, Renew. Sustain. Energy Rev. 14 (2010) 3156–3163.
[2] S. Azizi, M. Sanaye-Pasand, M. Abedini, A. Hassani, A traveling-wave-based methodology for wide-area fault location in multiterminal DC systems, IEEE Trans. Power Deliv. 29 (2014) 2552–2560.
[3] O. Gomis-Bellmunt, J. Liang, J. Ekanayake, R. King, N. Jenkins, Topologies of multiterminal HVDC-VSC transmission for large offshore wind farms, Electr. Power Syst. Res. 81 (2011) 271–281.
[4] N. Flourentzou, V.G. Agelidis, G.D. Demetriades, VSC-based HVDC power transmission systems: an overview, IEEE Trans. Power Electr. 24 (2009) 592–602.
[5] K. Sano, M. Takasaki, A surgeless solid-state DC circuit breaker for voltage-source-converter-based HVDC systems, IEEE Trans. Ind. Appl. 50 (2014) 2690–2699.
[6] V. Pathirana, P. McLaren, A hybrid algorithm for high speed transmission line protection, IEEE Trans. Power Deliv. 20 (2005) 2422–2428.
[7] X. Liu, A.H. Osman, O.P. Malik, Real-time implementation of a hybrid protection scheme for bipolar HVDC line using FPGA, IEEE Trans. Power Deliv. 26 (2011) 101–108.
[8] O. Nanayakkara, A.D. Rajapakse, R. Wachal, Traveling-wave-based line fault location in star-connected multiterminal HVDC systems, IEEE Trans. Power Deliv. 27 (2012) 2286–2294.
[9] O.M.K.K. Nanayakkara, A.D. Rajapakse, R. Wachal, Location of DC line faults in conventional HVDC systems with segments of cables and overhead lines using terminal measurements, IEEE Trans. Power Deliv. 27 (2012) 279–288.
[10] M.M. Saha, J.J. Izykowski, E. Rosolowski, Fault Location on Power Networks, Springer Science & Business Media, 2009.
[11] X. Zheng, T. Nengling, Y. Guangliang, D. Haoyin, A transient protection scheme for HVDC transmission line, IEEE Trans. Power Deliv. 27 (2012) 718–724.
[12] X. Liu, A. Osman, O. Malik, Hybrid traveling wave/boundary protection for monopolar HVDC line, IEEE Trans. Power Deliv. 24 (2009) 569–578.
[13] K. De Kerf, K. Srivastava, M. Reza, D. Bekaert, S. Cole, D. Van Hertem, R. Belmans, Wavelet-based protection strategy for DC faults in multi-terminal VSC HVDC systems, Gener. Transm. Distrib. IET 5 (2011) 496–503.
[14] W. Leterme, J. Beerten, D. Van Hertem, Nonunit protection of HVDC grids with inductive DC cable termination, IEEE Trans. Power Deliv. 31 (2016) 820–828.
[15] Z. Xiao-Dong, T. Neng-Ling, J.S. Thorp, Y. Guang-Liang, A transient harmonic current protection scheme for HVDC transmission line, IEEE Trans. Power Deliv. 27 (2012) 2278–2285.
[16] M. Hajian, L. Zhang, D. Jovcic, DC transmission grid with low-speed protection using mechanical DC circuit breakers, IEEE Trans. Power Deliv. 30 (2015) 1383–1391.
[17] S.P. Azad, W. Leterme, D. Van Hertem, A DC grid primary protection algorithm based on current measurements, 17th European Conference on Power Electronics and Applications (EPE15 ECCE-Europe), IEEE (2015) 1–10.
[18] A.E. Abu-Elanien, A.A. Elserougi, A.S. Abdel-Khalik, A.M. Massoud, S. Ahmed, A differential protection technique for multi-terminal HVDC, Electr. Power Syst. Res. 130 (2016) 78–88.
[19] D. Van Hertem, O. Gomis-Bellmunt, J. Liang, HVDC Grids: For Offshore and Supergrid of the Future, Vol. 51, John Wiley & Sons, 2016.
[20] M. Callavik, A. Blomberg, J. Häfner, B. Jacobsen, The hybrid HVDC breaker. An innovation breakthrough enabling reliable HVDC grids, ABB Grid Systems Technical Paper (2013).
[21] M. Valipour, Optimization of neural networks for precipitation analysis in a humid region to detect drought and wet year alarms, Meteorol. Appl. 23 (2016) 91–100.
[22] M. Valipour, M.E. Banihabib, S.M.R. Behbahani, Comparison of the ARMA, ARIMA, and the autoregressive artificial neural network models in forecasting the monthly inflow of Dez dam reservoir, J. Hydrol. 476 (2013) 433–441.
[23] M. Mirzaei, M. Ab Kadir, E. Moazami, H. Hizam, Review of fault location methods for distribution power system, Aust. J. Basic Appl. Sci. 3 (2009) 2670–2676.
[24] K. Silva, B. Souza, N. Brito, Fault detection and classification in transmission lines based on wavelet transform and ANN, IEEE Trans. Power Deliv. 21 (2006) 2058–2063.
[25] F. Martín, J.A. Aguado, Wavelet-based ANN approach for transmission line protection, IEEE Trans. Power Deliv. 18 (2003) 1572–1574.
[26] S. Le Blond, R. Bertho, D. Coury, J. Vieira, Design of protection schemes for multi-terminal HVDC systems, Renew. Sustain. Energy Rev. 56 (2016) 965–974.
[27] S.P. Le Blond, Q. Deng, M. Burgin, High frequency protection scheme for multi-terminal HVDC overhead lines, 12th IET International Conference on Developments in Power System Protection (DPSP 2014) (2014) 1–5.
[28] J. Liu, J. Duan, H. Lu, Y. Sun, Fault location method based on EEMD and traveling-wave speed characteristics for HVDC transmission lines, J. Power Energy Eng. 3 (2015) 106.
[29] S. Marx, B.K. Johnson, A. Guzmán, V. Skendzic, M.V. Mynam, Traveling wave fault location in protective relays: design, testing, and results, in: Proceedings of the 16th Annual Georgia Tech Fault and Disturbance Analysis Conference, Atlanta, GA, 2013.
[30] T.K. Vrana, Y. Yang, D. Jovcic, S. Dennetire, J. Jardini, H. Saad, The CIGRE B4 DC grid test system, System 500 (2013) D1.
[31] Q. Yang, S. Le Blond, F. Liang, W. Yuan, M. Zhang, J. Li, Design and application of superconducting fault current limiter in a multiterminal HVDC system, IEEE Trans. Appl. Supercond. 27 (2017) 1–5.
[32] J. Beerten, S. Cole, R. Belmans, Modeling of multi-terminal VSC HVDC systems with distributed DC voltage control, IEEE Trans. Power Syst. 29 (2014) 34–42.
[33] J. Li, M. Zhang, Q. Yang, Z. Zhang, W. Yuan, SMES/battery hybrid energy storage system for electric buses, IEEE Trans. Appl. Supercond. 26 (2016) 1–5.
[34] R.T. Pinto, P. Bauer, S.F. Rodrigues, E.J. Wiggelinkhuizen, J. Pierik, B. Ferreira, A novel distributed direct-voltage control strategy for grid integration of offshore wind energy systems through MTDC network, IEEE Trans. Ind. Electr. 60 (2013) 2429–2441.
[35] D. Jovcic, K. Ahmed, High Voltage Direct Current Transmission: Converter, Systems and DC Grids, John Wiley & Sons, 2015.
[36] J. Li, A.M. Gee, M. Zhang, W. Yuan, Analysis of battery lifetime extension in a SMES-battery hybrid energy storage system using a novel battery lifetime model, Energy 86 (2015) 175–185.
[37] C. Wadhwa, High Voltage Engineering, New Age International, 2007.
[38] A. Wasserrab, G. Balzer, The significance of frequency-dependent overhead lines for the calculation of HVDC line short-circuit currents, Electr. Eng. (2015) 1–11.
[39] J. Khazaei, Z. Miao, L. Piyasinghe, L. Fan, Minimizing DC system loss in multi-terminal HVDC systems through adaptive droop control, Electr. Power Syst. Res. 126 (2015) 78–86.
[40] J. Li, X. Wang, Z. Zhang, S. Le Blond, Q. Yang, M. Zhang, W. Yuan, Analysis of a new design of the hybrid energy storage system used in the residential m-CHP systems, Appl. Energ. 187 (2017) 169–179.
[41] X. Zhao, K. Li, Droop setting design for multi-terminal HVDC grids considering voltage deviation impacts, Electr. Power Syst. Res. 123 (2015) 67–75.
[42] T.M. Haileselassie, Control of Multi-terminal VSC-HVDC Systems, 2008, Online: https://daim.idi.ntnu.no/masteroppgaver/004/4126/masteroppgave.pdf. (Accessed May 2016).
[43] C. Dierckxsens, K. Srivastava, M. Reza, S. Cole, J. Beerten, R. Belmans, A distributed DC voltage control method for VSC MTDC systems, Electr. Power Syst. Res. 82 (2012) 54–58.
[44] J. Li, Q. Yang, F. Robinson, F. Liang, M. Zhang, W. Yuan, Design and test of a new droop control algorithm for a SMES/battery hybrid energy storage system, Energy 118 (2017) 1110–1122.
[45] J. Li, R. Xiong, Q. Yang, F. Liang, M. Zhang, W. Yuan, Design/test of a hybrid energy storage system for primary frequency control using a dynamic droop method in an isolated microgrid power system, Appl. Energy (2016) http://dx.doi.org/10.1016/j.apenergy.2016.10.066.
[46] A. Lindberg, T. Larsson, PWM and control of three level voltage source converters in an HVDC back-to-back station, Sixth International Conference on AC and DC Power Transmission (ACDCPT 1996), IET (1996) 297–302.
[47] Y. Guo, M. Kezunovic, D. Chen, Simplified algorithms for removal of the effect of exponentially decaying DC-offset on the Fourier algorithm, IEEE Trans. Power Deliv. 18 (2003) 711–717.
[48] E.C. Ifeachor, B.W. Jervis, Digital Signal Processing: A Practical Approach, Pearson Education, 2002.
[49] Q.-H. Wu, Z. Lu, T. Ji, Protective Relaying of Power Systems Using Mathematical Morphology, Springer Science & Business Media, 2009.
[50] T.S. Dillon, D. Niebur, Neural Networks Applications in Power Systems, CRL Publishing, London, 1996.

Design and Application of Superconducting Fault Current Limiter in a Multiterminal HVDC System

Qingqing Yang, Simon Le Blond, Fei Liang, Weijia Yuan, Min Zhang, and Jianwei Li

***Abstract*—Voltage source converter based HVdc (VSC-HVdc) systems are prone to high short-circuit current during transmission line faults. The situation for multiterminal HVdc (MTDC) systems is worse. The characteristics of superconducting material are ideal to limit the fault current in HVdc systems. This paper presents a novel use of the resistive type of superconducting fault current limiter (SFCL) in the MTdc network with the function of limiting the high current. The working principles of fault current limiter and a three-terminal HVdc system are modeled in detail using PSCAD/EMTDC software. The hybrid operation of the SFCL in the three-terminal HVdc system is tested in this paper for the fault response of the MTdc system. The performances of SFCL under different fault conditions are analyzed. The simulation results show that the fault current is effectively restrained and the SFCL can act as an efficient protective device for VSC-based multiterminal HVdc systems.**

***Index Terms*—DC line fault, dynamic analysis, multi-terminal VSC-HVDC, PSCAD/EMTDC, superconducting fault current limiter.**

I. Introduction

HVDC, especially multi-terminal HVDC systems have become a more and more attractive option for power system transmission [1]. VSC-HVDC technologies have been widely used in multi-terminal HVDC systems because of its full controllability [2]. A series inductor connected with the line in current source converter based HVDC (CSC-HVDC) can naturally withstand short circuit faults, but not applied in VSC-HVDC systems [3]. Compared with the traditional HVDC system, VSC-HVDC is subjected to high short circuit fault current caused by DC transmission line faults [4]. In addition, the DC fault current rises much more rapidly in MTDC system and has larger magnitude compared with the point-to-point HVDC systems [5]. Hence, the studies related to limit fault current for HVDC transmission system (especially the one using VSC technology and multi terminal converter stations) is necessary.

In many cases, shunt reactors (inductors) are used to decrease fault current while the fixed impedance in these devices will reduce system efficiency and may impair system stability [6]. Fault current limiters (FCLs) are developed with the capability of rapidly increasing their impedance, and thus limiting high fault currents. Superconducting material has been investigated to be use in many areas such as energy storages [7], [8], transportations [9] and so on. Superconducting fault current limiters (SFCLs) utilize superconducting materials to limit the fault current and improve power system reliability and stability.

Various design technology of FCL has been considered, the resistive SFCL, saturable-core SFCL, shielded-core SFCLand non-superconducting technologies. The FCL based on superconducting technology relies on the transition of superconductor from superconducting state to normal state (quenching process) and the non-superconducting technologies use DC HTS magnet windings to saturate an iron core [6]. For HVDC systems, the resistive SFCL is commonly designed as proposed in paper [10]–[12]. However, other types of SFCL are still applied in HVDC systems, such as the flux-coupling type of SFCL are used in [13]. A hybrid type of superconducting circuit breaker is introduced in [5].

The main purpose of this paper is to design and simulate the resistive types of SFCL, which have been applied in a three-terminal HVDC system. This research has emphasized the feasibility of SFCL in multi-terminal HVDC systems. An SFCL can suppress the large DC fault current in MTDC system to breakable values during the response time of DCCB and reduce the current interruption stress on DCCB components.

II. Superconducting Fault Current Limiter

Resistive type SFCL is one of the most promising SFCLs due to its simplicity, low weight, and volume. A low impedance value will be kept under normal operation and a higher value will be transformed during fault conditions. The resistance of SFCL is almost zero with the negligible influence on the system in normal operation [14]. The increased impedance makes the current decreasing to levels below the breaker limit during a fault situation, which can effectively reduce the fault current in the DC system [4]. In addition, the stability margins of the system will be enhanced by applying SFCL.

The performance of an SFCL is dominated by the interaction between High Temperature Superconductors (HTS) electromagnetism and thermal physics. With the second generation Yttrium barium copper oxide (YBCO) coated conductors, the SFCL can be built with high current density as well as fast transition and recovery. The wire used in this paper is 12 mm width and 0.15 mm thickness with 250 A rated current. The resistance is 0.104 Ω/m. 6 wires with 120 Ω resistance is in parallel, hence the total resistance is 20 Ω. The critical current is 1.5 kA in SFCLs.

Manuscript received September 6, 2016; accepted February 2, 2017. Date of publication February 14, 2017; date of current version March 6, 2017. *(Corresponding author: Jianwei Li.)*

The authors are with the Department of Electronic and Electrical Engineering, University of Bath, Bath BA2 7AY, U.K. (e-mail: jl977@bath.ac.uk).

Color versions of one or more of the figures in this paper are available online at http://ieeexplore.ieee.org.

Digital Object Identifier 10.1109/TASC.2017.2669152

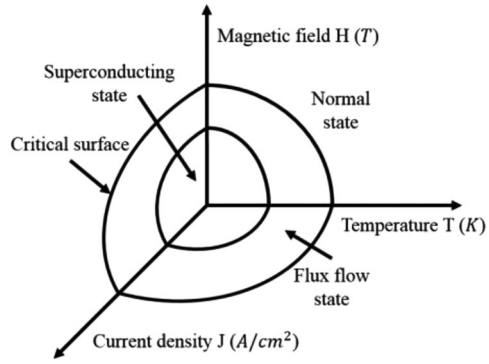

Fig. 1. 3-D phase diagram.

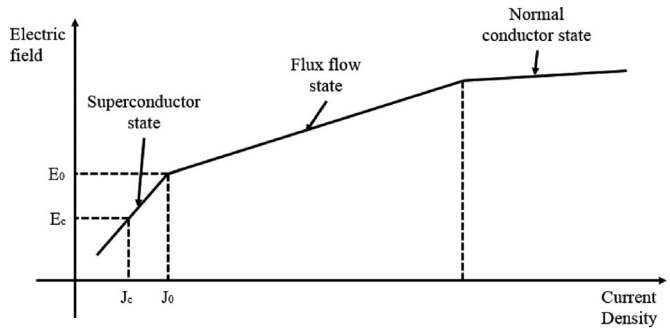

Fig. 2. E-J curve of HTS [16].

Three properties are used to describe the superconducting state, which are temperature (T), magnetic field (H) and current density (J). A 3-D phase diagram (Fig. 1) is generated to present the characteristics of the dependencies for HTS. The modes of operation of the SFCL can be described in three states: superconducting state, flux flow state, and normal conductor state, according to the value of the resistance, in addition to the recovery to the superconducting state.A maximum value can be reached when the other two critical parameters are set to be 0. The volume from the origin to the inner surface is regarded as the superconducting region. The variation of any of these three parameters can bring a transition between the superconducting and the normal conducting regime.

Electrical field and current density, which is known as E-J Power Law, as shown in Fig. 2, of HTS, is the best way to describe the electromagnetic properties of SFCLs. I_c and J_c represent the critical current and the critical current density respectively. J_c is normally defined as the current density value where the electric field E in the superconductor is 1 V/cm for simplicity and consistency. The critical current of the developed model is set to 1 kA. YBCO coated conductors usually have large n value of E-J power law [15]. Any current transient which exceeds critical current I_c will trigger the quench operation of the model.The flux flow resistance will increase in a step form within the first half cycle of the fault current. This piecewise linear conductance property is implemented in the simulation work to simulate the related SFCL. Therefore, the developed model of SFCL on PSCAD/EMTDC is represented as a constant resistance. The DC current is used to determine the critical point at which the SFCL will be converted to normal conducting state.

Because superconductors possess highly non-linear properties, superconductors are used to limit peak currents which depend on the non-linear response to temperature, current and magnetic field variations. The resistance transition of superconducting tapes in terms of temperature and current density is the best way to describe the characteristics of the resistive type SFCL current limiting behavior (1) [15].

$$R_{SFCL} = \begin{cases} 0 & J < J_c,\ T < T_c \\ f\left[\left(\frac{J}{J_c}\right)^n\right] & J > J_c,\ T < T_c \\ f(T) & T > T_c \end{cases} \tag{1}$$

Where: J is the current density of superconductor, T is the temperature, T_c and J_c represent the critical temperature and the critical current density respectively, and n represents the exponent of E-J power law relation.

The critical current density of superconductor is [14]:

$$\mathrm{J}_c = \mathrm{J}_{\mathrm{c0}}\left(\frac{\mathrm{T}_c - \mathrm{T}\,(\mathrm{t})}{\mathrm{T}_c - \mathrm{T}_o}\right)^{\alpha} \tag{2}$$

Where J_{c0} is the critical current density of superconducting at the initial temperature T_o, α is the cross-sectional area of the superconducting material and T_c is the critical temperature.

When the current exceeds the critical current, the resistivity starts to increase to very high values according to the following equation:

$$\rho_{\mathrm{sc}} = \frac{\mathrm{E}_0}{\mathrm{J}_c}\left(\frac{\mathrm{J}}{\mathrm{J}_c}\right)^{\mathrm{N}-1},\ \mathrm{T} < \mathrm{T}_c,\ \mathrm{J} > \mathrm{J}_{\mathrm{c}} \tag{3}$$

Then, the temperature of the YBCO is calculated as follows:

$$\mathrm{T}\,(\mathrm{t}) = \mathrm{T}_o + \frac{1}{\mathrm{C}_p}\int_0^{\mathrm{t}} \mathrm{Q}_{\mathrm{sc}}\,(\mathrm{t})\,\mathrm{dt} \tag{4}$$

Where: Q_{sc} is the net energy in the superconducting windings, T_o is the initial temperature of the material and C_p is the heat capacity of the material which describes the amount of heat needed to increase the material temperature by one degree.

In (1), when the condition $\mathrm{J} < \mathrm{J}_c,\ \mathrm{T} < \mathrm{T}_c$ is met, the SFCL will be in superconducting state which represents zero resistance. SFCL will transition to flux flow state when $\mathrm{J} > \mathrm{J}_c,\ \mathrm{T} < \mathrm{T}_c$. When the temperature reaches its critical value ($\mathrm{T} > \mathrm{T}_c$), the status will be in the normal resistive mode. The SFCL model is established in PSCAD/EMTDC which is a powerful tool for the system-level simulation [17]. The DC currents are measured on both ends of the transmission line. The superconducting resistance is a constant for different states and can be calculated for each transition to a new state.

The basic design of SFCL is shown in Fig. 3 established in PSCAD/EMTDC. Both the temperature and magnetic behaviour are considered in this paper. Once a fault occurs, the DC current will increase rapidly causing the temperature and magnetic behaviour to change, hence, the control model of the SFCL will work. The input selectors are a major component used to detect the mode of the SFCL by determining the critical

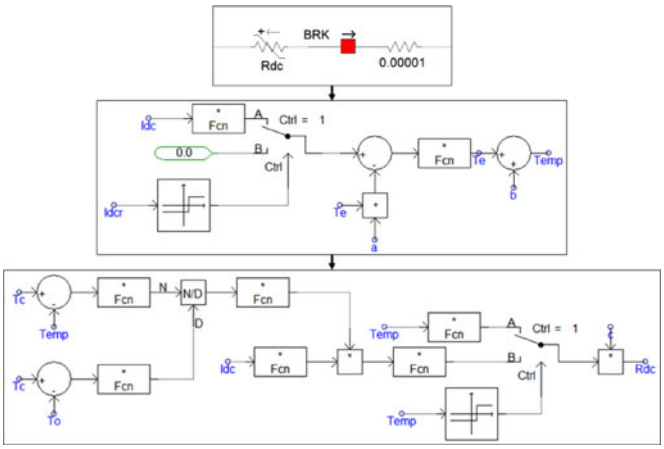

Fig. 3. SFCL model in PSCAD/EMTDC.

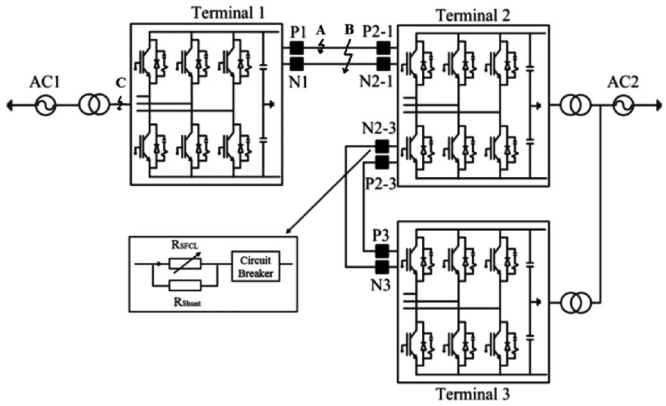

Fig. 4. The configuration of three-terminal HVDC system.

TABLE I
NOMINAL PARAMETERS OF THE SIMULATED TEST SYSTEM

Parameter	Nominal Value
Rated power	100 MVA
DC link voltage	±40 kV
R, L, C of DC overhead lines	10 mΩ/km, 0.56 mH/km, 0.26 μF/km
DC terminal reactor	300 mH
L-filter impedance ($r + j\omega L$)	(0.01 + j0.25) p.u.
Line-line AC voltage	24.5 kV
Two series capacitors	600 μF

temperature and critical current density. SFCL model compares the value of the incoming current with the setting current value. If the incoming current is less than the triggering current, the SFCL remains at minimum impedance. On the other hand, the SFCL will reach to higher impedance if the incoming current value is more than the triggering current.

III. THE MTDC SYSTEM MODELLING

A three-terminal VSC based HVDC system on the basis of CIGRE B4 programme [18] is developed in PSCAD/EMTDC software shown in Fig. 4 (parameters in Table I). For all

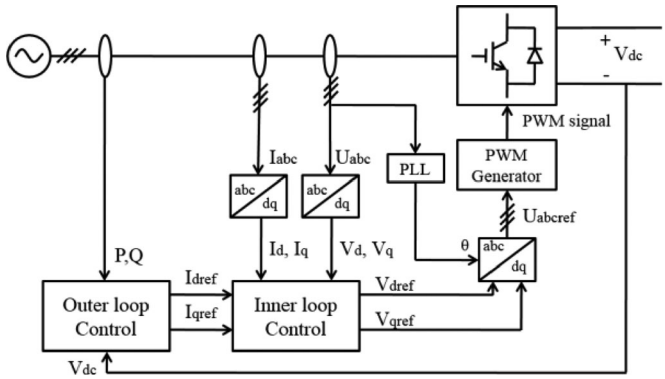

Fig. 5. VSC converter control.

transmission links a 200 km long overhead line with frequency-dependent model, which is illustrated, is adopted in this paper.

VSC based converter station control is presented in Fig. 5. VSC-HVDC systems function as an ideal voltage source at the DC terminals and can be connected in parallel without posing any technical difficulties [19]. The AC voltage waveform is synthesized using a two-level approach. In the established network, terminal 3 works as the sender to terminal 2. In addition, terminal 2 transport power to terminal 1.

Once the DC line fault occurs, the DCCBs operate and cut the fault at both ends of the line to keep stable operation with no power losses. Two SFCLs are applied at two ends of the transmission lines working together with circuit breakers. The main function of SFCL in DCCB is to suppress the increasing DC fault current to a lower level and significantly reduce the current interruption stress on DCCB components.

IV. SIMULATION RESULT AND DISCUSSION

In order to investigate the performance of multi-terminal VSC-HVDC system in Fig. 4 with the designed SFCL model, various simulation situations are carried out for the DC line faults on different sections and AC faults on different terminals. Pole to ground faults (Position A), pole to pole faults (Position B) and AC side faults (Position C) were simulated with different fault resistance as shown in Fig. 4. The fault is applied at 6 s and lasts 0.05 s. The first case is applying a DC line to ground fault for 50 ms duration. The fault is set at the positive pole and 40% of total line distance from terminal 1 with 0.01 Ω fault resistance.

The operating characteristics of SFCL when HVDC line-to-ground fault occurred are shown in Fig. 6 (1 p.u. = 1 kA). As depicted in Fig. 6, the peak fault current can reach up to approximately 4.75 times of the normal DC current on the faulted pole. With SFCL applied on both ends of the transmission line. It is shown that, with SFCL, the current peak is limited to about 2.51 p.u, while the prospective current is 3.82 p.u. on positive pole. This means the fault current is limited to 35% from the fault condition without SFCL.

The performances of SFCL during DC line to line fault are shown in Fig. 7. Because of the fault profile of line-to-line faults, the positive pole, and negative pole present the similar features

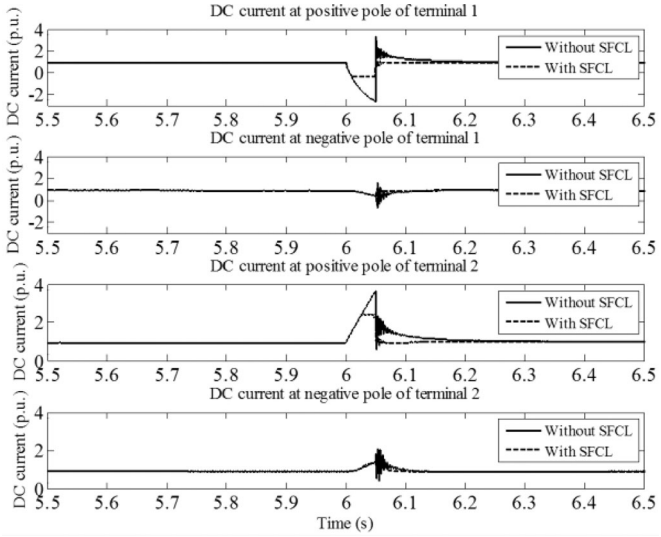

Fig. 6. Positive pole to ground fault.

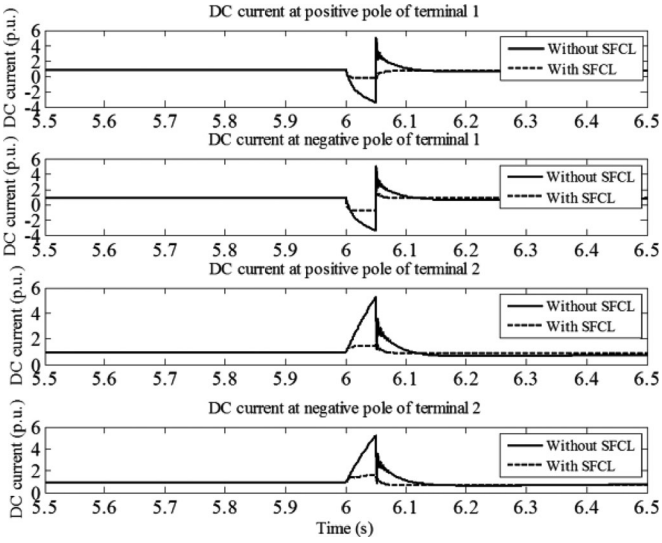

Fig. 7. Pole to pole fault.

of curve. 5.76 p.u. can be reached during a fault, which is 7 times the original current. With SFCL the fault currents can be limited to 65% for both ends and poles.

Using a three phase AC fault as an example, Fig. 8 shows the HVDC transmission line DC current under these conditions. In this case, 3.96 p.u. of maximum transient fault current on DC transmission line was observed. When SFCLs were applied, simulation result of DC current of transmission line was drastically decreased to 1.89 p.u., which means 50% fault current is limited by the SFCL. Through the analysis of the simulation results, the resistive SFCLs can effectively limit the first peak of fault current.

The SFCL responds together with the rest of the protection system and therefore can be complementary to circuit breakers reducing the fault current breaking requirement. It is figured out that the terminal 2-3 link will charge the DC side capacitor

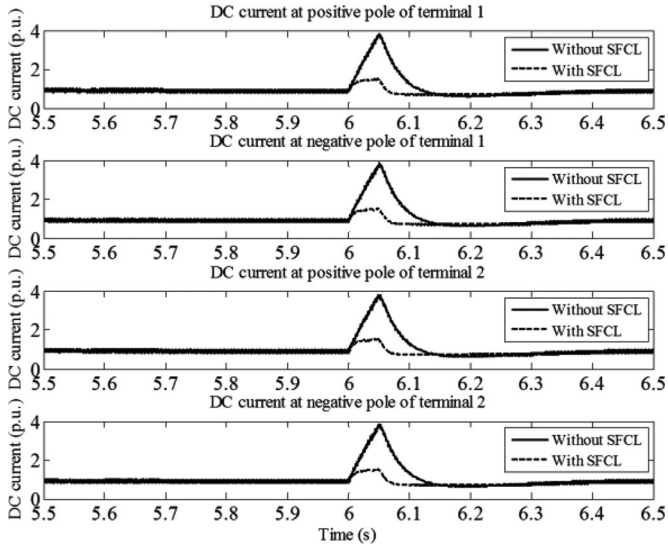

Fig. 8. Three phase AC fault.

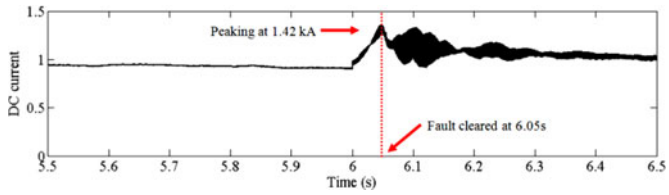

Fig. 9. Fault response on healthy link.

at terminal 2 under short circuit conditions on the terminal 1-2 link In the protection method, the directional element is usually used to tell the direction of the fault current, which works as the criterion to tell the whether the fault is internal or external. Hence, if the fault occurs between terminal 1 and terminal 2, because of the inverse current direction, the protection scheme between terminal 2 and terminal 3 will not come to action.

Actually, in the proposed MTDC system, the current in the healthy link will not go beyond the saturation limit even in the worst case. Fig. 9 shows the waveform of DC current on link 2-3 in the worst case that the fault happens on the link 1-2 and at 1% of the line length from terminal 2. As it can be seen from Fig. 9, the DC current starts to increase in the sixth second, when the fault occurs and peaks at 1.42 kA when the fault is cleared in the second of 6.05. Then the DC current begins to decrease till to the stable value. Neither the fault current during the period from 6s to 6.05s nor the restoring current after 6.05s goes beyond the saturation current (1.5 kA).

The fault current in HVDC system which only have resistance but no impedance effect will be very large compared to AC systems and the situation in MTDC system is more severe compared with point-to-point system. The most important thing need to be emphasized is the high limitation level (up to 80%). HTS SFCL could also reduce the loss during normal conditions, while IGBT DC breakers loss could not be neglected [20]. The necessity of adding SFCL is that resistive types of SFCL have a better performance suppressing the large fault current. The

damage to the system caused by DC transmission line fault will be significantly reduced, and the equipment will be protected from the high raised fault current. In addition, limiting fault current reduces the consequent voltage disturbances on the healthy parts of the system due to a fault. Mitigating these disturbances can help both load and generation ride through the fault. Consequently, the presence of an SFCL can lead to improved overall reliability for other devices in distribution systems.

The main elements affecting the cost of DC circuit breaker is the total fault clearing time which consists of the breaking time and fault clearing time and the reactor. A longer breaking time can lead to a very high level fault current which means a greater current breaking capability. Therefore, shorter breaking time is more desirable. The cost of SFCL depends on its current limiting capability. The investment for both devices can be very expensive. Combination of these two devices maybe a beneficial solution such as a combination of lower current limiting capability SFCL and a higher current breaking capability HVDC circuit breaker.

V. Conclusion

This paper has successfully integrated and evaluated the performance of VSC based multi-terminal HVDC system with resistive SFCL. An effective model of resistive type of SFCL has applied in VSC based multi-terminal HVDC system, considering the DC breakers overcurrent withstand capability. Based on the electric field intensity and current density characteristics, the SFCL has been modelled in this paper and it is successfully integrated into a VSC based MTDC system for fault current limitation under AC/DC faults. The transient analysis is carried out for different perturbations and from the simulation results. Simulation results show that SFCL not only reduces the current transients for DC faults but also for AC faults. The method was validated by time domain simulations undertaken with the PSCAD/EMTDC, and the results showed that the fault current could be reduced up to 65%. The use of SFCL can effectively suppress the short circuit fault on DC line. Hence, the robustness of VSC based multi-terminal HVDC system can be improved against the DC fault to a certain extent. The DC resistive SFCL is proved to be a very promising technology in multi-terminal HVDC systems.

References

[1] S. Le Blond, R. Bertho, D. Coury, and J. Vieira, "Design of protection schemes for multi-terminal HVDC systems," *Renewable Sustain. Energy Rev.*, vol. 56, pp. 965–974, 2016.

[2] C. Dierckxsens, K. Srivastava, M. Reza, S. Cole, J. Beerten, and R. Belmans, "A distributed DC voltage control method for VSC MTDC systems," *Electr. Power Syst. Res.*, vol. 82, pp. 54–58, 2012.

[3] N. Flourentzou, V. G. Agelidis, and G. D. Demetriades, "VSC-based HVDC power transmission systems: An overview," *IEEE Trans. Power Electron.*, vol. 24, no. 3, pp. 592–602, Mar. 2009.

[4] F. A. Mourinho *et al.*, "Modeling and analysis of superconducting fault current limiters applied in VSC-HVDC systems," in *Proc. 2015 IEEE Power Energy Soc. Gen. Meeting*, 2015, pp. 1–5.

[5] U. A. Khan, J.-G. Lee, F. Amir, and B.-W. Lee, "A novel model of HVDC hybrid-type superconducting circuit breaker and its performance analysis for limiting and breaking DC fault currents," *IEEE Trans. Appl. Supercond.*, vol. 25, no. 6, Dec. 2015, Art. no. 5603009.

[6] S. Eckroad, "Superconducting fault current limiters," *Electr. Power Res. Inst.*, Palo Alto, CA, USA, Tech. Rep. 1017793, 2009.

[7] J. Li, A. M. Gee, M. Zhang, and W. Yuan, "Analysis of battery lifetime extension in a SMES-battery hybrid energy storage system using a novel battery lifetime model," *Energy*, vol. 86, pp. 175–185, 2015.

[8] J. Li *et al.*, "Analysis of a new design of the hybrid energy storage system used in the residential m-CHP systems," *Appl. Energy*, vol. 187, pp. 169–179, 2017.

[9] J. Li, M. Zhang, Q. Yang, Z. Zhang, and W. Yuan, "SMES/battery hybrid energy storage system for electric buses," *IEEE Trans. Appl. Supercond.*, vol. 26, no. 4, Jun. 2016, Art. no. 5700305.

[10] Y. Chen, X. Liu, J. Sheng, L. Cai, Z. Jin, J. Gu *et al.*, "Design and application of a superconducting fault current limiter in DC systems," *IEEE Trans. Appl. Supercond.*, vol. 24, no. 3, Jun. 2014, Art. no. 5601305.

[11] H.-J. Lee, G. T. Son, J.-I. Yoo, and J.-W. Park, "Effect of a SFCL on commutation failure in a HVDC system," *IEEE Trans. Appl. Supercond.*, vol. 23, no. 3, Jun. 2013, Art. no. 5600104.

[12] J.-G. Lee *et al.*, "Assessment on the influence of resistive superconducting fault current limiter in VSC-HVDC system," *Physica C, Supercond.*, vol. 504, pp. 163–166, 2014.

[13] L. Chen, H. Pan, C. Deng, F. Zheng, Z. Li, and F. Guo, "Study on the application of a flux-coupling-type superconducting fault current limiter for decreasing HVdc commutation failure," *Can. J. Elect. Comput. Eng.*, vol. 38, pp. 10–19, 2015.

[14] F. Liang, W. Yuan, C. A. Baldan, M. Zhang, and J. S. Lamas, "Modeling and experiment of the current limiting performance of a resistive superconducting fault current limiter in the experimental system," *J. Supercond. Novel Magn.*, vol. 28, pp. 2669–2681, 2015.

[15] M. E. Elshiekh, D.-E. A. Mansour, and A. M. Azmy, "Improving fault ride-through capability of DFIG-based wind turbine using superconducting fault current limiter," *IEEE Trans. Appl. Supercond.*, vol. 23, no. 3, Jun. 2013, Art. no. 5601204.

[16] W. Paul, M. Chen, M. Lakner, J. Rhyner, D. Braun, and W. Lanz, "Fault current limiter based on high temperature superconductors–different concepts, test results, simulations, applications," *Physica C, Supercond.*, vol. 354, pp. 27–33, 2001.

[17] J. Li, R. Xiong, Q. Yang, F. Liang, M. Zhang, and W. Yuan, "Design/test of a hybrid energy storage system for primary frequency control using a dynamic droop method in an isolated microgrid power system," *Appl. Energy*, 2016. [Online]. Available: http://dx.doi.org/10.1016/j.apenergy.2016.10.066

[18] T. K. Vrana, Y. Yang, D. Jovcic, S. Dennetire, J. Jardini, and H. Saad, "The CIGRE B4 DC grid test system," *Electra*, vol. 270, pp. 10–19, 2013.

[19] T. Hammons *et al.*, "Role of HVDC transmission in future energy development," *IEEE Power Eng. Rev.*, vol. 20, no. 2, pp. 10–25, Feb. 2000.

[20] C. Peng, J. Wen, Y. Wang, J. Wu, and X. Chen, "Potential use of fault current limiter in VSC based DC transmission systems," in *Proc. 2012 Asia-Pacific Power Energy Eng. Conf.*, 2012, pp. 1–4.